PROCEEDINGS

INTERNATIONAL CONFERENCE ON

NONLINEARITY, BIFURCATION AND CHAOS:

THE DOORS TO THE FUTURE

I C N B C 9 6

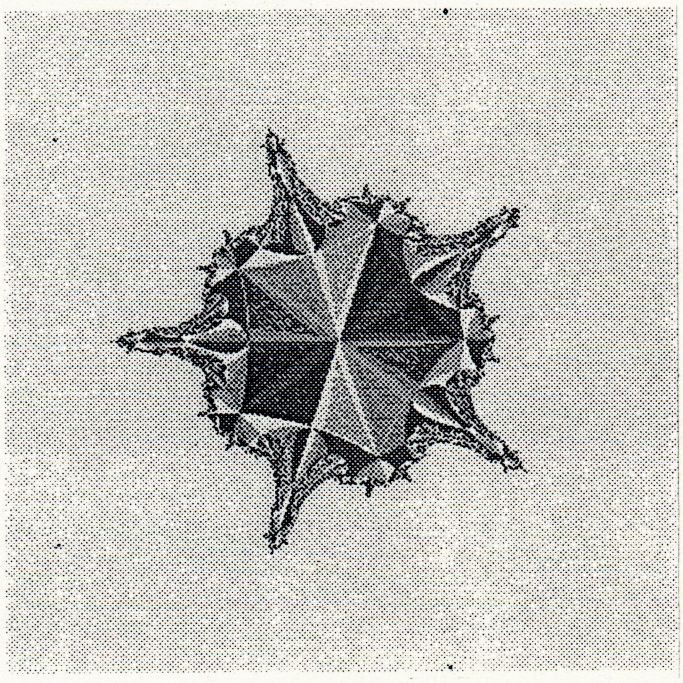

ŁODZ- DOBIESZKÓW - SEPTEMBER 16 -18, 1996

ORGANIZERS

Technical University of Lodź

Ecole Nationale des Travaux Publics de l'Etat

Publication of this programme was financially supported by

State Committee for Scientific Research of Poland (KBN)

and Ecole Nationale des Travaux Publics de l'Etat (France)

PROCEEDINGS OF THE ICNBC'96

INTERNATIONAL CONFERENCE ON

NONLINEARITY, BIFURCATION AND CHAOS:

THE DOORS TO THE FUTURE

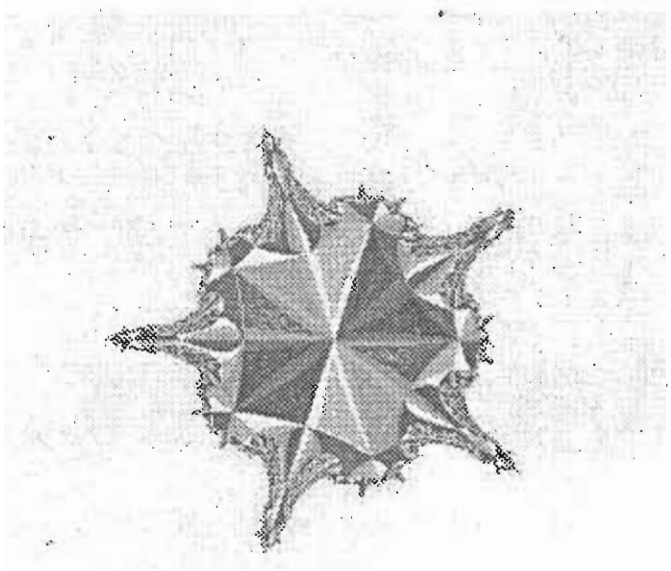

LODZ- DOBIESZKÓW - SEPTEMBER 16 -18, 1996

ORGANIZERS

Technical University of Lodź

Ecole Nationale des Travaux Publics de l'Etat

Publication of this programme was financially supported by

State Committee for Scientific Research of Poland (KBN)

and Ecole Nationale des Travaux Publics de l'Etat (France)

INTERNATIONAL SCIENTIFIC COMMITTEE

V.S. ANISHCHENKO (Saratov) J. AWREJCEWICZ (Lodź) I. BLEKHMAN (St.-Petersburg)

P. BOIS (Lille) D.-H. Van CAMPEN (Eindhoven) B.Y. CHIRIKOV (Novosibirsk)

L.O. CHUA (Berkeley) M. DUBOIS (Paris) Z. DŹYGADLO (Warsaw)

J.W. ELSNER (Częstochowa) C. GREBOGI (College Park) P. HAGEDORN (Darmstadt)

E. INFELD (Warsaw) L. JÉZÉQUEL (Lyon) M.A. KRASNOSEL'SKIJ (Moscow)

J. KUDREWICZ (Warsaw) C.-H. LAMARQUE (Lyon) A. LASOTA (Kraków)

R. LOZI (Nice) J. MARYNIAK (Warsaw) R. MENNICKEN (Regensburg)

F.C. MOON (New-York) M. OGORZALEK (Kraków) F. PFEIFFER (München)

G. REGA (L'Aquila) M. SCHATZMAN (Lyon) W. SCHWARZ (Dresden)

W. SZEMPLINSKA-STUPNICKA (Warsaw) H. TAMURA (Fukuoka)

H. TROGER (Wien) Y. UEDA (Kyoto)

Y.A. YORKE (College Park) H. ZORSKI (Warsaw)

ORGANIZING COMMITTEE

J. AWREJCEWICZ (chairman) Z. DŹYGADLO A. GALKOWSKI

E. INFELD J. KRYSIŃSKI (Rector) C.-H. LAMARQUE (co-chairman)

J.-M. MALASOMA J. MARYNIAK J. MROZOWSKI

M. OGORZALEK H. ZORSKI

The ICNBC'96 has been organized with the support of

the Committee of Mechanics of the Polish Academy of Sciences,

ENTPE (France), TU Lodź (Poland), Région Rhônes-Alpes (France),

Société Française de Mécanique, Association MV2 (France)

Polish Society of Theoretical and Applied Mechanics,

The New-York Academy of Sciences

State Committee for Scientific Research of Poland

Society of Applied Mathematics and Mechanics (GAMM, Germany)

EDITORS OF THE PROCEEDINGS

Jan AWREJCEWICZ

Technical University of Lódź

Division of Control and Biomechanics

1/15 Stefanowskiego, 90-924 Lódź, POLAND

Claude-Henri LAMARQUE

Ecole Nationale des Travaux Publics de l'Etat

Département Génie Civil Bâtiment URA CNRS 1652

Laboratoire Géo-Matériaux

1 rue Audin

F69 518 vaulx-en-Velin, Cedex, FRANCE

CONTENTS

INVITED PAPERS

CONTRIBUTED PAPERS

INVITED PAPERS

NOISY ON-OFF INTERMITTENCY

A. Čenys
Semiconductor Physics Institute, Vilnius LT 2600, Lithuania

Abstract: Statistical properties of the laminar lengths for the noisy on-off intermittency are studied analytically. The universal distribution of the laminar phases is obtained at the critical point. It can be well approximated by the power law with the exponent $-3/2$ and the exponential law describing fast falloff.

1. Introduction

Recently a particular type of intermittent bursting [Pikovsky, 1984, Fujisaka & Yamada 1985], called on-off intermittency [Platt *et al.*, 1993], have attracted wide attention. On-off intermittency differs essentially from the well known Pomeau-Manneville and crisis induced chaos-to-chaos intermittencies, although having common features with both of them. In dynamical systems it is related with a local bifurcation called *blowout bifurcation* [Ott & Sommerer, 1994]. This bifurcation defines the loss of stability of the smooth invariant manifold in phase space which exists due to the symmetry and contains the chaotic attractor. On-off intermittency can be defined as *Pomeau-Manneville type III intermittency with an irregularly driven bifurcation parameter*. Scaling properties of both intermittencies are similar [Heagy *et al.*, 1994, Čenys & Lustfeld, 1996]. Although exhibiting the same main statistical properties, the corresponding time dependent signals are essentially different. The laminar phases in the Pomeau-Manneville case represent regular dynamics for any choice of variables. For on-off intermittency the shape of the time dependent signal essentially depends on the measured variable and usually looks like chaos-to-chaos intermittency. To detect on-off intermittency in the experimental situation one has to look for *chaos-to-chaos intermittency with the characteristic exponents of the Pomeau-Manneville type III intermittency*.

Like other critical phenomena, the on-off intermittency is sensitive to the presence of external random noise unavoidable in experimental systems. The most prominent one is the appearance of a shoulder in the distribution of the laminar lengths. The shoulder above power law $-3/2$ curve precedes an exponent falloff at large lengths. It was predicted numerically [Platt *et al.*, 1994] and observed experimentally in electronic circuits [Hammer *et al.*, 1994, Čenys *et al.*, 1996] also ferromagnetic resonance [Rodelsperger *et al.*, 1995]. Platt *et al.* in their numerical

study have defined three regions of different behaviour in the distribution of the laminar lengths for noisy on-off intermittency, namely power law region, shoulder region and region of the exponential falloff. In this paper we show both analytically, exploiting Focker-Planck equation, and numerically that the shoulder and the exponential falloff are described by an unanimous exponential law.

2. Analytical model

The simplest model exhibiting the on-off intermittency in the presence of noise can be written as an one-dimensional map with external driving

$$r_{n+1} = a x_n r_n + \eta_n + f(r_n^2), \tag{1}$$

where random additive noise η is assumed to be small and function $f(r_n^2)$ represents nonlinear terms. For the dynamical systems the driving signal x_n is determined by the chaotic dynamics on the invariant manifold, while for the random maps it is determined by an external random force. In the later case both the driving signal x_n and the additive noise η_n can be of the same origin. The only difference is that multiplicative noise x_n should be of large amplitude as compared with the additive noise η_n.

The above model allows further simplifications. As it was shown earlier, the influence of both the additive noise η_n and the nonlinear term $f(r_n^2)$ can be modeled by two reflecting boundaries at r_1 and r_2 correspondingly. Moreover, diffusion defined by the linear term in Eq.(1) rather than nonlinearity, is responsible for the reinjection in this systems. As a result statistical properties of the first passage times, i.e. the time necessary for the system to pass the threshold r_{th} starting at some initial level $r_0 < r_{th}$ coincides with that of the laminar lengths.

Modeling both the additive noise and the nonlinear terms by the reflecting boundaries and introducing the logarithmic variable $y_n = \ln \mid r_n \mid$, Eq.(1) can be rewritten as

$$y_{n+1} = y_n + v + z_n. \tag{2}$$

The new driving variable $z_n = \ln \mid x_n \mid - < \ln \mid x_n \mid >$ has zero mean value $< z_n >= 0$ by definition ($< ... >$ denotes the time average). The new control parameter $v = (a - a_c)/a_c$ defines the deviation from the critical point a_c and it is assumed to be small $v \ll 1$. Noise free critical point a_c corresponds to the onset of the on-off intermittency in Eq.(1) without additive noise. It depends on the statistical properties of the driving signal x_n and can be estimated from the following relationship $\ln \mid a_c \mid =< \ln \mid x_n \mid >$.

Map (2) represents a biased "chaotic" walk, when driving signal z_n is generated by the chaotic system [Heagy *et al.*,1994]. However, long time behaviour of this map is well approximated by the usual random walk which assumes variable z_n to be Gaussian and δ-correlated. This approximation was extensively used in the previous analytical studies. For the uncorrelated Gaussian

driving, the probability density f of the variable y satisfies the Focker-Planck equation

$$\frac{\partial f}{\partial t} = -v\frac{\partial f}{\partial y} + \frac{D}{2}\frac{\partial^2 f}{\partial y^2}, \tag{3}$$

where the diffusion coefficient D is given by

$$D = \lim_{N\to\infty} N^{-1} < (\sum_{n=0}^{N-1} z_n)^2 > . \tag{4}$$

Expression (4) takes into account short time correlations present in the driving signal z_n.

To calculate the distribution of the first passage times, Eq.(3) should be solved with the initial condition

$$f(t=0,y) = \delta(y - y_0), \tag{5}$$

where $y_0 = \ln r_0$, and with absorbing boundary condition at the threshold defining laminar phases

$$f(t, y = y_{th}) = 0. \tag{6}$$

The distribution $P(\tau, y_0)$ of the first passage times τ then is proportional to the time dependent flow at the absorbing boundary $J(\tau, y = y_{th})$, where $J(t,y) \equiv -vf + \frac{D}{2}\frac{df}{dy}$. The second boundary condition

$$J(t, y = y_1) = 0 \tag{7}$$

is determined by the additive noise. It corresponds to zero flow at the reflecting barrier at $y_1 \equiv \ln r_1$.

In the noise free case with the second boundary condition at infinity ($y_1 \to -\infty$), an analytical solution of Eq.(3) is easily derived. It gives for the distribution of the first passage times $P(\tau, y_0^*)$ the following expression

$$P(\tau, y_0^*) = \frac{y_0^* \tau^{-3/2}}{\sqrt{2\pi D}} \exp\left[-\frac{(v\tau - y_0^*)^2}{2D\tau}\right], \tag{8}$$

where $y_0^* = \ln(r_{th}/r_0)$.

For the dominating diffusional reinjection we assume $y_0^* \ll 1$ and can neglect the second term in the exponent in the distribution (8). Then integration with the reinjection probability is trivial and for the distribution of the laminar lengths one obtains

$$P(\tau) \propto \frac{\tau^{-3/2}}{\sqrt{2\pi D}} \exp\left[-\frac{v^2\tau}{2D}\right]. \tag{9}$$

This noise free distribution has the same power law scaling and the exponential falloff as that obtained from the more complicated analysis of the random walk [Heagy, 1994].

In the presence of noise corresponding to the reflecting boundary at finite level y_1, Eq.(3) is solved using eigenfunctions and eigenvalues of the Focker-Planck operator. The straightforward application of the method gives following result for the distribution of the first passage times in the form of the infinite sum

$$P(\tau,\beta) = 2\tau_d^{-1} e^{\alpha\beta} \sum_{i=0}^{\infty} \frac{h_i^2 \sin(\beta h_i)}{2h_i - \sin 2h_i} \exp\left[-\frac{\tau}{2\tau_d}(\alpha^2 + h_i^2)\right], \tag{10}$$

where $\alpha = \mid v \mid D^{-1} \ln(r_{th}/r_1)$,$\beta = y_0^* \ln^{-1}(r_{th}/r_1)$ and eigenvalues h_i satisfy equation

$$\alpha \tan h = -h. \tag{11}$$

The parameter β depends on the ratio between reinjection r_0 and additive noise r_1. For small noise and diffusional reinjection, assumed in our model, $\beta \ll 1$. Parameter α defines which process - diffusion or drift, is a dominating one. It can be presented as a ratio $\alpha \equiv \tau_d/\tau_b$ between the diffusion time $\tau_d = D^{-1} \ln^2(r_{th}/r_1)$ and the drift time $\tau_b = \mid v \mid^{-1} \ln(r_{th}/r_1)$. The characteristic times τ_d and τ_b introduced here define the time needed for the system to reach threshold from the noise level due to diffusion and drift correspondingly.

The noise free critical point $\alpha = 0$ ($v = 0$) corresponds to the absence of the drift when the first passage time is completely determined by the diffusion process. In this case the transcendental equation (11) can be solved analytically and, taking into account $\beta \ll 1$, the distribution of the first passage times $P(\tau,\beta)$ at the critical point is given by

$$P(\tau,\beta) = \frac{\pi^2\beta}{4\tau_d} \sum_{i=0}^{\infty} (2i+1)^2 \exp\left[-\frac{(2i+1)^2\pi^2\tau}{8\tau_d}\right] \tag{12}$$

Like in the noise free case, only the norm of the distribution depends on the reinjection y_0 via parameter β. Therefore integration with the reinjection probability only eliminates the dependence on β and the distribution of the laminar lengths $P(\tau)$ is defined by the same function as the distribution of the first passage times $P(\tau,\beta)$. Moreover, the shape of the distribution (12) is universal, since it does not depend on the system's parameters if τ is measured in the units of the diffusion time τ_d. The universal distribution of the first passage times (12) at the critical point $v = 0$ is our main analytical result. It is shown in Fig. 1.

For small and large τ distribution (12) is well approximated by the power law and exponential behaviour correspondingly:

$$P(\tau) = \begin{cases} \beta\tau_d^{1/2}(2\pi)^{-1/2}\tau^{-3/2}, & \text{if} \quad \tau \le \tau_d, \\ \beta\pi^2(4\tau_d)^{-1} \exp\left[-\frac{\pi^2\tau}{8\tau_d}\right], & \text{if} \quad \tau \ge \tau_d, \end{cases} \tag{13}$$

As it can be easily seen in Fig. 1 the asymptotical curves approximate very well the range of both small and large laminar lengths. Moreover, the exponential asymptotic describes nearly

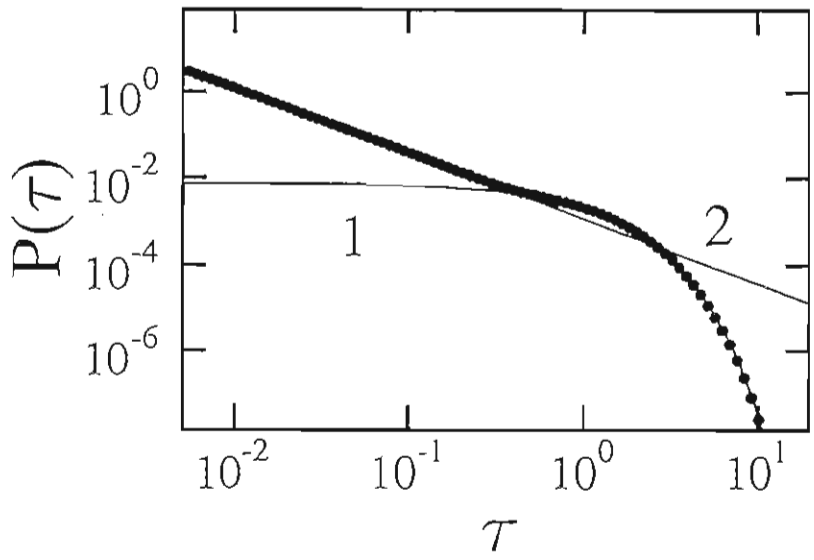

Figure 1: Universal distribution of the laminar lengths τ for noisy on-off intermittency (dots). 1 - exponential asymptotic for large τ; 2 - power law asymptotic for small τ.

whole shoulder region above power law straight line and transition between the two asymptotic is narrow. This result demonstrate that there are only two regions corresponding to the different behaviour in the universal distribution.

In the drift controlled region $\mid \alpha \mid \gg 1$ the exponential asymptotic of the distribution (3) for the large τ coincides with the results obtained by Ott *et al.* [1994a] For $v > 0$ it posses the same exponential falloff as in the noise-free case (9). This result corresponds to the fact that for $v \gg 1$ system reaches the threshold without reaching the noise level r_1 and an as a result additive noise influence is negligible. For $v < 0$ on the contrary, drift controlled region corresponds to the case when the system reaches fast noise level and stays close to this level for a long time. The rare bursts, during which the system can reach the threshold, are related with the tail in the Gaussian distribution and correspond to the pure imaginary eigenvalue of the Eq. (11) existing for $\alpha < -1$. The rare bursts cause the exponential falloff in the distribution $P(\tau)$ with a very large characteristic time $1/4\alpha^{-2}\exp(-2\alpha)$ ($\alpha < 0, \mid \alpha \mid \gg 1$). This result has the same scaling as that obtained by Ott *et al.* [1994a] and in addition allows to estimate the proportionality constant. However, this scaling is not universal for the all systems exhibiting on-off intermittency. It is related to the Gaussian approximation of the tails in the probability distribution which does not hold for all chaotic systems [Čenys & Lustfeld, 1996].

3. Conclusions

An analytical expression for the distribution of the laminar lengths for the noisy on-off intermittency is obtained from the analysis of the Focker-Planck equation. At the critical point of the onset of noise free on-off intermittency, it provides universal distribution independent on the parameters of a particular system. The distribution has only two regions corresponding to the different behaviour. These are power law region with the exponent $-3/2$ for the moderate laminar lengths and exponential law region describing fast falloff for the large lengths with the narrow transition region between them. The whole shoulder above power law straight line is described by the same exponential asymptotic.

4. Acknowledgments

This work was partially supported by the EEC under the contract No. CIPA-CT93-0255.

5. References

Čenys, A. & Lustfeld, H. [1996] "Statistical properties of the noisy on-off intermittency", J.Phys.A. **29**, 11-20.

Čenys *et al.* [1996] "On-off intermittency in chaotic synchronization experiment", Phys.Lett.A. **213**, 259-265.

Fujisaka, H. & Yamada, H. [1985]"A new intermittency in coupled dynamical systems", Prog.Theor.Phys. **74**, 918-921.

Hammer, P.W. *et al.* [1994] "Experimental observation of on-off intermittency", Phys.Rev.Lett. **73**, 1095.

Heagy, J.F., Platt, N, & Hammel, S.M. [1994] "Characterization of on-off intermittency", Phys.Rev.E **49**, 1140-1150.

Ott, E. & Sommerer, J.C. [1994] "Blowout bifurcations: the occurrence of riddled basins and on-off intermittency", Phys.Lett.A **188**, 39-47.

Ott, E. *et al.* [1994a] "The transition to chaotic attractors with riddled basins", Physica D **76**, 384-410.

Pikovsky, A.S. [1984] "On the interaction of strange attractors", Z.Phys.B **55**, 149-154.

Platt, N., Spiegel, E.A & Tresser, C. [1993] "On-off intermittency: a mechanism for bursting", Phys.Rev.Lett. **70**, 279-282.

Platt, N., Hammel, S.M. & Heagy, J.F. [1994] "Effects of additive noise on on-off intermittency", Phys.Rev.Lett. 72, 3498-3501.

Rodelsperger, F. Čenys, A. & Benner, H. [1995] "On-off intermittency in spin-wave instabilities", Phys. Rev. Lett. **75**, 2594-2597.

THE HIGHER MODES FOR THE CHAOTIC OSCILLATIONS OF A BUCKLED BEAM

Tatiana Reynolds[1], Earl H. Dowell[2]
Duke University, Durham, North Carolina 27708-0300

Abstract

We explore the use of the generalized Melnikov's method for determining the onset of chaos for a buckled beam with an external excitation. It is shown that the critical function of damping, forcing amplitude, and frequency for the *first component* of the Melnikov vector for the system of higher modal approximations and that for a single modal Duffing's equation are related, though not identical. Higher Melnikov vector components are also shown to be generally less critical.

Introduction

Obtaining the necessary conditions for chaos in Duffing-like equations from the intersection of unstable and stable manifolds is not new. The analysis of a single Duffing equation with small damping and periodic forcing is a classical example in standard texts (see, for example, [1]). In the last few years the analysis of a multi-dimensional Duffing's system has become a subject of intense discussion [2]. A series of works developed the Melnikov algorithm to show that chaotic motion may occur in systems similar to that which is analyzed in the present work. However, all results published to date are based upon the assumption that the second and higher order modal contributions to the chaotic motion are small. Therefore, all systems were effectively simplified to the one-dimensional case of a perturbed Hamiltonian system. Our analysis does *not* assume the amplitudes of the higher modes to be small perturbations. This fact makes the analysis more difficult and more interesting.

The physical system consists of a beam with ends which are simply supported. The beam is externally excited by the periodic force $P\cos\omega t$. In addition, an inplane load R_x is applied to the beam. This load will be always compressive and its value will vary above the critical buckling load, ie., the beam is buckled.

---

[1]Post-graduate Research Associate, Department of Mechanical Engineering and Materials Science.
[2]J. A. Jones Professor and Dean, School of Engineering, Fellow ASME.

A partial differential equation of the beam vibration is simpified using Galerkin's method [3]. It is assumed that the beam deflection takes the form of a summation of eigenmodes. Using the orthogonality of eigenmodes, we obtain the system of the ordinary differential equations:

$$\begin{aligned}
&\frac{d^2x_m}{dt^2} - m^2(R-m^2)x_m + \beta m^2 x_m \sum_{i=1}^{N}(ix_i)^2 \\
&= \varepsilon\left[\gamma_m \cos\tilde{\omega}t - \delta\frac{dx_m}{dt}\right] \\
&\text{for } m = 1, ..., N
\end{aligned} \tag{1}$$

where the beam deflection, $w(x,t)$, is given by the modal exapnsion $w(x,t) = \sum_{m=1}^{N} x_m(t)\sin\frac{m\pi x}{L}$ and $\gamma_m = \frac{1}{L}\int_0^L P\sin\frac{m\pi x}{l}dx$. R, δ, γ are nondimentional in-plane load, damping, and external excitation respectively. $\tilde{\omega}$ is the excitation frequency. All parameters and variables are nondimensionalized (see, [3, 4]).

Homoclinic Manifold

The question of integrability of the unperturbed system, i. e. (1) with $\varepsilon \equiv 0$, does not have a clear analytical answer. The set of N invariant functions is not obvious. and cannot be found in the family of elementary functions. There is only one first integral – the Hamiltonian

$$\begin{aligned}
H(x,y) &= \frac{1}{2}\times\sum_{r=1}^{N} y_r^2 + \frac{1}{4}\times(\sum_{r=1}^{N}(rx_r)^2)^2 \\
&- \frac{1}{2}\times\sum_{r=1}^{N} r^2(R-r^2)x_r^2
\end{aligned} \tag{2}$$

which is easy to establish for system (1). However, using the theorem proven by Poincare (see [5]) and the fact of the existence of the N homiclinic orbits, one can draw a conclusion about the existence of the homoclinic manifold and the integrability of the unpertubed system.

In general, calculation of the homoclinic manifold is a boundary value problem. We study the unperturbed system that is symmetrical about the subspace $y = 0$, i. e., if $(x(t), y(t))$ is a solution of equation (1) then $(x(-t), -y(-t))$ is a solution also. Hence, if the *positive* branch (x, y) crosses the $y = 0$ subspace the corresponding *negative* $(x, -y)$ one has

to cross it at the same point. Therefore, a boundary value problem can be replaced by an initial value problem with the initial condition

$$x(-T) = y(-T) = 0 \tag{3}$$

where $1/T \ll 1$. By integrating the system forward until $y_i = 0$ for $1 \leq i \leq N$ simultaneously, one obtains an unstable half of the manifold.

An interesting property of the phase plane projections of the homoclinic manifolds is the *shifted repeatability* of the shapes of the projections. The projection of the manifold on the coordinate plane $x_1 - y_1$ changes its size for systems with different dimensions. But qualitatively it is always a single loop in one of the half-planes. One can observe that whenever the number of modes increases by one, a new shape of the projections appears. The first mode repeats itself and all other modes shift their numbers from j to $j + 1$. The complete picture of the behavior of the manifold can be presented by a right isosceles triangle

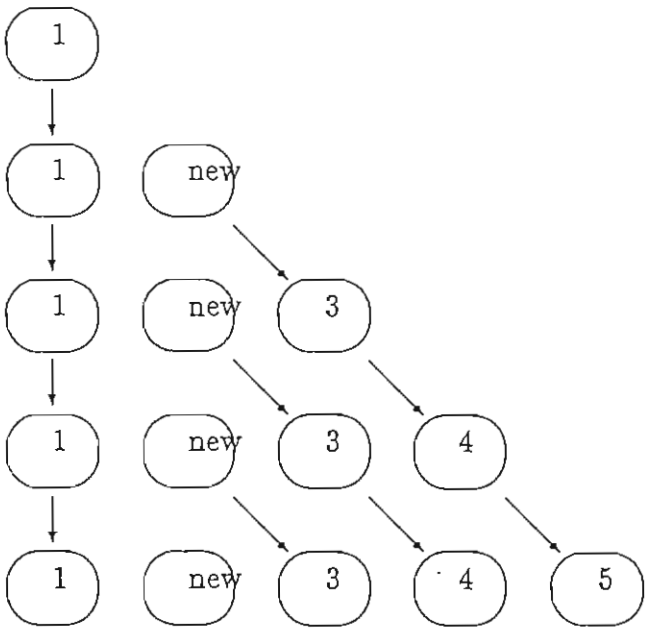

(see the sketch).

Energy Component of the Melnikov Vector

The second step of the multi-dimensional Melnikov algorithm is to calculate the vector which represents the distance between the stable and the unstable manifolds. However, only one of the integrals of motion has an analytical expression; thus we can follow the Melnikov algorithm by substituting the numerical data into the equation for the first or

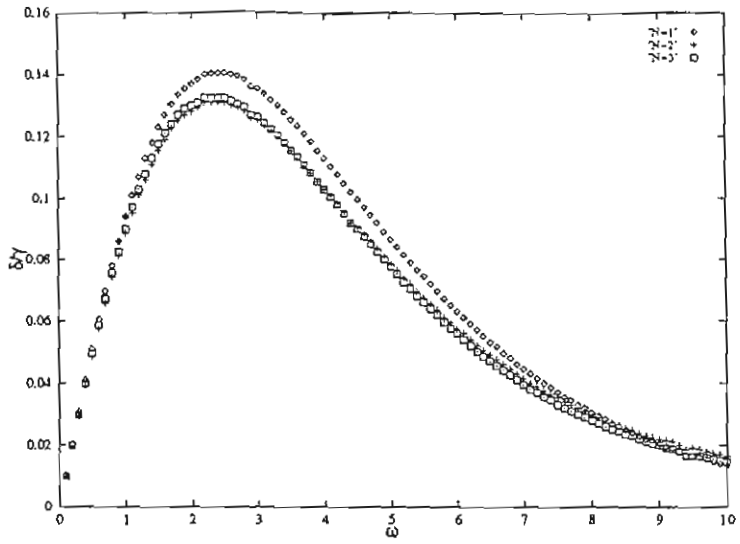

Figure 1: The influence of the second and third modes on the critical Melnikov curve, for $R = 11$.

energy component of the Melnikov vector. We will refer to this analytical technique involving some numerical data as $semi - analytical$.

After extensive computations for a broad range of parameter R, we have concluded that the critical curve obtained for the higher mode system is somewhat different from the similar curve calculated for the one-dimensional system (see, for example, Fig. 1). In order to include the effect of all modes into the analysis, we suggest the critical function be empirically approximated by a linear combination of terms whose form is suggested by the one mode result.

$$\frac{\delta}{\gamma} < \sum_{i^2 \leq N} coeff_i \frac{\omega}{\cosh \frac{\pi\omega}{2\sqrt{R-i^2}}}. \tag{4}$$

The influence of a particular mode is measured by the value of the corresponding coefficient in comparison to others. To make that comparison easier we rescale the vector of all coefficients $\vec{coeff}$ to make its length equal to 1, i. e.

$$Norm\vec{C}oeff = \frac{\vec{coeff}}{||\vec{coeff}||} \tag{5}$$

The normalized coefficients for R between 10 and 33 are shown in Fig. 2. The coefficients reach an asymptote for large R: $NormCoeff_1 \approx 0.475, NormCoeff_2 \approx -0.79, NormCoeff_3 \approx 0.365$. The fourth coefficient is very small (≈ 0.04) but clearly distinct from zero. The fifth

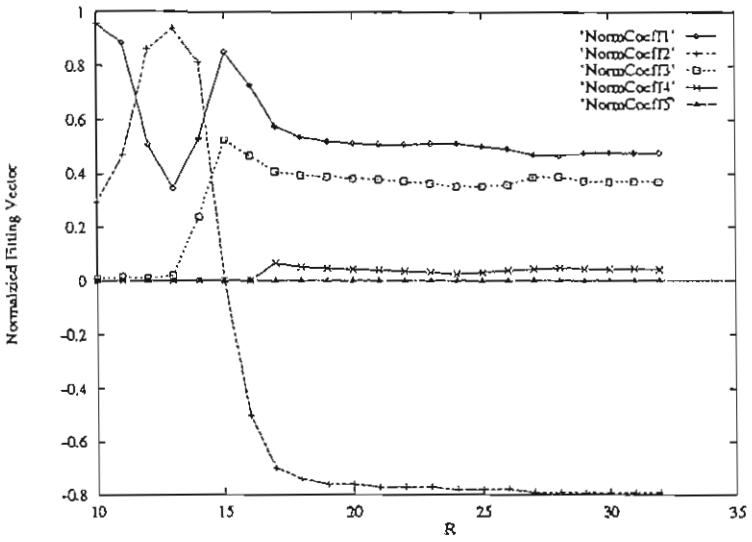

Figure 2: The mode influence evolution with respect to the axial load R.

coefficient is virtually zero (≈ 0.005). For $R < 10$, only the first mode component is significant.

Higher Components of the Melnikov Vector

The critical condtions for all components of the Melnikov vector can be obtained by numerically iterating the set of the dynamical parameters of the system until a certain component of the modified vector changes its sign. The condition for the possibility of a chaotic motion is for δ/γ to be in a region below the critical curve for each and every component. The results for the first component of the vector are known from the semi-analytical technique described above.

Let us begin with the simplest higher-dimensional system, $N = 2$, (see Fig. 3). One can conclude that the critical ratio for the *second* Melnikov component ≈ 0.3 and that it can be approximated by a horizontal line. Note the second component of the modified Melnikov vector begins to have zeros at much higher δ/γ ratios than the first component. This means that for an $N = 2$ system chaos may occur when ratio δ/γ is below the critical curve for the *energy* component.

Now we turn to higher dimensional dynamical structures hoping to show that the process for obtaining the critical condition for the system can be reduced to the search for

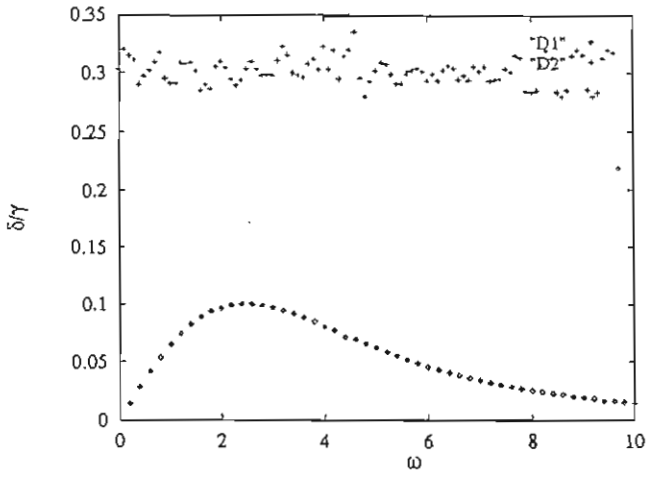

Figure 3: The critical relations of δ/γ for the components of the two-dimensional distance vector: $D1 = D_{1cr}$, $D2 = D_{2cr}$. $R = 17$

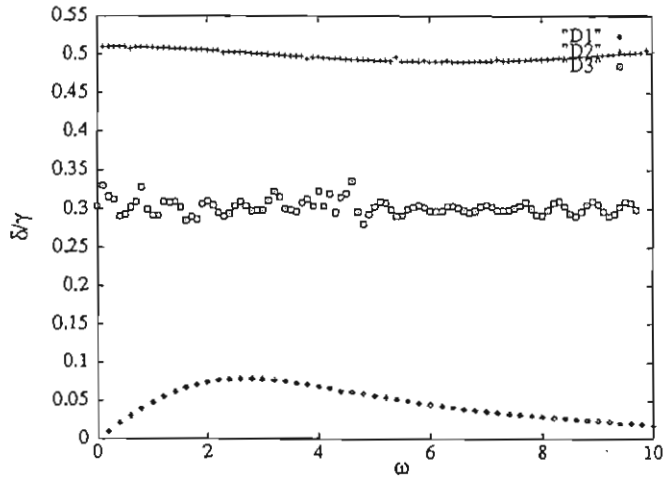

Figure 4: The critical relations of δ/γ for the components of the three-dimensional Melnikov vector. $D1 = D_{1cr}$, $D2 = D_{2cr}$, $D3 = D_{3cr}$. $R = 17$

the critical condition for the first component of the Melnikov vector only. Calculations were done for the $N = 3$ case. The results are given in Fig. 4. Reviewing these figures, one can reach the important conclusion that the critical curves for the higher components lie significantly above (≈ 0.3, ≈ 0.5) the critical curve (< 0.1) for the first component. Hence, the necessary condition for chaos can be based on the critical condition for the *energy* component only. One does not have to do the expensive and time consuming calculation of the manifold intersections. The only calculation required is the semi-analytical algorithm

decribed in the previous section.

Conclusions

A system of the Duffing's equations represents a buckeled plate with external excitation. After showing the existence of the N-dimensional homoclinic manifold analytically, for this system of Duffing's equations, we calculated its components numerically. The inductive structure of the homoclinic manifold was discovered and described. The homoclinic manifold was then used in the calculation of the first or energy component of the Melnikov vector.

Subsequently the distance between the manifolds in each coordinate plane of the higher dimensional phase space was determined. The critical condition for the higher components of the Melnikov vector are satisfied for a smaller excitation or higher damping than the first component. This allowed us to establish that the universal necessary condition for onset of chaos is defined by the critical condition for first or *energy* component only.

References

[1] S. Wiggins. *Introduction to Applied Dynamical Systems and Chaos.* Springer-Verlag, New York, 1990.

[2] S. Wiggins. *Global Bifurcations and Chaos*, chapter 4. Springer-Verlag, New York, 1988.

[3] E. H. Dowell and C. Pezeshki. On the understanding of chaos in Duffing's equation including comparison with experiment. *Journal of Applied Mechanics*, 53:5–9, 1986.

[4] J. Guckenheimer and P. J. Holmes. *Nonlinear Oscillations, Dynamical Systems, and Bifurcations of Vector Fields.* Springer-Verlag, New York, 1983.

[5] Henri Poincare. History of modern physics and astronomy. In Daniel L. Goroff, editor, *New Methods of Celestial Mechanics*, volume 13, pages 1055–1061. American Institute of Physica, 1991.

Controlling Complex Systems

Leon Poon[1,2] & Celso Grebogi[2,3]
[1]Department of Physics, University of Maryland, College Park, MD 20742
[2]Institute for Plasma Research, University of Maryland, College Park, MD 20742
[3]Institute of Physical Science and Technology, University of Maryland, College Park, MD 20742

Abstract - The dynamical properties of a simple mechanical system, which is found to possess a large number of coexisting periodic attractors, is studied. It is found that the system exhibits a rich dynamical behavior when it is subjected to small amplitude noise. This dynamical behavior is of great utility, and this is demonstrated by using small perturbations to gear and influence the dynamics toward a specific periodic behavior.

The study of nonlinear dynamical systems have yielded many rich and varied behaviors. While great strides have been made in the study of low-dimensional dynamics where only one or two attractors dominate the system's behavior, much less is known about dynamical systems where a multitude of coexisting attractors is the norm. In this paper, we examine a simple mechanical model that possesses a large number of coexisting periodic attractors for wide parameter ranges. We study the effects such a large number of coexisting attractors have on the global dynamics of the system and show how a small amount of noise can alter the qualitative behavior of the system. Furthermore, we show that small perturbations, if chosen judiciously, can control the dynamics of the system.

The dynamical system we are interested in models a kicked double rotor. The kicked double rotor consists of two connected massless rods (length l_1 and l_2) where one end of the first rod pivots about a fixed point while the other end is attached to and pivots about the middle of the second rod. A mass m_1 is placed at the end of the first rod and two masses $m_2/2$ are placed at each end of the second rod. The coefficients of friction at the pivots are denoted ν_1 and ν_2. Kicks of constant strength ρ is applied to one end of the second rod at periodic intervals. The state of the system after each kick is described by the angular displacements and velocities of the rods $(\theta_1, \theta_2, \dot{\theta}_1, \dot{\theta}_2)$. For more details about the double rotor map, please consult Grebogi *et al.* [1987] and Romeiras *et al.* [1992].

For simplicity, we set the two values of the coefficient of friction to be the same, that is, $\nu_1 = \nu_2 \equiv \nu$. The behavior of the system is therefore dependent on two factors: damping as indicated by the coefficient of friction ν and forcing as indicated by the strength of the periodic kick ρ. Without damping ($\nu = 0$), the double rotor map is a volume preserving map, and the system is known as a Hamiltonian system. In this case, the system is believed to possess infinitely many stable but nonattracting periodic orbits. There exists regular motion around these stable periodic orbits on the invariant Kolmogorov-Arnold-Moser (KAM) surfaces. Interspersed with these islands of stability in phase space are regions where orbits experienced persistent chaotic motion.

As small dissipation is introduced into the system ($0 < \nu \ll 1$), all the stable periodic orbits become attracting sinks [Lieberman & Tsang, 1985]. While it is believed that the number of periodic orbits in the Hamiltonian limit is infinite, there exist only finitely many coexisting periodic sinks when damping is nonzero. This is because many periodic orbits (especially the higher periodic orbits) lose their stability rapidly with increasing damping for a given value of forcing [Feudel *et al.*, 1996]. Nonetheless, the number of attractors can in principle be arbitrarily high if the damping is chosen small enough. Thus, the weakly dissipative double rotor system exhibits a rich dynamical behavior dominated by the appearance and disappearance of a multitude of periodic attractors as one varies damping and forcing [Poon *et al.*, 1996]. This interesting and less understood case is very important because, in practice, many systems are neither without dissipation nor strongly dissipative, but they are weakly dissipative.

Along with the conversion of stable periodic orbits into sinks, the region of chaos surrounding these islands of stability also plays a major role in the system's dynamics as small dissipation is introduced into the Hamiltonian double rotor system. While almost all orbits of the system eventually settle into one of the periodic sinks (the set that do not approach a periodic sink has measure zero and include points on the boundaries between the different sinks), they experience periods of long chaotic transients before falling into the sinks. In fact, except for small open neighborhoods around the periodic attractors, the majority of phase space in the double rotor system is occupied by heavily entangled fractal basin boundaries

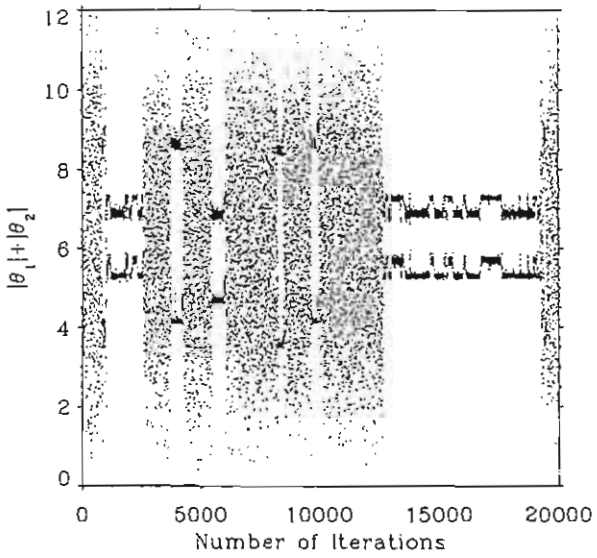

Figure 1: Time series of a typical noisy trajectory.

whose dimension is very close to the dimension of phase space [Poon & Grebogi, 1995]. The long chaotic transients can thus be attributed to the unstable chaotic sets embedded in the fractal basin boundaries [Grebogi *et al.*, 1988; Grebogi, *et al.*, 1983]. Even if every orbit's eventual behavior is periodic, the system is still very sensitive to initial conditions due to the fractal nature of the basin boundaries. Thus, a slight change in the initial condition will result in an orbit that is attracted to a totally different sink.

As a result, the system is extremely sensitive to noise, and the addition of small amplitude noise, typical of many physical systems, prevents the orbits from settling into any of the stable periodic behavior. What happens instead is that an orbit will come close to one of the periodic attractors and stay in its neighborhood for some time. This nearly periodic motion, however, is transitory, and noise will eventually move the orbit out of this state into the fractal boundary region. The orbit will then spend some amount of time within the massive basin boundary region executing an apparently chaotic motion before approaching the same or another periodic attractor. Hence, a typical noisy orbit alternates between intervals of chaotic motion and intervals of nearly periodic behavior near the "metastable" states (the former stable periodic attractors which are destabilized by noise) as shown in Fig. 1.

Hence, the dynamics of the noisy double rotor system tends to alternate among these

different behaviors and which of them are observed at a given time are often sensitive to minor perturbations. These two key attributes, accessibility to many states and sensitivity, present us with an opportunity to influence and manipulate the system's dynamics. Unlike low-dimensional chaotic systems that are commonly controlled using the ideas introduced in Ott *et al.* [1990], the weakly dissipative double rotor system is not characterized by the existence of one large chaotic attractor but by the coexistence of many attractors. While the existence of a large chaotic attractor is critical to those control schemes in Shinbrot *et al.* [1993], we show that the unstable chaotic sets in the boundaries of the double rotor system provide us with the necessary sensitivity and flexibility to gear the dynamics toward a specific periodic behavior using small perturbations. We can elect to stabilize an unstable periodic orbit embedded within a chaotic saddle in the boundary [Kovács *et al.*, 1994] or stabilize one of the (metastable) attracting sets as we show next.

Employing a simple feedback control scheme [Poon & Grebogi, 1995], we are able to control the dynamics of the noisy double rotor system. In Fig. 2, we follow a typical noisy orbit until it lands in a neighborhood of the desired metastable attractor we wish to control, then we turn on the control and let the system evolve further in the neighborhood of the desired attractor. Turning the control on means we add a small controlling term whose amplitude is a fraction (about 1/3) of the maximum noise amplitude at each step of the map. Hence, the controlling perturbation has a smaller amplitude than the case for the standard controlling chaos techniques [Shinbrot *et al.*, 1993]. After two thousand iterates, control is turned off, and we let the orbit wander until it falls near the next desired metastable attractor. In this fashion, we stabilize, say, four of the metastable attractors in the order we desire as demonstrated in Fig. 2. Furthermore, if the orbit is caught in the vicinity of a metastable state that is undesirable, we can destabilize it by applying small appropriate kicks (here too the magnitude of the kicks is about 1/3 of the maximum noise amplitude).

We have shown that a simple mechanical system with a small amount of dissipation can display the rich dynamical behavior where a multitude of coexisting periodic attractors appear and disappear over wide parameter ranges. In addition to these large number of sinks, the rest of phase space is filled with heavily intertwined fractal basin boundaries which

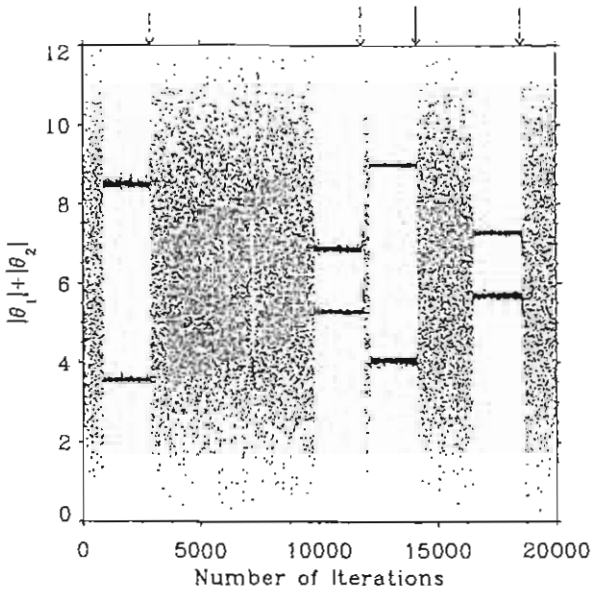

Figure 2: Time series showing the result of applying the simple feedback control scheme to successively control 4 different metastable states.

has two appreciable effects on the system: long chaotic transient behavior and final state sensitivity. Thus, small amounts of noise at each step of the dynamics can result in orbits that alternate between intervals of chaotic motion and intervals of nearly periodic behavior. In fact, the ability of the system to access many different states, combined with its sensitivity, offers great flexibility in controlling its dynamics. Using small perturbations (smaller than the maximum noise amplitude), we were able to stabilize the system about selected periodic behavior.

Acknowledgments

This work was supported by DOE (Office of Scientific Computing). The numerical computations reported here were supported by a grant from the W. M. Keck Foundation.

References

Feudel, U., Grebogi, C., Hunt, B., & Yorke, J.A. [1996] *Phys. Rev. E* (to appear).

Grebogi, C., McDonald, S.W., Ott, E. & Yorke, J.A. [1983] "Final state sensitivity: an obstruction to predictability," *Phys. Lett. A* **99**, 415.

Grebogi, C., Kostelich, E., Ott, E. & Yorke, J.A. [1987] "Multi-dimensioned intertwined basin boundaries: basin structure of the kicked double rotor," *Physica D* **25**, 347–360.

Grebogi, C., Nusse, H.E., Ott, E. & Yorke, J.A. [1988] "Basic sets: sets that determine the dimension of basin boundaries," in *Lecture Notes in Mathematics*, Vol. 1342, ed. J.C. Alexander (Springer-Verlag, New York) pp. 220–250.

Kovács, Z. , Szabó, K.G., & Tél, T. [1994] in *Nonlinearity and chaos in engineering dynamics*, ed. by J.M.T. Thompson & S.R. Bishop (Wiley, Chicheste).

Lieberman, M.A. & Tsang, K.Y. [1985] "Transient chaos in dissipatively perturbed near-integrable Hamiltonian systems" *Phys. Rev. Lett.* **55**, 908–911.

Ott, E., Grebogi, C., & Yorke, J.A. [1990] "Controlling Chaos" *Phys. Rev. Lett.* **64**, 1196–1199.

Poon, L. & Grebogi, C. [1995] "Controlling Complexity" *Phys. Rev. Lett* **75**, 4023–4027.

Poon, L., Feudel, U., Grebogi, C., & Yorke, J.A. [1996] "Dynamical properties of a simple mechanical system with a large number of coexisting periodic attractors" (in preparation).

Romeiras, F., Grebogi, C., Ott, E., & Dayawansa, W.P. [1992] "Controlling Chaotic Dynamical Systems" *Physica D* 58, 165.

Shinbrot, T., Grebogi, C., Ott, E. & Yorke, J.A. [1993] "Using Small Perturbations to Control Chaos" *Nature* **363**, 411–417 and references therein.

Stochastic Bifurcation: Concept and Examples

Volker Matthias Gundlach and Klaus R. Schenk-Hoppé
Institut für Dynamische Systeme
Universität Bremen, Postfach 330 440
28334 Bremen, Germany

Abstract: We present a concept to extend bifurcation theory from deterministic to stochastic models in dynamical systems and give reasons why this should be the natural way to deal with structural stability problems in random situations. In particular we present examples which show the naturality and strength of our approach.

1 Bifurcations

Bifurcation theory is concerned with qualitative changes in parametrized families φ_α of dynamical systems, e.g. those generated by a family of ordinary differential equations

$$\dot{x} = f_\alpha(x).$$

Of main interest are qualitative changes concerning the structural stability which describes the essential part of the dynamics. A parameter α_0 where structural stability is lost is called a bifurcation point.

In dimensions 1 and 2 there exists a well known classification of bifurcation scenarios into saddle-node, transcritical, pitchfork and Hopf bifurcations according to the changes in stability and types of equilibria. In normal form the corresponding families of ordinary differential equations can be presented as follows:

$$\dot{x} = \alpha - x^2 \text{ (saddle-node)}, \quad \dot{x} = \alpha x - x^2 \text{ (transcritical)}, \quad \dot{x} = \alpha x - x^3 \text{ (pitchfork)},$$

$$\text{in polar coordinates in } \mathbb{R}^2 : \ \dot{\theta} = c \neq 0, \quad \dot{r} = \alpha r - r^3 \text{ (Hopf)}.$$

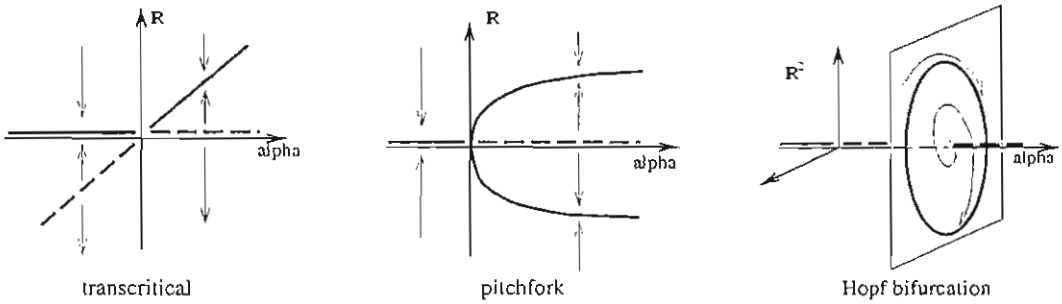

Figure 1: Bifurcation diagrams of above equations.

Moreover there exists a necessary condition for bifurcation: the linearized system has to become non-hyperbolic at the bifurcation point. For sufficient conditions the nonlinear part of the system has to be considered.

2 Random Dynamical Systems

In particular engineers often have to consider the situation that a system underlies a permanent influence of noise. Such a stochastic perturbation can have various effects on the system. A good way to describe such systems is the use of the concept *random dynamical systems* (RDS) (cf. Arnold [1]). It allows to embed stochastically perturbed systems in the standard theory of dynamical systems. Given a model for the noise in terms of a flow $(\vartheta_t)_{t\in\mathbb{R}}$ of measure-preserving transformations ϑ_t on a probability space $(\Omega, \mathcal{F}, \mathbb{P})$, the situation that a system evolves under this influence of $(\vartheta_t)_{t\in\mathbb{R}}$ on a phase space X can be described by a flow $(\Theta_t)_{t\in\mathbb{R}}$ on $\Omega\times X$ which due to the independence of the noise process on the dynamics on X should split as $\Theta_t(\omega, x) = (\vartheta_t\omega, \varphi(t,\omega)x)$. Because of this structure (Θ_t) is called a skew-product flow, while φ generates a cocyle, i.e. a mapping $(t,\omega,x)\mapsto\varphi(t,\omega)x$ satisfying $\varphi(t+s,\omega) = \varphi(t,\vartheta_s\omega)\circ\varphi(s,\omega)$. Of interest for the dynamics is only this cocyle φ and therefore it is also called a random dynamical system on X over $(\vartheta_t)_{t\in\mathbb{R}}$. While in the case of discrete time an RDS is given by applications of products of random mappings, for continuous time (which is the case we are considering exclusively here), there exist two ways to generate an RDS:

1. random differential equations $\dot{x} = f(\xi_t, x)$ representing the so-called *real noise* case, where (ξ_t) is a stationary stochastic process modelling noise,

2. (Stratonovich) stochastic differential equations $dx = f(x)dt+G(x)\circ dW$ representing the so-called *white noise* case, where W is standard Brownian motion.

Under rather mild conditions on the vector fields f the flow of such differential equations can be seen to define indeed a random dynamical system (cf. Arnold [1]). For the description of RDS invariant measures play a crucial role. These are probability measures on $\Omega\times X$ which are invariant under the skew product flow Θ and have marginal $\mathbb{P}$ on Ω in order to be in agreement with the noise model. Analogously to the dynamics one can also split the invariant measures into parts corresponding to realizations of the noise process, i.e. we can consider so called invariant random probability measures μ_ω, $\omega\in\Omega$ which are shifted in the same stationary way as the noise-trajectories, namely $\varphi(t,\omega)\mu_\omega = \mu_{\vartheta_\omega}$. These are the so-called disintegrations of the invariant measure μ.

We will be interested in one-parameter families of RDS corresponding to simple stochastic or random differential equations, in particular to noisy versions of the differential equations in normal form for bifurcations in dimension 1 and 2, and consider phenomena which could be called bifurcations.

3 Phenomenological Approach

The first main problem for stochastic bifurcation theory lies in the introduction of the right notion of structural stability. As orbits heavily underlie the influence of noise,

the concept of fixed or periodic points loses its importance and has to be replaced by a different one. An approach introduced by physicists (cf. Horsthemke and Lefever [5]) suggests to study in the white noise case qualitative changes on the level of invariant probability densities p_α. The latter are usually constructed as steady state solutions of the Fokker-Planck equation. They are in one-to-one correspondence with expectations $\mathbb{E}\mu_\omega$ of invariant random measures μ_ω, $\omega \in \Omega$ which are adapted to the past of the noise process.

Bifurcations can be associated with qualitative changes of the probability densities like transitions from one-peak to two-peak (see Fig. 2 below) to crater-like densities. Such

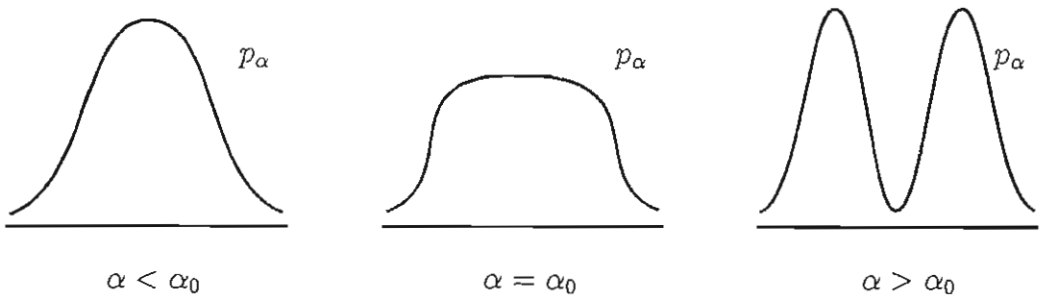

Figure 2: Qualitative change of probability densities

a bifurcation concept can be made rigorous, if we use an idea of Zeeman [7] and let structural stability for the stochastic systems be determined by smooth conjugation of the densities. The corresponding loss in structural stability is called a *phenomenological* or *P-bifurcation*.

This concept has the drawback to describe a static situation, as the invariant density measures the asymptotic proportion of time the system spends in a volume element. Also it does not pay any tribute to the stability of the system. Finally the concept of invariant probability densities is rather restrictive, as only Markovian situations can be considered and not all interesting and important dynamic phenomena are seized by such densities.

4 Dynamical Approach

For a description of structural stability taking care of dynamic aspects stationarity is the key to the solution of the problem. While in the deterministic situation stationarity can be expressed in terms of fixed or periodic points, in the stochastic situation this role is played by invariant measures in the sense above. For example, the random Dirac measure $\mu_\omega = \delta_{x(\omega)}$, where $x : \Omega \to X$ is a random variable, is the stochastic analogue of a fixed point in a deterministic system, if this measure is invariant, i.e. $\varphi(t,\omega)x(\omega) = x(\vartheta_t\omega)$.

Thus, if φ_α, $\alpha \in \mathbb{R}$ is a family of RDS with invariant measures μ_α, then $(\alpha_0, \mu_{\alpha_0})$ is called a *dynamical* or *D-bifurcation point*, if for each α in a neighbourhood of α_0 there exists a φ_α-invariant measure $\nu_\alpha \neq \mu_\alpha$ for which ν_α converges weakly to μ_{α_0} as α goes to α_0. So a dynamical bifurcation in random dynamical systems is associated with the appearance of new invariant measures.

This concept of bifurcation is much richer and closer to the one for deterministic systems. It is also possible to associate a stability notion with it. Namely for any invariant

measure μ_α the stability of the system φ_α can be characterized in terms of the Lyapuonv-exponents $\lambda_i(\mu_\alpha)$ for the linearization of φ_α, if multiplicative ergodic theory can be applied. Then a D-bifurcation is necessarily accompanied by the vanishing of a Lyapunov-exponent (see Arnold and Xu [2] which underlines that D-bifurcation is a concept concerning the dynamics of the system.

In the following we will demonstrate by two examples the applications of that concept and the differences between P- and D-bifurcations.

5 Stochastic Transcritical Bifurcation

The white noise version of the normal form for transcritical bifurcations is given by

$$dx = (\alpha x - x^2)dt + \sigma x \circ dW$$

where $\alpha \in \mathbb{R}$ and $\sigma > 0$. This stochastic differential equation can be explicitly solved to give a family of RDS φ_α

$$x \mapsto \varphi_\alpha(t,\omega)x = \frac{x \exp(\alpha t + \sigma W_t)}{1 + x \int_0^t \exp(\alpha s + \sigma W_s) ds}$$

with the only invariant measures given by

1. $\mu_\alpha = \delta_0$ for all $\alpha \in \mathbb{R}$,
2. $\nu_{\alpha,\omega} = \delta_{\kappa_\alpha(\omega)}$ with $\kappa_\alpha(\omega) = -(\int_0^\infty \exp(\alpha s + \sigma W_s) ds)^{-1}$ for $\alpha < 0$,
3. $\nu_{\alpha,\omega} = \delta_{\kappa_\alpha(\omega)}$ with $\kappa_\alpha(\omega) = (\int_{-\infty}^0 \exp(\alpha s + \sigma W_s) ds)^{-1}$ for $\alpha > 0$,

while the only invariant probability densities are given by

1. $p_\alpha = \delta_0$ for all $\alpha \in \mathbb{R}$,
2. $q_\alpha(x) = N_\alpha x^{\frac{2\alpha}{\sigma^2}-1} \exp(-\frac{2x}{\sigma^2})$ for $x > 0$ with a normalizing factor N_α and $q_\alpha(x) = 0$ for $x = 0$ provided $\alpha > 0$.

As $\lambda(\mu_\alpha) = \alpha$ and $\lambda(\nu_\alpha) = -\alpha$, we can conclude that a D-bifurcation takes place at $\alpha_0 = 0$. where the invariant measures exchange their stability. Thus we obtain the same bifurcation diagram as in the deterministic case (see Fig. 1), if we replace fixed points by invariant measures in that diagram. It is also easy to see that the density q_α undergoes a qualitative change at $\alpha = \sigma^2/2$ so that we have a P-bifurcation point at this parameter value. It was shown by Baxendale [3] that this point is characterized as a large deviations phenomenon in contrast to the stability phenomenon at the D-bifurcation point.

6 Stochastic Hopf Bifurcation

A far more difficult problem than the stochastic bifurcations in dimensions 1 presents the Hopf-bifurcation for stochastic systems. At the moment there does not exist a complete mathematical description of this phenomenon, though there exist extensive simulations which give us a very good impression of what seems to happen. We will try to illustrate

this by the example of the noisy Duffing-van der Pol oscillator (for a presentation of various bifurcation scenarios in this system see Schenk [6])given by

$$\begin{aligned} \dot{x}_1 &= x_2 \\ \dot{x}_2 &= (\alpha + \sigma\xi_t)x_1 + \beta x_2 - x_1^3 - x_1^2 x_2 \end{aligned}$$

where (ξ_t) denotes a real or white noise process and α, β present two bifurcation parameters. It is known that the deterministic system obtained for $\sigma = 0$ and $\alpha < 0$ held constant undergoes a Hopf bifurcation at $\beta = 0$. In the stochastic case $\sigma > 0$ simulations of the solution of the Fokker-Planck equation yielding invariant densities suggest the following P-bifurcation scenario (cf. Ebeling et al. [4]): there is a probability density q_β which arises at some $\beta_1 < 0$ which undergoes a P-bifurcation at $\beta = \beta_P$ to get the structure of a crater.

In order to draw a picture of the respective D-bifurcation scenario exhaustive simulations of invariant measures μ_ω are necessary. They lead us to believe in the following:

1. While in the deterministic case one finds for $\beta = 0$ a pair of complex-conjugate eigenvalues for the linearization, the respective Lyapunov-exponents $\lambda_1(0)$ and $\lambda_2(0)$ are different, i.e. noise splits the pair of complex conjugate eigenvalues. This is only possible with $\lambda_2(0) < 0 < \lambda_1(0)$ and if there exists $\beta_1 < 0$ with $\lambda_1(\beta_1) = 0$ so that a first D-bifurcation occurs earlier than in the deterministic case.

2. At β_1 the top Lyapunov-exponent $\lambda_1(\beta_1)$ vanishes and we have a first D-bifurcation from the stable Dirac-measure δ_0 to a stable measure $\nu^{(1)}_{\beta,\omega} = \frac{1}{2}(\delta_{x^{(1)}(\omega)} + \delta_{-x^{(1)}(\omega)})$ which is a convex combination of two Dirac measures and is the boundary of the unstable manifold of the saddle point $x = 0$.

3. At $\beta_2 > \beta_1$ the second Lyapunov-exponent $\lambda_2(\beta_2)$ vanishes and a second D-bifurcation from δ_0 takes place. A new measure $\nu^{(2)}_{\beta,\omega} = \frac{1}{2}(\delta_{x^{(2)}(\omega)} + \delta_{-x^{(2)}(\omega)})$ arises which is again a convex combination of two Dirac measures which correspond to random saddle points, while δ_0 has become unstable. The stable measure $\nu^{(1)}_{\beta,\omega}$ is the boundary of the unstable manifold corresponding to $\nu^{(2)}_{\beta,\omega}$. Both measures sit on an invariant random limit cycle which is stable and where the dynamics are hyperbolic.

These observations underline that P-bifurcation description only seize one part of the phenomenon, but leaves out the dynamical part (here the dynamics of the invariant circle). In the bifurcation diagram below we have put together P- and D-bifurcation scenarios obtained numerically.

References

[1] Arnold, L. [1995] *Six lectures on random dynamical systems*, Dynamical Systems (ed. Johnson, R.), Lecture Notes in Mathematics 1609, Springer-Verlag, Berlin *pp. 1-43.*

[2] Arnold, L. & Xu Kedai [1994] "Invariant measures for random dynamical systems, and a necessary condition for stochastic bifurcation from a fixed point", *Random & Computational Dynamics* 2, 165–182.

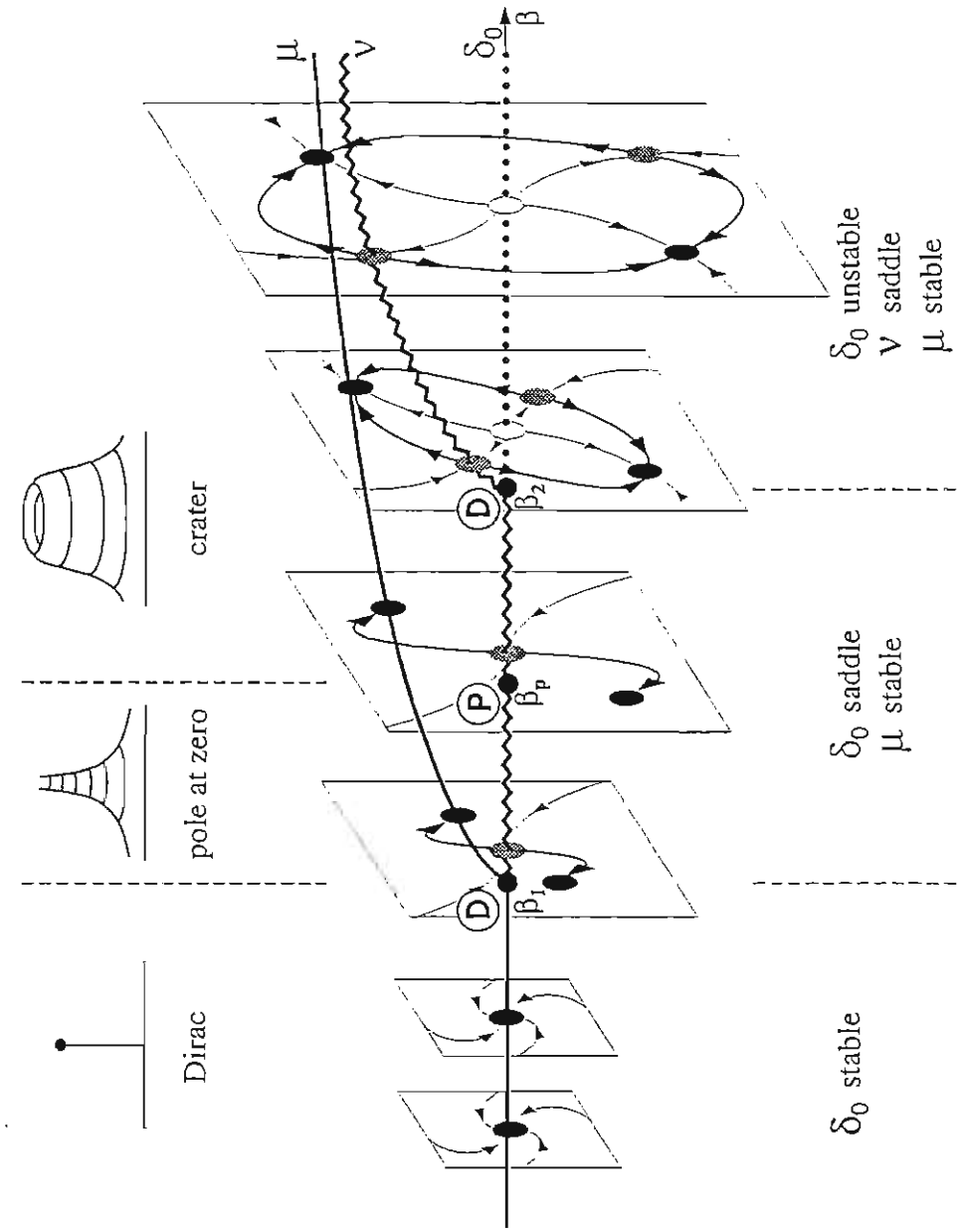

[3] Baxendale, P. [1994] "A stochastic Hopf bifurcation", *Probability Theory and Related Fields* 99, 581–616.

[4] Ebeling, W. & Herzel, H. & Richtert, W. & Schimansky-Geier, L. [1986] "Influence of noise on Duffing-Van der Pol oscillators", *Zeitschrift f. Angew. Math. u. Mechanik* 66, 141–146.

[5] Horsthemke, W. & Lefever, R. [1984] *Noise-induced transitions* Springer-Verlag, Berlin, Heidelberg, New York.

[6] Schenk–Hoppé, K.R. [1996] "Bifurcation scenarios of the noisy Duffing-van der Pol oscillator", *Nonlinear Dynamics* to appear.

[7] Zeeman, E.C. [1988] "Stability of dynamical systems", *Nonlinearity* 1, 115–155.

SPECTRAL PROPERTIES OF QUANTUM SYSTEMS UNDER CONDITIONS OF CHAOS

Marek Kuś

Center for Theoretical Physics, Polish Academy of Sciences, Warsaw, Poland

Abstract: Spectral properties of quantum systems which are chaotic in the classical limit are discussed. Theoretical predictions are confronted with results of experiments involving "macroscopic" models of quantum chaotic systems - microwave billiards.

1. Introduction

The quantitative distinction between regular and chaotic motion in classical mechanics uses extensively phase-space concepts, as it is best exemplified by the definition of Lyapunov exponent [Lichtenberg & Lieberman, 1992]. The strength of chaos in the system is characterized by its sensitivity to changes of initial conditions, i.e. the rate of temporal divergence of neighboring phase-space trajectories.

The straightforward translation of such concepts into the field of quantum systems is not possible due to the lack of the notion of the phase space in quantum mechanics. In the most obvious approach we could consider two initial wavefunctions $\psi(0)$ and $\phi(0)$ and try to measure the sensitivity to initial conditions by the fate of their overlap $d_q(t) := \langle\phi(t)|\psi(t)\rangle$. The overlap, however, remains constant in time due to the unitarity of the quantum evolution.

The above argument does not imply that in quantum mechanics the distinction between chaotic and regular evolution in not possible. It seems natural to try to differentiate between regular and chaotic motion using the most obvious quantum mechanical features of quantum systems, namely their spectral properties. Let us thus consider a quantum system with a well defined classical limit. Is it possible to predict whether the corresponding classical evolution is regular or chaotic by investigating simple features of the quantum spectrum of the system ?

It should be in fact not very astonishing that quantum systems share some of their spectral properties with other types of physical phenomena which can be described in terms of waves. In the last part of my talk I will describe some recent experiments in which some simple quantum mechanical chaotic systems are modeled by electromagnetic resonators.

2. Statistical Properties of Spectra

Intuitively we expect that spectra of systems which are chaotic on the quantum level should be "more complicated" then those of systems which are classically fully integrable. Closer examination of known solvable quantum problems reveals that, among systems which have classical counterparts, only for these, which are classically integrable we are able to find analytically their (energy) spectra. For all other systems we must invoke various perturbation techniques or numerical methods. As an obvious example we may consider quantum systems with many degrees of freedom like heavy atomic nuclei. For such systems the alternative method of description was proposed many years ago by Wigner [1951]. Borrowing ideas from classical statistical physics we embed their Hamiltonians in an statistical ensemble of random matrices, sharing only general features (like the total spin and the time reversal symmetry) with the system in question [Mehta, 1967]. Obviously the method does not allow us to find the spectrum, nevertheless it gives astonishingly good predictions concerning various *statistical* properties of energy levels. The perhaps most celebrated of such statistical characteristics is the probability density $P(s)$ of finding two neighboring energy level at the distance s one from the other on the energy scale. The Random Matrix Theory (RMT) predicts, for small s, $P(s) \sim s^{\beta}$, with the exponent β depending on the symmetries and spin of the system. The result can be interpreted as tendency of energy levels of "complicated" systems to repel each other, revealing strong correlations between individual levels. As mentioned, the strength of repelling measured by the exponent β depends on symmetries of the system, with the most important distinction between systems invariant under time reversal with $\beta = 1$ and those which do not possess time reversal symmetry for which $\beta = 2$ (in the simplest case of absence of spatial symmetries and integer spin).

It was a fruitful idea of Bohigas, Giannoni, and Schmit [1984] and Berry & Tabor [1977] to use RMT in order to find criteria discriminating between classically regular and chaotic dynamics on the quantum level. They conjectured that, like systems with many degrees of freedom, classically chaotic systems are characterized by the repulsion of levels. On the other hand, spectra of classically regular ones reveal no correlations which results in level clustering: $P(s) \sim \exp(-s)$. The conjecture has been since then supported by overwhelming numerical and empirical evidence.

The interesting ideas aiming at giving the Bohigas-Giannoni-Schmit conjecture somewhat more firm ground were developed by Pechukas [1983] and Yukawa [1985, 1986]. They consider a quantum evolution described by a parameter dependent Hamiltonian $H(\lambda) = H_0 + \lambda V$. We should think about H_0 as corresponding to a classically regular part and V as a integrability breaking perturbation, strength of which is controlled by the parameter λ. Now we can ask about the fate of the energy eigenvalues $q_n(\lambda)$ of $H(\lambda)$ when the parameter λ is changed. After a short calculation we find a nonlinear set of equations connecting the rates of change of the eigenvalues to various matrix elements of the perturbation V in the eigenbasis of $H(\lambda)$, namely $p_n(\lambda) := \langle\psi_n(\lambda)|V|\psi_n(\lambda)\rangle$ and

The resulting equations can be interpreted as describing the (Hamiltonian) dynamics of a one-dimensional gas of interacting particles with the eigenvalues q_n playing the roles of positions of particles an λ a fictitious time. The stationary canonical distribution gives then, to our satisfaction, results which are in complete agreement with predictions of RMT (also concerning the influence of symmetries) [Kuś *et al.*, 1987; Haake, 1991;].

This rather rough reasoning can be refined to be treated more seriously. [Kuś, 1988; Haake, 1991; Mnich, 1993; Dietz, 1994]. It can also be extended to the case of quantum systems which are periodically time-dependent or (what will be important in the next part of my lecture) dissipative [Huckleberry *et al.*, 1996].

3.Microwave Billiards as Testing Ground for Random Matrix Theory

Although experiments involving genuine quantum systems are of the main interest in support of conjectures I invoked in the previous sections, it is amusing to observe in macroscopic settings some of the intriguing properties characteristic for quantum chaotic systems.

First let me recall a paradigmatic example studied in classical dynamical systems, namely this of a planar billiard. A billiard is a connected region of a plane surrounded by impenetrable walls. A particle moves freely inside the region and bounces elastically from the walls respecting the classical laws of reflection.

It is known that integrability properties of billiards are determined by their shapes. In the most simple case of a rectangular billiard the evolution is fully integrable, whereas for more complicated shapes (e.g. the Sinai billiard i.e. a rectangular billiard with a circular hole inside - see Fig. 1a) can enjoy a fully chaotic motion.

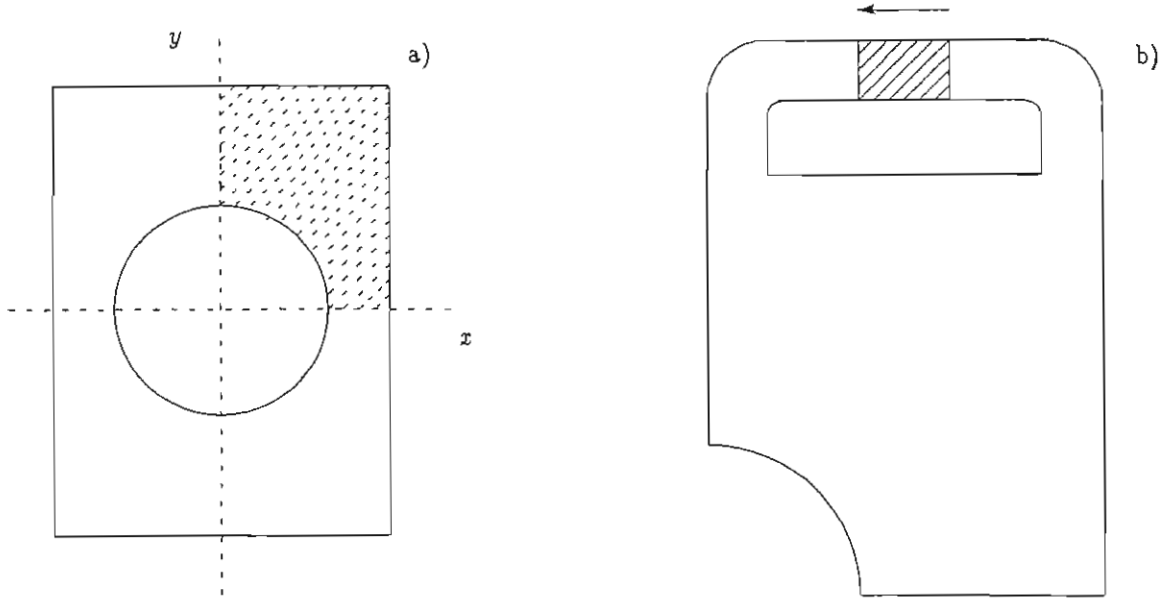

Figure 1: a) Chaotic Sinai billiard. In order to eliminate the obvious reflection symmetries with respect to the axis x and y we restrict the motion to one quarter of the full billiard (shaded area). b) Microwave resonator in the form of the Sinai billiard with an attached one-way waveguide breaking the time reversal invariance of the system.

The corresponding quantum problem is described by the free Schrödinger equation with appropriate boundary conditions

$$-\frac{\hbar^2}{2m}\left(\frac{\partial^2}{\partial x^2}+\frac{\partial^2}{\partial y^2}\right)\psi(x,y)=E\psi(x,y), \quad \psi|_S=0, \tag{1}$$

where S denotes the boundary of the billiard.

Consider now a quasi-two-dimensional metallic resonator of the shape of the billiard. The quasi-two-dimensionality means that the vertical dimension (the height) of the resonator is small enough. In the resonator we excite standing electromagnetic waves by injecting a microwave field through an attached waveguide. If the height of the resonator is smaller than the half wavelength of the microwaves we use in our experiment, only the ground modes in the vertical direction can be excited. The electromagnetic field in the resonator can be in this case described by a single scalar function $\phi(x,y)$ (proportional to the vertical component of the electric field) fulfilling the Helmholtz equation

$$\left(\frac{\partial^2}{\partial x^2}+\frac{\partial^2}{\partial y^2}\right)\phi(x,y)+k^2\phi(x,y)=0, \tag{2}$$

which should be supplemented by the known boundary conditions, $\phi|_S=0$, at a metallic boundary . It is thus obvious, that the quantum problem (1) and the electromagnetic one (2) are exactly equivalent after appropriate scaling of the variables.

The experiment consists thus of injecting microwaves to the resonator and observing at which frequencies of the incident field the electromagnetic field inside is excited, revealing

thus the eigen-frequencies of the boundary-value problem (2). Such experiments were performed by Stöckmann and Stein [1990] and, indeed, a clear distinction between the integrable (rectangular) and non-integrable (Sinai) billiards was observed. The measured eigen-frequencies of the first resonator tend to cluster together whereas in the second case linear repulsion (i.e. $P(s) \sim s$) was noticed.

As already mentioned the strength of repulsion between neighboring levels is changed to a quadratic one ($P(s) \sim s^2$) when the time reversal symmetry is broken. To observe it the chaotic microwave resonator was modified by attaching a so-called microwave isolator in the form of a one-directional waveguide as indicated in Fig. 1b [Stoffregen *et al.*, 1995].

In the ideal situation, such a one-way device should transmit perfectly microwaves propagating in one direction and absorb ones going in the opposite direction. The fact that energy is absorbed by the system invalidates the previous approach which uses the Helmholtz equation (2). Instead we can describe the system in terms of scattering theory (treating the waveguide through which microwaves enter the system as an incoming channel and the antenna which we use to measure the field inside the resonator as an outgoing one). The resonant eigenmodes of the resonator can be then characterized by their frequencies and lifetimes (which are finite due to the energy dissipation). As long as the lifetimes are long we can resolve individual resonant frequencies and measure their tendency to cluster or repel each other. It is intuitively obvious, and also easy to show, that unidirectionality of the attached waveguide leads to the breaking of the time reversal invariance of the system [Stoffregen *et al.*, 1995]. The careful analysis of the scattering process reveals that we should then really expect the nonlinear repulsion between eigenvalues [Haake *et al.*, 1996; Albeverio *et al.*, 1996]. These findings were fully confirmed by experiments [Stoffregen *et al.*, 1995].

References

Albeverio, S., Haake, F., Kurasov, P., Kuś, M. & Šeba, P. [1996] "S-matrix, resonances, wavefunctions for microwave transport through billiards with leads", *J. Math. Phys.* , in print.

Berry, M. V. & Tabor, M. [1977] "Level clustering in the regular spectrum", *Proc. Roy. Soc. A* **356**, 375.

Bohigas, O., Giannoni, M. J. & C. Schmit [1984] "Characterization of quantum spectra

and universality of level fluctuations law", *Phys. Rev. Lett.* **52**, 1.

Dietz, B. [1994] "Random matrix theory and equilibrium statistics for the quasienergies of classically chaotic systems", *Z. Phys. B* **96**, 271.

Haake, F. [1991] *Quantum Signatures of Chaos* (Springer, Berlin).

Haake, F., Kuś, M., Šeba, P., Stöckmann, H.-J. & Stoffregen, U. [1996]"Microwave billiards with broken time reversal invariance", *J. Phys. A*, in print.

Huckleberry, A. T., Zaitsev, D., Haake, F., & Kuś, M. [1996] "Reduction of symmetry and molified microcanonical ensembles", *to be published*, 1996.

Kuś, M., Haake, F., & Scharf, R. [1987] "Symmetry versus degree of level repulsion for kicked quantum systems", *Z. Phys. B* **66**, 129.

Kuś, M "Dynamics and statistics of quasi-energy levels for kicked quantum systems", *Europhys. Lett.* **5**, 1, 1988.

Lichtenberg, A. J. & Lieberman,M. A. [1992] *Regular and Chaotic Dynamics* (Springer, New York).

Mehta, M. L. [1967] *Random Matrices and the Statistical Theory of Energy Levels* (Academic Press, New York) 1967.

Mnich, K. [1993] "A complete set of constants of motion for the generalized Sutherland-Moser system", *Phys. Lett. A* **176**, 189.

P. Pechukas, P. [1983] "Distribution of energy levels in the irregular spectrum", *Phys. Rev. Lett.* **51**, 943.

Stöckmann, H.-J. & Stein, J. [1990] " "Quantum" chaos in billiards with broken time reversal symmetry", *Phys. Rev. Lett.* **64**, 2215.

Stoffregen, U., Stein, J., Stöckmann, H.-J., Kuś, M. & Haake, F. [1995] "Microwave billiards with broken time reversal symmetry", *Phys. Rev. Lett.* **74**, 2666.

Wigner, E. P. "On the statistical distribution of the widths and spacing of nuclear resonance levels", *Proc. Cambridge Phil. Soc.* **47**, 790.

Yukawa, T. [1985] "New approach to the statistical properties of energy levels", *Phys. Rev. Lett.* **54**, 1883.

Yukawa, T. [1986] "Lax form of the quantum mechanical eigenvalue problem", *Phys. Lett. A* **116**, 227.

Turbulence and Coherent Structures in Subsonic Jets. Control of the Turbulence

P. S. Landa
Department of Physics, Moscow State University
Moscow 119899, Russia

Abstract

The onset of turbulence and formation of large scale patterns (coherent structures) in subsonic jets is considered from oscillation theoretical standpoint. It is hypothesized that these phenomena are results of a noise-induced nonequilibrium phase transition of the second kind. It is shown by the example of noise-induced oscillations of a pendulum with a randomly vibrating suspension axis that such a transition can be controlled by an additional harmonic action. The known possibility of notable attenuation or intensification of turbulence in jets by means of a slight acoustic action at one or another frequency can be attributable to such control.

It is known that because of the Kelvin–Helmholtz instability hydrodynamic waves are excited and amplified in the jet's boundary layer. These waves can propagate only downstream with a velocity of order of the flow velocity. The distinctive feature of hydrodynamic waves is their random character. Nevertheless, against the background of this randomness there are comparatively regular large scale patterns (the concentrations of vorticity) called *coherent structures*.

Excitation of coherent structures, as noted above, is caused by the Kelvin–Helmholtz instability, but in their formation nonlinear effects play a dominant role. This is associated with the fact that in jet flows there is non-linear feedback resulting in the occurrence of the so called *pairing* of vortices observed experimentally in the jet's mixing layer (see, for example, [Vlasov & Ginevsky, 1986]).

Today there is an extensive literature devoted to the instability of the boundary layer of jets and wakes resulting in their turbulization and in the formation of large-scale coherent structures (see, e.g., [Michalke, 1984; Vlasov & Ginevsky, 1986]). The theory of these phenomena is based mainly on views fully formed in response to either direct numerical simulation or simulation by the so called *discrete vortex technique* [Belotserkovsky & Ginevsky, 1995]. When the latter is used it is assumed that vortices are already formed, and only their interaction is considered. The problem of vortex excitation in itself is studied in a very small number of works. Among them the first work carried out by Rayleigh as early as 1879 [Rayleigh, 1879] should be noted. In the last three tens of

years these problems were studied primarily by Michalke, Crighton, Gaster, and Plaschko (see, for example, [Crighton & Gaster, 1976; Michalke, 1984; Plaschko, 1979]). In these works a profile of the mean flow velocity was given and the linearized Euler equations for deviations were approximately solved. Because the coefficients of these equations depend on the coordinates, an exact analytical solution cannot be obtained. Numerical calculations performed by the authors indicated above are in reasonably good agreement with experimental data.

Issuing from a nozzle, a fluid jet always noticeably diverges. This is associated with the fact that owing to viscosity increasingly more neighboring fluid layers are involved in the motion. The profile of mean flow velocity changes essentially in the process. At the nozzle exit it is near rectangular, whereas away from the nozzle it becomes bell-shaped, see Fig. 1. The fluid layer within which the mean velocity changes significantly is called

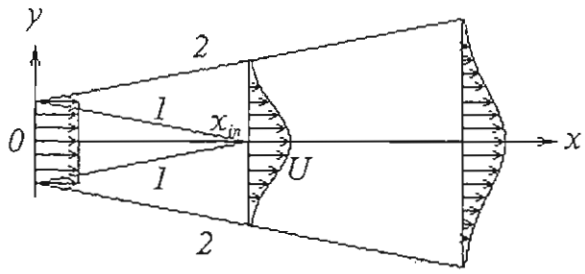

Figure 1: Schematic image of a free jet illustrating change of its mean velocity profile and widening the mixing layer. The curves labelled 1 and 2 correspond to internal and external boundaries of the mixing layer respectively.

the boundary layer or *the mixing layer*. It is interesting that the coherent structures are formed just in this layer. It is seen from Fig. 1 that the mixing layer's thickness increases approximately linearly with distance from the nozzle. At a certain distance away from the nozzle $x = x_{\text{in}}$ the thickness of the internal part of the mixing layer δ_1 becomes equal to the half-width of the nozzle's outlet for a plane jet or the nozzle's radius for a circular jet, whereupon a continuous boundary layer is formed. The jet's part for $x \leq x_{\text{in}}$ called *the initial part*.

Owing to its strong instability a fluid jet is an amplifier with a sufficiently high spatial gain factor [Landa, 1996]. A small acoustic disturbance at some frequency f_a lying in the region of resonance, being given near the nozzle, turns into an amplifying hydrodynamic wave. This is evidenced by experimental results of Crow and Champagne [1971]. It follows from these results that, from a certain value of the acoustic wave amplitude onward, the dependence of the relative root-mean-square pulsation of the longitudinal component of the hydrodynamic velocity $\epsilon_u =< u^2 >^{1/2} /U_0$ on the acoustic wave frequency f_a, measured in terms of Strouhal numbers $\mathrm{St} = f_a D/U_0$, where D is the nozzle's diameter and U_0 is the mean fluid velocity on the jet axis, turns out to be resonant. For $\epsilon_{ua} =< u_a^2 >^{1/2} /U_0 = 0.02$, where u_a is the acoustic velocity, this dependence is shown in Fig. 2 *a*.

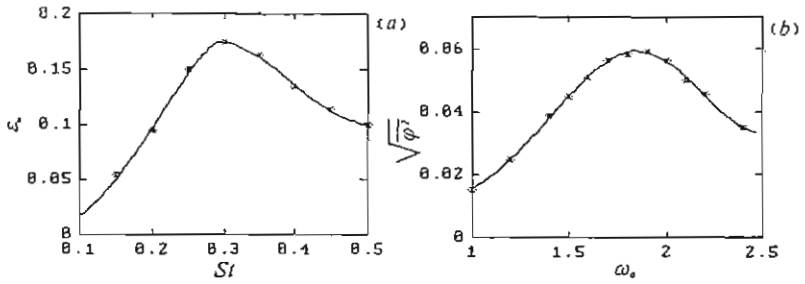

Figure 2: (a) The dependence of ϵ_u on St for $\epsilon_{ua} = 0.02$, $x/D = 4$, where x is the distance from the jet nozzle, D is the nozzle's diameter; (b) the dependence of $\overline{\varphi^2}^{1/2}$ on ω_a for $a = 0.5$. When the additional disturbance is absent, $\epsilon_u \approx 0.04$ and $\overline{\varphi^2}^{1/2} \approx 0.0317$.

We see that ϵ_u is maximal for St ≈ 0.3.

One of the interesting manifestations of nonlinear effects in a jet is the possibility of notable attenuation or intensification of hydrodynamic waves by a slight acoustic action at one or another frequency. The attenuation of hydrodynamic pulsations occurs if the frequency of the acoustic action is rather high, whereas the intensification occurs if the frequency of the acoustic action is rather low. The experimental dependence of the relative root-mean-square pulsation of the longitudinal component of the hydrodynamic velocity $\widetilde{\epsilon}_u$ on the acoustic pressure for St $= 2.35$ is shown in Fig. 3 a. We see that the turbulent pulsations first decrease as the amplitude of acoustic wave increases and then they increase.

As for the reasons of the appearance of turbulence and coherent structures in a jet, we hold to the idea that this appearance is caused by a noise-induced phase transition. Such transitions are known for certain systems (see, for example, [Van den Broeck et al., 1994]. A simple example is excitation of oscillations of a pendulum with a randomly vibrating suspension axis [Landa & Zaikin, 1996]. Surprisingly, this process has much in common with turbulent processes.

We studied, both analytically and numerically, the following equation:

$$\ddot{\varphi} + 2\beta\left(1 + \alpha\dot{\varphi}^2\right)\dot{\varphi} + \omega_0^2\left(1 + \xi(t)\right)\sin\varphi = 0, \qquad (1)$$

where φ is the pendulum's angular deviation from the equilibrium position, $2\beta\left(1 + \alpha\dot{\varphi}^2\right)\dot{\varphi}$ is the value proportional to the moment of the friction force which is assumed to be nonlinear, ω_0 is the natural frequency of small pendulum's oscillations, and $\xi(t)$ is the acceleration of the suspension axis that is assumed to be a comparatively wide-band random process with nonzero power spectrum density at the frequency $2\omega_0$.

When the intensity of the suspension axis vibration is in excess of a certain critical value proportional to the friction factor β, the excitation of pendulum's oscillations occurs that makes itself evident in the fact that the variance of the pendulum's angular deviation becomes nonzero. It follows from the results obtained that close to the excita-

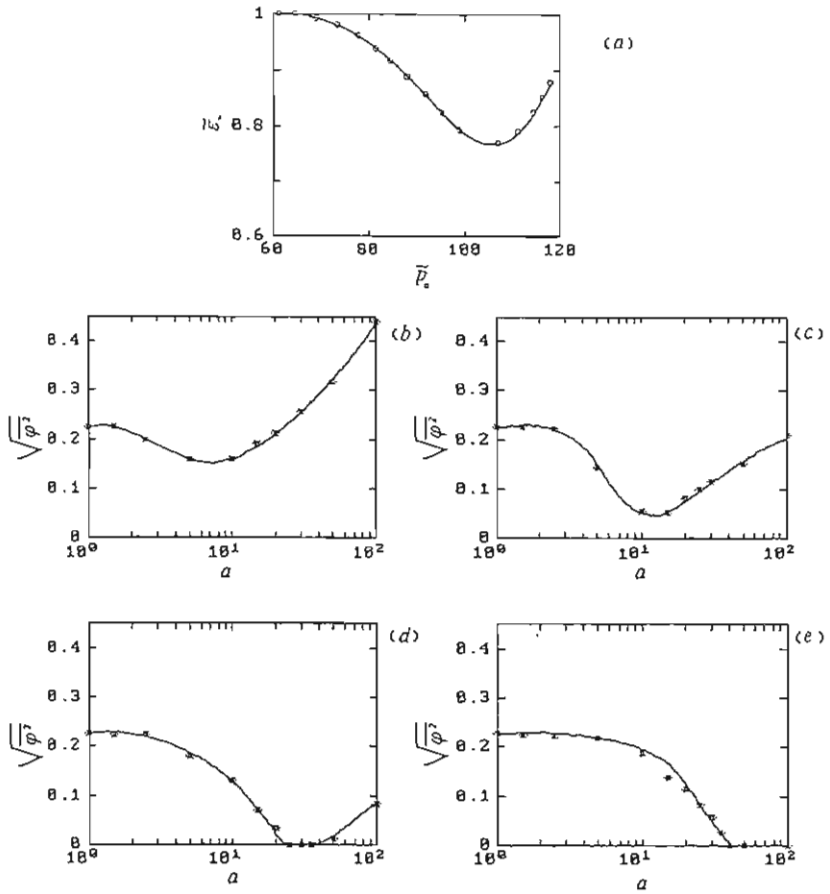

Figure 3: (a) The experimental dependence of $\tilde{\epsilon}_u$ on the relative amplitude of acoustic pressure $\tilde{p}_a$ measured in decibels for St $= 2.35$, $x/D = 8$; the dependencies of $\overline{\varphi^2}^{1/2}$ on a for $\omega_0 = 1$, $\beta = 0.1$, $\alpha = 100$, $\kappa(2)/\kappa_{cr}(2) = 5.6$, ($b$) $\omega_a = 3.5$, (c) $\omega_a = 6$, (d) $\omega_a = 11$, (e) $\omega_a = 19.75$.

tion threshold the pendulum's oscillations possess the property of intermittency, i.e. over prolonged periods the pendulum oscillates in the immediate vicinity of its equilibrium position (so called 'laminar' phases); these slight oscillations alternate with short splashes ('turbulent' phases). Away from the threshold the duration of laminar phases decreases and of turbulent increases, and laminar phases ultimately disappear. The variance of the pendulum's angular deviation increases in the process. We emphasize that turbulence for transient Reynolds numbers exhibit also this property. It is no chance that the first theoretical works concerning the intermittency phenomenon were made by the specialists in the field of turbulence [Pomeau & Manneville, 1980].

If the intensity of the suspension axis random vibration is under its threshold value then the excitation of pendulum's oscillations can be initiated by small additional low-frequency vibration of the suspension axis. The inclusion of this vibration can be carried out by substitution into Eq. (1) of $\xi + a\cos\omega_a t$ in place of ξ, where a and ω_a are, respectively, the amplitude and frequency of the additional vibration of the suspension axis. The results of numerical simulation of Eq. (1) for different values of a are represented

in Fig 4 *a*. We see that the excitation of oscillations, as the amplitude a increases,

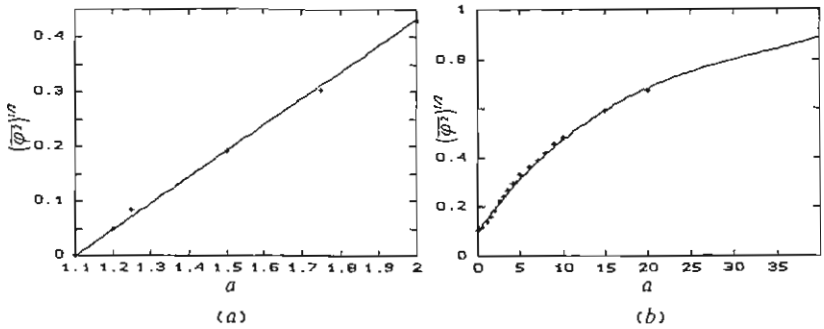

Figure 4: The dependence of $\overline{\varphi^2}^{1/2}$ on a for $\omega_0 = 1$, $\beta = 0.1$, $\alpha = 100$, (a) $\kappa(2)/\kappa_{cr}(2) = 0.51$, $\omega_a = 0.318$ (the straight line $\overline{\varphi^2}^{1/2} = 0.48(a - 1.1)$ is shown as a solid line), (b) $\kappa(2)/\kappa_{cr}(2) = 2.23$, $\omega_a = 1.5$.

is of a threshold character. For $\omega_a = 0.318$ the threshold value of a is equal to 1.1. The dependence of $\sqrt{\overline{\varphi^2}}$ on the difference between the amplitude a and its threshold value is found to be approximately linear. For $a > a_{cr}$ the oscillations excited are not distinguished from those excited due to random vibration only. The oscillation intensity is the greater, the larger a. By this is meant that the low-frequency vibration initiates the noise-induced phase transition and the birth of the induced attractor. If for $a = 0$ noise-induced pendulum's oscillations exist then low-frequency vibration intensifies these oscillations. An example of such intensification is shown in Fig. 4 *b*.

Now let us consider a possibility of depressing noise-induced pendulum's oscillations by high-frequency harmonic action. Numerical simulation of Eq. (1) with $\xi + a\cos\omega_a t$ in place of ξ, where $\omega_a > 2$, shows that such depression do occur. The results of the simulation are represented in Fig. 3 *b, c, d, e*. It is seen from these figures that, for small amplitudes of the high-frequency action, this action has little or no effect on the noise-induced oscillations existing. As the amplitude increases the intensity of the noise-induced oscillations decreases to a certain minimal value which is the smaller the larger is the action frequency. True, this minimal value is attained for the larger action amplitudes the higher is the frequency. For sufficiently high frequencies the oscillations can be depressed entirely.

So, we have shown that the profound parallels between such seemingly dissimilar phenomena as turbulence in jets and noise-induced pendulum's oscillations exist. It is of interest that these parallels are founded not on the similarity of equations of motion but on the generality of laws of oscillation theory. Undoubtedly, additional grave investigations must be called on to be sure that these parallels are not illusory, but they adequately depict the essence of the phenomena. Nevertheless, the mere presence of such the parallels reinforce once again the known fact that the nature obeys unified laws. These unified laws fall just into the subject of such universal science as oscillation theory.

References

Vlasov, Ye.V. & Ginevsky, A.S. [1986] "Coherent structures in turbulent jets and wakes", in *VINITI AN SSSR, Itogi Nauki i Tekhniki, Mekhanika Zhidkosti i Gasa*, 20, pp. 3–84 (in Russian).

Michalke A. [1984] "Survey on jet instability theory", *Progr. Aerosp. Sci.*, 21(3), 159–199.

Belotserkovsky, S.M. & Ginevsky, A.S. [1995] *Simulation of Turbulent Jets and Wakes by Discrete Vortex Technique* (Nauka, Moscow) (in Russian).

Rayleigh (Strutt, J.W.) [1879] "On the instability of jets", *Proc. London Math. Soc.*, 10, 4–13.

Crighton, D.G. & Gaster, M. [1976] "Stability of slowly diverging jet flow", *J. Fluid Mech.*, 77, 397–413.

Plaschko, P. [1979] "Helical instabilities of slowly diverging jets", *J. Fluid Mech.*, 92, 209–215.

Landa, P.S. [1996] *Nonlinear Oscillations and Waves in Dynamical Systems* (Kluwer Academic Publishers, Dordrecht–Boston).

Crow, S.C. & Champagne, F.H. [1971] "Orderly structure in jet turbulence", *J.Fluid Mech.*, 48, 547–591.

Van den Broeck, C. et al. [1994] "Noise-induced nonequilibrium phase transition", *Phys. Rev. Lett.*, 73(25), 3395–3398.

Landa, P.S & Zaikin, A.A. [1996] "Noise-induced phase transitions in a pendulum with a randomly vibrating suspension axis" (submitted in Phys. Rev. E).

Pomeau, Y. & Manneville, P. [1980] "Intermittent transition to turbulence in dissipative dynamical systems" *Comm. Math. Phys.*, 74(2), 189–197.

MARKOV OPERATORS AND FRACTALS

A. Lasota
Institute of Mathematics, Silesian University,
Bankowa 14, 40-007 Katowice, Poland

J. Myjak
Dipartimento di Matematica Pura ed Applicata
Università di L'Aquila, via Vetoio, 67100 L'Aquila, Italy

Abstract: We adjoin to an arbitrary Markov–Feller operator P a function Γ which maps closed sets into closed sets. This function has many properties of an iterated function system. In particular the iterates $\Gamma^n(A)$ converge (under appropriate assumptions) to the support of a measure invariant with respect to P.

1. Introduction

Iterated function systems allow one to construct fractals in two different ways. Namely, fractal can be obtained as the limit of a sequence of sets or as the support of an invariant measure. The second approach is strongly related to the theory of Markov operators and gives better analytical possibilities. However, even if a Markov operator P is asymptotically stable and for every choice of the initial measure μ the sequence $(P^n\mu)$ converges to a unique invariant measure μ_*, the corresponding sequence of supports (supp $P^n\mu$) need not converge to the support of μ_*.

To study this problem we introduce the notion of condensing Markov operators. For these operators the convergene of the sequence $(P^n\mu)$ implies the convergence of supports. We also show that the classical operators appearing in the fractal theory (Barnsley [1988]) are condensing.

2. Limiting properties of supports

Let (X, ϱ) be a metric space. In what follows we assume that X is separable and this assumption will not be repeated in the statements of theorems. By $K(x, r)$ we denote the closed ball with center x and radius r. For a subset A of X, cl$A$ stands for the closure of A. By $\mathcal{F}_0$ we denote the space of all closed subsets of X.

Let (A_n), $n = 0, 1, \ldots$, be a sequence of subsets of X. We define the *lower bound* LiA_n and the *upper bound* LsA_n by the following conditions. A point x belongs to LiA_n

if for every $\varepsilon > 0$ there is an integer n_0 such that

$$A_n \cap K(x, \varepsilon) \neq \emptyset \tag{2.1}$$

for $n \geq n_0$. A point x belongs to $\mathrm{Ls}A_n$ if condition (2.1) is satisfied for infinitely many n. Finally, if $\mathrm{Li}A_n = \mathrm{Ls}A_n$ we say that the sequence (A_n) is convergent and we denote the set $\mathrm{Li}A_n = \mathrm{Ls}A_n$ by $\mathrm{Lt}A_n$. It is called the *topological limit* of the sequence A_n.

By $\mathcal{B}_X$ we denote the σ–algebra of Borel subsets of X and by $\mathcal{M}$ the family of all finite Borel measures (nonnegative, σ–additive) on X. By $\mathcal{M}_1$ we denote the subset of $\mathcal{M}$ such that $\mu(X) = 1$ for $\mu \in \mathcal{M}_1$. The elements of $\mathcal{M}_1$ will be called *distributions*.

As usually by $C(X)$ we denote the space of all bounded confinuous functions $f : X \to \mathbb{R}$ with the norm

$$\|f\| = \sup_{x \in X} |f(x)|.$$

For $f \in C(X)$ and $\mu \in \mathcal{M}$ we write

$$\langle f, \mu \rangle = \int_X f(x)\mu(dx).$$

Given $\mu \in \mathcal{M}$ we define the support of μ by the formula

$$\text{supp } \mu = \{x \in X : \ \mu(K(x, r)) > 0 \quad \text{for every} \ \ r > 0\}.$$

Evidently supp μ is a closed set and $\mu(A) = 0$ for $A \subset X \setminus \text{supp } \mu$.

We say that a sequence $(\mu_n) \subset \mathcal{M}$ converges weakly to a measure $\mu \in \mathcal{M}$ (shortly $(w) \lim_{n \to \infty} \mu_n = \mu$) if

$$\lim_{n \to \infty} \langle f, \mu_n \rangle = \langle f, \mu \rangle \qquad \text{for} \quad f \in C(X).$$

We start this section with a version of the Alexandrov theorem for supports. Recall that the classical Alexandrov theorem assures that for every open subset U of X the limiting measure $\mu(U)$ is smaller that the $\liminf_{n \to \infty} \mu_n(U)$. It is easy to prove a similar property of supports.

Theorem 2.1. *Assume that (μ_n), $\mu_n \in \mathcal{M}$, converges weakly to $\mu \in \mathcal{M}$. Then*

$$\mathrm{Li} \text{ supp } \mu_n \supset \text{supp } \mu.$$

A family of measures $\{u_t : \ t \in T\} \subset \mathcal{M}$ is called *condensed at a point $x \in X$* if for every $\varepsilon > 0$ there is $\eta > 0$ such that

$$\inf\{\mu_t(K(x, \varepsilon)) : \ t \in T_\eta\} > 0$$

where

$$T_\eta = \{t \in T : \ K(x,\eta) \cap \text{supp } \mu_t \neq \emptyset\}.$$

As usually we admit that the infimum of the empty set is equal $+\infty$. A family $\{\mu_t : t \in T\}$ is called *condensed on* X (or shortly *condensed*) if it is condensed at every point $x \in X$.

Theorem 2.2. *Assume that a sequence of measures* $(\mu_n), \mu_n \in \mathcal{M}$, *converges weakly to a measure* $\mu \in \mathcal{M}$. *Then the following conditions are equivalent:*

(i) (μ_n) *is condensed on* X,

(ii) Lt supp $\mu_n =$ supp μ.

3. Markov set function

An operator $P : \mathcal{M} \to \mathcal{M}$ is called a *Markov operator* if it satisfies the following two conditions:

$$P(\lambda_1\mu_1 + \lambda_2\mu_2) = \lambda_1 P\mu_1 + \lambda_2 P\mu_2 \qquad \text{for} \quad \lambda_1, \lambda_2 \in \mathbb{R}_+ \ \text{ and } \ \mu_1, \mu_2 \in \mathcal{M};$$

$$P\mu(X) = \mu(X) \qquad \text{for} \quad \mu \in \mathcal{M}.$$

A Markov operator P is called a *Feller operator* if there is an operator $U : C(X) \to C(X)$ such that

$$\langle Uf, \mu\rangle = \langle f, P\mu\rangle \tag{3.1}$$

for every $f \in C(X)$ and $\mu \in \mathcal{M}$. Operator U is called *dual* to P.

Using condition (3.1) it is easy to verify the following proposition.

Proposition 3.1. *If* P *is a Feller operator and* supp $\mu_1 =$ supp μ_2, *then* supp $P\mu_1 =$ supp $P\mu_2$.

Let a Feller operator $P : \mathcal{M} \to \mathcal{M}$ be given. We adjoin to P a mapping $\Gamma : \mathcal{F}_0 \to \mathcal{F}_0$ by the condition

$$\Gamma(A) = \text{supp } P\mu, \qquad \text{where} \quad A = \text{supp } \mu. \tag{3.2}$$

According to Proposition 3.1, condition (3.2) defines a function Γ in a unique way.

Proposition 3.2. *The function* $\Gamma : \mathcal{F}_0 \to \mathcal{F}_0$ *given by formula* (3.2) *has the following properties:*

(i) $\Gamma(\emptyset) = \emptyset$;

(ii) $\Gamma(\text{cl} \bigcup_{t\in T} A_t) = \text{cl} \bigcup_{t\in T} \Gamma(A_t)$ *for every family* $\{A_t\}_{t\in T}$ *of closed sets;*

(iii) *If* Γ_1 *and* Γ_2 *are generated by Feller operators* P_1 *and* P_2, *then* $\Gamma_1 \circ \Gamma_2$ *is generated by* P_1P_2.

4. Stability results

Let $P : \mathcal{M} \to \mathcal{M}$ be a Markov operator. A measure μ is called *invariant* (or *stationary*) with respect to P if $P\mu = \mu$.

A Markov operator P is called *asymptotically stable* if there exists a stationary measure $\mu_* \in \mathcal{M}_1$ such that

$$(w) \lim_{n\to\infty} P^n\mu = \mu_* \qquad \text{for every} \quad \mu \in \mathcal{M}_1. \tag{4.1}$$

Obviously a measure μ_* satisfying condition (4.1) is unique.

Now we are going to study the behaviour of the iterates of the Markov set function Γ generated by an asymptotically stable Markov operator.

Theorem 4.1. *Let P be a Feller operator and let Γ be the corresponding Markov set function. Assume that P is asymptotically stable and denote by A_* the support of the probabilistic invariant measure μ_*. Then*

$$\text{Li } \Gamma^n(B) \supset A_* \qquad \textit{for} \quad B \in \mathcal{F}_0 \setminus \{\emptyset\}.$$

Corollary 4.1. *Let P, Γ and A_* be as in Theorem 4.2. Then*

$$\text{Lt } \Gamma^n(B) = A_* \qquad \textit{for} \quad B \in \mathcal{F}_0 \setminus \{\emptyset\},\ B \subset A_*.$$

This corollary shows that the support A_* of the invariant measure for an asymptotically stable operator has a regeneration property typical for semifractals [Lasota & Myjak 1996]. A stronger property characteristic for fractals requires additional assumptions concerning the iterates $(P^n\mu)$.

A Feller operator P will be called *condensing* if for every $\mu \in \mathcal{M}$ with bounded support the sequence $(P^n\mu)$ is condensed.

From Theorem 4.2 we obtain immediately the following corollary.

Corollary 4.2. *Let P, Γ and A_* be as in Theorem 4.2. Assume moreover that P is condensing. Then*

$$\text{Lt } \Gamma^n(B) = A_* \qquad \textit{for every bounded set} \quad B \in \mathcal{F}_0 \setminus \{\emptyset\}.$$

5. Applications to iterated function systems and fractals

We are going to apply our results to Markov operators generated by iterated function systems. These systems under the name of "systems with a complete connection" were studied by Onicescu and Mihoc [1935]. More recently they are studied because of the close connection with fractals [Barnsley 1988, Lasota & Mackey 1994] and other areas of applied mathematics.

An *Iterated Function System* (shortly *IFS*) is given by a sequence of continuous transformations

$$S_i : X \to X, \qquad i = 1, \ldots, N,$$

and a probabilistic vector

$$p_i : X \to \mathbb{R}, \qquad i = 1, \ldots, N,$$

where p_i are continuous functions satisfying

$$p_i(x) > 0, \quad \sum_{i=1}^{N} p_i(x) = 1 \qquad \text{for} \quad x \in X.$$

Such a system is shortly denoted by $(S, p)_N$. Having IFS $(S, p)_N$ we define the corresponding Markov operator $P : \mathcal{M} \to \mathcal{M}$ by setting

$$P\mu(A) = \sum_{i=1}^{N} \int_{S_i^{-1}(A)} p_i(x)\mu(dx) = \sum_{i=1}^{N} \int_X 1_A(S_i(x)) p_i(x)\mu(dx). \tag{5.1}$$

It is easy to verify that P is a Feller operator.

The probabilistic interpretation of IFS $(S, p)_N$ can be described as follows. Let a probabilistic space $(\Omega, \Sigma, \text{prob})$ be given. We consider a sequence of random elements $x_n : \Omega \to X$ and a sequence of random variables $\xi_n : \Omega \to \{1, \ldots, N\}$, $n = 0, 1, \ldots$, and we assume that these sequences are related by conditions:

$$\text{prob}\,(\xi_n = k | x_n = x) = p_k(x) \qquad \text{for} \quad k = 1, \ldots, N, \quad n = 0, 1, \ldots,$$

and

$$x_{n+1} = S_{\xi_n}(x_n) \qquad \text{for} \quad n = 0, 1, \ldots.$$

By μ_n we denote the distribution of x_n, i.e.

$$\mu_n(A) = \text{prob}\,(x_n \in A) \qquad \text{for} \quad A \in \mathcal{B}_X, \quad n = 0, 1, \ldots.$$

The operator P is a transition operator for the sequence (x_n), i.e. $\mu_{n+1} = P\mu_n$ for all n. The set function Γ corresponding to P is given by the formula

$$\Gamma(A) = \text{cl}\left(\bigcup_{i=1}^{N} S_i(A)\right).$$

Operators of the form (5.1) are used for the construction of fractals. In our terminology the Barnsley definition of a fractal can be expressed as follows: A *fractal* is the support of the unique invariant measure corresponding to an asymptotically stable and condensing operator of the form (5.1).

Sufficient conditions for the asymptotic stability of Markov operators of the form (5.1) are well known [Barnsley *et al.* 1988, Lasota & Yorke 1994]. Here we are going to show a sufficient condition for the condensation.

Theorem 5.1. *Let an IFS* $(S,p)_N$ be given. Assume that

$$\varrho(S_i(x),S_i(y)) < \varrho(x,y) \qquad for \quad x,y \in X,\ x \neq y,\ i=1,\ldots,N, \tag{5.2}$$

and that for every bounded set K there is a bounded set $B \supset K$ such that

$$S_i(B) \subset B.$$

Then the operator P given by (5.1) is condensing.

It should be noted that condition (5.2) does not imply asymptotic stability of the operator P if the mappings $p_i,\ i=1,\ldots,N$ are only continuous.

References

Barnsley, M. F. [1988] *Fractals Everywhere* (Academic Press, New York), Chap. 9, pp. 334–380.

Barnsley, M. F., Demko, S. G., Elton, J. H. & Geronimo, J. S. [1988] "Invariant measures arising from iterated function systems with place dependent probabilities", *Ann. Inst. Henri Poincaré* 24(3), 367–394.

Lasota, A. & Mackey, M. C. [1994] *Chaos, Fractals and Noise–Stochastic Aspects of Dynamics* (Springer Verlag, New York), Chap. 12, pp. 393–446.

Lasota, A. & Myjak, J. [1996], "Semifractals", *Bull. Pol. Acad. Sci. Mathematics* 44(1), 5–21.

Lasota, A. & Yorke, J. A. [1994] "Lower bound technique for Markov operators and iterated function systems", *Random and Comput. Dynamics* 2(1), 41–77.

Onicescu, O. & Mihoc, G. [1935] "Sur les chaines de variables statistiques", *Bull. Sci. Math.* 59, 174–192.

APPLICATIONS AND POTENTIAL OF THE VOLTERRA SERIES FOR NONLINEAR STRUCTURAL DYNAMICS PROBLEMS

G. R. Tomlinson, Department of Mechanical Engineering,
The University of Sheffield, Mappin Street,
Sheffield, S1 3JD.

Abstract: From a mathematical point of view, the Volterra series provides a strong foundation for studying particular classes of nonlinear systems. This paper presents some interesting ways in which the Volterra series can be used as a basis for identifying and simulating the effects of faults in engineering structures.

1. Introduction

Damage detection, condition monitoring and fault location in engineering structures is a subject of considerable interest because it relates directly to cost and operational reliability.

Structural damage deterioration such as cracks, delaminations loose joints are normally related to nonlinear phenomena, particularly when the structure/component is subject to dynamic excitation [Chance, 1996, Natke and Yao, 1993]. Strictly speaking, the Volterra series [Volterra, 1959] can only be applied to structures with nonlinear properties that are analytic i.e. polynomial type functions. Thus faults such as cracks, which often appear as bilinear functions, do not have a Volterra series representation but they can be approximated over any interval, using a polynomial formulation as guaranteed by the Weierstrass approximation theorem [Simmons, 1963]. One principal advantage of using the Volterra series is that with many nonlinear problems only the first few terms in the series, (e.g. kernels up to order 3) are needed to capture the principal dynamic characteristics of the response. A disadvantage is that it is difficult to measure the kernels accurately in practice [Chance, 1996]. However, by estimating the kernels in the time domain or their equivalent, the Higher Order Frequency Response Functions in the frequency domain, as a function of a controlled input level of excitation, the presence of faults can be detected. Conversely, in many applications

where health/condition monitoring methods are employed to detect faults, validation of the monitoring system cannot be carried out in-situ. A method of inducing 'pseudo-faults' into a structure which produces the same dynamic characteristics as the real fault could prove valuable to the test engineer.

This paper describes the ways in which the Volterra series can be used as the basis for detecting faults in engineering structures, hence demonstrating the potential of the Volterra series for nonlinear structures dynamics problems.

2. Representation of a Nonlinear System Response

2.1 Volterra series definition

Given that a single input x(t) to a nonlinear system will produce an output y(t) it can be shown [Wiener, 1942] that for a wide class of systems

$$y(t) = y_1(t) + y_2(t) + y_3(t) + \ldots + y_n(t) + \ldots \tag{1}$$

where,
$$y_n(t) = \int_{-\infty}^{+\infty} \ldots \int_{-\infty}^{+\infty} d\tau_1 \ldots d\tau_n \, h_n(\tau_1, \ldots, \tau_n) \prod_{i=1}^{n} x(t-\tau_i) \tag{2}$$

The terms $h_1(\tau_1), h_2(\tau_1,\tau_2), \ldots, h_n(\tau_1,\ldots,\tau_n)$ are known as the first, second, third, ..., n^{th}-order Volterra kernels or impulse response functions of the time - invariant system which can be shown to be symmetric i.e. $h_2(\tau_1,\tau_2) = h_2(\tau_2,\tau_1)$ etc.

As in the linear case, there exists a dual frequency-domain representation for nonlinear systems based on the *higher-order* FRFs or *Volterra kernel transforms*

$$H_n(\omega_1,\ldots,\omega_n) = \int_{-\infty}^{\infty} \ldots \int_{-\infty}^{\infty} d\tau_1 \ldots d\tau_n h_n(\tau_1,\ldots,\tau_n) e^{-i(\omega_1\tau_1+\ldots+\omega_n\tau_n)} \tag{3}$$

It can be shown that the kernel transforms are also symmetric in their arguments. In addition, they satisfy a reflection property,

$$H_1(-\omega) = H_1^*(\omega), \qquad H_2(-\omega_1,-\omega_2) = H_2^*(\omega_1,\omega_2), \tag{4}$$

2.2 Frequency Response Representation

The frequency domain representation of the Volterra series is of the form

$$Y(\omega) = Y_1(\omega) + Y_2(\omega) + Y_3(\omega) + \ldots Y_n(\omega) + \ldots \tag{5}$$

$$
\begin{aligned}
Y(\omega) &= H_1(\omega)X(\omega) \\
&+\left(\frac{1}{2\pi}\right)\int_{-\infty}^{+\infty} d\omega_1\, H_2(\omega_1, \omega-\omega_1)X(\omega_1)X(\omega-\omega_1) \\
&+\left(\frac{1}{2\pi}\right)^2\int_{-\infty}^{+\infty}\int_{-\infty}^{+\infty} d\omega_1 d\omega_2\, H_3(\omega_1,\omega_2,\omega-\omega_1-\omega_2) \\
&\qquad \times X(\omega_1)X(\omega_2)X(\omega-\omega_1-\omega_2) \\
&+\ldots+\left(\frac{1}{2\pi}\right)^{n-1}\int_{-\infty}^{+\infty}\ldots\int_{-\infty}^{+\infty} d\omega_1\ldots d\omega_{n-1} H_n(\omega_1,\ldots,\omega_{n-1},\omega-\omega_1-\ldots-\omega_{n-1}) \\
&\qquad \times X(\omega_1)\ldots X(\omega_{n-1})X(\omega-\omega_1-\ldots-\omega_{n-1})+\ldots
\end{aligned}
\tag{6}
$$

where the n^{th}-order component of the response in the frequency domain may be written

$$
\begin{aligned}
Y_n(\omega) = \left(\frac{1}{2\pi}\right)^{n-1}\int_{-\infty}^{+\infty}\ldots\int_{-\infty}^{+\infty} d\omega_1\ldots d\omega_{n-1} H_n(\omega_1,\ldots,\omega_{n-1},\omega-\omega_1-\ldots-\omega_{n-1}) \\
\times X(\omega_1)\ldots X(\omega_{n-1})X(\omega-\omega_1-\ldots-\omega_{n-1})
\end{aligned}
\tag{7}
$$

If the leading diagonals are employed $(\omega_1+\omega_2=\ldots\omega)$ and a range of excitation amplitude levels are used one can write [Chance, 1996, Ewan, 1980],

$$[Y] = [X]\,[H]$$

$$[Y(\omega)] = \begin{bmatrix} Y_1(\omega) \\ Y_2(\omega) \\ \vdots \\ Y_n(\omega) \end{bmatrix},\quad [H_{2n-1}] = \begin{bmatrix} H_1(\omega) \\ H_3(\omega,\omega,-\omega) \\ \vdots \\ H_{2n-1}(\omega,\omega,\ldots-\omega) \end{bmatrix}$$

with,

$$[X] = \begin{bmatrix} X_1 & aX_1^3 & bX_1^5 \\ X_2 & aX_2^3 & bX_2^5 \\ X_3 & aX_3^3 & bX_3^5 \end{bmatrix},\ a=\frac{3}{4},\ b=\frac{5}{8}$$

and

$$[H_{2n-1}] = [X]^{-1}[Y(\omega)] \tag{8}$$

$$[Y(2\omega)] = \begin{bmatrix} Y_1(2\omega) \\ Y_2(2\omega) \\ \vdots \\ Y_n(2\omega) \end{bmatrix}, [H_{2n}] = \begin{bmatrix} H_2(\omega,\omega) \\ H_4(\omega,\omega,\omega,-\omega) \\ \vdots \\ H_{2n}(\omega,\omega\ldots,\ldots\omega) \end{bmatrix}$$

$$[X] = \begin{bmatrix} cX_1^2 & cX_1^4 & dX_1^6 \\ cX_2^2 & cX_2^4 & dX_2^6 \\ cX_3^2 & cX_3^4 & dX_3^6 \end{bmatrix}, c = \frac{1}{2}, d = \frac{15}{32}$$

$$[H_{2n}] = [X]^{-1}[Y(2\omega)] \tag{9}$$

$$[Y(3\omega)] = \begin{bmatrix} Y_1(3\omega) \\ Y_2(3\omega) \\ \vdots \\ Y_n(3\omega) \end{bmatrix}, [H_{n+2}] = \begin{bmatrix} H_3(\omega,\omega,\omega) \\ H_5(\omega,\omega,\omega,\omega,-\omega) \\ \vdots \\ H_{n+2}(\omega,\omega\ldots,\ldots-\omega) \end{bmatrix}$$

$$[X] = \begin{bmatrix} eX_1^3 & fX_1^5 \\ eX_2^3 & fX_2^5 \\ eX_3^3 & fX_3^5 \end{bmatrix}, e = \frac{1}{4}, f = \frac{5}{16}$$

and $$[H_{n+2}] = [X]^{-1}[Y(3\omega)] \tag{10}$$

Equations (8) (9) and (10) provide a means of estimating the higher order FRFs when harmonic excitation is used with a series of controlled input levels. If a structure is tested in its 'virgin' state, only the $H_1(\omega)$ will be significant if the structure behaves in a linear manner. However, if a fault occurs then the presence of the higher order FRFs can signify a 'change' in the state of the structure which may be related to a reduction in the integrity.

2.3 Impulse response representation

When the excitation is an impulse of magnitude A, i.e. $x(t) = A\delta(t)$ the use of eq. (1) and (2) leads to [Manson, 1996, Thomas, 1995]:

$$y(t) = Ah_1(t) + A^2h_2(t) + \ldots A^nh_n(t) + \ldots \tag{11}$$

$$\text{i.e. } y(t) = \sum_{i=1}^{\infty} A^i h_i(t) \tag{12}$$

If a range of N impulses of magnitude $A=A_m$ (m=1...N) are used, eq. (12) can be expressed as,

$$[y] = [A][h]$$

where,

$$[y] = \begin{bmatrix} y^1(t) \\ \vdots \\ y^N(t) \end{bmatrix}, [h] = \begin{bmatrix} h_1(t) \\ \vdots \\ h_N(t) \end{bmatrix}$$

$$[A] = \begin{bmatrix} A_1^1 & A_1^2 & \cdots & A_1^N \\ A_2^1 & A_2^2 & \cdots & A_2^N \\ \vdots & & & \\ A_N^1 & \cdots & & A_N^N \end{bmatrix}$$

and provided that the matrix [A] is invertible,

$$[h] = [A]^{-1}[y] \tag{13}$$

By utilising the concept of energy with the estimated kernels one can formulate a nonlinear energy ratio [Thomas, 1995],

$$\rho(A) = \frac{\sum_{i=2}^{N} A2\eta_i}{\sum_{i=1}^{N} A^{2i}\eta_i}; \quad \eta_i = \int h_i(t,t\ldots t)^2 dt \tag{14}$$

This ratio provides an indicator function for the presence of nonlinearity and its dependence on the magnitude of the impulse. Figure (taken from [Thomas, 1995]) shows how $\rho(A)$ varies for two different types of nonlinearity, whose nonlinear dominant characteristics were quadratic and cubic respectively.

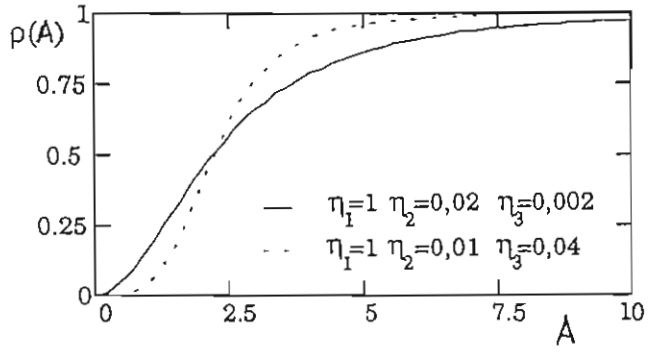

Figure 1: Variation of the nonlinear energy ratio with magnitude of the impulse.

3. Applications

3.1 Sine excitation

A cantilever beam incorporating a simulated crack shown in Fig. 2 was excited over the frequency range 100-400 rad/s with a stepped sine excitation which encompassed only the second flexural mode of vibration. The higher order FRFs were obtained from eqs. (8), (9) and (10).

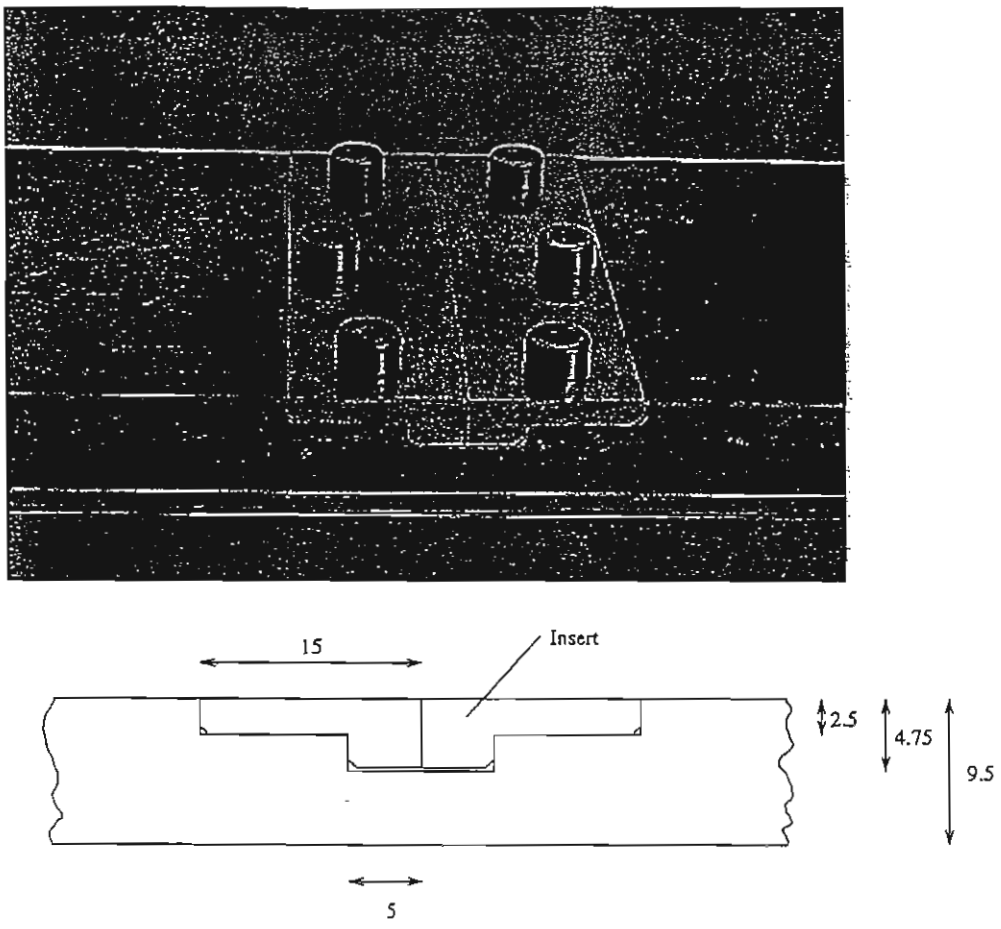

Figure 2 : Experimental beam incorporating inserts to simulate a breathing crack.

Figure 3 shows H_{11} (the linear frequency response function) for the faulted beam with the resource ω_2 = 339 rad/s. H_{22} displays an additional peak at $\omega_2 / 2$ indicating a quadratic effect. H_{33} has an additional peak at $\omega_2 / 3$ indicating a cubin effect. These clear results demonstrate the presence of a general polynomial type nonlinearity which are indicative of a bilinear stiffness function.

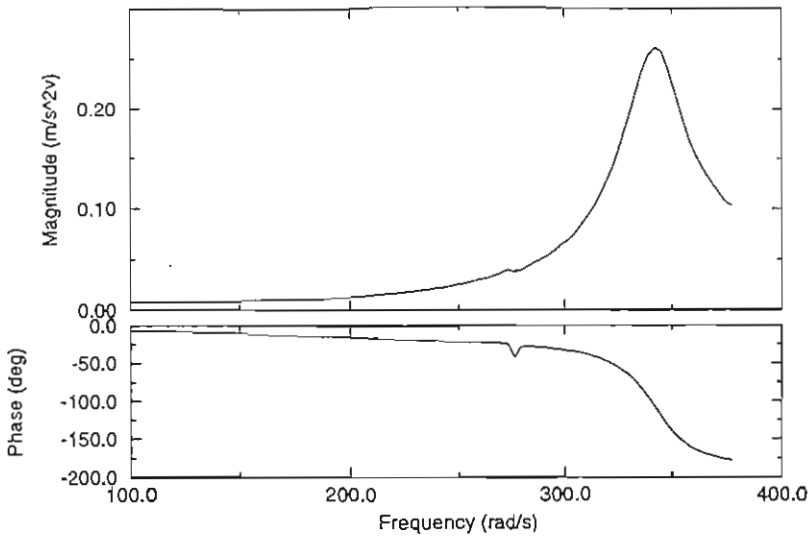

Experimental H_{11} from faulted beam.

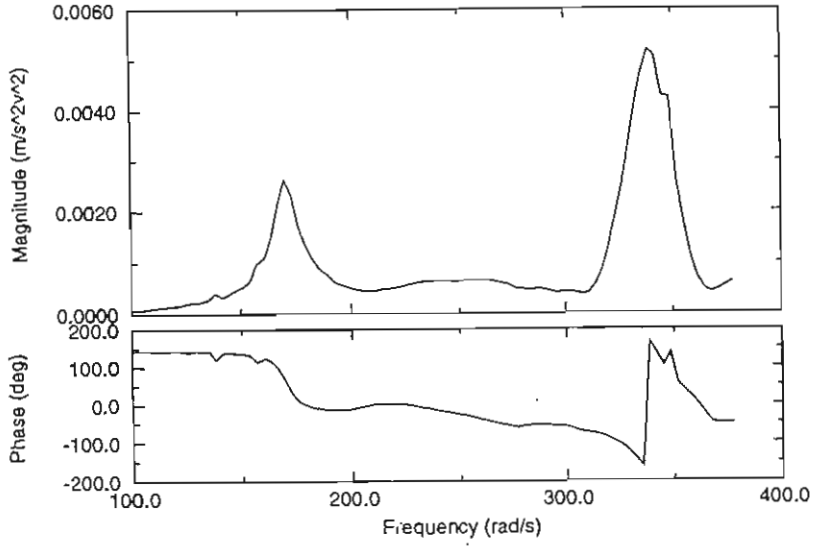

Experimental leading diagonal $(\omega_1 = \omega_2)$ of H_{22} from faulted beam.

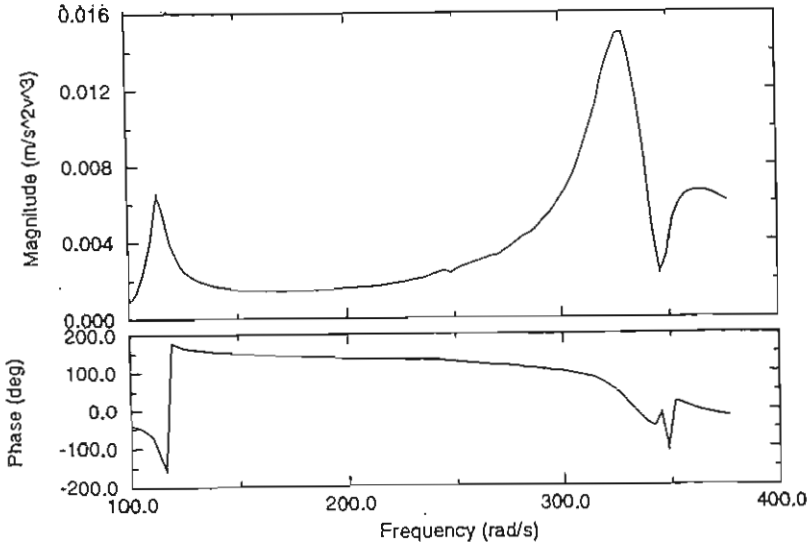

Experimental H_{33} from faulted beam along the diagonal $(\omega_1 = \omega_2 = \omega_3)$

Figure 3: Experimental Frequency Response Functions from the Faulted Beam

3.2 Impulse excitation

These results are taken from [Thomas, 1995]. The results are from tests on an electric Pylon with and without a loose joint. The force was applied using tensile (cable) loading and release mechanism. The transient response was recorded for a range of force levels (5.5, 7.5, 15kN) for the 'undamaged' pylon and repeated (5.5, 8, 10kN) with a loose joint in the pylon. Using eqs. (13) and (14) the results shown in Fig. 4 were obtained.

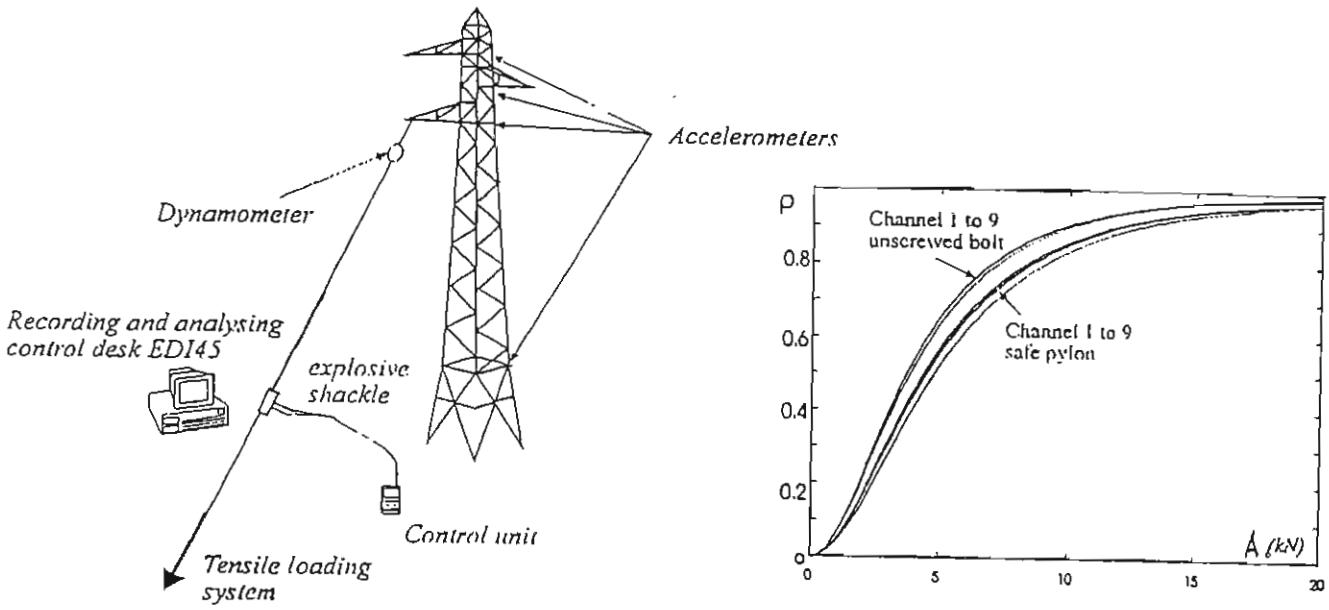

Figure 4: Tension release testing of pylon

4. Pseudo-fault method

This is a method which allows one to make a linear system behave as if it had a given nonlinearity present at a prescribed location. The object is to allow experimental validation of on-line fault detection systems.

The principle is as follows [Manson *et al*, 1996]. Consider a linear system S_1, excited at a location labelled i with an input $x^{(i)}(t)$ as shown in Fig. 5a. The response at point j is given by

$$y_\ell^{(j:i)}(t) = y_1^{(j:i)}(t) = \int_{-\infty}^{\infty} d\tau_1 h_1^{(j:i)}(\tau_1 - t) x^{(i)}(\tau_1)$$

Now suppose S_ℓ is replaced by $S_{n\ell}$, a nonlinear system but with the same linear part as S_ℓ (i.e. the same structure but with a fault). If the same input $x^{(i)}(t)$ is applied, assuming the Volterra series exists, the response at j is now given by, (Fig. 5b),

$$y_{n\ell}^{(j:i)}(t) = y_1^{(j:i)}(t) + y_2^{(j:i)}(t) + y_3^{(j:i)}(t) + \ldots + y_n^{(j:i)}(t) + \ldots$$

where

$$y_n^{(j:i)}(t) = \int_{-\infty}^{\infty} \ldots \int_{-\infty}^{\infty} d\tau_1 \ldots d\tau_n \times h_n^{(j:i)}(t-\tau_1, \ldots, t-\tau_n) x^{(i)}(\tau_1) \ldots x^{(i)}(\tau_n)$$

The object of the exercise is to produce $y_{n\ell}(t)$ the *nonlinear* response to $x^{(i)}(t)$ in the *linear* system. This is accomplished by exciting with an auxiliary signal $x_{n\ell}^{(k)}(t)$ at point k say (Fig. 5c).

If $x_{n\ell}^{(k)}(t)$ is applied in addition to $x^{(i)}(t)$, by the principle of superposition (valid for the linear S_ℓ), the response at j is

$$y^{(j)}(t) = y_\ell^{(j:i)}(t) + y_{n\ell}^{(j:k)}(t)$$

where

$$y_{n\ell}^{(j:k)}(t) = \int_{-\infty}^{\infty} d\tau \, h_1^{(j:k)}(t-\tau) x_{n\ell}^{(k)}(\tau)$$

So, in order that $y^{(j)}(t)$ be equal to the nonlinear response, $y_{n\ell}^{(j:i)}(t)$, it is required that

$$y_{n\ell}^{(j:k)}(t) = y_2^{(j:i)}(t) + y_3^{(j:i)}(t) + \ldots + y_n^{(j:i)}(t) + \ldots$$

The Fourier transforms of both sides of this equation leads to,

$$X_{n\ell}^{(k)}(\omega) = \frac{1}{2\pi H_1^{(j:k)}(\omega)} \{$$

$$\int_{-\infty}^{\infty} d\omega_1 H_2^{(j:i)}(\omega_1, \omega-\omega_1) X^{(i)}(\omega_1) X^{(i)}(\omega-\omega_1) +$$
$$\frac{1}{(2\pi)} \int_{-\infty}^{\infty} \int_{-\infty}^{\infty} d\omega_1 d\omega_2 H_3^{(j:i)}(\omega_1, \omega_2, \omega-\omega_1-\omega_2) \times$$
$$X^{(i)}(\omega_1) X^{(i)}(\omega_2) X^{(i)}(\omega-\omega_1-\omega_2) + \ldots$$
$$+ \frac{1}{(2\pi)^{n-2}} \int_{-\infty}^{\infty} \ldots \int_{-\infty}^{\infty} d\omega_1 \ldots d\omega_{n-1} \times$$
$$H_n^{(j:i)}(\omega_1, \ldots, \omega_{n-1}, \omega-\omega_1-\ldots-\omega_{n-1}) \times$$
$$X^{(i)}(\omega_1) \ldots X^{(i)}(\omega_{n-1}) X^{(i)}(\omega-\omega_1-\ldots-\omega_{n-1})$$
$$+ \ldots \}$$

Suppose the excitation is harmonic i.e. $x^{(i)}(t) = X\cos(\Omega t)$, the auxiliary input has the form [Worden *et al*, 1993],

$$x_{n\ell}^{(k)}(t) = \sum_{n=2}^{n=\infty} \frac{X^n}{2^{n-1}} \left\{ \sum_{p=0}^{p=m(n)} A(n,p) \left| \frac{H_n^{(j:i)}(\Omega,\Omega,\ldots,-\Omega}{H_1^{(j:k)}((n-2p)\Omega)} \right| \times \cos\left[(n-2p)\Omega t + \angle\left(\frac{H_n^{(j:i)}(\Omega,\Omega,\ldots,-\Omega}{H_1^{(j:k)}((n-2p)\Omega)} \right) \right] \right\}$$

where

$$\begin{aligned} m(n) &= \frac{n-1}{2} && n \text{ odd} \\ m(n) &= \frac{n}{2} && n \text{ even} \\ A(n,p) &= \frac{n!}{p!(n-p)!} && p \neq \frac{n}{2} \\ a(n,p) &= \frac{n!}{2p!(n-p)!} && p = \frac{n}{2} \end{aligned}$$

and in the $H_n^{(j:i)}(\Omega,\Omega,\ldots,-\Omega)$ terms are p negative frequencies and (n-p) positive frequencies.

The procedure was applied to a single degree of freedom experimental rig [Manson *et al*, 1996] where the objective was to inject an auxiliary input to the rig (the linear system) in order to produce an output which corresponded to the linear system plus a cubic stiffness junction. Validation was carried out by connecting a nonlinear spring (a clamped beam) to the linear system and the new response was measured. This was then compared to the linear system plus the auxiliary input. Parametric models of the linear and nonlinear system were obtained in order the HFRFs would be calculated and used to derive the auxiliary input for the nonlinear system. Figure 6 shows a comparison between the experimental nonlinear system response (due to a sinewave input) and that from the linear rig with the auxiliary input. A good comparison is clearly achieved.

Conclusions

Three applications of methods for treating nonlinear structures have been outlined, all based on the Volterra series. Although some of these applications are based on relatively simple structures, they serve to show that the Volterra series offers potential for dealing with real problems. Many aspects have not been discussed which are important when one is utilising the Volterra series such as truncation of the series, bounds on the excitation levels and range of validity. In addition, the application of the pseudo-fault method should be evaluated on continuous (MDOF) multi-input multi-output systems before it can be claimed to be fully general.

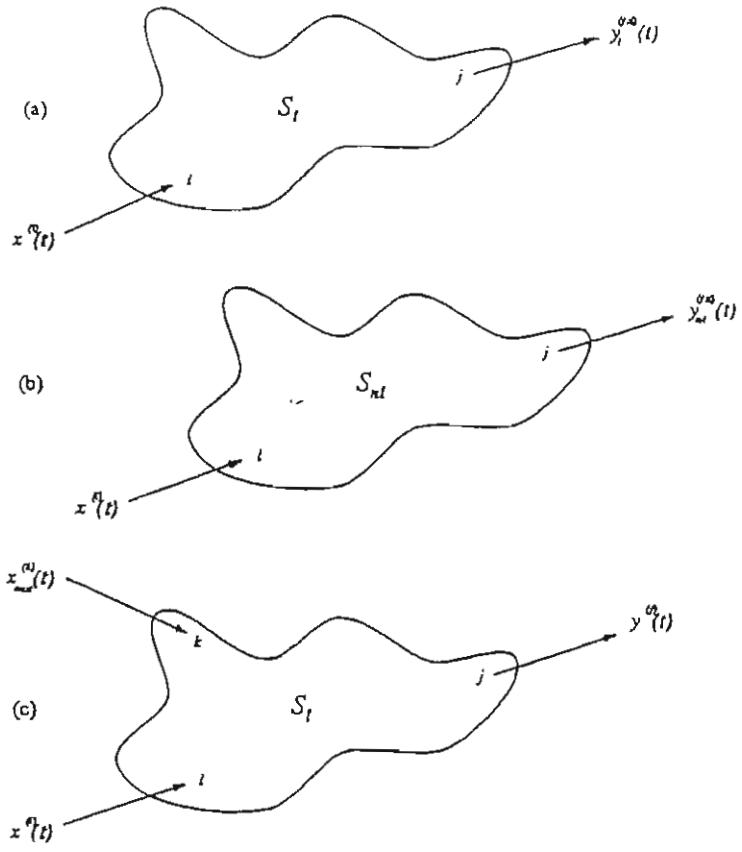

Figure 5: Schematic illustrating the pseudo-fault method.

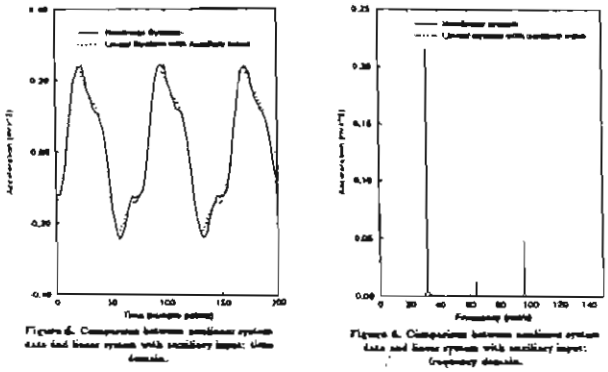

Acknowledgements

The author wishes to acknowledge Drs Worden, Manson and Chance for the material that they provided for this paper.

References

Chance, J. E., [1996], "Structural fault detection employing linear and nonlinear dynamic characteristics", PhD Thesis, University of Manchester.

Ewen, E. J. and Wiener D. D.,[1980], "Identification of weakly nonlinear systems using input and output measurements", IEEE Trans., CA-27, No. 12.

Manson, G. [1996], "Analysis of nonlinear mechanical systems using the Volterra series", PhD Thesis, University of Manchester.

Manson, G., Worden, K., Chance, J. E. and Tomlinson G. R. [1996], "Experimental Study of the Pseudo-Fault Method", Proc. 2nd European Euromech 'Non linear Oscillation Conference", Prague.

Natke, H. G. and Yao, J. T. P.[1993], "Detection and location of damage causing nonlinear behaviour", in Safety Evaluation Based on Identification Approaches, Eds., Natke, Tomlinson, Yao, Vieweg.

Simmons, G. F. [1963], "Introduction to topology and modern analysis", New York, McGraw-Hill.

Thomas, J. J. [1995], "Contrôle non destructif des materiaux et des structures par analyse dynamique nonlinéaire", École Poly Technique, Palaisena, France.

Volterra, V. [1959], "Theory of functionals and of Integral and integro-differential equations", New York, Dover.

Wiener, N. [1942], "Response of a nonlinear device to noise", Radiation Laboratory, M.I.T. Report 129.

Worden, K., Manson, G. and Tomlinson, G. R., [1993], "Pseudo-nonlinearities in engineering structures", Procs. Royal Soc. London A 445, pp193-220.

CONTRIBUTED PAPERS

TIME-HIERARCHY AND BIFURCATIONS IN BIOMOLECULAR SYSTEMS. DYNAMICAL AND NOISE CONTROL OF PHASE TRANSITIONS.

G.Abgarian*, V.Kharkyanen and G.Weinreb
Division of Physiscs of Biological Systems of Institute for Physics NASci of Ukraine,
Pr-t Nauki, 46, Kiev-22, 252650
*Erevan State Medical University, Erevan, Armenia

Abstract: Biomolecular systems such as DNA, RNA, proteins that construct different type of functional structures (ion channels, photoreaction centers, etc.) are very mobile dynamic and stochastic systems with a complex behavior. The corresponding system of equations contain different time scales. External factors, such as flows of charged particles, light or chemical reagents can influence the system behavior. Taking into account both time hierarchy and interactions between biomolecule and flows of reagents we develop theoretical approach describing real biomolecular systems such as ion channels of biomembranes, photoreaction centers, etc. We show that self-organization effects could be induced by both pumping as well noise in these systems.

Biological macromolecules play important role in the functioning of alive systems. They provide important biological functions such as charge transfer through the membrane, enzymatic functions and a lot of others. During the functioning they change their configurations. For example, ion channels of biological membrane providing specific path for ion transport through membrane have several conformations that determine the channel conductivity (open, closed states) [Hille, 1992]. Photoreaction centers of bacteria change their conformations and change the rates of electron tunneling in processes of photoreception [Parson & Cogdel, 1975].

It is well known that proteins are characterised by time scales from picoseconds to seconds [Careri, 1983]. We'll consider a generalized two dimensional molecular machine of charge transport as a non-linear stochastic system of different time-scales. In this case the system Hamiltonian is reasonable to represent in the form: $H(x,r)=H_{mol}(x)+H_{charge}(r)+H_{int}(x,r)$. Here $H_{mol}(x)$ is an energy of the macromolecule's structural group with charges out of the system; $H_{charge}(r)$ is the charge energy in the system without taking into account the

interaction with conformational degrees of freedom; $H_{int}(x,r)$ is the energy of the charge-conformational interaction.

It is reasonable to introduce a set of distribution functions P_i. These functions determine the probability density of conformational coordinate x, number of charges in the system and the probability density of their localization within macromolecule. For instance, if macromolecule has a single binding site we can introduce functions $P_0(x,t)$ and $P_1(x,t)$ that determine distribution densities of conformational variable x in the empty system (index 0) or in an occupated one (index 1). We can write equations for these functions:

$$\left.\begin{aligned} \frac{\partial P_0(x,t)}{\partial t} &= \frac{1}{\tau_x}\frac{\partial}{\partial x}\left[\frac{\partial H_0(x)}{\partial x}P_0 + kT\frac{\partial P_0}{\partial x}\right] + P_1 k_{10} - P_0 k_{01}, \\ \frac{\partial P_1(x,t)}{\partial t} &= \frac{1}{\tau_x}\frac{\partial}{\partial x}\left[\frac{\partial H_1(x)}{\partial x}P_1 + kT\frac{\partial P_1}{\partial x}\right] + P_0 k_{01} - P_1 k_{10}, \end{aligned}\right\} \quad (1)$$

where $H_0(x)=H_{mol}(x)$, $H_1(x)=H_{mol}(x)+H_{int}(x)$, $\sum_i \int P_i(x,t)dx = 1$. The time-hierarchy in the system is manifasted in the fact that charge transport is highly faster than the conformational motions. (In ion channels ion transfer lies in time range $\sim 10^{-7}$ sec, meanwhile gate processes (conformational motions) lies in range $\sim 10^{-3}$ sec). Using the Haken's slaving principle [Haken, 1983] let us determine equation for the distribution function of slow conformational variable x:

$$\rho(x,t) = P_0(x,t) + P_1(x,t). \quad (1)$$

Thus, we suppose that $P_1k_{10}=P_0k_{01}$ and obtain

$$\frac{\partial \rho(x,t)}{\partial t} = \frac{1}{\tau_x}\frac{\partial}{\partial x}\left[\frac{\partial V}{\partial x}\rho + kT\frac{\partial \rho}{\partial x}\right], \quad (2)$$

where

$$-\frac{\partial V(x)}{\partial x} = -\frac{\partial H_{mol}}{\partial x} - \frac{\partial H_{int}}{\partial x}\frac{N_0W_{01} + N_2W_{21}}{W_{10} + W_{12} + N_0W_{01} + N_2W_{21}} \quad (3)$$

is the mean force with respect to the fast charge motion; V(x) is effective conformational potential; N(x) is the probability that the channel is occupied by

ion; $W_{ij} = \Omega_i \exp\left[\frac{E_i - E_{ij}}{kT}\right]$, k is the Boltzmann constant and T is the absolute temperature. Equation (2) is a generalized equation for biomolecular system with one binding site, of fast charge transfer and slow conformational degree of freedom. Let us suppose that barrier E_{12} is mobile (see Fig.1). The extrema of the stationary distribution function $\rho_{st}(x)$ are determined by condition that its derivative is equal to zero. In the case when $H_{mol}(x) = \kappa(x-x_0)^2/2$ (the system has a single conformation without charge-conformational interaction) and when $H_{int}(x)=x_\infty x$ we obtain a nonlinear equation:

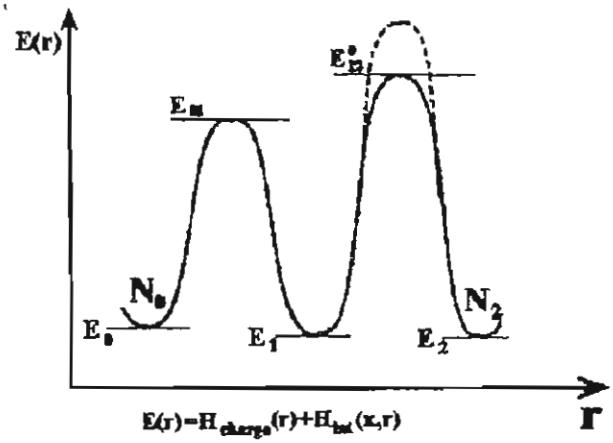

Figure 1. Energy profile of ion channel with one binding site (energy E_1). N_0 and N_2 are proportional to the ion concentrations in bath solutions.

$$\kappa(x-x_0) = -x_\infty N(x). \qquad (4)$$

This equation could have several solutions that are determined by both dynamic

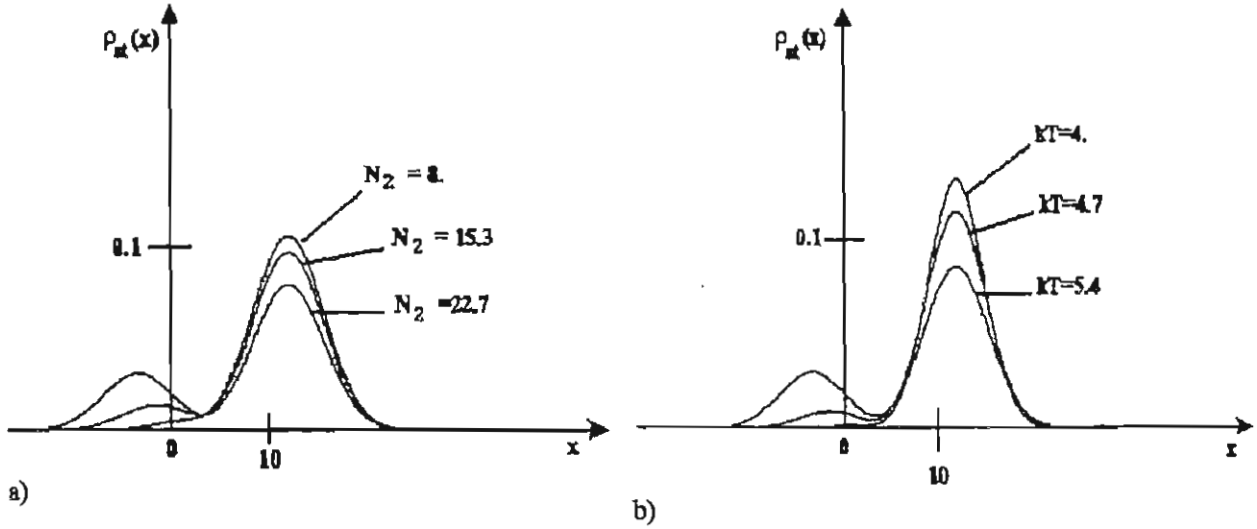

a) b)

Figure 2. Self-organization in ion channel induced by pumping (N_2, fig. a)) and by temperature (kT, fig.b). Parameters: x_∞=10, κ=0.45, x_0=12, N_0=0, W_{10}=0.001, W^0_{12}=0.1, W_{01}=0.1, W^0_{21}=0.01, $E_{12}=E^0_{12}+H_{int}(x)$. All values are given in arbitrary units.

(N_0 and N_2) and stochastic (T) control parameters. In Figs.2 we show results of computations. One can see that the distribution function $\rho_{st}(x)$ could have one, two or three extrema depending on control parameters N_0, N_2, T. Thus, in these molecular systems of time-hierarchy both the pumping (N_0 and N_2) [Chinarov *et al.*,1992, Kharkyanen, Panchouk, & Weinreb, 1994] as well noise (T) can induce self-organization effects. Using these parameters one can control phase transitions and regulate the processes of charge transport in biomolecules.

REFERENCES.

Careri, G. [1983] *Structure and Dynamics of Biomolecules Viewpoint from Physics.* from *Structure and Dynamics: Nucleic Acids and Proteins* (Adenine Press, N.Y.), pp. 5-12.

Chinarov V.A., Gaididei Yu.B., Kharkyanen V.N., Sit'ko S.P. [1992] "Ion pores in biological membranes as self-organized bistable systems", *Phys.Rev.A,* **46(8)**, 5232-5241.

Haken, H. [1983] *Advanced Synergetics. Instability Hierarchies of Self-Organizing Systems and Devices* (Springer-Verlag, Berlin Heildelberg New York Tokyo), p.419.

Hille, B. [1992] *Ionic Channels of Excitable Membranes* (Sinauer Associates, Sunderland, Massachusetts), p.607.

Kharkyanen, V.N., Panchouk, A.S. & Weinreb, G.E. [1994] "Self-Organization Effects Induced by Ion-Conformational Interaction in Biomembrane Channels", *J.Biol.Phys.* **19**, 259-272.

Parson,W.E. & Cogdel, R.I. [1975] "The primary photochemical reaction of bacterial photosynthesis", *Biochim.Biophys.Acta* **416**, 105.

DETECTION OF STICK-SLIP CHAOTIC OSCILLATIONS USING MELNIKOV'S METHOD

J. Awrejcewicz, M. M. Holicke
Technical University of Łódź, Division of Control and Biomechanics (I-10),
1/15 Stefanowskiego St, 90-924 Łódź, Poland

Abstract: In this paper we predict stick-slip chaotic dynamics in a one-degree-of-freedom non-autonomous oscillator using the Melnikov's technique. Numerical simulation confirms a validity of our approach.

1. Introduction

Self-excited oscillations caused by friction are often observed in nature and belong to one of the oldest problems of nonlinear mechanics [Stoker, 1950; Andronov et al., 1966]. A decreasing part of the friction coefficient versus a relative velocity between sliding bodies is responsible for an occurrence of self-excited oscillations. When this relative velocity equals zero then a static friction can occur (stick), otherwise we have a slip mode corresponding to the dynamic friction. In this paper an attention is focused on analytical prediction of stick-slip chaotic motion in a one-degree-of-freedom oscillator with friction periodically driven using the Melnikov's method. Chaotic stick-slip dynamics of coupled oscillators has been reported earlier by simulation [Awrejcewicz & Delfs, 1990 a, b].

2. Analysed System, Melnikov's Method and Results

Stick-slip one-degree-of-freedom oscillations are governed by the following set of first order ODE's

$$\begin{aligned} \dot{x} &= v, \\ \dot{v} &= ax - bx^3 + \varepsilon\left[\gamma \cos\omega t - T(v - v_*)\right], \end{aligned} \tag{1}$$

where

$$T(v - v_*) = T_0 \operatorname{sign}(v - v_*) - \alpha(v - v_*) + \beta(v - v_*)^3. \tag{2}$$

In Eq. (1) and Eq. (2) $\varepsilon > 0$ is the perturbation parameter and v_* corresponds to the velocity of the belt on which the considered mechanical system lies. T_0, α, β are friction coefficients, a and b are stiffness' coefficients, whereas γ and ω are the amplitude and frequency of excitation, respectively. For $\varepsilon = 0$ we have the unperturbed system with the following Hamiltonian

$$H = \frac{1}{2}\left(v^2 - ax^2 + \frac{1}{2}bx^4\right), \tag{3}$$

and there are three critical points for a, $b > 0$: two centres at $\left(\pm\sqrt{a/b},0\right)$ and a hyperbolic saddle at the origin with the homoclinic orbit satisfying the equation

$$\frac{dx}{dt} = x\sqrt{a - b\frac{x^2}{2}} = \sqrt{a}x\sqrt{1 - \frac{b}{a}\frac{x^2}{2}}. \tag{4}$$

Integrating Eq. (4) in respect to t, we obtain

$$x_0(t) = \sqrt{\frac{2a}{b}}\,\mathrm{sech}\,t, \quad v_0(t) = \pm a\sqrt{\frac{2}{b}}\,\mathrm{sech}\,t\tanh t. \tag{5}$$

After some transformations the Melnikov's function is obtained:

$$\begin{aligned} M(t_0) = {} & -a\sqrt{\frac{2}{b}}\gamma\sin t_0\int_{-\infty}^{\infty}(\mathrm{sech}\,\tau\tanh\tau\sin\omega\tau)d\tau - T_0 a\sqrt{\frac{2}{b}}\left\{\int_{-\infty}^{\infty}[\mathrm{sech}\,\tau\tanh\tau d\tau\times\right. \\ & \left.\times\mathrm{sign}(\mathrm{sech}\,\tau\tanh\tau - v_*)]d\tau\right\} - 4\beta\frac{a^4}{b^2}\int_{-\infty}^{\infty}\mathrm{sech}^4\tau\tanh^4\tau d\tau + \\ & +3\beta v_* a^3\left(\frac{2}{b}\right)^{3/2}\int_{-\infty}^{\infty}\mathrm{sech}^3\tau\tanh^3\tau d\tau + +2(\alpha - 3\beta v_*^2)\frac{a^2}{b}\int_{-\infty}^{\infty}\mathrm{sech}^2\tau\tanh^2\tau d\tau + \\ & -(\alpha - \beta v_*^2)v_* a\sqrt{\frac{2}{b}}\int_{-\infty}^{\infty}\mathrm{sech}\,\tau\tanh\tau d\tau, \end{aligned} \tag{6}$$

where $\tau = t - t_0$.

The first integral of Eq. (6) can be calculated using the method of residues and it yields

$$a\sqrt{\frac{2}{b}}\gamma\sin t_0\int_{-\infty}^{\infty}(\mathrm{sech}\,\tau\tanh\tau\sin\omega\tau)d\tau = \pi\omega a\sqrt{\frac{2}{b}}\gamma\sin t_0\,\mathrm{sech}\left(\frac{\pi\omega}{2}\right). \tag{7}$$

To calculate the second integral we use

$$v_0(\tau)\,\mathrm{sign}[v_0(\tau) - v_*] = \begin{cases} -v_0(\tau), & v_0 < v_* \\ v_0(\tau), & v_0 > v_* \end{cases} \tag{8}$$

If τ_{1*}, τ_{2*} are the solutions of $v_* = v_0(\tau) = a\sqrt{\frac{2}{b}}\,\mathrm{sech}\,\tau\tanh\tau$, then we have

$$\mathrm{sech}\,\tau_{1*} = \sqrt{\frac{1}{2} - \sqrt{\frac{1}{4} - \frac{b}{2a^2}v_*^2}} \text{ and } \mathrm{sech}\,\tau_{2*} = \sqrt{\frac{1}{2} + \sqrt{\frac{1}{4} - \frac{b}{2a^2}v_*^2}} \text{ for } v_* \le \frac{a}{\sqrt{2b}}. \tag{9}$$

Therefore, we have

$$T_0 a\sqrt{\frac{2}{b}}\int_{-\infty}^{\infty}\operatorname{sech}\tau\tanh\tau\,\operatorname{sign}\left[\operatorname{sech}\tau\tanh\tau-\nu_*\right]d\tau=$$

$$=T_0 a\sqrt{\frac{2}{b}}\left[-\int_{-\infty}^{\tau_{1*}}\operatorname{sech}\tau\tanh\tau d\tau+\int_{\tau_{1*}}^{\tau_{2*}}\operatorname{sech}\tau\tanh\tau d\tau-\int_{\tau_{2*}}^{\infty}\operatorname{sech}\tau\tanh\tau d\tau\right]= \quad (10)$$

$$=2T_0 a\sqrt{\frac{2}{b}}\left[\sqrt{\frac{1}{2}+\sqrt{\frac{1}{4}-\frac{b}{2a^2}\nu_*^2}}-\sqrt{\frac{1}{2}-\sqrt{\frac{1}{4}-\frac{b}{2a^2}\nu_*^2}}\right].$$

If $\nu_* > \frac{a}{\sqrt{2b}}$ then $\tau_* \notin \mathbf{R}$ and

$$T_0 a\sqrt{\frac{2}{b}}\int_{-\infty}^{\infty}\operatorname{sech}\tau\tanh\tau\,\operatorname{sign}\left[\operatorname{sech}\tau\tanh\tau-\nu_*\right]d\tau=T_0 a\sqrt{\frac{2}{b}}\int_{-\infty}^{\infty}\operatorname{sech}\tau\tanh\tau d\tau=0. \quad (11)$$

Calculating the rest of the integrals, we finally obtain

$$M(t_0)=-a\sqrt{\frac{2}{b}}\pi\gamma\omega\operatorname{sech}\left(\frac{\pi\omega}{2}\right)\sin\omega t_0-\frac{16}{35}\beta\frac{a^4}{b^2}+\frac{4}{3}\left(\alpha-3\beta\nu_*^2\right)\frac{a^2}{b}+$$

$$-\begin{cases}2T_0 a\sqrt{\frac{2}{b}}\left[\sqrt{\frac{1}{2}+\sqrt{\frac{1}{4}-\frac{b}{2a^2}\nu_*^2}}-\sqrt{\frac{1}{2}-\sqrt{\frac{1}{4}-\frac{b}{2a^2}\nu_*^2}}\right] & \text{for } \nu_*<\frac{a}{\sqrt{2b}}\\ 0 & \text{for } \nu_*\geq\frac{a}{\sqrt{2b}}.\end{cases} \quad (12)$$

Then, the Melnikov's criterion of chaos is given by

$$\pi\gamma\omega\operatorname{sech}\left(\frac{\pi\omega}{2}\right)>\frac{16}{35}\beta\frac{a^3}{b\sqrt{2b}}-\frac{4}{3}\left(\alpha-3\beta\nu_*^2\right)\frac{a}{\sqrt{2b}}+$$

$$+\begin{cases}2T_0\left[\sqrt{\frac{1}{2}+\sqrt{\frac{1}{4}-\frac{b}{2a^2}\nu_*^2}}-\sqrt{\frac{1}{2}-\sqrt{\frac{1}{4}-\frac{b}{2a^2}\nu_*^2}}\right] & \text{for } \nu_*<\frac{a}{\sqrt{2b}}\\ 0 & \text{for } \nu_*\geq\frac{a}{\sqrt{2b}}.\end{cases} \quad (13)$$

The obtained results are shown in the (γ,ν_*) plane in Fig. 1.

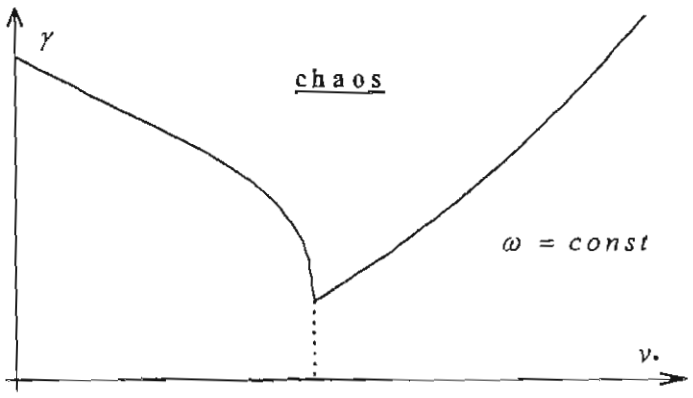

Fig. 1. Chaotic threshold in the (γ,ν_*) plane.

3. Concluding Remarks

In order to check a validity of our results we have taken $a = b = 1$, $\alpha = \beta = T_0 = 0.3$, $\omega = 2$, $\nu_* = 0.4$ and we have obtained $\gamma_c = 0.64$. The MATLAB-SIMULINK package has been used to simulate the analysed system. The obtained results are shown in Fig. 2 and illustrate a good agreement with the analytical method used.

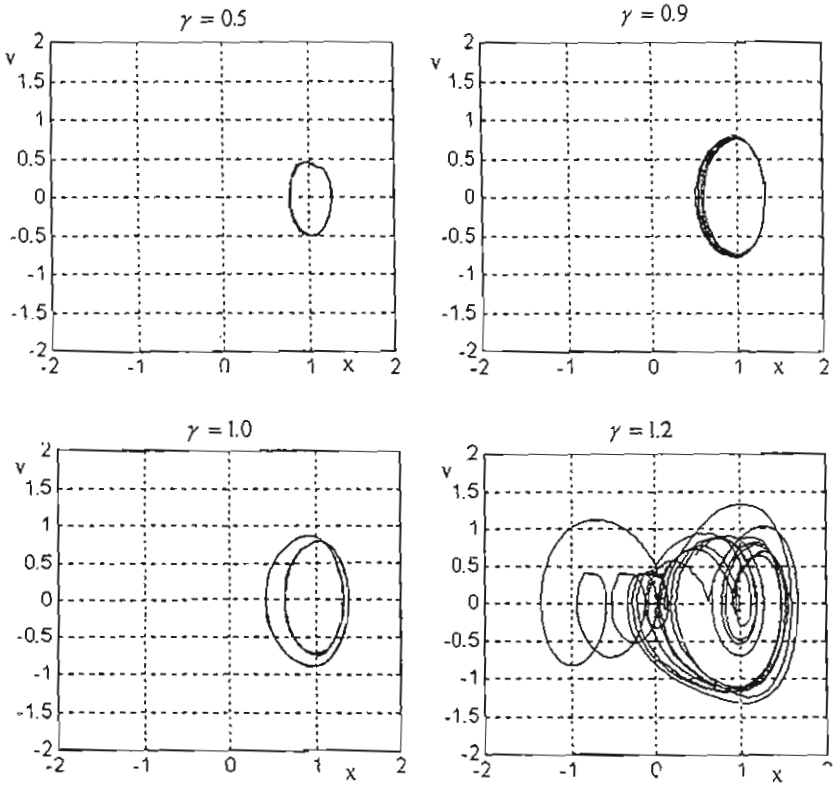

Fig. 2. Phase portraits of the analysed system for different values of γ parameter.

References

Andrianov, A. A., Vitt, A. A. & Khaikin, S. E. [1966] *Theory of Oscillators* (Pergamon Press).

Awrejcewicz, J. & Delfs, J. [1990] "Dynamics of a self-excited stick-slip oscillator with two degrees of freedom. Part I. Investigation of equilibria", *European J. Mech. A/Sol.* **9**(4), 269-282.

Awrejcewicz, J. & Delfs, J. [1990] "Dynamics of a self-excited stick-slip oscillator with two degrees of freedom. Part II. Slip-stick, slip-slip, stick-slip transitions, periodic and chaotic orbits", *European J. Mech. A/Sol.* **9**(5), 397-418.

Stoker, J. J. [1950] *Nonlinear Vibrations* (Interscience Publishers, New York).

CHAOS IMPLIES EXTREMELY HIGH ORDER

J. Awrejcewicz, †C.-H. Lamarque
Technical University of Lódź, Division of Control and Biomechanics (I-10)
1/15 Stefanowskiego St., 90-924 Lódź, POLAND
Tel: (4842) 312225; Fax: (4842) 361383
†Département Génie Civil et Bâtiment, Ecole Nationale des Travaux
Publics de l'Etat, Rue Maurice Audin - 69518, Vaulx-en-Velin Cedex, FRANCE
Tel: (33) 72047066; Fax: (33) 72047156

Abstract. Chaotic and hyperchaotic behaviour of the Chossat-Golubitsky map is analyzed.

1 Introduction

In this paper an attention is focused on exploring dynamical properties of aperiodic behaviour displayed by two-dimensional maps. A key investigation is oriented on an symmetry property analysis based on consideration of simple symmetric maps rather than an artificial construction of a system of coupled oscillators with symmetry. The Chossat-Golubitsky map [Chossat, Golubitsky 1988] (symmetric and non-invertible) is used and it exhibits periodic, quasi-periodic, chaotic and hyperchaotic dynamics and a great number of bifurcations. Among others, a sudden change of regular dynamics has been explained via a saddle (period-8) - node (period-4) bifurcation occurring on a boundary of the umbrella-shape set of saddles and a sudden route to infinity via the crisis of two peculiar structures of saddles on the border of the period-4 unstable orbits set are illustrated and analyzed.

2 Results and Conclusions

The numerical techniques applied are described in references [Nusse & Yorke, 1994; Awrejcewicz 1991; Parker & Chua, 1989]. Consider the Chossat-Golubitsky map

$$Z \to \left(A\left|Z^2\right| + B\,\mathrm{Re}\left(Z^{\mathrm{I}}\right) + C\right) Z + D\left(Z^*\right)^{\mathrm{I}-1}, \tag{1}$$

where: $Z = X + \mathrm{i}Y$ $(\mathrm{i}^2 = -1)$, $Z^* = X - \mathrm{i}Y$, $A, B, C, D \in \mathbb{R}$, $\mathrm{I} \in I$ (integer) and $A = 1.0$, $C = -1.775$, $D = 0.5$, $\mathrm{I} = 5$ For $B = 0.1$ we have the umbrella-like attractor and a set of period-4 orbits (Fig. 1a, b).

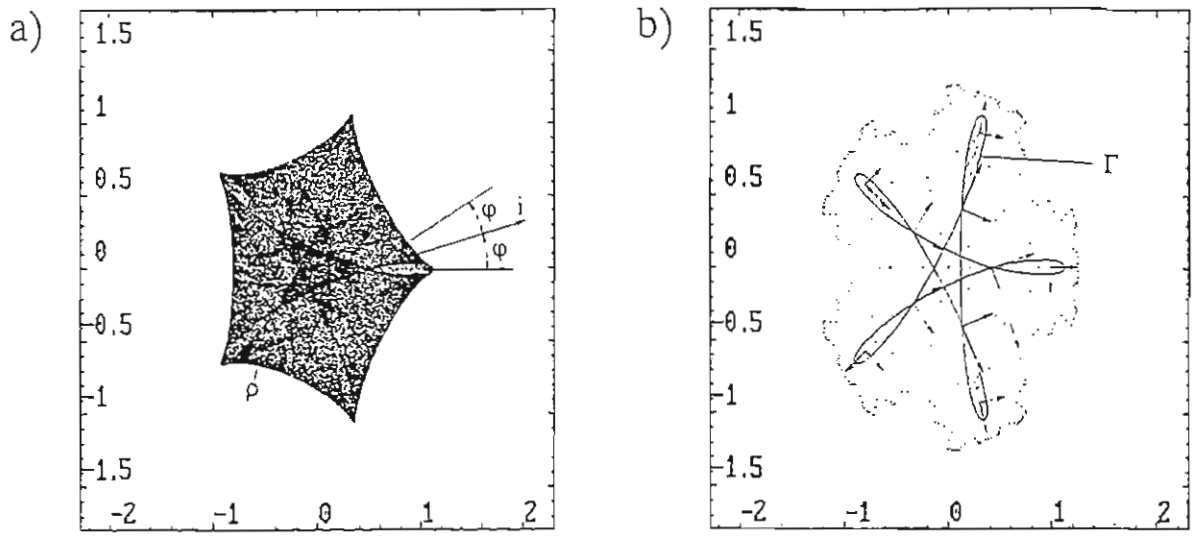

Fig. 1: The umbrella hyperchaotic attractor with the Lyapunov numbers 1.48 and 1.25 (a) and a set of the period-4 orbits with marked eigenvectors (b)

In Fig. 1a one can see arcs intersecting each other and creating a star-like set of points. These curves (invariant) are repeated again in Fig. 1b and it is seen that the period-4 orbit (previously stable) has appeared and it lies in the five dashed leave-like areas. Now these points are saddles with the eigenvalues $\sigma_1 = -7.07$ and $\sigma_2 = 6.12$ and with the marked eigenvectors. In the case of the points lying on the star-like spikes, they are also saddles with the same eigenvalues and marked eigenvectors with one exception – in the right arm of the star there is another point with the very large, approximately opposite situated eigenvectors $(1.125 \cdot 10^9)$ and $(1.17 \cdot 10^9)$. Note that the eigenvectors of the three points described are tangent to the marked curve and their directions indicate that the points cannot move along this curve. (Note that here a tangent is a generalization of the classical tangent).

Let us focus our attention on a tangency structure of 1 - set in $\mathbb{R}^2$ and divide an original hyperchaotic set (Fig. 1) into two sets

$$S = \bigcup_{i=2} S_i, \tag{2}$$

where $S_1 = \Gamma$ corresponds to the extracted set of points presented in Fig. 1b. Approximating the umbrella-like set by infinitely many points, Γ becomes a continuous and compact set. Because $F : (X_i, Y_i) \to \mathbb{R}^2$ is a continuous map and $F(X_1, Y_1) \neq F(X_2, Y_2)$, then $F[(X_1, Y_1), (X_2, Y_2)]$ contains a curve joining $F(X_1, Y_1)$ and $F(X_2, Y_2)$. On the

basis of iterations we have a curve (the map is non-invertible). As a result of such an approach we get a curve, which is a regular 1-set, and $(S - \Gamma)$ which is an irregular, so-called "curve-free" set.

The points in Fig. 1a are mainly concentrated along the extracted curve Γ, and the condition of "all points" can be substituted by "almost all". Regular curves are characterized by tangents, and according to Besicovitch [Falconer 1985] our set in $\mathbb{R}^2$ has a tangent at (X, Y) in a direction of the unit vector $\bar{i}\,(i_x,\, i_y)$ if

$$\overline{D}^{\delta}\left(S,(X,Y)\right) > 0 \wedge \bigwedge_{\varphi>0} \lim_{r\to 0} D_H\left(S \cap \left(B_r\left(X,Y\right) \setminus s\left((X,Y)\,\bar{i},\varphi\right)\right)\right) = 0, \tag{3}$$

where

$$\overline{D}^{\delta}\left(S,\,(X,\,Y)\right) = \lim_{r\to 0} \frac{D_H\left(S \cap B_r\left(X,\,Y\right)\right)}{(2r)^{\delta}}, \tag{4}$$

and $S\left((X,Y)\,\bar{i},\varphi\right)$ denotes a double sector with the (X,Y) vertex and 2φ angle (see Fig. 1a). (Note that here φ is small enough in order to separate another branch of the Γ curve). Such a description is intuitively true, because a tangent traces a direction with significantly many more points than the rest of the points in the marked sector.

The most interesting phenomenon detected here is that the corresponding five vortexes of the star correspond to the period-4 saddle with the above mentioned eigenvalues and eigenvectors. It means (from a topological point of view) that a regular subset of the irregular strange attractor is controlled by the eigenvectors of particular periodic orbits (here period-4). Because Γ can be treated as the rectifiable curve, then it possesses a tangent at almost all its points, which implies its differentiability in almost all points. Increasing continuously the control parameter, we have observed that the star spikes move towards the border of the limit points. The explosion takes place exactly when these points touch the border. At this critical state we have observed a specially organized structures of the eigenvectors (they are parallel correspondingly), whereas two eigenvectors with a very high length become parallel reaching (probably) the plus and minus infinity, which causes that the infinity becomes the attractor.

We have investigated the B parameter interval where only the 2-periodic orbit has been found, this time looking for the unstable periodic orbits and we have found infinitely many of them to form a non-attracting invariant chaotic saddle which exhibits

the horseshoe-like dynamics. During the increase of B, a structure as well as stability of this invariant set changes and also, correspondingly, a chaotic attractor suddenly appears or vanishes as a result of an interior crisis (a collision between the chaotic saddle with the stable period-14 orbit or vice-versa, i.e. a collision between the chaotic attractor and the unstable period-14 orbit).

Note that a structure of the chaotic attractor is a result of extremely high order (which has its limit in infinity) of infinitely many flip and regular saddle-type periodic orbits. To exhibit and analyse this structure we limit our consideration to $B = -0.01592$. During numerical simulations we have observed how the period-1 saddles create a boundary of the bounded region of the phase space which then is more strongly established by the period-3 and 6 orbits. Because it is easy to recognise (during computer simulations) that the period-14 saddle orbit traces a shape of the chaotic attractor, therefore, we have concluded that the chaotic strange attractor is a result of the collision between the unstable period-14 saddle orbit and the stable period-14 orbit. Note also that during a further increase of B parameter, an activity of other periodic saddles is invoked.

References

Nusse, H. E. & Yorke, J. A. [1994] *Dynamics: numerical explanations.* Springer Verlag, New York.

Parker, T. S. & Chua, L. O. [1989] *Practical numerical algorithms for chaotic systems.* Springer Verlag, New York.

Awrejcewicz, J. [1994] *Bifurcation and chaos in coupled oscillators.* World Scientific, Singapore.

Chossat, P. & Golubitsky, M. [1988] *Symmetry increasing bifurcation of chaotic attractors.* Physica 32D, 423-436.

Falconer, K. J. [1985] *The geometry of fractal sets.* Cambridge.

CONTROLLING SYSTEMS WITH IMPACTS

J. Awrejcewicz, K. Tomczak, †C.-H. Lamarque
Technical University of Lódź, Division of Control and Biomechanics (I-10),
1/15 Stefanowskiego Str., 90-924 Lódź, POLAND
†Département Génie Civil et Bâtiment, Ecole Nationale des Travaux
Publics de l'Etat, Rue Maurice Audin - 69518, Vaulx-en-Velin Cedex, FRANCE

Abstract. The method of controlling and improvement of stability of periodic orbits of vibro-impact systems is proposed. This method is based on the feedback loop control with a time delay.

1 Introduction

In this paper we consider control of steady-state vibro-impact motion with a possibility of its stability improvement. The vibro-impact dynamics can be observed in hammer-like devices, ball and race dynamics, a ball bearing assembly, and, depending on a purpose, stabilisation or destabilisation of the vibro-impact periodic motion is needed. Although there are many control methods (feedback control with a time delay, sliding mode control, repetitive control, iterative learning control, adaptive control) an applied control usually proposed is on a basis on the numerical observations of the required results by an introduction of the control coefficients [Hara it et al., 1988; Arimoto, 1990; Slotine & Li, 1991; Youcef-Toumi & Wu, 1992]. In this paper we are focused on the vibro-impact dynamics control with a delay feedback supported by an analytical prediction.

2 Delay Feedback Control

The analysed one-degree-of-freedom vibro-impact system is governed by the following equation

$$\ddot{x} + c\dot{x} + \alpha^2 x = P_0 \cos\omega t + A\left[x(t) - x(t-T)\right] + B\left[\dot{x}(t) - \dot{x}(t-T)\right], \tag{1}$$

where: $P_0 = y_0 k_2/m$, $c = c_1/m$, $\alpha^2 = (k_1 + k_2)/m$, $A = k_2 a/m$, $B = k_2 b/m$, and $T = 2\pi/\omega$. Above y_0 and ω are the amplitude and the frequency of kinematic excitation; k_1, k_2 are the stiffnesses coefficients; c_1 is the damping coefficient; m is the mass; a, b are control coefficients.

A key point of such a control is that a periodic solution possesses the same period as the excitation, i.e. $x_0 = x_0(t - T)$, and x_0 is a particular solution of both the controlled and uncontrolled system [Krodkiewski & Faragher, 1995].

We assume damping of the same order as ε, and from (1) we obtain

$$\ddot{x} + \alpha^2 x = P_0 \cos\omega t + \varepsilon A\left[x(t) - x(t-T)\right] + \varepsilon B\left[\left(1 - \frac{c}{B}\right)\dot{x}(t) - \dot{x}(t-T)\right]. \tag{2}$$

Introducing

$$x = z + \frac{P_0}{\alpha^2 - \omega^2}\cos\omega t, \tag{3}$$

we get

$$\ddot{z} + \alpha^2 z = \varepsilon f(a, \eta, \psi), \tag{4}$$

where:

$$f(a,\eta,\psi) = \varepsilon A\left[z + \frac{P_0}{\alpha^2-\omega^2}\cos\omega t - z(t-T) - \frac{P_0}{\alpha^2-\omega^2}\cos\omega(t-T)\right] +$$
$$+\varepsilon B\left[\left(1-\frac{c}{B}\right)\left(\dot{z} - \frac{P_0\omega}{\alpha^2-\omega^2}\sin\omega t\right) - \dot{z}(t-T) + \frac{P_0\omega}{\alpha^2-\omega^2}\sin\omega(t-T)\right],$$
$$\eta = \omega t, \quad \psi = \alpha t.$$

Using the KBM method we have truncated the ε series up to the order $O(\varepsilon)$ and after integration of the two first ordered ODE's we get

$$x = \frac{P_0}{\alpha^2-\omega^2}\cos(\omega t + \varphi) + \mathrm{e}^{Rt}(C\cos\alpha_0 t + D\sin\alpha_0 t), \tag{5}$$

where:

$$a(t) = C_0\mathrm{e}^{Rt}, \quad \psi(t) = \alpha_0 t + \theta_0, \quad R = \frac{1}{2\alpha}\left\{A\sin\alpha T - \omega\left[c - B(1-\cos\alpha T)\right]\right\},$$
$$\alpha_0 = \alpha - \frac{A}{2\alpha}(1-\cos\alpha T) + \frac{B\omega}{2\alpha}\sin\alpha T, \quad C = C_0\cos\theta_0, \quad D = -C_0\sin\theta_0, \tag{6}$$
$$C_0 = \sqrt{C^2 + D^2}.$$

3 Stability Control

Before the impact number l, the mass possesses the velocity x_{l-}. This causes the following perturbation solution to occur

$$x + \delta x_l = \mathrm{e}^{R\tau_l}\left[(C + \delta C_l)\cos\alpha_0\tau_l + (D + \delta D_l)\sin\alpha_0\tau_l\right] + a\cos(\omega\tau_l + \varphi + \delta\varphi_l). \tag{7}$$

A new time τ is measured from the l-th impact $\tau_l = \tau + \delta\tau_l$. For example, the next impact occurs for $\tau_{l+1} = \frac{2\pi}{\omega} + \delta T_l$, where δT_l denotes the period $T = 2\pi/\omega$ perturbation.

The following boundary conditions are introduced:

$$\begin{aligned} &l: \quad \tau = 0, \quad \delta\tau_l = 0, \quad \delta x_l = 0, \quad \delta\dot{x}_l = \delta\dot{x}_{l+}, \\ &l+1: \quad \tau = \frac{2\pi k}{\omega} + \delta\tau_l, \quad \delta\tau_l = \delta T_l, \quad \delta x_l = 0, \quad \delta\dot{x}_l = \delta\dot{x}_{(l+1)-}. \end{aligned} \tag{8}$$

After some calculations we have obtained the following equations

$$\begin{aligned} &\delta C_l - a\delta\varphi_l\sin\varphi = 0, \\ &\mathrm{e}^{2\beta R}\left[(\delta\varphi_{l+1} - \delta\varphi_l)\frac{RC - \alpha_0 C\tan\beta\alpha_0}{\omega} + \delta C_l\cos 2\beta\alpha_0 + \delta D_l\sin 2\beta\alpha_0\right] - \delta C_{l+1} = 0, \\ &R_\tau\mathrm{e}^{2\beta R}\left[(\delta\varphi_{l+1} - \delta\varphi_l)\frac{(R^2 - \alpha_0^2)C - 2R\alpha_0 C\tan\beta\alpha_0}{\omega} + R\delta C_l\cos 2\beta\alpha_0 + R\delta D_l\sin 2\beta\alpha_0\right. \\ &\quad \left. -\delta C_l\alpha_0\sin 2\beta\alpha_0\right] + R\delta C_{l+1} + \alpha_0\delta D_{l+1} - (R_\tau + 1)a\omega\delta\varphi_{l+1}\cos\varphi = 0, \end{aligned} \tag{9}$$

where $\beta = \pi k/\omega$ and $R_r \leq 1$ as usual denotes the restitution coefficient.

Assuming that

$$\delta\varphi_l = \delta\varphi_0 + \sum_{i=1}^{l} \omega \delta T_i, \tag{10}$$

and introducing

$$\delta C_l = a_1\gamma^l, \quad \delta D_l = a_2\gamma^l, \quad \delta\varphi_l = a_3\gamma^l \tag{11}$$

we get the following characteristic equation

$$b_2\gamma^2 + b_1\gamma + b_0 = 0, \tag{12}$$

where:

$$\begin{aligned}
b_2 &= \left(-\mathrm{e}^{2\beta R}\frac{RC - \alpha_0 C\tan\beta\alpha_0}{\omega} + a\sin\varphi\right)\alpha_0, \\
b_1 &= \mathrm{e}^{2\beta R}\sin 2\beta\alpha_0\left[R_r\mathrm{e}^{2\beta R}\frac{(R^2-\alpha_0^2)C - 2R\alpha_0 C\tan\beta\alpha_0}{\omega} - (R_r+1)a\omega\cos\varphi\right] \\
&\quad -\mathrm{e}^{4\beta R}R_r\frac{RC-\alpha_0 C\tan\beta\alpha_0}{\omega}(R\sin 2\beta\alpha_0 + \alpha_0\cos 2\beta\alpha_0) + \\
&\quad +\alpha_0\mathrm{e}^{2\beta R}\frac{RC-\alpha_0 C\tan\beta\alpha_0}{\omega} - a\mathrm{e}^{2\beta R}\sin\varphi\left[\alpha_0\cos 2\beta\alpha_0 + \right. \\
&\quad \left. -R_r(R\sin 2\beta\alpha_0 + \alpha_0\cos 2\beta\alpha_0) - R\sin 2\beta\alpha_0\right], \\
b_0 &= R_r\mathrm{e}^{4\beta R}\sin 2\beta\alpha_0\frac{(R^2-\alpha_0^2)C - 2R\alpha_0 C\tan\beta\alpha_0}{\omega} + \\
&\quad +R_r\mathrm{e}^{4\beta R}\frac{RC-\alpha_0 C\tan\beta\alpha_0}{\omega}(R\sin 2\beta\alpha_0 + \alpha_0\cos 2\beta\alpha_0) + \\
&\quad -aR_r\mathrm{e}^{4\beta R}\sin\varphi\left[\cos 2\beta\alpha_0\,(R\sin 2\beta\alpha_0 + \alpha_0\cos 2\beta\alpha_0) + \right. \\
&\quad \left. +\sin 2\beta\alpha_0\,(R\cos 2\beta\alpha_0 - \alpha_0\sin 2\beta\alpha_0)\right].
\end{aligned} \tag{13}$$

The problem of stability is reduced to consideration of the second order characteristic Eq. (11). If the roots of Eq. (12) are $|\gamma_{1,2}| < 1$, then according to the assumed solutions (11) δC_l, δD_l and $\delta\varphi_l$ approach zero for $l \to \infty$, and the solutions will be asymptotically stable.

4 Simulation Results and Conclusions

During numerical simulations we have used the MATLAB-Simulink package and the MATLAB-model for equation (1) with the boundary conditions.

We have taken the following parameters: $m = 1[kg]$, $k_1 = 3[N/m]$, $k_2 = 1[N/m]$, $c_1 = 0$ $[Ns/m]$, $x_0 = 1[m]$, $T = 0.4\pi[s]$, $R_r = 0.65$, $s = 0.01[m]$, $a = -0.01[N/m]$, $b = -0.045[Ns/m]$.

For these parameters according to (6) we get $R = -0.103$, which shows that the delay loop control coefficients A and B allow us to obtain quicker damping of free oscillations in the solution (5) than without control (Fig. 1). Additionally, for the given parameters we have

found from Eq. (12) that $|\gamma_{1,2}|$ are lying closer to the origin for the system with the control coefficients than without control (with the delay loop $|\gamma_{1,2}| = 0.576$, whereas without the loop $|\gamma_{1,2}| = 0.65$).

For the given parameters numerical simulations confirm analytical predictions.

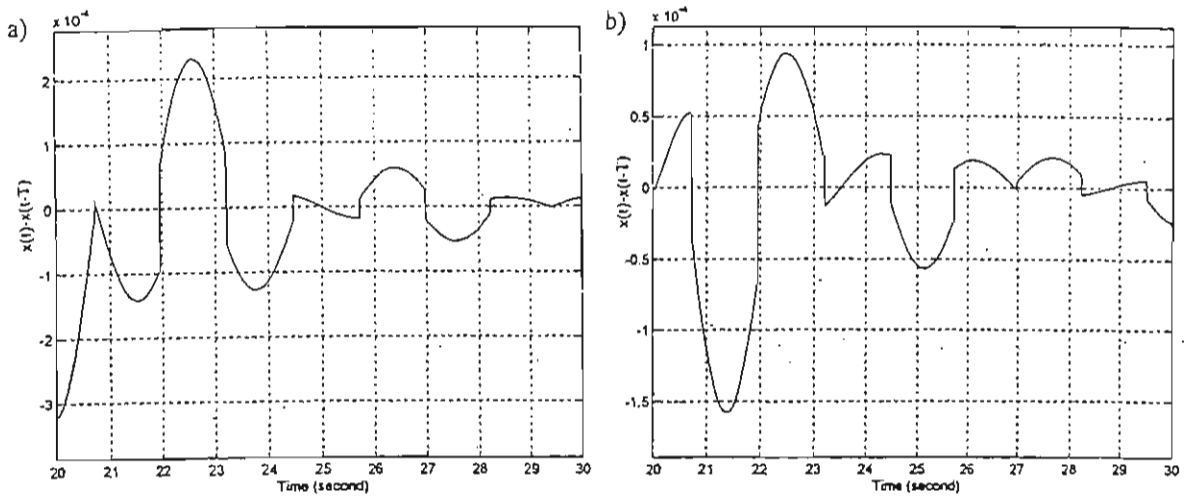

Fig. 1: Difference between two transients $x(t) - x(t-T)$ approaching periodic orbit for the system: (a) without control and (b) with control ($a = -0.01$, $b = -0.045$)

It can be seen in Fig. 1, that with control the transients vanish quicker than in the case without control. In the case presented above the periodic orbit is achieved after about 24.1 seconds for the system analysed without the delay loop and after 21.8 seconds for the system analysed with the delay loop ($|\mu| \leq 10^{-4}$), respectively.

References

Hara, S.; Yamamoto, Y.; Omata, T. & Nokano, M. [1988] "Repetitive Control System: A New Type Servo System for Periodic Exogenous Signals", *IEEE Transactions on Automatic Control*, Vol. 33, No 7, pp. 659-668.

Arimoto, S. [1990] "Learning Control Theory for Robotic Motion". *International Journal of Adaptive Control and Signal Processing*, Vol. 4, pp. 549-564.

Slotine, J.-J.E. & Li, W. [1991] *Applied Nonlinear Control* (Prentice-Hall, Englewood Cliffs, New Jersey).

Youncef-Toumi, K. & Wu, S.-T. [1992] "Input-Output Linearization Using Time Delay Control", *Journal of Dynamics Systems, Measurement and Control*, Vol. 114, pp. 10-19.

Krodkiewski, J.M. & Faragher, J.-S. [1995] "Stability of the Periodic Motion of Non-linear Systems", *Proceedings of the International Conference on Vibration and Noise*, Venice.

On Synchronization and Anti-Synchronization in Piecewise Linear Systems.

M.A. Aziz Alaoui(*) and A.N. Sharkovsky(**)

(*) Laboratoire GEMH, Université du Havre
Faculté des Sciences, BP 540 76058
LeHavre cedex, France. Fax 33. 35. 19. 57. 15
Tel 35 19 57 17; e.mail aziz@fst.univ-lehavre.fr

(**) Institute of Mathematics, National Academy of Sciences, 252601 Kiev, Ukraine
e.mail : asharkov@math.carrier.kiev.ua

Abstract : The purpose of this paper is to present some results on the synchronization and anti-synchronization of chaotic systems. A new algorithm is developed to recover a trajectory of a chaotic piecewise linear system from its $\varepsilon-$trajectory. Such a problem may be applied to the extraction of an information bearing signal from an input signal.

1 Introduction

Recently, there has been much interest in the chaotic synchronization and control of dynamical systems, following various methods leading to various applications, for example encoding electronic messages for secure communications, [Pecora & Carroll, 1990 ; Kocarev et al, 1992 ; Lozi & Chua, 1993 ; Lozi & Aziz-Alaoui, 1994] and other references given in the bibliography, theoritical results can be found in Wu & Chua [1994].

Chua's circuit, which is well known to exhibit a strong strange attractor [Chua 1992], is often used as a basic model. One essential property of a chaotic signal is that it is not asymptotically stable, for chaotic systems there is sensitive dependance on intial data and every trajectory on the strange attractor is unstable. Synchronization of all corresponding variables is possible only if there are control connections between the systems which have to synchronize, thereby generating one new connected system. In the classical methods, to prove synchronization, we require the computation of numerical quantities as conditional Lyapunov exponents. But, if there are no control connections between the systems then generally one cannot resolve by means of synchronization the problem of extracting the information bearing signal $s_i, i = 0, 1 \cdots$ from the input signal $\bar{x}_i = x_i + s_i$, where x_i is some unknown trajectory of one of the receiving systems. Let us note that this problem is equivalent to the problem of recovering the trajectory x_i of the system from its $\varepsilon-$trajectory $\bar{x}_i$, [Sharkovsky, 1995].

For these reasons the notion of anti-synchronization, which we give here, may be useful.

2 Synchronization and Anti-Synchronization

2.1 Definitions and main theorem

In this section we will define the notion of anti-synchronization in one or more dimensionnal dynamical systems, and we will give the main result. Let us first give some necessary definitions; most of them are done for discrete one-dimensional dynamical systems, but they may be easily written for any dimension and also in continuous time.

Definition 1. *The sequence $\bar{x}_0, \bar{x}_1, \cdots, \bar{x}_N$ is an* $\varepsilon-$**trajectory** *of a dynamical system $x_{n+1} = f(x_n)$, if $|\bar{x}_i - f(\bar{x}_i)| < \varepsilon$ for $i = 0, 1, \cdots, N-1$.*

It has long been known that certain well-behaved maps exhibit shadowing property. For example numerical computations can lead to spurious results because of finite floating point arithmetic. Near a numerically computed orbit there exists a *true* orbit which, however, may be the orbit of a different initial value than the one intended, see Bowen [1975]. There is below a definition of this important property which has been established at some parameter values of various maps (the logistic one for example, [Hammel et al, 1987]), and which holds for structurally stable systems.

Definition 2. *A dynamical system $x_{n+1} = f(x_n)$ has the* **shadowing property** *if there exists $\varepsilon_0 > 0$ such that for any $\varepsilon-$trajectory $\bar{x}_0, \bar{x}_1, \cdots, \bar{x}_N$ with $\varepsilon < \varepsilon_0$, the dynamical system has trajectory $x_0, x_1, \cdots, x_N$ such that $|\bar{x}_i - x_i| < \varepsilon$ for $i = 0, 1, \cdots, N$.*

For dynamical systems (both in continuous and discrete time) which have this property, the problem of reconstructing trajectory from some $\varepsilon-$trajectory, can be successfully resolved in admissible time.

Definition 3. *A dynamical system $x_{n+1} = f(x_n)$ has the* **anti-synchronization** *property if there exist $\varepsilon_0 > 0$ and λ, $0 < \lambda < 1$, such that for any two $\varepsilon-$closed (with $\varepsilon \leq \varepsilon_0$) trajectories $x_0, x_1, \cdots, x_N$ and $x'_0, x'_1, \cdots, x'_N$ (that is $|x_i - x'_i| < \varepsilon$ for $i = 0, 1, \cdots, N$), we have $|x_0 - x'_0| < const \times \lambda^N$.*

This definition may be generalized in an obvious way to systems of any dimension and to continuous-time systems.

Important remarks

1. For a dynamical system having the anti-synchronization property, we can always recover any piece of any trajectory with any given accuracy by knowing some $\varepsilon-$trajectory of fairly large length which is $\varepsilon-$close to this trajectory.

2. If the dimension of a dynamical system is greater than one and there are both positive and negative Lyapunov exponents of the trajectories on the attractor of this system, the problem of the transmission of information via such a system is resolved by the use of both synchronization effects (for the negative exponents) and anti-synchronization effects (for the positive exponents).

We can now come to the main result given in the following theorem.

Theorem 4. *: (Main result)*

Let us have a dynamical system, $f^t : X \longrightarrow X$, where X is some compact, and let $\mathcal{A} \subset X$ be a hyperbolic (strange) attractor of this system. Then there is some $\varepsilon_0 > 0$ such that for any $\varepsilon < \varepsilon_0$ and any $\varepsilon-$trajectory $\{\bar{x}_0, \bar{x}_1, \cdots, \bar{x}_N\}$ (N being sufficiently large) belonging to $\varepsilon-$neighbourhood of the attractor $\mathcal{A}$, there exists (true) trajectory $\{x_0, x_1, \cdots, x_N\}$ on $\mathcal{A}$ such that $||\bar{x}_i - x_i|| < \varepsilon$ for $0 \leq i \leq N$.

Furthermore, for any $\delta > 0$ there exist $m_1, m_2 > 0$ ($m_1 + m_2 < N$) such that for any two trajectories $\{x_0^{(q)}, x_1^{(q)}, \cdots, x_N^{(q)}\}$ ($q = 1, 2$) on $\mathcal{A}$ for which $||\bar{x}_i - x_i^{(q)}|| < \varepsilon$ for $0 \leq i \leq N$ and $q \in \{1, 2\}$, we have $||x_i^{(1)} - x_i^{(2)}|| < \delta$ for $m_1 \leq i \leq N - m_2$.

Corollary Under the same hypothesis, if $\bar{x}_i = x_i + s_i$, $0 \leq i \leq N$, with $|s_i| < \varepsilon$, then for any $\delta > 0$, there are $m_1, m_2 > 0$ such that each trajectory $x'_i, i = 0, 1, \cdots, N$ for which $|\bar{x}_i - x'_i| < \varepsilon$ if $o \leq i \leq N$ on the time interval $[m_1, N - m_2]$ has the following property: $|x'_i - x_i| < \delta$ and thus $|s'_i - s_i| < \delta$ where $s'_i = \bar{x}_i - x'_i$, $m_1 \leq i \leq N - m_2$.

2.2 Algorithm for piecewise linear systems

Let s_i be an information bearing signal and $\bar{x}_i = x_i + s_i$ be the input signal, where x_i is some unknown trajectory of one of the receiving systems. We want to realize secure communications via a strange attractor, then to extract s_i, $i = 0, 1, \cdots$ from $\bar{x}_i$; (this problem is equivalent to the problem of recovering the trajectory x_i, $i = 0, 1, \cdots$ of the system from its $\varepsilon-$trajectory $\bar{x}_i$, $i = 0, 1, \cdots$).

For that purpose we have to realize an algorithm and to write a program to find x'_i if we know $\bar{x}_i$. We use Lozi-map, f, as an example. This map exhibits a hyperbolic strange attractor, it is given as follows :

$$\begin{cases} x_{n+1} &= - a|x_n| + y + 1 \\ y_{n+1} &= bx_n \end{cases}$$

Let λ_j, $j = 1, 2$ denote the Lyapunov exponents of the map f, the main steps of our algorithm can be summed up as follows :

(i) Firstly, for a given initial condition (x_0, y_0), we have two sequences $\{\bar{x}_0, \bar{x}_1, \cdots, \bar{x}_i, \cdots\}$, $(\bar{x}_i = x_i + s_i)$,with $|\bar{x}_i - x_i| < \varepsilon$ and $\{\bar{y}_1, \bar{y}_2, \cdots, \bar{y}_i, \cdots\}$, with $|\bar{y}_i - y_i| < \varepsilon'$, (for Lozi-map, $\varepsilon' = b\varepsilon$).

Let us denote k_i and m_i $(i = 0, 1, 2 \cdots)$, the integers verifying:

. $m_0 = 0 < k_1 < m_1 < k_2 < m_2 \cdots$,

. $\bar{x}_i \geq 0$ if $m_{s-1} < i \leq k_s$, where $s = 1, 2 \cdots$,

. $\bar{x}_i < 0$ if $k_s < i \leq m_s$, where $s = 1, 2 \cdots$.

(ii) Secondly, we define the sets :

- If $|\lambda_1 \lambda_2| < 1$ (case of synchronization)
  $V_i^0 = \{(x, y) \in I\!R^2, \bar{x}_i - \varepsilon < x_i < \bar{x}_i + \varepsilon$ and $\bar{y}_i - \varepsilon < y_i < \bar{y}_i + \varepsilon\}$ if $m_{s-1} < i \leq k_s$, $s = 1, 2 \cdots$,
  $Z_i^0 = \{(x, y) \in I\!R^2, \bar{x}_i - \varepsilon < x_i < \bar{x}_i + \varepsilon$ and $\bar{y}_i - \varepsilon < y_i < \bar{y}_i + \varepsilon\}$ if $k_s < i \leq m_s$, $s = 1, 2 \cdots$,
- If $|\lambda_1 \lambda_2| > 1$ (case of anti-synchronization)
  $U_i^0 = \{(x, y) \in I\!R^2, \bar{x}_i - \varepsilon < x_i < \bar{x}_i + \varepsilon$ and $\bar{y}_i - \varepsilon < y_i < \bar{y}_i + \varepsilon\}$ if $m_{s-1} < i \leq k_s$, $s = 1, 2 \cdots$,
  $W_i^0 = \{(x, y) \in I\!R^2, \bar{x}_i - \varepsilon < x_i < \bar{x}_i + \varepsilon$ and $\bar{y}_i - \varepsilon < y_i < \bar{y}_i + \varepsilon\}$ if $k_s < i \leq m_s$, $s = 1, 2 \cdots$,

(iii) Finally, we define the sets below by iteration, for $l = 1, 2, \cdots N$,

- Case of synchronization
  $V_i^l = V_i^{l-1} \cap f(V_{i-1}^{l-1})$, if $m_{s-1} < i \leq k_s$, $s = 1, 2 \cdots$,
  $Z_i^l = Z_i^{l-1} \cap f(Z_{i-1}^{l-1})$, if $k_s < i \leq m_s$, $s = 1, 2 \cdots$,
- Case of anti-synchronization
  $U_i^l = U_i^{l-1} \cap f^{-1}(U_{i+1}^{l-1})$, if $m_{s-1} < i \leq k_s$, $s = 1, 2 \cdots$,
  $W_i^l = W_i^{l-1} \cap f^{-1}(W_{i+1}^{l-1})$, if $k_s < i \leq m_s$, $s = 1, 2 \cdots$,

Each of these sets is a subset of the previous one (i.e. $V_i^0 \supset V_i^1 \supset V_i^2 \cdots \supset V_i^N \ni x_i$). Hence we can recover x_i with the given accuracy δ after $N(\delta)$ iterations.

3 Bibliography

Aziz-Alaoui,M.A. & Lozi,R. [1995], "Numerical Results on Nolinear Filtering for Coupled Chua Oscillators", *Proc. of 2nd Int. Conf. ODE, Marrakech.*

Bowen, R. [1975], "ω−limit set for Axiom A diffeomorphisms",*J.Differential Aquations,18.*

Carroll,T. & Pecora,L. [1992], "A circuit for Studying the Synchronization of Chaotic Systems", *Int. J. of Bifurcation and chaos Vol. 2 No 2, 659-667.*

Chua,L.O. [1992], "The Genesis of Chua's Circuit",*Int. J.Electron.comun. 46(1992) 250-257.*

Hammel,S.M., Yorke, J.A. & Grebogi,C.[1987], "Do Numerical Orbits of Chaotic Dynamical Processes Represent True Orbits?", *J. Complexity,3, 136-145.*

Hammel,S.M., Yorke, J.A. & Grebogi,C.[1988], "Numerical Orbits of Chaotic Dynamical Processes Represent True Orbits?", *Bull. Amer. Math. Soc. 19, 465-469.*

Kocarev,Lj. , Halle,K.S., Eckert,K., Chua,L.O. & Parlitz,U. [1992], "Experimental Demonstration of Secure Communication via Chaotic Synchronization", *Int. J. of Bifurcation and Chaos Vol. 2, No 3, 709-713.*

Lozi,R. & Chua,L.O. [1993],"Secure communications via chaotic synchronization II: Noise Reduction by Cascading two Identical Receivers", *Int. J. of Bifurcation and chaos, Vol. 3, No 5, 1319-1325.*

Lozi,R., & Aziz-Alaoui,M.A. [1994], "Secure Communications Via Chaotic Synchronization in Chua's Circuit: Numerical Analysis of the Errors of the Recovered Signal", *Proc. of the Symposium On Nonlinear Theory and its Application, Kagoshima, pp. 145-148.*

Pecora,L.M. & Carroll,T. [1990], "Synchronization in Chaotic Systems", *Phys. Rev. lett.* **64**,*821-824.*

Sharkovsky, A.N. [1995] "From One -dimensional to Infinite-dimensional Dynamical Systems", *Proc. of the 3rd Int. Specialist Workshop on Nolinear Dynamics of Electronic Systems. Dublin, Ireland 28-29 Jul. 95.*

Wu, C.W. & Chua,L.O. [1994], "A Unified Framework for Synchronization and Control of Dynamical Systems", *Int. J. of Bifurcation and chaos Vol. 4 No 4, 979-998.*

NON-LINEAR OSCILLATIONS OF HAMILTONIAN SYSTEM WITH ONE DEGREE OF FREEDOM ON THE BOUNDARY OF PARAMETRIC RESONANCE DOMAIN.

Dr. Boris Bardin
Post-doctoral studies, Institute B of Mechanics, University of Stuttgart
Pfaffenwaldring 9, D-70550 Stuttgart, FRG
(on leave from the Moscow Aviation Institute)

Abstract: Non-linear oscillations of a nearly integrable time-periodic Hamiltonian system with one degree of freedom are investigated in a small finite neighbourhood of its equilibrium. It is assumed that multipliers of the linearized system are multiple and the characteristic exponents $\pm iN$ are imaginary (N is an integer).

It is shown that for most initial data the motions are quasi- periodic in the neighbourhood of the equilibrium. The existence of stable 2π-periodic motions near an unstable equilibrium position is established. It is shown that, irrespective of instability, trajectories beginning sufficiently close to an equilibrium point will always remain at a finite distance from it. The chaotic nature of the motions near trajectories asymptotic to the equilibrium point is discussed.

1 Formulation of the Problem

Consider a system with one degree of freedom whose motion is described by Hamiltonian differential equation. The Hamiltonian is 2π-periodic in time t, analytic in canonical variables q, p and a small parameter ε. Assume that when $\varepsilon = 0$ the origin $q = p = 0$ is a stable equilibrium position. By an appropriate choice of variables q, p the Hamiltonian can be written in the form

$$H = \frac{1}{2}\omega(q^2 + p^2) + \frac{1}{4}c(q^2 + p^2)^2 + O((q^2 + p^2)^3) + O(\varepsilon) \tag{1}$$

where ω is a frequency of linear oscillations. We assume that the constant $c \neq 0$.

In this paper we analyze the behaviour of the system in a small finite neighbourhood of equilibrium by a parametric resonance $\omega \approx N$, where N is an integer. The case of the parametric resonance $2\omega \approx N$ was investigated in [Markeyew, 1995a].

2 Unperturbed System

In the case $\omega = N - \varepsilon\beta$ (β is a constant) the Hamiltonian can be reduced by a non-linear canonical 2π-periodic in t change of variables $q, p \to x_1, x_2$ to the form

$$\begin{aligned} H \;=\; & 2b\Big\{\frac{1}{2}\varepsilon[(\mu-1)x_1^2 + (\mu+1)x_2^2] - \varepsilon[f_{30}x_1^3 + f_{21}x_1^2x_2 + f_{12}x_1x_2^2 + f_{03}x_2^3] + \\ & \frac{1}{4}(x_1^2 + x_2^2)^2\Big\} + O((x_1^2 + x_2^2)^3) + \varepsilon O_4 + O(\varepsilon^2) \end{aligned} \tag{2}$$

where $b, \mu, f_{ij}(i + j = 3)$ are constant and O_4 denotes a series that begins with fourth- or higher order terms in the variables x_1, x_2

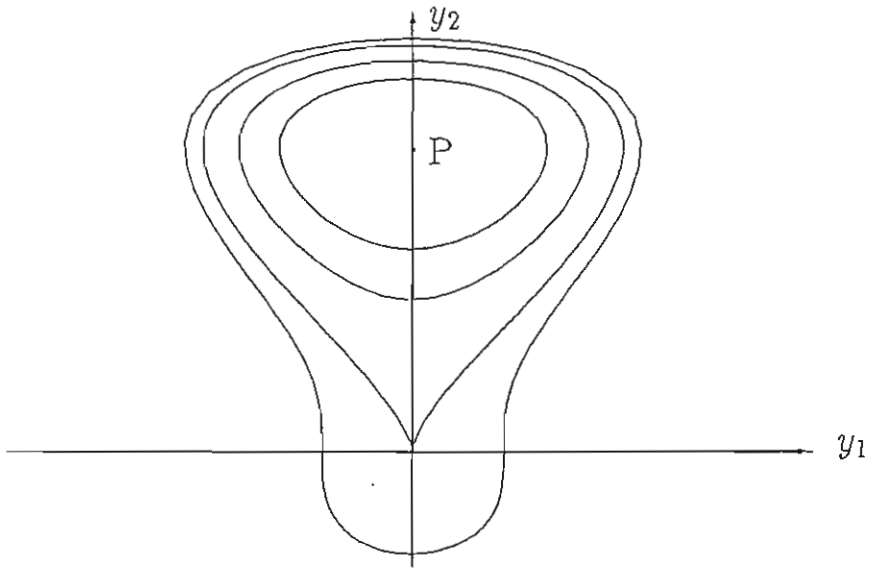

Fig.1 The phase portrait of the unperturbed system

If $|\mu| \neq 1$ then all terms of third degree of the Hamiltonian can be killed by means of a non-linear canonical change of variables. This case was investigated in [Markeyew, 1995b]. We shall investigate the case $\mu = -1$.

We introduce the variables u_1, u_2 through the generating function

$$S = x_1 u_2 - \frac{1}{2} f_{30} x_1^2 u_2 - \frac{1}{4} f_{21} x_1 u_2^2 - \frac{1}{6} f_{12} u_2^3 \tag{3}$$

and carry out rescaling by means of the formulae

$$u_1 = \varepsilon^{\frac{3}{2}} f_{03}^2 y_1, \quad u_2 = \varepsilon f_{03} y_2, \quad \tau = -2b f_{03} \varepsilon^{\frac{3}{2}} t \tag{4}$$

In the new variables y_1, y_2 the Hamiltonian has the form

$$H = y_1^2 - y_2^3 + \frac{1}{4} y_2^4 + \varepsilon \frac{1}{4} (2 f_{03}^2 y_1^2 y_2^2 - 4 f_{04}(\tau) y_2^4 - f_{03} f_{21} y_2^5) + O(\varepsilon^{\frac{3}{2}}) \tag{5}$$

where the function $f_{04}(\tau)$ is periodic in τ.

Putting $\varepsilon = 0$, we obtain a unperturbed system with the Hamiltonian

$$H_0 = y_1^2 - y_2^3 + \frac{1}{4} y_2^4 \tag{6}$$

The unperturbed system has the energy integral $H_0 = h$ and is a integrable system. Its phase portrait is shown in Fig.1. Motions of the system can occur only when $h \geq -\frac{27}{4}$. The value $h = -\frac{27}{4}$ corresponds to a equilibrium position (point P in the Fig.1) with the coordinates $y_1 = 0, \quad y_2 = 3$. If $-\frac{27}{4} < h < 0$ or $h > 0$ the phase trajectories are closed curves. The value $h = 0$ corresponds to the separatrix and the origin of coordinates.

Outside of the separatrix the solutions of the unperturbed system can be expressed in terms of elliptic functions

$$y_2 = \frac{\alpha \sqrt{\lambda}\, \mathrm{cn}(u,k) + \beta}{\sqrt{\lambda}\, \mathrm{cn}(u,k) + 1} \tag{7}$$

where $u = \omega_0(\tau - \tau_0)$, the $\lambda, \alpha, \beta, \omega_0, k$ can be expressed through the energy constant h. The quantity τ_0 is an arbitrary constant. On the separatrix we have (taking $y_1(0) = 0$)

$$y_1 = \frac{\tau}{(\tau^2 + \frac{1}{4})^2}, \quad y_2 = \frac{1}{\tau^2 + \frac{1}{4}} \tag{8}$$

Outside of the separatrix expressing in the action-angle variables w, I the Hamiltonian has the following form $H_0 = h(I)$. Calculations show that outside of the separatrix the condition for non-degeneracy of the system $\frac{d^2h}{dI^2} \neq 0$ is fulfilled.

3 Non-linear Oscillations of the Perturbed System

Consider now the perturbed system with the Hamiltonian (5). According to Ivanov & Sokol'skii [1980], Merman [1964] and Bardin [1991] its equilibrium position $y_1 = y_2 = 0$ is unstable and there are exactly two single-parameter families of asymptotic solutions, one of them tends asymptotically to the origin as $t \to +\infty$ and other as $t \to -\infty$. If, however, the asymptotic trajectories are pairwise confluent in the unperturbed system, forming separatrix, then in the full system the separatrix in general decouple [Arnold, *et al.* 1988], and there is a stochastic layer in their neighbourhood .

Since outside a sufficiently small neighbourhood of the separatrix the Hamilton function (5) written in the action-angle variables is analytic and its unperturbed part is non-degenerate, most closed trajectories in Fig.1 generate conditionally-periodic motions when $0 < \varepsilon \ll 1$ [Arnold, *et al.* 1988]. The Lebesgue measure of the completion of the set of these generating trajectories is of the order $\exp(-c_1\varepsilon^{-1})$ (where $c_1 > 0$ a constant) [Neishtadt,1981]. Thus, in spite of the fact that the equilibrium $y_1 = y_2 = 0$ is unstable in the perturbed system trajectories that begin sufficiently close to the origin of coordinates remain in a bounded neighbourhood of the origin.

According to Poincare's theory the equilibrium position P of the unperturbed system are replaced by $2\pi-$periodic (with respect variable t) motion of the full system which depend analytically on ε. Since the unperturbed system is non-degenerate, from Moser's theorem on invariant curves these periodic motions are stable.

We use Chirikov's [1977] method to obtain an estimate of the width of the stochastic layer. The general solution of the unperturbed system can be written in the form

$$y_1 = y_1(\tau + \sigma, h), \quad y_2 = y_2(\tau + \sigma, h) \tag{9}$$

where σ and h are arbitrary constant and h is the energy constant. In the full system σ and h are slowly changing functions of τ. Ignoring terms of order above $\varepsilon^{\frac{3}{2}}$ in the Hamiltonian (5) we consider the separatrix mapping

$$h_1 = h_0 + \varepsilon\chi\lambda e^{-2q\lambda}\sin\alpha_0, \quad \alpha_1 = \alpha_0 + aq\lambda|h|^{-\frac{1}{6}} \tag{10}$$

where $\alpha = q\lambda\sigma + \delta_1$, h_0, σ_0 are the value of h, σ correspondingly at $\tau = 0$ and h_1, σ_1 are the value of h, σ correspondingly over a time interval equal to one cycle of a motion near separatrix. χ, δ_1, q are some numbers and $\lambda = (2b|f_{03}|\varepsilon^{\frac{3}{2}})^{-1}$.

We linearize the mapping (10) in the neighbourhood of the stationary points $h_* = \pm (aq\lambda/2\pi n)^6$

$$P_1 = P_0 + K \sin \lambda_0, \quad \alpha_1 = \alpha_0 + P_1 \tag{11}$$

where $K = \varepsilon\chi\lambda^2 e^{-2q\lambda} qa/6h_*^{\frac{7}{6}}$. The new variable P was introduced by means the following formula

$$h = h_* - 6h_*^{\frac{7}{6}}(aq\lambda)^{-1}P \tag{12}$$

According to Chirikov's method from the condition $|K| > 1$ we determined that width of the stochastic layer is the order of $\varepsilon^2 \exp(-c\varepsilon^{-\frac{3}{2}})$, where $c = (b|f_{03}|)^{-1}$.

Acknowledgments

The author worked on this paper at the Institute for Problems of Mechanics, Russian Academy of Science and during the visits to the Institute B of Mechanics, University of Stuttgart. The research in Germany was sponsored by the Germany Service of Changes (DAAD) and in Russia by the Russian Foundation for Basic Research (93-013-16257) and International Science Foundation (MFG300). Prof. W. Schiehlen and Prof. A.P. Markeyew are gratefully acknowledged for useful discussions and their interest in this work.

References

1.Arnold, V.I., Kozlov V.V., Neishtadt A.I., [1988] *Mathematical aspects of classical mechanics.* Dynamical Systems III (Springer-Verlag, Berlin) Chap. 6, pp. 220-231.

2.Bardin, B.S. [1991] "Asymptotic solutions of Hamiltonian systems at first-order resonance", *J. Appl. Maths. Mechs.* 55(4), 469-474.

3.Chirikov, B. V. [1977] *Non-linear Resonances.* (Izd. Novosib. Gos. Univ., Novosibirsk) Chap. 4, pp. 41-61.

4.Ivanov, A. P. & Sokol'skii, A.G. [1980] "On the stability of a non-autonomous Hamiltonian system under parametric resonance of essential type", *J. Appl. Maths. Mechs.* 44(6), 687-691.

5.Markeyew, A.P. [1995a] "The behavior of a non-linear Hamiltonian system with one degree of freedom at the boundary of a parametric resonance domain", *J. Appl. Maths. Mechs.* 59(4), 541-551.

6.Markeyew, A.P. [1995b] "Parametric resonance and non-linear oscillations of a heavy solid in a neighbourhood of its planar rotations", *Mechanics of solids* 30(5), 34-44.

7.Merman, G.A. [1964] "Asymptotic solution of a canonical system with one of freedom in the case of vanishing characteristic exponents", *Bull. Inst. Teoret. Astron. Akad. Nauk SSSR* 9(6), 394-424.

8.Neishtadt,A.I. [1981] "Estimates in Kolmogorov theorem on conservation of conditionally-periodic motions", *J. Appl. Maths. Mechs.* 45(6), 766-772.

2D topological defects and solution of nonlinear boundary value problems by inverse scattering transform method

A.B.Borisov, VV.Kiseliev

Institute of Metal Physics, S.Kovalevskaya 18, GSP-170,
Ekaterinburg 620219, Russia
pressure@ufm.e-burg.su

By now inverse scattering transform (IST) method is apparently a powerful systematic tool to solve nonlinear PDE and by significance may be compared with the Fourier transforms method for the theory of linear differential equation. But from the outset IST had form suitable to solve the Cauchy problem for nonlinear equations (NE) of hyperbolic types. The 2D elliptic sine-Gordon equation

$$(\partial_x^2 + \partial_y^2)u = \sin(u) \tag{1}$$

describes in good approximation quite a lot of nonlinear phenomena in the condensed matter physics: two-dimensional Josephson junctions, magnetic films, incommensurate structures in crystals and so on. In this paper the modification of the IST is proposed to solve boundary value problems for NE with L-A pairs.

Single vortex with topological charge $Q = \oint \nabla u \cdot dr$, dipoles of vortices with $Q = \pm 1, \pm 2, ...$ have been studied using IST modification proposed in [1, 2, 3, 4]. The outline of our procedure is following: 1) the direct and inverse problems are considered in both half- plane $x > 0$ and $x < 0$ separately, 2) the boundary conditions when allow us to determine only part of the scattering data, 3) we match the scattering problems in the left and right half-planes and

determine the all scattering data. Then Dirichlet problem reduces to solution of the Gelfand-Levitan-Marchenko linear equations. Vortex dipole formed by charges is represented by 2π -kinks of finite length that are terminating on the vortex centers. It has simple boundary conditions: $u(x,y) \to 0$, as $r \to \infty$. In this case we obtained the following systems of inverse problem equations:

$$(-1)^{i+1} 4N_i(y,z) + \varepsilon_{1i} F_0(y+z) + \int_y^\infty [M_1(y,t) \cdot F_0(t+z) +$$

$$\varepsilon_{ik} N_k(y,t) \cdot F_1(t+z)]dt = 0, \quad \varepsilon_{ik} = -\varepsilon_{ki}, \quad \varepsilon_{12} = 1,$$

$$4M_i(y,z) + \varepsilon_{1i} F_1(y+z) + \int_y^\infty [|\varepsilon_{ik}| M_k(y,t) \cdot F_1(t+z) + \qquad (2)$$

$$\varepsilon_{ik} N_k(y,t) \cdot F_2(t+z)]dt = 0, \qquad i,k = 1,2$$

$$F_p(x,y) = \frac{1}{2\pi} \int_{-\infty}^{\infty} d\lambda \, \lambda^{-1} w_1^p(\lambda) \exp\left\{ \frac{w_2(\lambda)}{2} y - w_1(\lambda) x \right\} S(\lambda), \qquad p = 0,1,2$$

which for given scattering data $S(\lambda)$ (λ is spectral parameter, $w_1 = \frac{\lambda + \lambda^{-1}}{2}$, $w_2 = \frac{\lambda - \lambda^{-1}}{2}$) define kernels $N_i, M_i$of Jost functions and solution of (1) by $u(x,y) = -4 \arctan 2N_2(x,y,t=y)$. We find that vortex dipole (centers of vortices are situated at the points $x = 0, y = \pm l$)are described by continuous spectrum with singularity:

$$S(\lambda) = 0 \qquad (x \cdot \lambda) \le 0, \qquad S(\lambda) = -w_1 . sign(\lambda) \cdot \frac{\pi Q \sinh l \cdot w_2}{w_2} \qquad (x \cdot \lambda) \ge 0.$$

Spiral dipole is represented spiral-shaped $2\pi-$kink section. Near the spiral centers ($x = 0, y = \pm l$) the field u can be asymptotically expanded

$$u \to \pm \arctan \frac{y \pm l}{x} + \frac{f_\mp}{4\pi} \ln \left[(y \pm l)^2 + x^2 \right] \qquad (x \to 0, \; y \to y \pm l) .$$

The first item has singularity of vortex ($Q = \pm 1$), the second item represents logarithmic singularity of point sourse with $f_\pm$strength. We show that solution of corresponding boundary problem is defined by (2) with scattering data

$$S(\lambda) = sign(\lambda) \left[-\frac{\pi}{w_2} \cdot w_1 \cdot \sinh(w_2 \cdot l) + \frac{f_+}{4} \exp(-w_2 \cdot l) + \frac{f_-}{4} \cdot \exp(w_2 \cdot l) \right]$$

for $(x \cdot l > 0)$ and $S(\lambda) = 0$ for $(x \cdot l < 0)$. The asymptotic behavior of $u(x,y)$ as $r^2 = x^2 + y^2 \to \infty$ have the simple form :

$$\partial_y u(x,y) = \left(\partial_x - \frac{f_+}{2\pi}\partial_y\right) K_0\left(|\overrightarrow{r} - \overrightarrow{r_+}|\right) - \left(\partial_x + \frac{f_-}{2\pi}\partial_y\right) K_0\left(|\overrightarrow{r} - \overrightarrow{r_-}|\right), \tag{3}$$

where $K_0(r)$ is zero-order McDonald function and $\overrightarrow{r_\pm} = (0, \pm l)$. Just as we investigated vortex dipole and spiral dipole (with $x = 0$, $y = \pm l$ centers) against background of the cnoidal wave

$$u_0 = 4\arctan\left[cn\left(\frac{x}{k}\right)/1 + sn\left(\frac{x}{k}\right)\right] \tag{4}$$

which corresponds to the ground state of the junction for definite values of the external magnetic field,to the ground state of some incommensurate magnetics and crystals. Using obtained scattering data [2] we find leading terms of the asymptotes of $u(x,y)$ (adiabatic approximation)

$$u \to u_0(x + \alpha(x,y) + \beta(x,y)) \qquad r \to \infty, \tag{5}$$

$$\alpha(x,,y) = \frac{k}{2}\left(\arctan\frac{y_+}{x_+} - \arctan\frac{y_-}{x_+}\right), \qquad x_+ = \frac{x}{\sqrt{K_1}}, \qquad y_\pm = \frac{y \mp l}{\sqrt{K_2}},$$

$$\beta(x,y) = \frac{-k}{4\pi k'}\left(f_+ \ln\frac{r_+}{R} + f_- \ln\frac{r_-}{R}\right), \qquad K_1 = \frac{4Kk'^2}{k^2 E}, \qquad K_2 = \frac{4E}{k^2 K}$$

where R is truncation radius, K, E are complete elliptic integral of the first and second kind respectively and $r_\pm^2 = x_+^2 + y_\pm^2$. Such solution describes the two-dimensional deformation of the cnoidal wave (or lattice solitons) in the presence a magnetic spiral dipole. It is known that when the junction is cooled below its superconducting transition temperature Abrikosow vortices are trapped and created a magnetic dipole ($f_\pm = 0$) [5] or spiral dipole ($f_\pm \neq 0$) on the defects. We note that firstly the single singular spiral was found in [6] by numerical simulation and our results for dipoles are in accordance with that results.

References

[1] A.B.Borisov, Phys.Lett. A 143 (1990) 52.

[2] A.B.Borisov, V.V.Kiseliev, Inverse Problem 5 (1989) 959.

[3] A.B. Borisov, S.N Ionov, Physica D, (1996) to be published.

[4] A.B.Borisov, V.V.Kiseliev, Physica D 87 (1995) 64.

[5] J.Manhard, J.Bosh, R.Gross, R.P.Huebener, Phys.Rev.B 35 (1987) 5208.

[6] A.G.Shagalov, Phys.Lett. A 165 (1992) 412.

CHAOS IN A TWO DEGREES OF FREEDOM SYSTEM WITH FRICTION

Anita Ciekot
Institute of Mathematics & Computer Science
Technical University of Częstochowa

Abstract

In this paper the two degrees of freedom system (TDOFS) with friction which describes belt conveyor will be investigated. The area of parameters when the movement is chaotic will be calculated. The equations describing these model are nonlinear so that their chaotic characteristic: the shape of solution, the phase orbit, the Poincare map, the spectral density function, the autocorrelation function will be taken into account. Additionally, an initial conditions influence the vibrations form has been considered (the simple celluar method). The results has been presented graphically.

1 Introduction

The technical dynamical systems are described mostly with ordinary differential equations called 'equations of motion'. They have the form $\dot{\mathbf{x}} = \mathbf{f}(t, \mathbf{x})$ with the initial conditions $\mathbf{x}(t_0) = \mathbf{x}_0$, where $\mathbf{x} = [x_1, x_2, \ldots, x_N]^T$ and $\mathbf{f} = [f_1, f_2, \ldots, f_N]^T$. It is assumed that one or more of the functions f_i are nonlinear.

Solutions of such equations may be chaotic, quasi-periodic or periodic. There are some characteristics making possible to distinguish it: the shape of solution, the phase orbit, the Poincaré map, the spectral density function, the autocorrelation function, the Lyapunov exponent value.

2 The analysis of two-degrees-of-freedom chaotic system with friction

In this paper the two-degrees-of-freedom dynamical system with friction is analysed. It is a system which consist of two mass: m_1, m_2, two springs: k_1, k_2 and moving belt with speed $v_0 = const$. This system is given in Fig.1. The equations of motion of this system are:

$$m_1\ddot{x}_1 = -k_1x_1 - k_2x_2 + k_2x_2 + T_1(w_1) \qquad m_2\ddot{x}_2 = -k_2x_2 + k_2x_1 + T_2(w_2)$$

where:

$T_1(w_1)$ - is the friction force of mass m_1 dependes on the relative velocity $w_1 = v_0 - \dot{x}_1$

$T_2(w_2)$ - is the friction force of mass m_2 dependes on the relative velocity $w_2 = v_0 - \dot{x}_2$

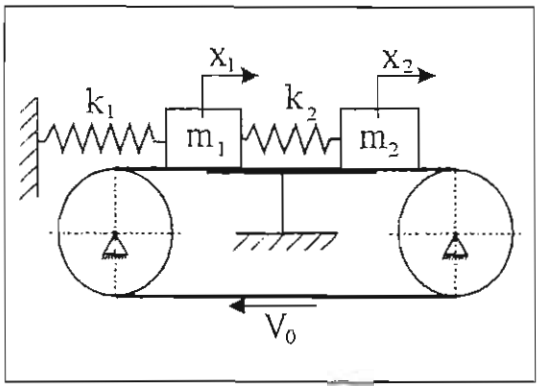

Figure 1:

$\dot{x}_1, \dot{x}_2$ - mass velocities m_1, m_2

Functions T_1 and T_2 are defined by:

$T_1(w_1) = T_{01} sgn W_1 - \alpha_1 W_1 + \beta_1 W_1^3 \quad T_2(w_2) = T_{02} sgn W_2 - \alpha_2 W_2 + \beta_2 W_2^3$

For the numerical analysis it has been assumed that:
$m_1 = 4,\ m_2 = 3, \alpha_1 = 5.518, \alpha_2 = 4.9,\ \beta_1 = 0.1569,\ \beta_2 = 0.1816,$
$T_{01} = 29.43, T_{02} = 19.62, v_0 = 0.5 k_1 = 11.77, k_2 = 7.85$ and zero initial conditions.

Equations of motion have been solved numerically using the Runge-Kutta-Merson method. Next, the chaotic characteristics have been derived from the solution with the programs described in [4]. Figures 2 and 3 show two of them: the Poincaré map for mass m_1 and m_2 which suggestes that the system is chaotic. Remaining characteristics of chaos which were used in the investigations are the following: non-regular displacement, non-existence of limit cycles in phase plane, wide spectrum, shape of the autocorrelation function will be presented during the conference.

The influence of the varying of initial conditions on the nature of motion is analysed with a simple cellular method [3]. Fig. 4 shows an influence of initial conditions for system solutions.

References

[1] Awrejcewicz, J., *Chaos in simple mechanical systems with friction*, Journal of Sound and Vibrations, 109(1), 1986.

[2] Feeny, B., *Chaos and friction*, PhD thesis, Cornell University, 1990.

[3] Leszczynski, J.S., *Some modification of the simple cellular method for solution of the chaotic systems*, XI Polish Conference on Computer Methods in Mechanics, Kielce-Cedzyna, 1993, 501-505

[4] Pękala, W., *Pakiet programów CHAOS do obliczania charakterystyk układów chaotycznych*, IX Conference METODY KOMPUTEROWE W MECHANICE, Kraków-Rytro 1989.

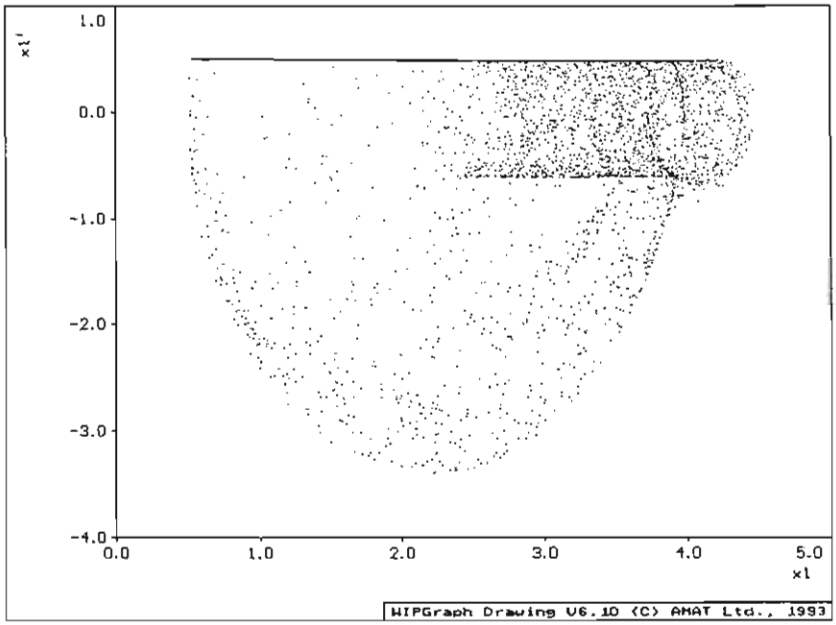

Figure 2:

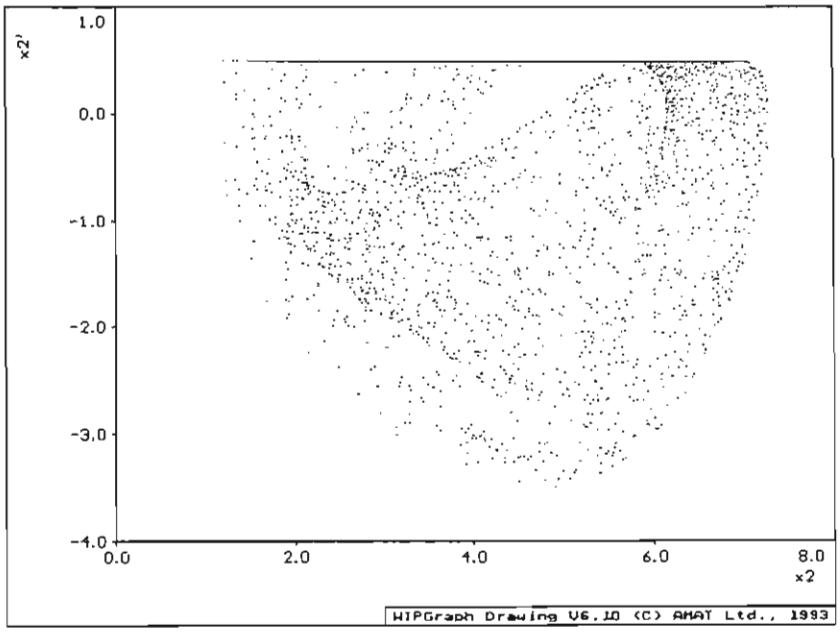

Figure 3:

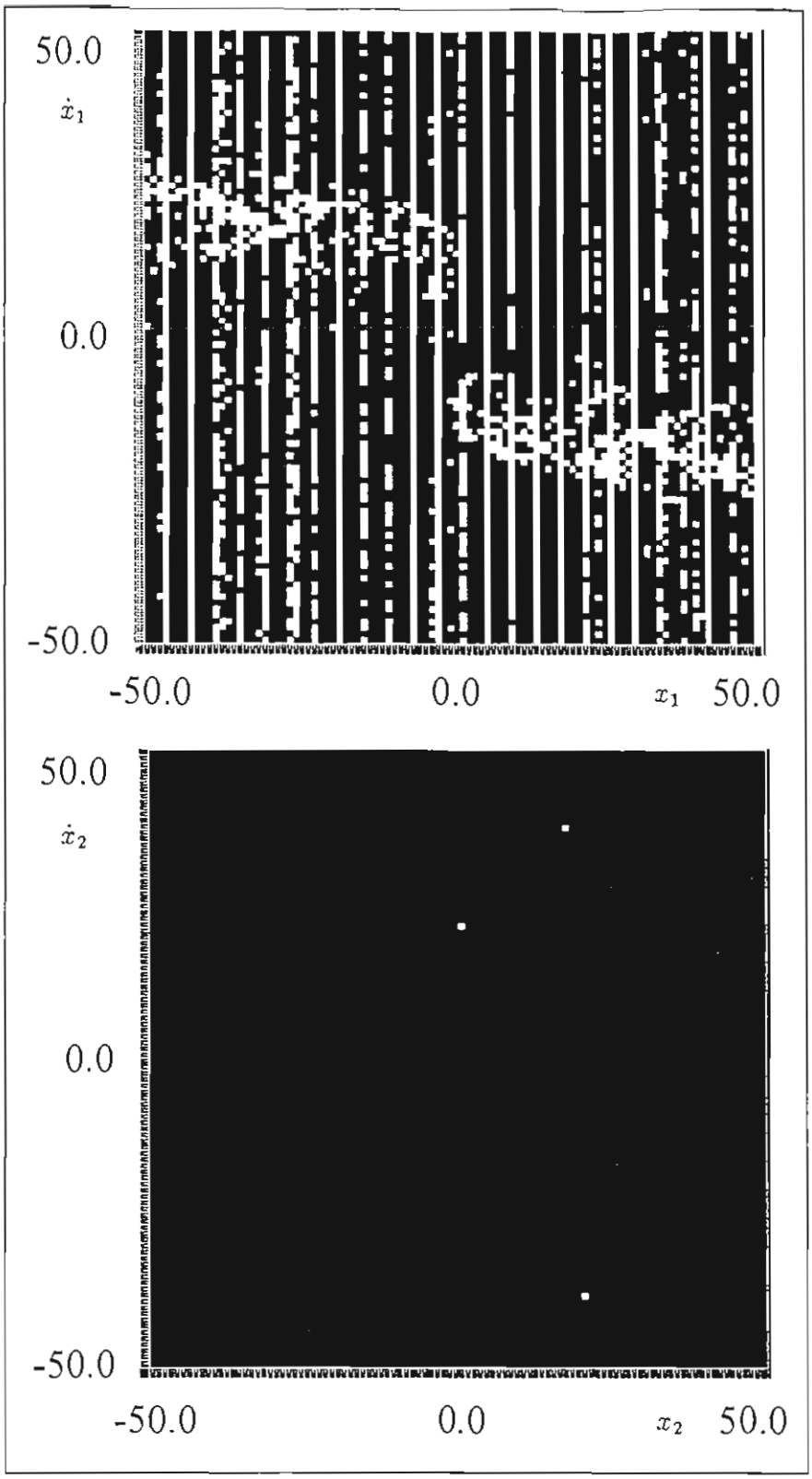

Figure 4:

Linear stability theory applied to the transitions to periodic flows in a thermally–driven square cavity

J.M. CORNET†*, C.H. LAMARQUE‡*

† Laboratoire des Sciences de l'Habitat, Ecole Nationale des Travaux Publics de l'Etat. 1 rue Audin, 69120 Vaulx–en–Velin, France. JeanMichel.Cornet@entpe.fr

‡ Laboratoire Géomatériaux, Ecole Nationale des Travaux Publics de l'Etat. 1 rue Audin, 69120 Vaulx–en–Velin, France. Claude.Lamarque@entpe.fr

* Département Génie Civil et Bâtiment, URA CNRS 1652, Ecole Nationale des Travaux Publics de l'Etat. 1 rue Audin, 69120 Vaulx–en–Velin, France.

Abstract : We intend to establish a methodology suited to the search of the first bifurcations of convective flows using a linear stability analysis, allowing us to define a relation between amplitude and frequency of the perturbation. A particular combination of various numerical methods to compute on one hand the basic solution and on the other hand the perturbation is applied to the search of the bifurcations in a thermally–driven cavity. This method shows a good agreement with available experimental and numerical data and can provide a significant accuracy for a reduced cost in comparison with other well–known techniques like direct simulation.

Introduction

The transitions from steady state to unsteady flows in a thermally–driven cavity with conductive horizontal walls provide a test problem in the field of natural convection. They have been investigated in many different works. Observations from experiments [1] show that instabilities inside a tri–dimensional cubic cavity are bi–dimensional ones. Transitions lead to three successive frequencies that occur in the interval $[3 \times 10^6; 10^7]$ of the Rayleigh number. Numerical approaches of square cavity confirm these results either by using the method of control–volumes [2,3] or by making use of spectral methods [4] or by analyzing the linear stability from a finite element method [5]. The different authors of papers [2—5] announce some frequencies that seem to be in good agreement with experimental results. But an uncertainty is remaining about the critical Rayleigh number. The reason is that to characterize the instability of sub–critical Hopf type is difficult directly by numerical simulations. In this paper, in order to determine with a good accuracy the bifurcation threshold of the flow, an analysis of the linear stability is proposed which is fairly adapted to this problem.

1. Mathematical setting

We are dealing with the Navier–Stokes equations coupled with heat equation in the

case of Boussinesq hypothesis. We choose nondimensional variables for convective terms

$$\frac{\partial u}{\partial t} + (\mathbf{u} \cdot \mathrm{grad})\,\mathbf{u} = \frac{Pr}{Ra^{1/2}}\Delta \mathbf{u} - \frac{\partial p}{\partial x} + Pr\,T\,\mathbf{k}$$
$$\frac{\partial T}{\partial t} + (\mathbf{u} \cdot \mathrm{grad})\,T = \frac{1}{Ra^{1/2}}\Delta T \qquad (1)$$

$$\mathrm{div}\,\mathbf{u} = 0$$

The boundary conditions are written in the following form

$$\mathbf{u}(\pm 1/2, z) = \mathbf{u}(x, \pm 1/2) = 0 \qquad (2)$$

$$T(-1/2, z) = -T(1/2, z) = 1/2, \qquad T(x, \pm 1/2) = -x$$

(perfectly conductive horizontal walls).

2. Analysis of the linear stability

Let us denote $\mathbf{u}_0 = (u_0, w_0)$, T_0, P_0 the basic solution (without any bifurcation). The previous system of partial differential equations (1) with boundary conditions (2) is now written by using a vorticity Ω_0 and stream function form: it is expanded at first order in the neighbourhood of the basic solution. This procedure leads to a non-autonomous perturbed system in φ and τ (respectively the stream function and the temperature of the perturbation),

$$\varphi(x, z, t) = \varphi(x, z)\exp(\sigma t)$$
$$\tau(x, z, t) = \tau(x, z)\exp(\sigma t)$$

Thus, this system is resolved by making use of some expansions of the functions $\varphi(x, z)$ and $\tau(x, z)$ over a basis of polynomials well adapted to the boundary conditions. This basis is orthonormalized by using a Gram–Schmidt procedure.

Several different techniques have been compared in reference [6]. It occurs that the best procedure is the method of collocation: it provides the results at the lowest computational cost and it processes the highest speed of convergence when the size of the bases of functions is increasing.

The basic solution is looked for according to the grid of Gauss–Lobatto–Chebycheff collocation points. The meshes of the grid are irregular: thus, we prefer to build a finite element method associated with this grid of collocation points. We choose a P_2 approximation of velocity field and a P_1 approximation of the temperature and pressure fields with triangular elements, according to the inf-sup condition [7].

Pressure is known except for a constant. We remove this difficulty by setting a discrete pressure of null-mean inside the cavity. We get rid of the condition $\mathrm{div}\,\mathbf{u} = 0$ of the system of equations (1) by iterating a variant of the algorithm of augmented

Lagrangian [8] well–adapted to our problem. The iteration matrix obtained according to this procedure is better conditionned and the GMRES iterative method [9] readily leads to the solution of linear systems. This last method includes a reduced storage related to the coefficients of the matrices different from zero.

The steady–state is calculated by demanding $\partial/\partial t \equiv 0$ in the system of equations (1). The non–linear equations obtained from the finite element method are solved by using the Newton algorithm. The problem of how to choose the initial condition before running the Newton algorithm has a solution with several steps, when increasing the Rayleigh number from a low value.

The basic solution that as been calculated according to this procedure is now introduced in the perturbed equations. The derivatives are estimated by Taylor expansions adapted to the irregular grid in order to guaranty a second order approximation. The perturbed system is transformed into a generalized eigenvalue problem $A\,\mathbf{x} = \sigma B\,\mathbf{x}$, solved by the QZ algorithm [10].

3. Results

We deal with the three critical situations provided by experiments. By using from 16×16 polynomials to 28×28 polynomials, we have localized the critical point round the non–dimensional frequency $f = 0.252$ corresponding to the Rayleigh number 2.6×10^6 (Fig.1). We obtain a good agreement with the data that could be found in literature.

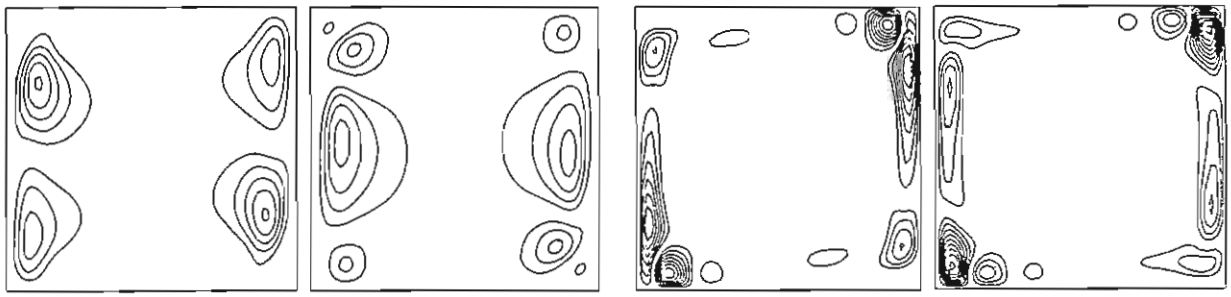

Figure 1: Real and imaginary parts of the eigenvector corresponding to the first bifurcation. Streamlines and isotherms of the unsteady part of the flow.

The convergence of critical points when the number of polynomials is increased show that the frequency and the logarithm of the Rayleigh number simultaneously converge. Thus, this gives explanation for the difficulty of determining the critical values of this last parameter. Therefore, our technique provides a significant convergence for numbers of polynomials small enough (1% error for the critical frequency and the logarithm of the Rayleigh number with a basis of 20×20 polynomials).

Conclusion

This work associated several numerical methods which guaranty a rather fast con-

vergence towards the critical points of parameters (σ_i, Ra) of the flow. The linear analysis of stability can be achieved whithout any analytical knowledge of the basic solution.

This method allows a comparison of new results with the values given by direct numerical simulations of the unsteady flow.

Now we are directing attention to the good qualities of the convergence of this method of analyzing the linear stability. We focus on the computational cost of this new method: we are able to provide convergence towards results at a computational cost lower than the computational cost of all other approaches.

Bibliography

[1] **Briggs, D.G., Jones, D.N.** Two-dimensional periodic natural convection in a rectangular enclosure of aspect ratio one. *Journal of Heat Transfer*, 1985, Vol.107, p.850—855.

[2] **Jones, D.N., Briggs, D.G.** Periodic two-dimensional cavity flow: effect of linear horizontal thermal boundary condition. *Journal of Heat Transfer*, 1989, Vol.111, p.86—91.

[3] **Henkes, R.A.W.M.** *Natural convection boundary layers.* Ph.D. Thesis: Delft University, 1990.

[4] **Le Quere, P.** Onset of unsteadiness, routes to chaos and simulations of chaotic flows in cavities heated from the side: a review of present status. *Heat Transfer 1994.* Edited by G.F. Hewitt. Warwickshire: Institution of Chemical Engineers, 1994. Vol.1, p.281—296. ISBN 0-85295-345-3.

[5] **Winters, K.H.** Hopf bifurcation in the double-glazing problem with conducting boundaries. *Journal of Heat Transfer*, 1987, Vol.109, p.894—898.

[6] **Cornet, J.M.** *Approche modale des transferts aérauliques dans le bâtiment: mécanismes d'instabilité, bifurcations et dynamique non-linéaire.* Ph.D. Thesis: INSA Lyon, 1995.

[7] **Brezzi, F.** On the existence, uniqueness and approximation of saddle-point problems arising from lagrangian multipliers. *Revue Française d'Automatique, Informatique et Recherche Opérationnelle*, 1974, n°R-2, p.129—151.

[8] **Fortin, M., Glowinski, R.** *Augmented lagrangian methods.* Amsterdam: North-Holland, 1983.

[9] **Saad, Y., Schultz, M.H.** *GMRES: a generalized minimal residual algorithm for solving nonsymmetric linear systems.* New Heaven: Yale University, Department of Computer Science, 1983. Report n°YALEU/DCS/RR-254.

[10] **Moler, C.B., Stewart, G.W.** An algorithm for generalized matrix eigenproblems. *SIAM Journal of Numerical Analysis*, 1973, Vol.10. p.241—256.

Unimodal 2-endomorphisms and Chaos in the Sence of Li & Yorke

V. A. Dobrynskiy

Institute of Mathematics of National Academy of Science of Ukraine
(Tereshchenkovskaya str. 3, 252601 Kiev, UKRAINE)

Abstract: It is shown an existence of two open sets in a parameters space such that mappings associated with parameters belonging to these sets have areas with chaotic in the sense of Li & Yorke behaviour of trajectories. Mechaniques which generate chaos differ one from another for mappings associated with each of domains. A measure of chaotic area may be so small that it is impossible to find one with computer-assistant calculations.

Let $Int(T)$ be a set of interior points of $T \subset I^2=[0,1]*[0,1]$ and $\Gamma(T)=T\setminus Int(T)$ be its boundary.

A 2-endomorphism of I^2 into itself

$$\Phi:\ (x,y) \longrightarrow (\Phi(x,y),x), \qquad (1)$$

where $(x,y) \in I^2$ is called unimodal one if $\Phi(x,y)$ is such a smooth function that $\Phi(x,0)=\Phi(x,1)=\Phi(0,y)=\Phi(1,y)$ and there is only one point $(\bar{x},\bar{y}) \in Int(I^2)$ such that both partial derivatives of $\Phi(x,y)$, $\Phi'_1(x,y)$ and $\Phi'_2(x,y)$, evaluated at $(\bar{x},\bar{y})$ are simultaneously equal to 0 and besides $\Phi(\bar{x},\bar{y}) > \Phi(x,y) > 0$ for any $(x,y) \in Int(I^2)$ such that (x,y) is not equel to $(\bar{x},\bar{y})$ [Dobrynskiy,1995].

From our point of view this definition is one of the most natural generalizations of the notion of one-dimensional unimodal mapping on the two-dimensional case. Below we study properties of the following 2-parameters family of such mappings:

$$F:\ (x,y) \longrightarrow (\ \lambda f(x)[h\{f(y)\}]^s\ ,\ x\ ). \qquad (2)$$

where λ, s: $0 < \lambda \leqslant 1$, $s > 0$ are parameters, $f(t)$ is smooth unimodal on $[0,1]$ function such that $f(0)=f(1)=0$, $f(q)=1$, where q is a point of the extreme value of $f(t)$, with the derivative $f'(t)$ satisfying the relation $(t-q)f'(t) < 0$ for all $t \in [0,1]\setminus\{q\}$ and

where $h(t)$ is a diffeomorphism of $[0,1]$ such that $h(0)=0$, $h'(t)>0$ for all $t \in [0,1]$.

A critical set $K=K(F)$ of F is a closure of the locus of $Int(I^2)$, where Jacobian $||DF||$ of F being equal zero. The set K is differ from I. Gumowski's & C. Mira's [1980] *LC*. Get analytical expressions for K and its two first images and preimages. They are $K=\{(x,y): y=q,\ 0 \leq x \leq 1\}$, $F(K)=\{(x,y): x=\lambda f(y),\ 0 \leq y \leq 1\}$, $F^2(K)=\{(x,y): x=\lambda f(y)[h(y/\lambda)]^s,\ 0 \leq y \leq \lambda\}$, $F^{-1}(K)=\{(x,y): x=q,\ 0 \leq y \leq 1\}$, $F^{-2}(K)=\{(x,y): q=\lambda f(x)[h\{f(y)\}]^s\}$. Note that $F^{-2}(K)$ exists only if $\lambda \geq q$.

Denote by $R^{(n)}=F^{n+2}(I^2)$. Obviously $R^{(i)} \subset R^{(j)}$ if $i > j$, i.e. $R^{(n)}$ are embedded one into another and $NW(F) \subset \bigcap_{n=0}^{\infty} R^{(n)}$, where $NW(F)$ is a non-wandering set of F. The sets $R^{(n)}$ form a system of compact neighbourhoods of $\bigcap_{n=0}^{\infty} R^{(n)}$ and preimages of K dissect each of them on parts. Let J, L, N are natural numbers. A connected part of $\Gamma(T)$ is called a base of T if it lies in an arc belonging to $\left[R^{(n)} \cap F^{-j}(K)\right]_{j=0}^{J}$. Two bases are different one from another if they belong to the distinct arcs of $\left[R^{(n)} \cap F^{-j}(K)\right]_{j=0}^{J}$. A supplement of bases till whole $\Gamma(T)$ is called sides of T. Each connected component of the supplement forms one side of T. Let N be a number of elements of partition. Denote by $\underline{i} \in \{\underline{1}, \underline{2}, \ldots, \underline{N}\}$ corresponding the number of $i \in \{1,2,\ldots,N\}$ the element of partition.

Sets $F^L(\underline{j})$, $\underline{i}$ are called one-dimensionally correctly intersecting if $\underline{i}$ has two bases and two sides, bases of $\underline{i}$ and F^L-images of bases of $\underline{j}$ do not intersect one another and if there is a simple connected component $\xi \subset F^L(\underline{j}) \cap \underline{i}$ having also only two bases and two sides with bases lying in the different bases of $\underline{i}$ and sides non-intersecting sides of $\underline{i}$. Sets $F^L(\underline{j})$, $\underline{i}$ are called two-dimensionally correctly intersecting if $Int(F^L(\underline{j})) \supset \underline{i}$.

Now we are able to use a symbolical dynamics in such a manner. According to one of the mentioned above definitions assign to each pair of numbers j,i an element π_{ji} of a matrix of admissible

transitions π so that π_{jl} is equal to 1 if sets $F^L(j)$, $\underline{i}$ intersect correctly and it is equal to 0 in opposite case.

In accodance with this matrix π constitute of all kinds bounded from the left sequences of symbols $1,2,\ldots,N$. There is a natural correspondence between sequences and subsets of $\bigcap_{n=0}^{\infty} R^{(n)}$.
So, it is easy to show for each periodic of period M sequence of symbols there is at least one invariant with respect to F^{LM} subset of $\bigcap_{n=0}^{\infty} R^{(n)}$. Further, it is not heavy to prove an existence the fixed point inside every of mentioned above F^{LM}-invariant subsets of $\bigcap_{n=0}^{\infty} R^{(n)}$. The number Q_M of periodic of period M sequences, as it has been proved by V.M.Alexeev [1976], is given by formula $Q_M = Sp[\pi^M] = \sum_{\mu_k \in \beta} \mu_k^M$, where $Sp[\pi^M]$ is a spur of the matrix π^M, μ_k are eigenvalues of π and β is its spectrum. There is an equality $\mu_0 = \lim_{M\to\infty} \sqrt[M]{Q_M}$, where μ_0 is the largest positive eigenvalue of π.

So, the number Q''_M of periodical of period M points of F^L can be estimated in such a manner: $Q''_M \geq Sp[\pi^M] = \sum_{\mu_k \in \beta} \mu_k^M$, $\mu_0 \leq \lim_{M\to\infty} \sqrt[M]{Q''_M}$.

It is resonable to ask whether the mapping of (2) having mentioned above properties exists. The answer is "yes".

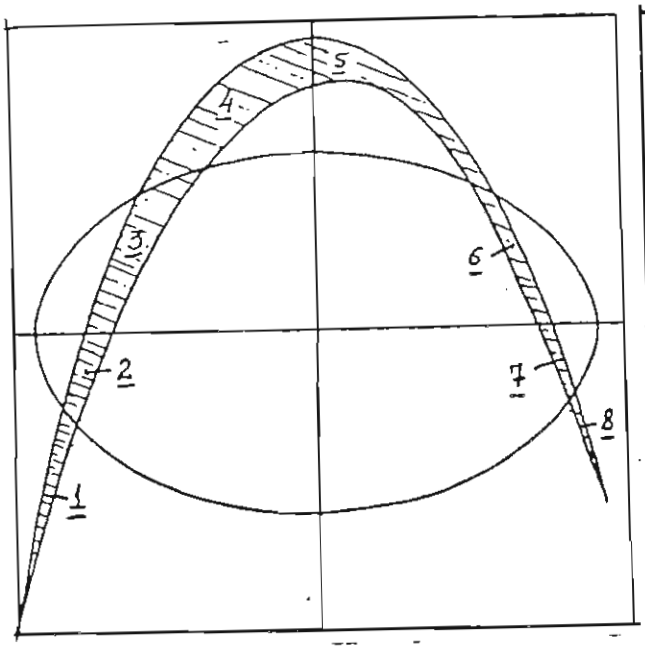

Fig. 1.

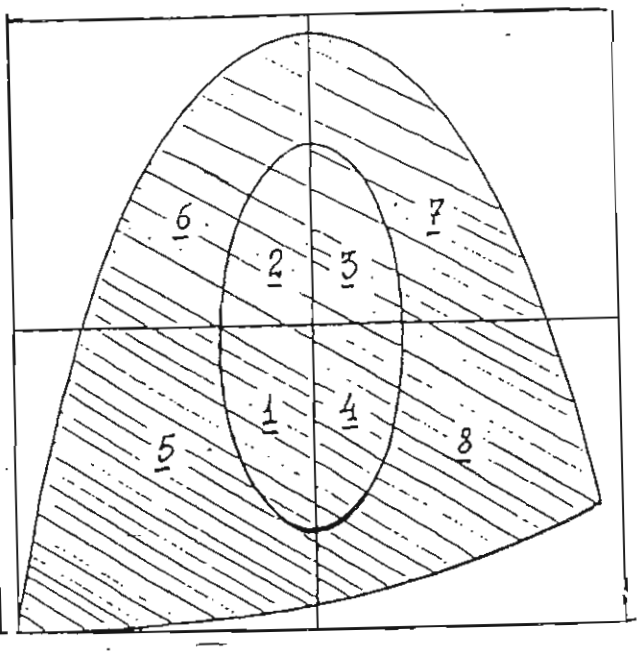

Fig. 2.

Theorem 1. There are $\bar{\bar{\lambda}}$, $\bar{\bar{s}}$: $q < \bar{\bar{\lambda}} < 1$, $\bar{\bar{s}} > 0$ and natural L such that for any collection of numbers λ, s, n, J such that $n=0,1,\ldots$, $J=2,3,\ldots$, $\bar{\bar{\lambda}} \leqslant \lambda \leqslant 1$, $0 < s \leqslant \bar{\bar{s}}$ $\left[\text{ or } s \geqslant 1/\bar{\bar{s}}\right]$ constituted for the mapping F^L the matrix Π is non-trivial in the sense of existing periodical sequences of symbols among of all kinds those constituted in accodance with the matrix Π.

For example consider the neighbourhood R and its partition by arcs beloning to $\left[R \cap F^{-j}(K)\right]_{j=0}^{2}$ for λ, s picked out as in the Theorem 1. They are pictured in Figs. 1-2.

Denote by $S(f(t)) = \dfrac{f'''(t)}{f'(t)} - \dfrac{3}{2}\left[\dfrac{f''(t)}{f'(t)}\right]^2$ Schwarzian (the derivative of Schwarz) of $f(t)$.

Theorem 2. Let $S(f(t)) < 0$ in $[0,1]\setminus\{q\}$ then there are $0 < \bar{\bar{\lambda}} < 1$, $\bar{\bar{s}} > 0$ such that the mapping of (2) has at least one saddle-type hyperbolic periodic of period 3 point and one bi-asymptotically tends to it trajectory consisting of transversal intersections of stable and unstable manifolds of this periodic point for all λ, s such that $0 < s \leqslant \bar{\bar{s}}$, $\bar{\bar{\lambda}} \leqslant \lambda \leqslant 1$.

Theorem 3. There are $0 < \bar{\bar{\lambda}} < 1$, $\bar{\bar{s}} > 0$ such that the mapping of (2) has a fixed point being the snap-back repeller [Marotto,1978] for all λ, s such that $s \geqslant 1/\bar{\bar{s}}$, $\bar{\bar{\lambda}} \leqslant \lambda \leqslant 1$.

Proving of both last theorems is connected with a treatment of certain subsets of the partitions of R. In first case this is the element 8 of the partition described in Fig. 1 and in second one this is the element 3 of the partition described in Fig. 2.

Theorem 4. For the mapping F a measure of area of chaos in the sense of Li & Yorke [1975] tends to zero as s tends to infinity.

In conclusion we notice that proofs of all theorems mentioned above can be found in [Dobrynskiy,1995a].

R E F E R E N C E S.

Alexeev V. M. [1976] *Simbolic dynamics (Eleventh mathematical school)* (Edition of Institute of mathematics, Ukrainian Acad. Sci., Kiev, 210 pp. (Russian).

Dobrynskiy V. A. [1995] "Critical sets and unimodal mappings of square", *Doklady Russian Acad. Sci.*, 341(4), 442-445 (Russian).

Dobrynskiy V. A. [1995a] "Critical sets and unimodal mappings of square", *Matematicheskiye zametki*, 58(5), 669-680 (Russian).

Li T.-Y. & Yorke J. A. [1975] "Period three implies chaos", *Amer. Math. Monthly*, 82, 985-992.

Marotto F. R. [1978] "Snap-back repellers imply chaos in R^n", *Journal Math. Anal. Appl.*, 63(1), 199-223.

Gumowski I. & Mira C. [1980] *Dynamique chaotique. Transformations ponctuelles. Transition order-desorder* (Editions Cepadues, Toulouse) 478 pp.

CHAOTIC VIBRATONS OF A HELICOPTER

Zbigniew Dżygadło and Grzegorz Kowaleczko
Military University of Technology
ul. Kaliskiego 2, 01-489 Warszawa, Poland

Abstract: A helicopter is a rotorcraft which can be subjected, during its motion, to various types of vibrations. For some of these vibrations there can appear bifurcations and regular or chaotic motions. Spatial motion dynamics of a helicopter-autopilot system is considered. A complete set of nonlinear differential equations describing the fuselage motion and all the blades motions is applied. The control laws for static autopilot have been formulated on the basis of the method of motions separation. Some results of numerical analysis are presented, which show phase plane plots and power spectrum diagrams for several flight parameters.

1. Introduction

Recently some investigations have been made of dynamic models of helicopter-autopilot systems (cf. [1]-[3]). In [4] the flap-lag motion of a rotor has been studied, where regular and chaotic transient response has been found.

In the present paper a nonlinear dynamic model of a helicopter-autopilot system is considered which enables us to determine regular and chaotic motions of the helicopter.

For the analysis it is assumed that the helicopter fuselage is a rigid body and the motion of rigid blades about flap hinges, lead-lag hinges and axial hinges is considered, while the tail rotor is treated as a hingeless and weightless source of thrust equilibrating the drag moment and ensuring directional control of helicopter.

The induced velocity has been determined making use of the Biot-Savart law and a simplified model of vortex field has been applied, spatial structure of tip vortex trajectories being taken into consideration.

2. Formulation of the Problem

On the basis of physical model presented above, a set of nonlinear differential equations has been obtained, which describes the dynamics of translatory and rotating motion of the helicopter and the blade motions around flap, lead-lag and axial hinges. The kinematic relations are also included in this set.

Several systems of coordinates have been applied in the problem under study. Equations of dynamic equilibrium of forces and moments have been determined in the system

$Ox_k y_k z_k$ fixed with the fuselage and blade motion has been considered in the systems of coordinates $P_H x' y' z'$ and $P_V xyz$ fixed with the hinges P_H and P_V.

Finally we obtain a set of 25 nonlinear differential equations with periodic coefficients which can be presented in the form:

$$A(t,X)\dot{X} = f(t,X,S) \tag{1}$$

where X is the vector of flight parameters:

$$X = (U,V,W,P,Q,R,\dot{\beta}_i,\beta_i,\dot{\zeta}_i,\zeta_i,\Theta,\Phi,\Psi)^T, \quad i=1,2,3,4 \tag{2}$$

and U, V, W are linear velocities of the centre of fuselage mass in the coordinate system $Ox_k y_k z_k$ fixed with the fuselage, P, Q, R are angular velocities of the fuselage in the same coordinate system, Θ, Φ, Ψ are pitch, roll and yaw angles of the fuselage, β_i - i-th blade flap rotation about flap hinge P_H, ζ_i - i-th blade lead-lag rotation about lead-lag hinge P_V.

Vector S is the vector of control parameters: $S = (\theta_0, \kappa_s, \eta_s, \varphi_{so})^T$ (3)

where: θ_0 is angle of collective pitch of the main rotor, κ_s is control angle in the longitudinal motion, η_s is control angle in the lateral motion and φ_{so} is angle of collective pitch of the tail rotor. Detailed way of determining Eqs.(1) can be found in [1] to [3].

It has been assumed that the helicopter is performing a steady horizontal trimmed flight without sideslip. The terms of this flight are:

- linear and angular accelerations are equal to zero: $\dot{U} = \dot{V} = \dot{W} = \dot{P} = \dot{Q} = \dot{R} = 0$ (4)

- angular velocities are: $P = Q = R = 0$ (5)

- and the velocity component parallel to the Oy_k axis is: $V = 0$ (6)

On the basis of Eqs.(4)-(6), making use of Eq.(1), the following vector of flight parameters can be obtained: $X_0 = (U_0,0,W_0,0,0,0,\dot{\beta}_{i0},\beta_{i0},\dot{\zeta}_{i0},\zeta_{i0},\Theta_0,\Phi_0,\Psi_0)^T$, $i=1,2,3,4$ (7)

and the vector of control parameters: $S_0 = (\theta_0, \kappa_S, \eta_S, \varphi_{SO})_0^T$ (8)

Vectors (7) and (8) define the initial conditions for further calculations of flight parameters.

The control of helicopter under consideration is carried out by means of a static autopilot for which the law of control can be described by the expression:

$$S(t) = S_0 + Tx(t) \tag{9}$$

where $x(t)$ is the vector of increases in flight parameters (2) and T is a matrix of stabilizing coefficients. Method of determining the matrix T can be found in [2].

3. Solution of the Problem

The set of Eqs.(1) together with the law of control (9) has been applied to numerical simulations for Polish „Sokol" helicopter with the static autopilot for four values of flight velocity: 0, 100, 200 and 300 km/h.

Some results of computation are presented in this paper. In Figs. 1 and 2 the phase plane plots for blade flap motion β and blade lead-lag rotation ζ are shown. It is seen that all these motions are regular and periodic ones.

Similar courses can be found for the pitch angle Θ of fuselage, while for the angles of roll Φ and yaw Ψ there appear small chaotic perturbations. Linear components of velocity U,V,W have regular courses and for angular components P,Q,R we obtain chaotic perturbations. In Figs. 3 to 5 power spectrum diagrams (PSD) are shown for angular velocities P,Q,R at the velocity V=300km/h. It is seen that there occur period doubling bifurcations and chaotic perturbations appear.

In Figs. 6 to 8 power spectrum diagrams are presented for control parameters θ_0, κ_s and η_s at V=300km/h. Period doubling bifurcations and chaotic perturbations are also shown in these figures.

References

1. Dżygadło Z., Kowaleczko G., *Analysis of Spatial Motion Dynamics of a Helicopter for Various Models of Induced Velocity Field*, J. Tech. Phys., v. XXXIV, 2, 1993.
2. Dżygadło Z., Kowaleczko G., *Dynamic Analysis of a Helicopter-Autopilot System*, J. Tech. Phys., v. XXXIV, 4, 1993.
3. Kowaleczko G., *The Mathematical Model of an Astatic Autopilot of a Helicopter Including Couplings between Longitudinal and Lateral Motions*, J. of Theor. and Appl. Mech., v. 32, 4, 1994.
4. Tang D.M., Dowell E.H., *Damping Prediction for a Stalled Rotor in Flap-Lag with Experimental Correlation*, J. of the American Helicopter Society, v. 40, 4, 1995.

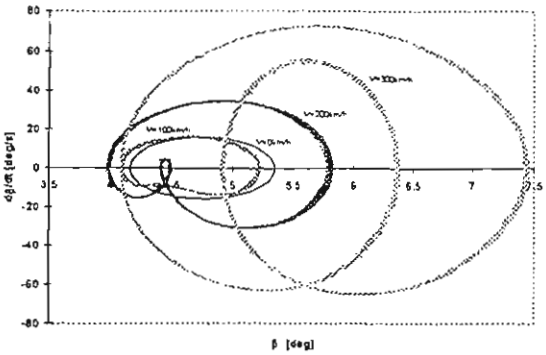

Fig.1. The phase plane plots for blade flap motion β

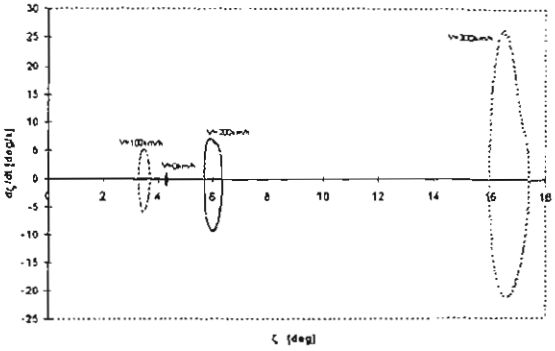

Fig.2. The phase plane plots for blade lead-lag motion ζ

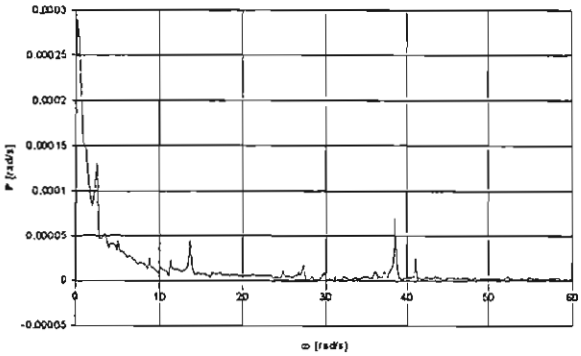

Fig.3. PSD plot for angular velocity P at V=300km/h

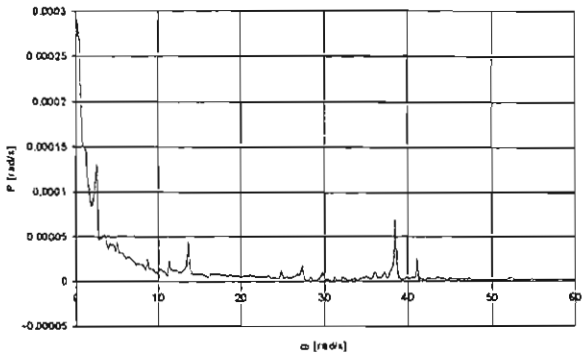

Fig.4. PSD plot for angular velocity Q at V=300km/h

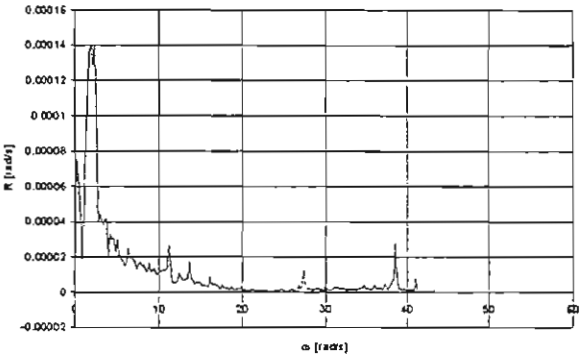

Fig.5. PSD plot for angular velocity R at V=300km/h

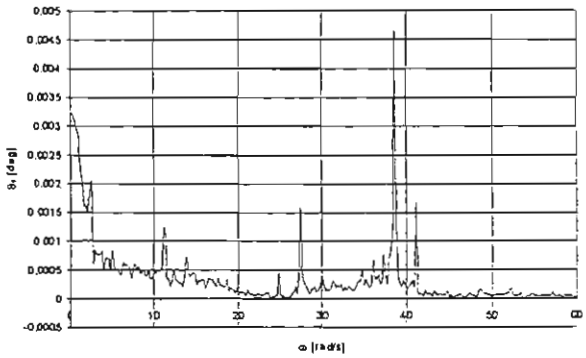

Fig.6. PSD plot for angle of collective pitch Θ_0 at V=300km/h

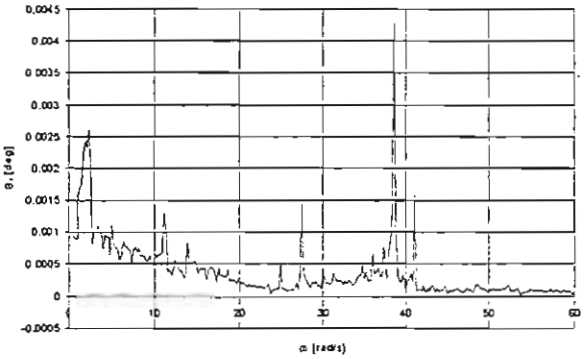

Fig.7. PSD plot for control angle κ_s at V=300km/h

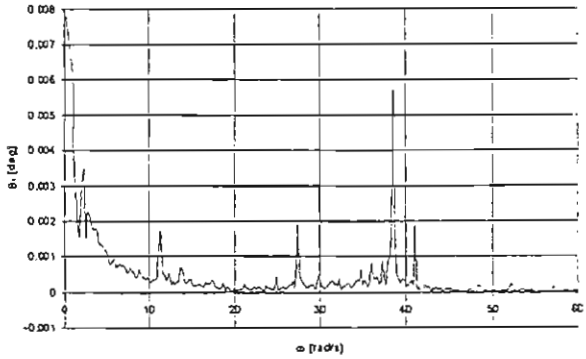

Fig.8. PSD plot for control angle η_s at V=300km/h

REGULAR AND CHAOTIC VIBRATIONS OF AN AIRFOIL IN SUPERSONIC FLOW

Zbigniew Dżygadło, Idzi Nowotarski and Aleksander Olejnik
Military University of Technology, ul. Kaliskiego 2, 01-489 Warszawa, Poland

Abstract: An airfoil in supersonic flow, having deformable supports, is an aeroelastic system for which can appear various types of bifurcations and regular or chaotic motions. The airfoil has two degrees of freedom: plunge displacement and angle of pitch displacement. The stiffness force and moment for those motions are assumed to be nonlinear ones. The airfoil is subjected to the pressure difference produced by its motion in supersonic flow.

Types of bifurcations occuring in the system and limit cycles of self-excited vibrations as well as regions of regular or chaotic motions are investigated.

1. Introduction

Recently some investigations have been made of nonlinear vibrations of aeroelastic systems in which regular and chaotic motions have been studied (cf. for instance [1]-[3]).

In the present paper nonlinear vibrations of an airfoil in supersonic flow are considered (Fig. 1). The airfoil is subjected to the pressure difference caused by its motion in the gas stream and this pressure difference has been determined on the basis of the potential theory of supersonic flow [4].

Finally, we obtain a set of two nonlinear differential equations describing the motion of the system under consideration which enables us to study regular and chaotic vibrations.

2. Equations of Motion

The airfoil has two degrees of freedom (Fig. 1), where $z_c=z_c(t)$ is plunge displacement and $\alpha=\alpha(t)$ is angle of pitch displacement. Equations of motion can be written in the form

$$m\frac{d^2z_c}{dt^2}-S\frac{d^2\alpha}{dt^2}=Q_z+P_k \quad ; \quad I\frac{d^2\alpha}{dt^2}-S\frac{d^2z_c}{dt^2}=Q_\alpha+M_k \tag{1}$$

where m, S, I are mass, static moment and moment of inertia, respectively, per unit span of the airfoil and

$$P_k=P_k(z_c)=-k_z(z_c+\beta_z z_c^3) \quad ; \quad M_k=M_k(\alpha)=-k_\alpha(\alpha+\beta_\alpha\alpha^3) \tag{2}$$

represent nonlinear stiffness force and moment for motion of the airfoil, while Q_z and Q_α are aerodynamic force and moment.

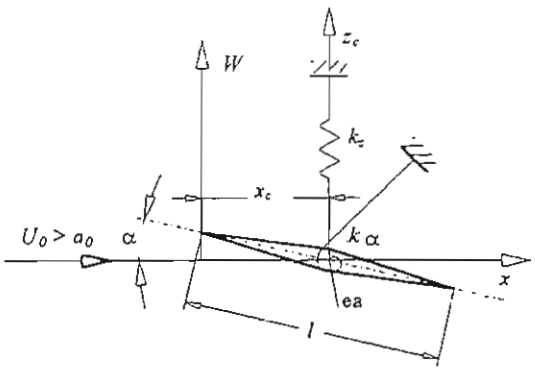

Fig. 1

The pressure difference produced by the airfoil motion in supersonic flow can be determined in the form (cf. [4])

$$\Delta p = p_l - p_u = -\frac{2\rho_0 U_0}{\mu}\left[U_0\frac{\partial W}{\partial x} + \left(1-\frac{1}{\mu^2}\right)\frac{\partial W}{\partial t}\right] \quad (3)$$

where $\mu^2 = M^2 - 1, \qquad M = \dfrac{U_0}{a_0} > 1 \qquad (4)$

ρ_0, a_0, M density, sound velocity and Mach number of unperturbed flow and

$$W = W(x,t) = z_c(t) + \alpha(t)(x_c - x) \quad (5)$$

Aerodynamic force and moment can be obtained as

$$\begin{aligned} Q_z &= \int_0^l \Delta p\,dx = \frac{2\rho_0 U_0^2 l}{\mu}\,\alpha - \frac{2\rho_0 U_0 l}{\mu}\left(1-\frac{1}{\mu^2}\right)\left[\dot z_c + \dot\alpha\left(x_c - \frac{l}{2}\right)\right] \\ Q_\alpha &= \int_0^l \Delta p(x_c - x)\,dx = \frac{2\rho_0 U_0^2 l}{\mu}\left(x_c - \frac{l}{2}\right)\alpha - \frac{2\rho_0 U_0 l}{\mu}\left(1-\frac{1}{\mu^2}\right)\left[\left(x_c - \frac{l}{2}\right)\dot z_c + \left(x_c^2 - x_c l + \frac{l^2}{3}\right)\dot\alpha\right] \end{aligned} \quad (6)$$

The problem will be considered in a dimensionless form assuming that the displacement z_c is referred to the cord length of airfoil l and time t to $1/\omega_\alpha$, where

$$\omega_\alpha = \sqrt{\frac{k_\alpha}{I}}, \qquad \omega_z = \sqrt{\frac{k_z}{m}} \quad (7)$$

are natural frequencies of uncoupled vibrations of the airfoil under study.

Equations of motion (1), (2), (6) are then obtained in the form

$$\ddot z - e\ddot\alpha + \chi_z(z + \bar\beta_z z^3) = \gamma_1 r^2\alpha - \gamma_1\delta r^2(\dot z + \xi_0\dot\alpha) \;\; ; \;\; \ddot\alpha - \frac{e}{r^2}\ddot z + \alpha + \beta_\alpha\alpha^3 = \gamma_1\xi_0\alpha - \gamma_1\delta[\xi_0\dot z + (\xi_0^2 + \tfrac{1}{12})\dot\alpha] \quad (8)$$

where

$$\gamma_1 = \frac{2\rho_0 U_0^2 l^2}{\mu k_\alpha}; \qquad \delta = \frac{l\omega_\alpha}{a_0 M}\left(1-\frac{1}{\mu^2}\right); \qquad \chi_z = \frac{\omega_z^2}{\omega_\alpha^2}; \qquad e = \frac{S}{ml}; \qquad r^2 = \frac{I}{ml^2}$$
$$\xi_0 = \frac{x_c}{l} - \frac{1}{2}; \qquad \bar\beta_z = \beta_z l^2; \qquad z = z_c/l; \qquad \tau = \omega_\alpha t \quad (9)$$

Equations (8) together with relations (9) are applied to the analysis of the airfoil vibrations. In these equations, the coefficient γ_1 defines the reduced dynamic pressure of supersonic flow, which is decisive for self-excitation of the system, $\gamma_1\delta$ is the coefficient of aerodynamic damping and ξ_0 is the dimensionless distance of the elastic axis ea from the mid-chord point (Fig. 1).

3. Numerical Analysis of Stability and Nonlinear Vibrations of the Airfoil

At the beginning Eqs. (8) are linearized assuming that

$$\beta_\alpha = \overline{\beta}_z = 0 \tag{10}$$

and the solution of Eqs. (8), (10) can be found in the form

$$z(\tau) = z_0 e^{p\tau} \quad , \quad \alpha(\tau) = \alpha_0 e^{p\tau} \tag{11}$$

We then obtain the frequency equation from which critical parameters of self-excited vibrations

$$\gamma_1 = \gamma_{1cr}; \quad p = \omega_{cr} \tag{12}$$

and critical parameters of divergence $\gamma_1 = \gamma_{1div}; \quad p = 0$ (13)

can be determined depending on values of parameters of the problem under study.

For the analysis of nonlinear vibrations, the complete set of Eqs. (8) is applied. Making use of numerical methods course of vibrations is determined, regular and chaotic limit cycles are examined.

Numerical calculations have been performed for the following data: χ_z=0.2; e=0.125; r^2=0.12; β_z=0; β_α=20 and δ=0.001, 0.01, 0.1, while ξ_0=0 to 0.5.

Some results of computational analysis are presented in this paper for ξ_0=0.4; γ_1=1.2, 5 and δ=0.001, 0.1 in Figs. 2-4, where the effect of γ_1 and δ on the course of limit cycle vibrations is investigated.

References

1. Zhao, L. C. and Yang, Z. C., Chaotic Motions of an Airfoil with Non-Linear Stiffness in Incompressible Flow, J. of Sound and Vibration, v.138,2,1990.
2. Tang, D. M. and Dowell, E. H., Flutter and Stall Response of a Helicopter Blade with Structural Nonlinearity, J. of Aircraft, v. 29,5,1992.
3. Dżygadło, Z., Nowotarski, I. and Olejnik, A., Nonlinear, Regular and Chaotic vibrations of a Plate in Supersonic Flow, XII Polish Conf. on Computational Methods in Mechanics, Warszawa - Zegrze 1995.
4. Dżygadło, Z., On nonautonomous Boundary Value Problems of Plates Oscillating in Supersonic Flow, Fluid Dynamics Transactions, v. 4, IFTR, PAS, Warszawa 1969.

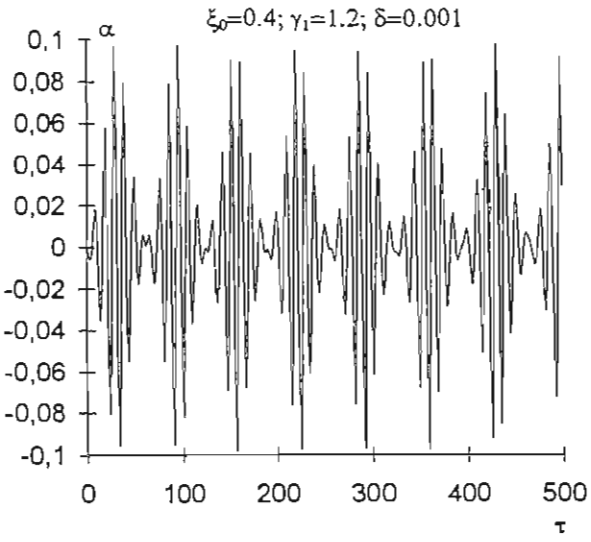

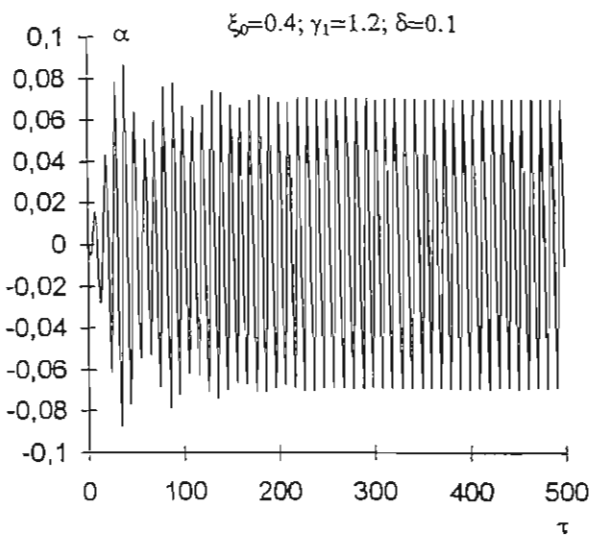

Fig. 2. Time histories of limit cycle vibrations near the flutter critical speed for γ_1=1.2 and δ=0.001, 0.1

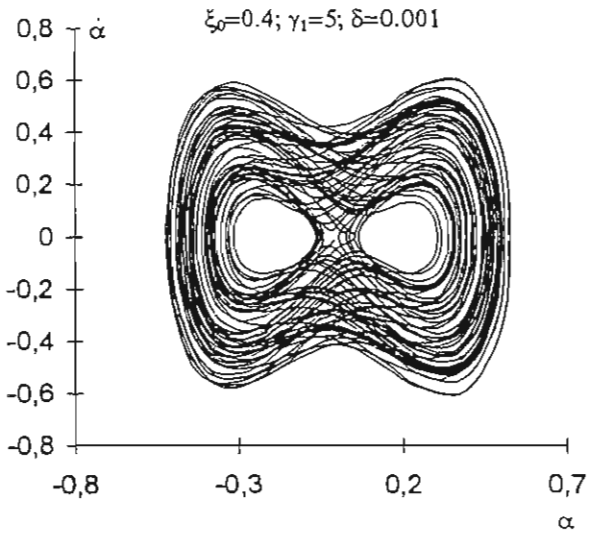

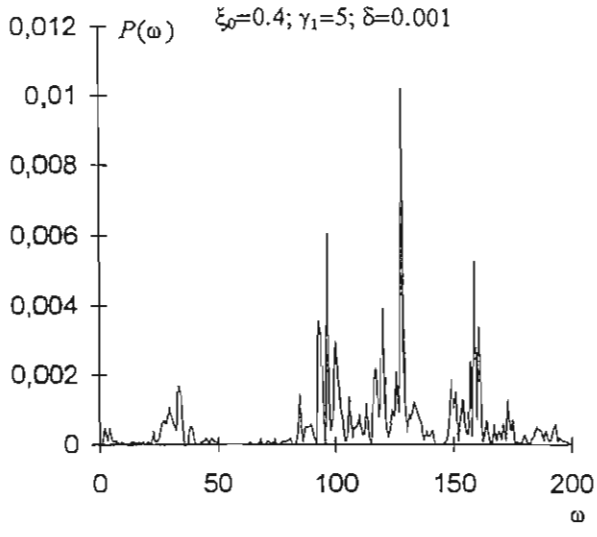

Fig. 3. Chaotic limit cycle vibration and its PSD for γ_1=5 and δ=0.001.

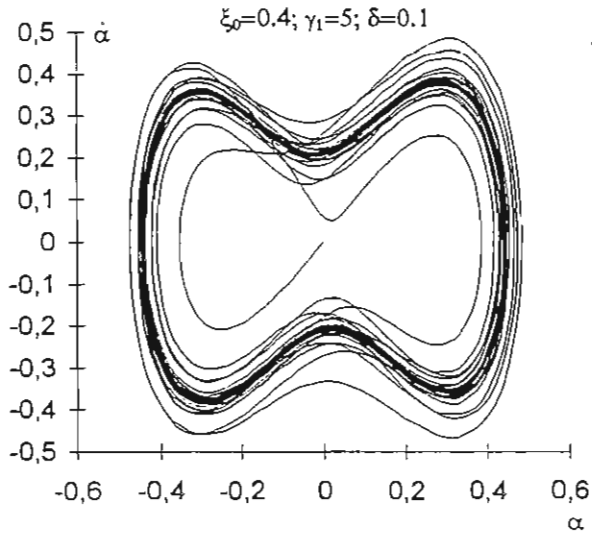

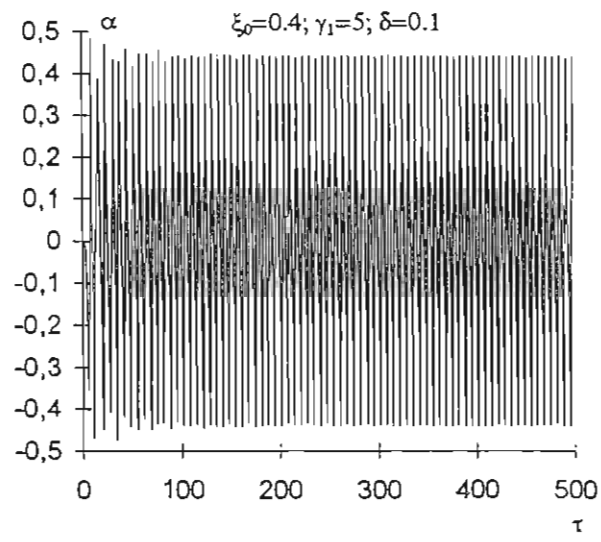

Fig. 4. Periodic limit cycle vibration for γ_1 = 5 and δ=0.1.

Lyapunov Design of Synchronizing Systems

A. Yu. Pogromsky, A.L.Fradkov
Institute for Problems of Mechanical Engineering
61, Bolshoy, VO, St. Petersburg, 199178, RUSSIA
sasha@ccs.ipme.ru, alf@ccs.ipme.ru

Abstract. The direct Lyapunov method is applied to the design of synchronizing systems. Sufficient conditions of sinchronization are established based on recent results of nonlinear control theory.

1. Introduction

Synchronization of dynamic systems is a commonly known phenomenon well studied in systems with periodic solutions. It has been recognized recently that under sertain conditions synchronization phenomenon may also be observed in systems with chaotic behavior (see, e.g. [Wu & Chua, 1994] and references therein) that is important for various applications. In the existing definitions (see Blekhman, 1971; Afraimovich, *et. al* 1987; Blekhman, *et. al* 1995) the problem of synchronization was stated as one of analysis. From the different point of view this problem can be reformulated as one of control design (Fradkov, 1994). Notice that controller which ensures synchronization can depend on parameters of interacting subsystems which may be unknown in practice. This leads to the problem of adaptive synchronization which can be posed as follows [Fradkov, 1994].

Definition 1 *Adaptive synchronization problem statement.*

Given equation of r interacting systems:

$$\dot{x}_i = F_i(x_i, u, t, \xi), \quad i = 1 \dots r, \tag{1}$$

where $x_i \in \mathcal{R}^{n_i}$ *and* $\xi \in \Xi$ *is the vector of unknown parameters.*

Find equation of the connection system:

$$u(t) = U_t[x_1(s), x_2(s), \dots, x_r(s), \theta(s), 0 \le s \le t], \tag{2}$$

where $u \in \mathcal{R}^m$ *and equation of the adaptation algorithm*

$$\theta(t) = \Theta_t[x_1(s), x_2(s), \dots, x_r(s), \theta(s), 0 \le s \le t], \tag{3}$$

ensuring the goal $|x_i(t) - \bar{x}_i(t)| \le \Delta$ *for* $t \ge t_*$, *where* $\bar{x}(t)$ *is some solution, perhaps unknown* a priori.

2. Decomposition based synchronization

Consider an n-dimensional system governed by a state equation of the form:

$$\dot{x} = f(x)$$

where $x \in \mathcal{R}^n$. Divide the system state vector into two parts in an arbitrary way: $x = (z_d, y_d)^T$. Pecora and Carrll [1990] suggested building an identical copy of this system and "drive" it with the y_d variables coming from the original system as follows:

$$\textit{Drive system} \qquad \begin{cases} \dot{z}_d = Z(z_d, y_d) \\ \dot{y}_d = Y(z_d, y_d) \end{cases} \tag{4}$$

$$\textit{Response system} \qquad \begin{cases} \dot{z}_r = Z(z_r, y_d) \\ \dot{y}_r = Y(z_r, y_r) \end{cases} \tag{5}$$

where $y_d \in \mathcal{R}^l$ and $(z_d, y_d)^T, (z_r, y_r)^T$ are the state vectors of the so-called drive and response systems [1]. Notice that variable y_d (output of the drive system) is used "to drive" the response system. Notice also that the first equation of the response system can be represented in the form:

$$\dot{z}_r = Z(z_r, y_r) + u$$

where $u = U(z_r, y_r, y_d)$. Therefore, introduced decomposition solves the problem of synthesis of synchronizing systems. The decomposition (4-5) was introduced in [Pecora & Carroll, 1990] in order to achieve the following goal of synchronization:

$$|z_d(t) - z_r(t)| \to 0, \quad as \quad t \to \infty$$

For the sake of completenes we will consider the additional synchronization goal:

$$|y_d(t) - y_r(t)| \to 0, \quad as \quad t \to \infty$$

To investigate the system behavior write down the error equation:

$$\dot{e}_z = f_0(e_z, t) \qquad \dot{e}_y = f_1(e_z, e_y, t)$$

where $e_z = z_d - z_r, e_y = y_d - y_r$. Obviously this error system is non-autonomous. The following result is valid:

Theorem 1 *Assume that*
A1. *For any initial conditions $z_d(0), z_r(0), y_d(0)$ solutions $z_d(t), y_d(t)$ exist on infinite time interval and equilibrium $e_z = 0$ of $\dot{e}_z = f_0(e_z, t)$ is globally uniformly asymptotically stable.*
A2. *$\dot{e}_y = f_1(e_z, e_y, t)$ is input-to-state (ISS)[2] stable with e_z as input.*
Then for any initial conditions the synchronization goal is achieved.

3.High-gain synchronization

Consider the following system:

$$\dot{x}_1 = f(x_1) + g(x_1)(y_2 - y_1) \qquad \dot{x}_2 = f(x_2) + g(x_2)(y_1 - y_2) \tag{6}$$

where $x_1 \in \mathcal{R}^n$ and $x_2 \in \mathcal{R}^n$ are states variables, $y_1 \in \mathcal{R}^l$ and $y_2 \in \mathcal{R}^l$ are outputs of the first and second subsystems given by

$$y_1 = h(x_1) \qquad y_2 = h(x_2)$$

We will assume that f, g and h are smooth enough to ensure existence of the solution of (6) at least on some time interval. The problem of synchronization is to find appropriate g such that $|x_1(t) - x_2(t)| \to 0$ as $t \to \infty$ for all initial conditions $x_1(0), x_2(0)$ from the given compact set. It is seen from (6) that synchronous motion in our case is a solution of the following system:

$$\dot{z} = f(z)$$

which as we will assume is well defined for all initial conditions $z(0) \in \mathcal{R}^n$ on infinite time interval.

[1] For our convinience we changed notions of the drive and response systems introduced in [Pecora & Carroll, 1990]

[2] *see, e.g. [Sontag, 1995]*

It is worth mentioning that $(y_2 - y_1)$ can be considered as a control input and in this case number of inputs is equal to the number of outputs: $m = l$. In the study of high-gain synchronization we will assume that each system to synchronize has relative degree $(1, \ldots, 1)^T$. Recall that this assumption means that matrix $L_g h(x)$ [3] is nonsingular in the neighborhood of origin. If, moreover, the distribution spanned by the vector fields $g_1(x), \ldots, g_m(x)$ is involutive, it is possible to find coordinate transformation $z = \Phi(x), z \in \mathcal{R}^{n-m}$, locally defined near $x = 0$ such that in new coordinates the system is represented in the *normal form*. Assume that such a transformation is *globally* defined (see Theorem 5.5 in [Byrnes & Isidori, 1991]). Then (6) can be rewritten as follows:

$$\begin{aligned} \dot{z}_1 &= q(z_1, y_1) \\ \dot{y}_1 &= a(z_1, y_1) + b(z_1, y_1)(y_2 - y_1) \\ \dot{z}_2 &= q(z_2, y_2) \\ \dot{y}_2 &= a(z_2, y_2) + b(z_2, y_2)(y_1 - y_2) \end{aligned} \tag{7}$$

where $a(z) = L_f h(\Phi^{-1}(z)), b(z) = L_g h(\Phi^{-1}(z))$. The problem is to find appropriate parameters of b which ensure synchronization. We will assume that the vector function b can be parametrized in the form $b(z, y) = \gamma b_\gamma(z, y)$ where $\gamma \in \mathcal{R}^1$ is the synchronization gain, also refered in the literature to as a *coupling constant*. As we will see under the certain conditions if γ exceeds some threshold value then synchronization occurs for all initial conditions from the given compact set. Imposing constraint $y_1 - y_2 = 0$ one can easily find dynamics of the constrained system (7):

$$\begin{aligned} \dot{z}_1 &= q(z_1, y_1) \\ \dot{z}_2 &= q(z_2, y_1) \\ \dot{y}_1 &= a(z_1, y_1) \end{aligned} \tag{8}$$

System (8) provides *zero dynamics* of system (7).

Now we are in position to formulate the main result of this section:

Theorem 2 *(High-gain synchronization). Assume that*
A1. $q \in C^1$, $a \in C^1$, $b \in C^1$.
A2. For all initial conditions $z_1(0), z_2(0), y_1(0)$ *system (8) has bounded trajectories which exponentially converge to the set* $z_1 = z_2$, *that is, there exist a* C^1*-smooth function* $V_0 : \mathcal{R}^{m-n} \rightarrow \mathcal{R}_+$ *and positive numbers* $\alpha_1, \ldots, \alpha_4$ *satisfying quadratic type inequalities:*

$$\alpha_1 ||z_1 - z_2||^2 \leq V_0(z_1 - z_2) \leq \alpha_2 ||z_1 - z_2||^2,$$

$$(\nabla V_0(z_1 - z_2))^T (q(z_1, y_1) - q(z_2, y_1)) \leq -\alpha_3 ||z_1 - z_2||^2,$$

$$||\nabla V_0(z_1 - z_2)|| \leq \alpha_4 ||z_1 - z_2||,$$

A3. For any $z_i \in \mathcal{R}^{n-m}$, $y_i \in \mathcal{R}^m$ *matrix* $b_\gamma(z_i, y_i)$ *is uniformly positive definite:*

$$b_\gamma(z_i, y_i) > \beta I_m, \beta > 0$$

A4. System (7) is bounded-input-bounded-state (BIBS) stable with $y_1 - y_2$ *as input.*
Then for any compact set Ω *of initial conditions* $z_1(0), z_2(0), y_1(0), y_2(0)$ *there exists* $\bar{\gamma}_\Omega$ *such that the goal of synchronization is achieved for all* $\gamma > \bar{\gamma}_\Omega$.

[3] $L_g f$ stands for Lie derivative of f with respect to vector field g

Theorem 2 establishes sufficient conditions under which two system synchronize as long as their initial conditions belong to some compact set Ω. Once this set is known it is possible to find number $\bar{\gamma}_\Omega$ such that the gain $\gamma > \bar{\gamma}_\Omega$ ensures synchronization. From the practical point of view this result is not always satisfactory. Indeed, to find $\bar{\gamma}_\Omega$ the model of the system must he known with its stable invariant set. Thus it is interesting to find an adaptive algorithm which tunes γ untill synchronization occurs. Such an algorithm can he easily found. The following result is valid:

Theorem 3 *(Gain scheduling). Assume that hypotesis of Theorem 2 holds and the synchronization gain is updated by*

$$\gamma(t) = (y_1(t) - y_2(t))^T \Lambda_1 (y_1(t) - y_2(t)) + \int_0^t (y_1(s) - y_2(s))^T \Lambda_2 (y_1(s) - y_2(s)) ds$$

where Λ_1, Λ_2 are semipositive and positive definite $m \times m$ matrices.
Then the trajectory $\gamma(t)$ is bounded and the goal of synchronization is achieved for arbitrary initial conditions $z_i(0), y_i(0), \gamma(0)$.

4. Conclusion

In this notes we have discussed some results which can help in design of synchronizing systems. One of them relates concept of Input-to-State stability, the other is based on the fact that exponentially minimum- phase system of relative degree one can be semiglobally stabilized. It is also to be said that this semiglobally stabilizing feedback makes the overall system semiglobally feedback passive. Therefore one can apply nonlinear version of the Kalman-Yakubovich lemma (see, e.g. [Byrnes *et. al.*, 1991]) to find adaptive control laws which provide synchronization under parameter mismatch.

Proofs of the presented theorems and results of computer simulation will be included in the full version of the paper.

The authors are supported in part by RFBR Grant 96-01-01151.

5. References

Afraimovich V.S.,Verichev N.N.,Rabinovich M.I., (1987) Stochastic synchronization of oscillations in dissipative systems. *Radiophysics and Quantum Electronics (RPQEAC)*, Plenum Press, vol.32, pp.795-803, 1987.

Blekhman, I. (1971) *Synchronization of dynamic systems*, (Moscow-Nauka), in Russian.

Blekhman I.I., Landa P.S., Rozenblum M.G. (1995) Synchronization and Chaotization in interacting dynamical systems. *Applied Mechanics Reviews*, vol.48(11), part 1, Nov. 1995.

Byrnes C.I. and A. Isidori (1991) "Asymptotic stabilization of minimum phase nonlinear systems", *IEEE Trans. Automat. Control*, vol. 36(10), pp. 1122-1137.

Byrnes C.I., A. Isidori and J.C. Willems (1991) "Passivity, feedback equivalence, and the global stabilization of minimum phase systems", *IEEE Trans. Automat. Control*, vol. 36(11), pp. 1228-1240.

Fradkov A.L. (1994) Nonlinear adaptive control: regulation - tracking - oscillations. Proc. *IFAC Workshop "New trends of Control Systems Design"*, Smolenice, 1994, pp.426-431.

Pecora, L.M. and T.L. Carroll (1990) "Synchronization in chaotic systems," *Phys. Rev. Lett.*, vol. 64, pp. 821-823.

Sontag E.D. (1995) "On the Input-to-State Stability Property" *European Journal of Control* vol. 1, pp. 1-24.

Wu, C.W. and L.O. Chua (1993) "A unified framework for synchronization and control of dynamical systems," *Int'l Journal Bifurcation Chaos*, vol. 4, pp. 979-998.

PERTURBATION SOLUTIONS OF STRONGLY NONLINEAR DOUBLE–WELL DUFFING OSCILLATORS

C. FRANCIOSI and S. TOMASIELLO

Department of Structural Engineering, University of Basilicata

Via della Tecnica 3, 85100, Potenza, Italy

Abstract: Two perturbation methods for strongly nonlinear oscillators have been applied to the supercritical Duffing equation, in order to obtain a close approximation to the frequency–amplitude relationship. A preliminary step introduces a modified version of the original equation, and then the perturbation methods can be applied in a highly automatized version. In the first case a hybrid Lindstedt–Poincarè–Galerkin approach is used, whereas in the second case a modified perturbation parameter is defined, which allows the introduction of strong nonlinearities. The performances of both the methods are checked against the corresponding numerical simulations by means of a symbolic code written in *Mathematica*

1. Introduction

It is well–known that the dynamic behaviour of a slender beam subjected to an axial force can be modelled, in first approximation, by a Duffing equation:

$$\ddot{x} + \alpha x + \beta x^3 = 0 \tag{1}$$

If the axial force is lower than a critical value, then the linear stiffness coefficient α is positive, and the resulting oscillator has a single stable equilibrium point at the origin. In this case the standard perturbation techniques give excellent results, even for strong nonlinearities (see Hayashi [1964], for example).

As the axial force increases beyond the critical value, the linear stiffness coefficient becomes negative, the equilibrium point at the origin becomes unstable, and two stable equilibrium points are created through a pitchfork bifurcation. The standard perturbation methods cannot be used, because the system has no linear frequency, and it is usual to employ Melnikov–like techniques (cfr. Wiggins [1990], Holmes [1979]).

In this paper two perturbation methods for strongly non–linear oscillators are adapted for this particular case, and then their performances are compared with some numerical

trajectories. In both the cases, the original equation will be written in the modified form:

$$\ddot{x} + \alpha x + \varepsilon(\beta x^3 - 2\alpha x) = 0 \tag{2}$$

with $\alpha > 0$, and then the "perturbation" parameter ϵ will be assigned the value 1, recovering the original equation.

The first perturbation technique (see Geer and Anderson [1991]) combines the well-known Lindstedt–Poincarè method with a Galerkin technique, and our results generalize in some sense the approximations given in Geer and Anderson [1991].

In the second approach, a nonlinear parameter transformation is defined, which allows the use of standard Lindsted–Poincarè even for strong nonlinearities. The method has been proposed in Cheung et al. [1991], where it has been applied to single–well Duffing oscillators.

Finally, a symbolic program written in *Mathematica* allowed us to obtain several terms in the approximation procedure, so enabling a crude convergence check.

2. Preliminaries and Results

Let us briefly review the classical Linstedt–Poincarè method, as it is the starting point for the subsequent modified perturbation techniques.

First of all, the time rescaling $\tau = \omega t$ should be performed, where ω is the (unknown) frequency of the response, so that (2) becomes:

$$\omega^2 \ddot{x} + \alpha x + \varepsilon(\beta x^3 - 2\alpha x) = 0 \tag{3}$$

where now the dot denotes differentiation with respect to the new parameter τ.

Then, the following series expansions can be written:

$$x(\tau) = x_0(\tau) + \varepsilon x_1(\tau) + \varepsilon^2 x_2(\tau) + \varepsilon^3 x_3(\tau) + \ldots \tag{4}$$

$$\omega = \sqrt{\alpha} + \varepsilon\omega_1 + \varepsilon^2\omega_2 + \ldots \tag{5}$$

and inserted into eqn.(3). A set of linear equations can be deduced and solved sequentially. If N terms of the series expansions have been calculated, then a solution is expressed as (cfr. Geer and Anderson [1991]):

$$\tilde{x}(\tau) = x_0(\tau) + \delta_1 x_1(\tau) + \delta_2 x_2(\tau) + \ldots + \delta_{N-1} x_{N-1}(\tau) \tag{6}$$

where the $N-1$ amplitudes δ_i can be determined by inserting the previous *ansatz* into the Duffing equation, and by imposing that the residual must be orthogonal to the coordinate functions x_k.

$$\int_0^{2\pi} \left[\tilde{\omega}^2 \ddot{\tilde{x}} + \alpha\tilde{x} + \epsilon\left(\beta\tilde{x}^3 - 2\alpha\tilde{x}\right)\right] x_k d\tau = 0; \qquad \text{k=1,...,N} \tag{7}$$

In this way, N nonlinear equations can be obtained, which will be solved to give the amplitudes δ_i and the frequency $\tilde{\omega}^2$.

If, for example, two coordinate functions are employed, then a trivial application of the Lindstedt–Poincarè method gives:

$$x_0 = A\cos(t); \qquad x_1 = -\frac{A^3}{8}\cos(t)\sin(t)^2 \tag{8}$$

as coordinate functions. According to the Galerkin approach, the solution will be expressed as $u = x_0 + \delta_1 x_1$ and the two resulting nonlinear equations can be easily solved. Unfortunately, the results are too long to be given here.

The second approach is even simpler, and can be essentially reduced to the following steps (cfr. Cheung et al. [1991]):

— instead of the ω series expansion (cfr. eqn.5), it is convenient to expand ω^2:

$$\omega^2 = \omega_0^2 + \epsilon\omega_1 + \epsilon^2\omega_2 + \epsilon^3\omega_3 \ldots \tag{9}$$

— a new perturbation parameter is introduced, as follows:

$$\nu = \frac{\epsilon\omega_1}{\omega_0^2 + \epsilon\omega_1} \tag{10}$$

so that ν will be less than one for every $\epsilon\omega_1$ value.

— the series expansion in term of ϵ is replaced by the new series expansion in terms of the new parameter ν.

A classical Lindstedt–Poincarè approach can now be followed. The first terms of the relationship frequency–amplitude are given by:

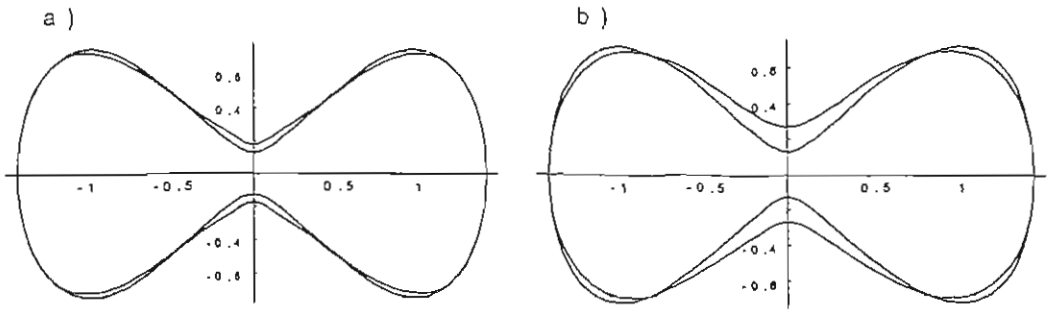

Figure 1. Comparison between numerical and perturbe solutions.

a) Lindstedt–Poincarè–Galerkin with four coordiante functions vs. numerical solution

b) Modified Lindstedt–Poincarè with six terms vs. numerical solution.

$$\omega^2 = 1 - \frac{3\,A^4\,\epsilon^2}{8\,(3\,A^2-8)^2} - \frac{51\,A^8\,\epsilon^4}{512\,(3\,A^2-8)^4} - \frac{213\,A^{12}\,\epsilon^6}{4096\,(3\,A^2-8)^6} \tag{11}$$

3. Numerical Results

As already said, a symbolic computer program was written, which greatly simplifies the tedious calculations of the perturbation methods, and makes possible to obtain a close approximation to the true results. In Fig. 1 the perturbed solution is compared in the phase plane with the corresponding numerical simulation for $\alpha = \beta = \epsilon = 1$ and for an amplitude A equal to 1.42, which is quite near to its limiting value (cfr. Wiggins [1990]).

4. References

Cheung Y.K., Chen S.H., Lau S.L. [1991] "A Modified Linstedt–Poincarè method for certain strongly non–linear oscillators", *Int. J. Non–linear Mech.*, 26 (3/4), 367–378

Geer J.F., Andersen C.M. [1991] "Resonant frequency calculations using a hybrid perturbation – Galerkin technique", *Appl. Mech. Rev.* 44 (11), S76–S88

Hayashi C. [1964], *Nonlinear Oscillations in Physical Systems* (McGraw–Hill, New York)

Holmes P.J. [1979] "A nonlinear oscillator with a strange attractor", *Trans. Roy. Soc.*, 292 , 419–447

Wiggins S. [1990] *Introduction to Applied Nonlinear Dynamical Systems and Chaos*, (Springer Verlag)

Controlling Chaos for Magneto-Elastic Beam by Delayed Feedback Control

Takashi HIKIHARA
Department of Electrical Engineering, Kansai University
Yamate-cho, 3-3-35, Suita, Osaka, 564 JAPAN
Fax : +81-6-388-8843
hikihara@ipcku.kansai-u.ac.jp

Abstract

The delayed feedback control method has a potential to stabilize the unstable periodic orbit embedded in the chaotic attractor. In this paper, the stabilization of the unstable periodic orbit in the magneto-elastic system is discussed experimentally.

1. Introduction

The controlling chaos is a hot research field in nonlinear dynamics and numerous papers have been published [1]. Among them the delayed feedback control method, which is proposed by Pyragas [2], is an interesting controlling method on the standpoint of application to real systems. We have already applied the method to stabilize the chaotic motion appeared in a magneto-elastic system [3-5]. The magneto-elastic beam is well-known to appear the chaotic motions in the external forcing condition [6]. The system can be described by Duffing's equation. As for the real system, however, it is difficult to describe the nonlinearities and the exact parameter. As results of the experiments, it was shown that the delayed feedback control is effective to stabilize the unstable periodic orbit embedded in the chaotic attractor of the magneto-elastic beam [5].

Many of the methods proposed for the controlling chaos should wait for the moment when the state of the system comes close to the well-known unstable periodic orbit. The linear feedback theory plays the role only in the neighbourhood of the expected orbit. In the case of the delayed feedback control, the stabilized unstable periodic orbit cannot be predicted until the motion is stabilized. However, the control can be acheived without the knowledge of the unstable periodic orbit. In this paper some aspects ablut the controlling method is discussed experimentally.

2. Experimental Setup and Control Method

The magneto-elastic beam system is well-known as a system that shows the chaotic motion [6]. The elastic beam that is fixed on the frame at the one end is vibrated between the two magnets placed on the frame. The system can be identically modeled by the Duffing's equation:

$$\ddot{x} + 2\delta\dot{x} + f(x) = B\cos\omega t \tag{1}$$

When the feedback control is applied to the system the system can be represented by

$$\ddot{x} + 2\delta\dot{x} + f(x) = B\cos\omega t + u(t) \tag{2}$$

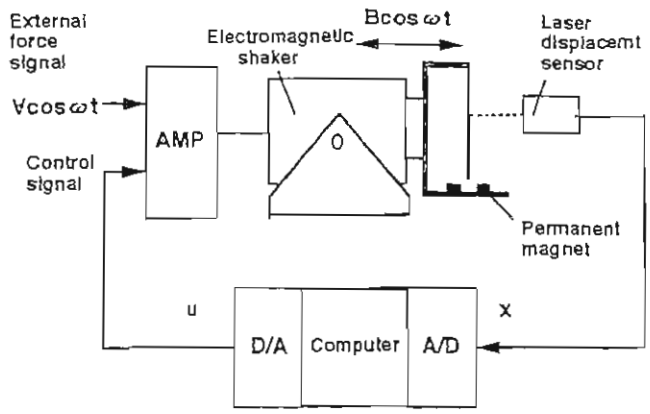

Figure 1: System configuration.

Here the feedback value u(t) is depending on the controlling method. To establish the delayed feedback loop in the experiment, the feedback signal can be induced by the error between the output state values and the delayed ones of the forced magneto-elastic system. To make the experimental system simple, the loop is composed only of the velocity of the elastic beam. When the delayed time is set at τ,

$$u(t) = K(\dot{x}(t) - \dot{x}(t-\tau)) \tag{3}$$

In the case Eq. (2) becomes the difference-differential equation. Fig. 1 shows the detail experimental system. The control signal is superposed to the forcing sinusoidal signal of the electro-magnetic shaker. To stabilized an unstable period-one orbit, the delayed time is set at the same as the forcing period. Moreover, the stabilization of the unstable period-N orbit is expected when the delayed time is set at the N times forcing period [2, 5]. Once the motion of the magneto-elastic beam is stabilized, the control signal becomes extremely low level. However, if we begin the control at the arbitrary timing of the chaotic motion, the stabilization cannot be insured at every trial. The reason is that the feedback gain has a limmit in the real system. The delayed feedback control means that the original system (differential equations) is converted into an infinite dynamical system (difference-differential equation) when the system is controlled. Therefore the theoretical analysis is extremely difficult.

3. Experimental Results and Discussion

As the nonlinearity depends on the relation between the beam and the magnets, there is some varieties of the nonlinearity. In this case the potential well by the nonlinearity is the double well shape. We will not discuss whether the system shows the chaotic motion or not. At first, in order to confirm the effectiveness of the control method, the stabilization of the unstable periodic motion with the period 1T, which exists after the period doubling bifurcation, is considered. The results is shown in Fig.2.

The figure shows that the unstable periodic orbit is stabilized on the phase plane, where two period-two stable orbit and one unstable periodic orbit exist at least. The result implies that the delayed feedback control has a possibility to select the unstable periodic orbit only by setting the delayed time. When we repeat the switching the control on and off, the stabilization is achieved by every controled interval as shown in Fig.3.

In the chaotic attractor, the infinite number of unstable periodic orbits are embedded. Potentially, the arbitrary unstable periodic orbit can be stabilized by using the delayed

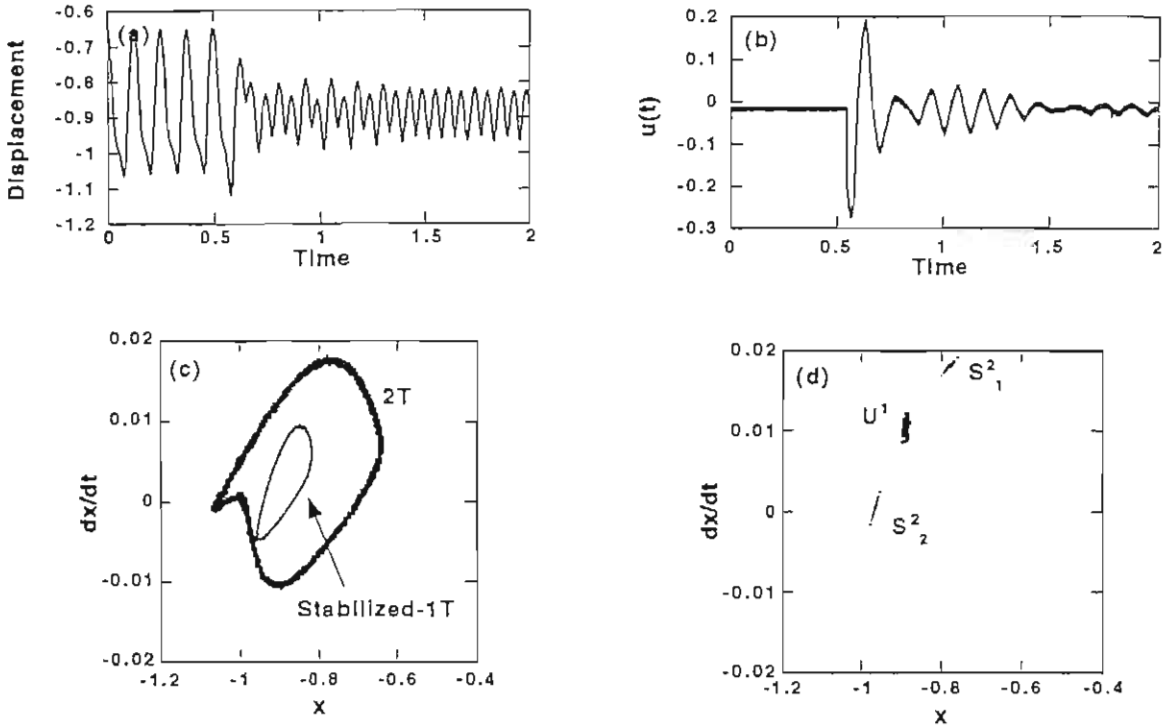

Figure 2: Stabilization of the unstable periodic orbit embedded in the period -two motion; (a) displacement, (b) control signal, (c) trajectories of the period 2T motion and stabilized 1T motion, and (d) Poincaré map of 2T and stabnilized 1T motion.

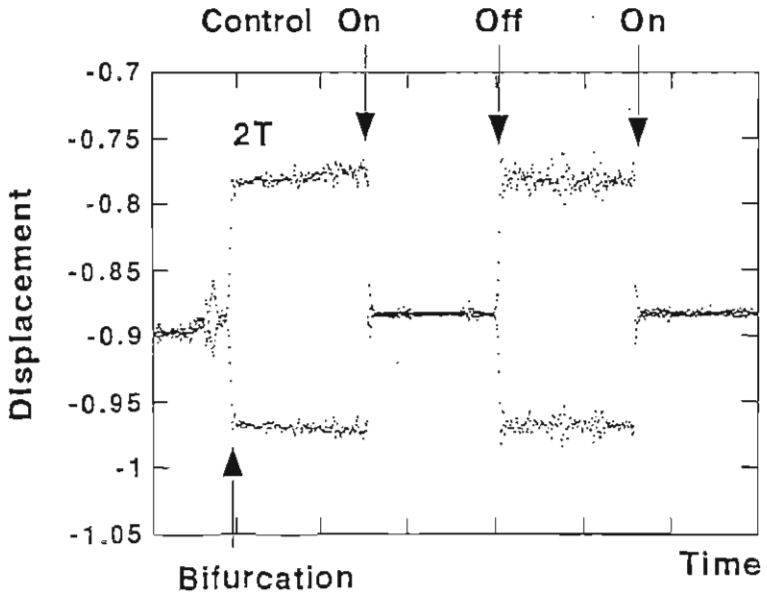

Figure 3: Stability by switching the control on and off.

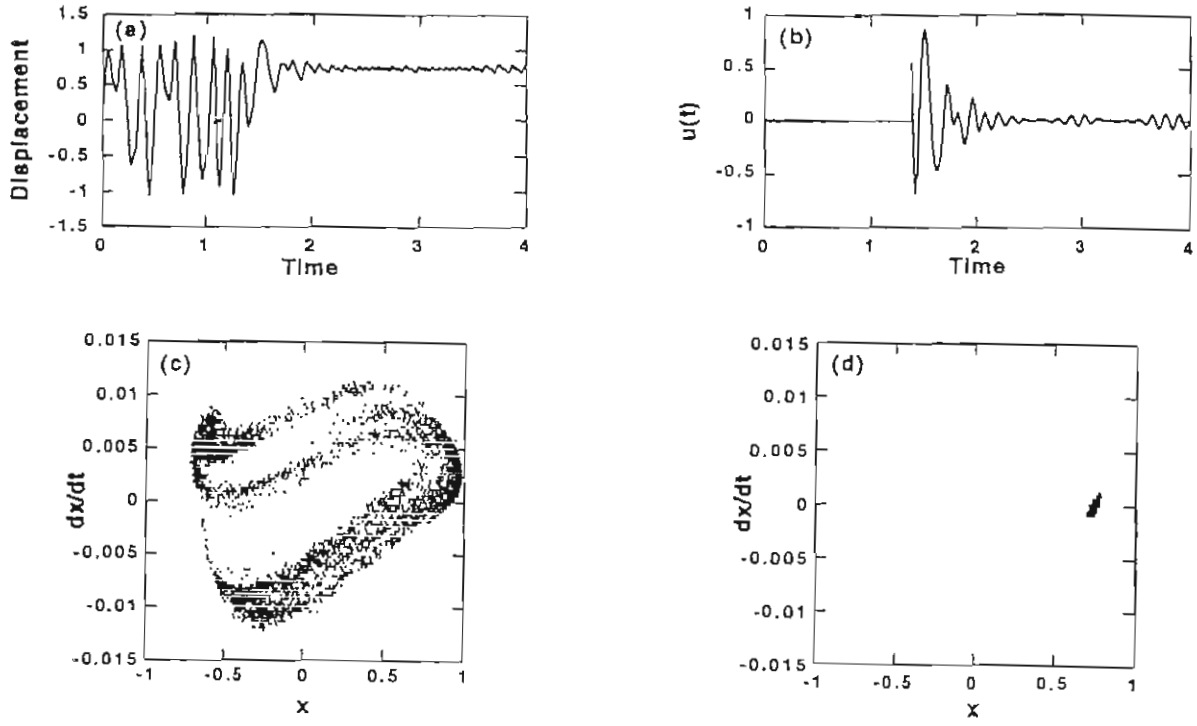

Figure 4: Stabilization of the unstable periodic orbit embedded in the chaotic motion; (a) displacement, (b) control signal, (c) Poincaré map of the chaotic motion, and (d) Poincaré map of stabilized unstable periodic motion.

feedback control. However, the each basin of the periodic orbit is considered to be narrow and besides to the basin of other periodic orbit. Then it is difficult to stabilize every unstable periodic orbit experimentally. The stabilized unstable periodic orbit is liable to go to the most possible one as shown in Fig.4.

4. Conclusion

In this paper it is shown that the unstable periodic orbit of the magneto-elastic beam system can be stabilized by the delayed feedback control both in the periodic state and the chaotic state. These results should be a clue to the theoretical analysis of the delayed feedback control and further experimental applications.

References

[1] G.Chen, ftp : "uhoop.egr.uh.edu/pub/TeX/ chaos.tex".

[2] K.Pyragas, Phys. Lett. A, 170 (1992) 421.

[3] T.Kawagoshi & T.Hikihara, Tech. Rep. of IEICE Japan, NLP94-80 (1994).

[4] T.Hikihara & T.Kawagoshi, Phys. Lett. A, 211 (1996) 29.

[5] T.Hikihara & M.Touno, 1995 Proceedings of International Synposium Nonlinear Theory and Its Applications, Las Vegas, Dec.10-14, 981.

[6] F.C.Moon, Chaotic and Fractal Dynamics (John Wiley Sons, 1992).

DYNAMIC LOADS IN A DRIVE MECHANISM

Victor Hinko
State University "Lviv Politechnic"
290070, Lviv-70, Khotktvich Str., 64/25, Ukraine

Abstract: Dynamic phenomena occuring in drive elements of a lifting mechanism of drill string are considered, taking into account the change jf the cable length and resistance of the environment in an out-pipe space.

Equations of the cable and string motion are built with consideration of a linear speed of cable-over-drum wrapping, difference of gravitation constants during motion inair and liquid.

The work of drill strings when fullfilling technological operations in the process of making wells is connected with considerable dynamic loads in the elements of a lifting mechanism. For convinience of investigation, the lifting mechanism of the drillstring is divided into component elements which are funtionally interdependent and interconnected by means of a pneumatic coupling.

From differential equations taking into account initial and boundary conditions of the problem, we pass over to integral-differential equations with are studied dy the methods of Bogolubow-Mytropolskyi assymptote theory using a small parameter, as well as by application of "cable functions".

The work of drill strings when fullfilling technological operations in the process of making wells is connected with considerable dynamic loads in the elenents of a lifting mechanism. For convinience of investigation, the lifting mechanism of the drill string isdivided into component elements which are funtionally interdependent and interconnected by means of a pneumatic coupling.

Structurally, the lifting mechanism comprizes the following elements:

1. Drive which is divided into diesel, diesel-hydraulic (is used with power aggregates СА-6, СА-10 and СА-1АДГ-1000), ac electrical and do electrical motors.

2. Transmission which consists of summing reductor, decreasing reductor and gear box.

3. Drill winch which depending on the design may be of the following types: (У2-5-5, ЛБУ-1000, ЛБУ-1700 and ЛБУ-3000).

4. Pulley block system which consists of crownwheel, load rope, and hooked pulley block.

5. Drill pipe column which corporates drill column, loaded bottom and face motor.

6. Chisel feed control is an auxiliary elements in drilling and is designed to form and regulate on-face axial force value.

All the mentioned elements of the lifting mechanism are connected each with other by means of tire-and-air flux clutches.

Depending on the design, each element of the lifting mechanism may be either in the form of a eparate assembly, or together with other elements of this mechanism. Each of the lifting mechanism's components is of a particular design, and therefore, the investigation is carried out by different dynamic models. Basad on the analysis of kinematic schemes,the eguivalent dynamic schemes have been built; they permit to study each element and obtain, as a result, calculation parametrs which will be initial when investigating the subsequent element of the lifting mechanism. As an example, let's consider kinematic and equivalent dynamic model of the direct current electric drive.

For the given drive the following operation variants are inherent: 1 and 2 - operation of the electric motors I or II when they are linked with the winch's shaft; 3 - simultaneous operation of the electric motors I or II; 4 and 5 - operation of the electric motor I and II via lowering chain transmission (this operating variant is used for lifting maximum load 4MN or for pulling pulley block system); 6 - operation of the lifting mechanism with the chisel feed control.

Mathematical models for each of the above variants of a drive are composed based on the second type Lagrange equation, taking into account non-linear characteristics of elastic coupling links, factual mechanic characterictics of the drive, the effect of time-variable lengths of load-carrying ropes, variable inertia moments of the drum.

For example, let's consider mathematical models for the first and second variants. For the first variant, mathematical model is described by the set of equations as follows:

$$I_1 \frac{d^2\varphi_1}{dt^2} + \nu_{11}\left(\frac{d\varphi_1}{dt} - \frac{d\varphi_{12}}{dt}\right) + c_{11}(\varphi_1 - \varphi_{12}) = T_1(t); \qquad (1)$$

$$J_{36}\frac{d^2\varphi_{12}}{dt^2} + \nu_{12}\left(\frac{d\varphi_{12}}{dt} - \frac{d\varphi_{13}}{dt}\right) + \nu'_{13}\left(\frac{d\varphi_{12}}{dt} - \frac{d\varphi_{35}}{dt}\right) - \nu_{11}\left(\frac{d\varphi_1}{dt} - \frac{d\varphi_{12}}{dt}\right) +$$
$$+ c_{12}(\varphi_{12} - \varphi_{13}) - c'_{13}(\varphi_{12} - \varphi_{35}) - c_{11}(\varphi_1 - \varphi_{12}) = 0; \qquad (2)$$

$$J_{37}\frac{d^2\varphi_{35}}{dt^2}+\nu_{35}\frac{d\varphi_{35}}{dt}+\nu'_{13}\left(\frac{d\varphi_{12}}{dt}-\frac{d\varphi_{35}}{dt}\right)-c_{35}\varphi_{35}-c'_{13}(\varphi_{12}-\varphi_{35})=0; \quad (3)$$

$$J_{2M3}\frac{d^2\varphi_{13}}{dt^2}+\nu_{13}\left(\frac{d\varphi_{13}}{dt}-\frac{d\varphi_{d}}{dt}\right)-\nu_{12}\left(\frac{d\varphi_{12}}{dt}-\frac{d\varphi_{13}}{dt}\right)+c_{13}(\varphi_{13}-\varphi_{d})-c_{12}(\varphi_{12}-\varphi_{13})=0; \quad (4)$$

$$J_d(t)\frac{d^2\varphi_{d}}{dt^2}+J_d(t)\frac{d\varphi_{d}}{dt}+\nu_{13}\left(\frac{d\varphi_{13}}{dt}-\frac{d\varphi_{d}}{dt}\right)+c_{13}(\varphi_{13}-\varphi_{d})=-T_r(t); \quad (5)$$

For the second variant, mathematical model is described by the set of equations as follows:

$$I_{11}\frac{d^2\varphi_{11}}{dt^2}+\nu_{21}\left(\frac{d\varphi_{11}}{dt}-\frac{d\varphi_{21}}{dt}\right)+c_{21}(\varphi_{11}-\varphi_{21})=T_{11}(t); \quad (6)$$

$$J_{36}\frac{d^2\varphi_{21}}{dt^2}-\nu_{21}\left(\frac{d\varphi_{11}}{dt}-\frac{d\varphi_{21}}{dt}\right)+\nu_{22}\left(\frac{d\varphi_{21}}{dt}-\frac{d\varphi_{d}}{dt}\right)+\nu_{23}\left(\frac{d\varphi_{21}}{dt}-\frac{d\varphi_{31}}{dt}\right)-$$
$$-c_{21}(\varphi_{11}-\varphi_{21})+c_{22}(\varphi_{21}-\varphi_{d})+c_{23}(\varphi_{21}-\varphi_{31})=0; \quad (7)$$

$$J_{37}\frac{d^2\varphi_{31}}{dt^2}+\nu_{31}\frac{d\varphi_{31}}{dt}-\nu_{23}\left(\frac{d\varphi_{21}}{dt}-\frac{d\varphi_{23}}{dt}\right)+c_{31}\varphi_{31}-c_{23}(\varphi_{21}-\varphi_{23})=0; \quad (8)$$

$$\left[J_d(t)+J_{2M3}\right]\frac{d^2\varphi_{d}}{dt^2}+J_d(t)\frac{d\varphi_{d}}{dt}-\nu_{22}\left(\frac{d\varphi_{21}}{dt}-\frac{d\varphi_{d}}{dt}\right)-c_{22}(\varphi_{21}-\varphi_{d})=-T_r(t). \quad (9)$$

Similarly, one can compose equations for the other operation variants of the direct current drive. In equtions 1...9 quantity $J_d(t)$ is determined by the formula:

$$J_d(t)=J_0+0{,}5q_1\omega_d\sum_{1}^{3}(R_0+ih)\,t_i. \quad (10)$$

In order to solve the above differential equation sets we used the program **PUSK** with a subprogram **DMOM5** that defines values of quantities T_I T_{II} from the dependency 11:

$$T=C_M\Phi i_a, \quad \text{where} \quad \Phi=\Phi(i_a,\ i_f). \quad (11)$$

Here C_M is constant coefficient, and work flow is the function of anchor chain current i_a and free field winding i_f.

Indicating p as time differentiation we write down

$$pi_a=S_a u_a+T_a u_f+E_a, \quad pi_f=S_f u_f+T_f u_a+E_f, \quad (12)$$

where

$$S_a=1/(L_r-L_{nf}L_{af}/L_{ff}); \quad T_a=-S_a L_{nf}/L_{ff};$$
$$E_f=-(L_{fa}E_a+r_f i_f)/L_{ff}; \quad T_f=S_a L_{nf}/L_{ff}; \quad (13)$$
$$S_f=(1-L_{fa}T_a)/L_{ff};$$
$$E_a=S_a(L_{nf}r_f i_f/L_{ff}-C_E\omega\Phi-\Delta u-r_a i_a).$$

Coefficients L_{jk} are determined as

$$L_{jk}=d\Psi_j/di_k, \quad j=a,\ n,\ D,\ f, \quad k=a,\ f,$$

where Ψ_a, Ψ_n, Ψ_f, Ψ_d are full flux-linkage of anchor winding, sequential and free field winding, and winding of additional poles.

$$L_r = L_{aa} + L_{na} + L_{Da}; \qquad L_{rf} = L_{af} + L_{nf} + L_{Df}., \tag{14}$$

r_a, r_f is resistance of anchor chain and field winding;

u_a, u_f is voltage;

Δu is voltage cut down in a brush contact;

ω_1 is angle speed of a rotor which is defind by the formula 15

$$\omega_1 = p\int_0^t \left[(T_i - T_r)/J\right]dt. \tag{15}$$

Here, p is a number of pole paifs; T_r is statistic moment of resistance on a shaft; J is concentrated inertia moment of the system which is initiated.

Dynamicity coefficients K_d on the shaft of a drill winch in start at $T_r = 40$ kNm, and start time in 4s equals for each of the variants: 1.216 - for the first; 1.218 - for the second; 1.209 - for the third; 1.295 - for the fourth; 1.303 - for the fifth, and 1.446 - for the sixth variant. The maximum value K_d is obtained during drilling. As lifting time increases, the dynamicity coefficient decreases.

Resistance moment T_r which is applied to the winch drum is calculated from the relationship

$$T_r(t) = F(x, t)R_d(d), \tag{16}$$

where $F(x, t)$ is force in the rope branch which is reeled over the drum: $R_d(t)$ is variable radius of rope reel over the drum, which is determined from the dependency

$$R_d(t) = R + h(z + \operatorname{sign} t). \tag{17}$$

The force value $F(x, t)$ is determined when solving the equations of the rope and drill pipe column movements

$$\frac{du_1^2(x_1, t)}{dt^2} - a_1^2 \frac{du_1^2(x_1, t)}{dx_i^2} = q \pm \frac{dv_d(t)}{dt}; \tag{18}$$

$$\frac{du_2^2(x_2, t)}{dt^2} + 2\nu \frac{du_2^2(x_2, t)}{dt} - a_2^2 \frac{du_2^2(x_2, t)}{dx_2^2} = q_0. \tag{19}$$

In these equation $u_1(x_1, t)$, $u_2(x_2, t)$ are longitudinal displecements of cross-sections of the cable and the drill string; a_1, a_2 are speeds of propagation of alastic waves of deformations in the cable and the drill string; g, g_0 is gravitation constant during motion in the air liquid; ν is resistance of motion of the drill string in the out-pipe space; $v_d(t)$ is speed of cable-over-drum wrapping of the drill winch

$$g_0 = g\left(1 - \gamma_p / \gamma_t\right), \tag{20}$$

where γ_p, γ_t is density of drilling mud and the pipe material.

Solution of equation 18 must satisfy the following boundary conditions, at:

$$x_3 = 0 \qquad M_3 u_{2t} - E_2 A_2 u_{2\times 3} = M_3 g_0; \tag{21}$$

$$x_3 = 1 \qquad M_2 u_{2t} + E_2 A_2 u_{2\times 3} = M_3(g \pm v_d) + f(x,\ t). \tag{22}$$

In section at $x_2 = l_2$, coordinates $X_2 = 0$ and $X = l_0$.

In the point of rope reel over the drum $X = l(t)$ the boundary condition is expresed by the dependency

$$u_1[l(t),\ t] = \int_0^t u_{1x}[l(t),\ t](t)dt \tag{23}$$

where the rope length

$$l(t) = \int_0^t v_d dt \tag{24}$$

Initial conditions when solving equations 18...19 in a general case are functions 25:

$$\begin{aligned} u_1(x) &= \varphi_1(x) \qquad & u_{1t}(x) &= \varphi_2(x) \\ u_2(x) &= \psi_1(x_3) \qquad & u_{2t}(x_3) &= \psi_2(x_3) \end{aligned} \tag{25}$$

In connection with the fact that doundary condition 21 is not being integrated, we come from equations 18 to integral-differential equation 24

$$V_1(x,\ t) = -\int_{l(t)}^{l_0} K[s, x, l(t)]\rho(s)V_{1t}(s,\ t)ds - \{V_{1x}[l(t),\ t](t)\}_t \times$$

$$\times \int_{l(t)}^{l_0} K[s, x, l(t)]\rho(s)ds - \int_{l(t)}^{l_0} K[s, x, l(t)]\rho(s)(g \pm v_d)ds. \tag{26}$$

Having investigated the latter by Boholiubov-Mytropolskyi asymptotic theory, we obtain analytyical dependencies to determine vibration frequency forces in cross-sections of the rope reel over the drum:

$$p_0 = \left\{3E_1A_1M^{-2}q_1 / \left[3 + \alpha[l(t)]\alpha[l(t)]\right]\right\}^{0,5}, \tag{27}$$

where $M = M_1 + M_2 + m_2 / 3, \qquad \alpha(l[t]) = q_1[l_0 - l(t)] / M,$

when q_1 is running mass of the rope.

Analysing curves we can see thet an error in calculation by the exact and approximate formulas will be larger at smaller length of the pulley block. So. for the drill rig winch ЛБУ-3000 values δF_{max} which are received by the exact formula at $l_p = 1m$ equal 175 kN and at length l_p=50m, 38 kN.

Thus, at the average and large length of a pulley block, forces can be determined by approximate formulas, and at the small length 27 and 28, in order to raise accuracy, it is necessary to use exact solutions.

To conclude, I can say that the analytical investigation performed permits to determine vibration frequencies, deformations and forces in drive links of the lifting mechanism of the drill rig.

A SIMPLE CRITERION FOR THE OCCURRENCE OF CHAOS

Kazumasa Hirai
Dept. of Applied Mathematics, Konan University,
8-9-1, Okamaoto, Higashi-Nada, Kobe, Japan 658

Abstract: A simple method to analyze the occurrence condition of chaos in a nonlinear control system is investigated. The basic idea for this analysis is that, if every equilibrium point becomes unstable and there exists an unstable limit surface surrounding them, then chaos may occur. The describing function method is applied for this analysis and the parameter region for the occurrence of chaos is shown for several transfer functions.

1. Introduction

It can be considered that, if all equilibrium points are unstable and there exists a closed stability boundary surrounding these points in the state space, every trajectory starting from the inside of the boundary surface does not converge to the equilibrium points and also does not diverge. Then, every trajectory may wander in the state space. This phenomenon may be a chaotic motion [Khbnik et al,1993], [Kuramitsu,1995]. In the following let call this stability boundary an unstable limit surface, from where every trajectory starting from the inside or outside of this surface goes away [Fukuda & Hirai,1995].

In this paper, based on the above considerations, the occurrence conditions of chaos will be studied. The prediction method proposed here is simple and applicable for higher order system. A parameter region for the occurrence of chaos will be shown for several transfer functions.

2. The Occurrence Condition of Chaos

The first step to study the occurrence condition of chaos is to investigate the conditions for every equilibrium point to be unstable and next step is to find the existence condition of an unstable limit surface surrounding them.

However, since it is not easy to obtain the existence condition of an unstable limit surface, we may consider the existence condition of an unstable limit cycle at first. Since a limit cycle is a closed curve and not surface, the additional conditions must be considered for the trajectory not to diverge and to remain in some closed regions in the state space.

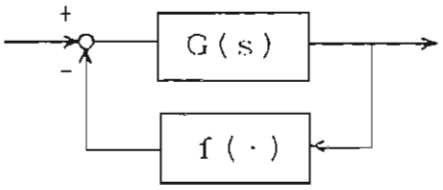

Fig.1 Nonlinear control system

Now, a nonlinear control system shown in Fig.1 is considered. The transfer function $G(s)$ and nonlinear function $f(x)$ are

assumed to be represented by

$$G(s) = N(s) / D(s) \quad (1)$$

$$N(s) = b_0 s^m + \cdots + b_{m-1} s + b_m$$

$$D(s) = s^n + a_1 s^{n-1} + \cdots + a_{n-1} s + a_n \ (n \geq m) \quad (2)$$

$$f(x) = x^3 - kx,$$

where we assume that, G(s) has a low pass filter characteristic and $b_m \neq 0$.

This equation can be represented in the form of the state equation as

$$\left.\begin{aligned} \dot{x}_1 &= x_2,\ \dot{x}_2 = x_3, \cdots \\ \dot{x}_n &= -(a_1 x_n + a_2 x_{n-1} + \cdots + a_n x_1 + f(y)) \end{aligned}\right\} \quad (3)$$

$$y = b_0 x_{m+1} + b_1 x_m + \cdots + b_m x_1 \quad (4)$$

2.1 Bifurcation of equilibrium points

From Eq.(3), the equilibrium points are given by

$$P^0:\ x_1 = x_2 = \cdots = x_n = 0$$

$$p^{\pm}:\ x_1 = \pm\sqrt{(kb_m - a_n)/b_m^3}$$

$$x_2 = x_3 = \cdots = x_n = 0$$

Clearly the equilibrium points $P^{\pm}$ can only exist if $k > a_n / b_m$. Linearizing Eq.(3) around each equilibrium point and investigating the roots of characteristic equations, the stability and the bifurcation mode of each equilibrium point can be obtained. For example, it will be shown that if k increases, P^0:unstable $\Rightarrow$ $P^{\pm}$:stable $\Rightarrow$ $P^{\pm}$:unstable (Hopf bifurcation). In this final state three equilibrium points becomes unstable.

2.2 Limit cycle

Next, the existence condition of an unstable limit cycle surrounding three unstable equilibrium points is now studied. Assume that one stable limit cycle around one of $P^{\pm}$ is represented by

$$x_1(t) = A + B\sin\omega t \quad (5)$$

The output $f(x_1)$ can be approximated as

$$f(x_1) = N_0(A.B)A + N_1(A.B)\sin\omega t, \quad (6)$$

where N_0 and N_1 are represented by

$$N_0(A,B) = \frac{1}{2\pi}\int_{-\pi}^{\pi} f(A + B\sin\omega t)d\omega t$$

$$= -k + A^2 + \tfrac{3}{2}B^2 \quad (7)$$

$$N_1(A,B) = \frac{1}{2\pi}\int_{-\pi}^{\pi} f(A + B\sin\omega t)\sin\omega t d\omega t$$

$$= -k + 3A^2 + \tfrac{3}{4}B^2 \quad (8)$$

It is to be noted that this approximation can be satisfied if the linear part $G(j\omega)$ has a property of a low pass filter. From Fig.1, we have

$$-\{G(0)N_0(A,B)A + G(j\omega)N_1(A,B)B\sin\omega t\} = A + B\sin\omega t \quad (9)$$

Then, the following equations are obtained:

$$1 + G(0)N_0(A,B) = 0 \quad (10)$$

$$1 + G(j\omega)N_1(A,B) = 0 \quad (11)$$

Substituting Eq.(7) into Eq.(10), we have

$$A = \pm\sqrt{k - \tfrac{3}{2}B^2 - g_0} \quad (12)$$

where $g_0 = 1/G(0)$, and the sign $\pm$ of A corresponds to $p^{\pm}$.

Hence, from Eq.(8),

$$N_1(A,B) = N_1(B) = 2k - \tfrac{15}{4}B^2 - 3g_0 \quad (13)$$

The describing function method will now be applied [Gelb,A. et al, 1968]. From Eq.(11), if there exists a limit cycle, two loci, $G(j\omega)$ and $-1/N_1(A,B)$ must have an intersection on the complex plane.

Since $N_1(A,B)$ is real number, $\mathrm{Im}\,G(j\omega) = 0$ at the intersection. Now let $\mathrm{Im}\,G(j\omega_p) = 0$, and $\mathrm{Re}\,G(j\omega_p) = 1/l_0$. Then, from Eq. (13), we have

$$B = B_s = \sqrt{\tfrac{4}{15}(2k - 3g_0 + l_0)} \quad (14)$$

Substituting Eq. (14) into Eq. (12), we have

$$A = \pm\sqrt{\tfrac{1}{5}(k + g_0 - 2l_0)} \quad (15)$$

The stability of a limit cycle can be determined by checking the relative location

of the both loci.

Next, the existence condition of an unstable limit cycle surrounding the equilibrium points is now studied. Since the limit cycle has no bias component in this case, we put $A = 0$ in Eq. (5). Then from Eqs. (8) and (11), we have

$$B = B_u = \sqrt{\tfrac{4}{3}(k - I_0)}. \tag{16}$$

By plotting two loci, it will be made clear that this limit cycle is unstable.

Summarizing above, the amplitude of stable and unstable limit cycle, and the bias component are given by Eqs. (14), (16) and (15), respectively.

In order for the unstable limit cycle to encircle stable limit cycles,

$$B_s + |A| \le B_u \tag{17}$$

Substituting Eqs. (14), (15), (16) into Eq. (17) and using $I_0 < 0$, we have

$$2I_0 - g_0 \le k \le -14I_0 + 15g_0 \tag{18}$$

However, the left-hand side condition is included in $k \ge (3g_0 - I_0)/2$ obtained from Eq.(14).

Therefore, k must be satisfied

$$\tfrac{1}{2}(3g_0 - I_0) \le k \le -14I_0 + 15g_0 \tag{19}$$

It is to be noted that the left-hand side condition is equal to the condition for every equilibrium point to be unstable.

Next, the problem that the trajectory starting from the inside of the unstable limit cycle does not diverge in the state space must be studied.

It will be clear, that since $x_1(t)$ is bounded, if a_1 is positive, all state variables do not diverge from Eq.(3).

Summarizing the above, it can be said that Eq.(19) and $a_1 > 0$ is the necessary condition for the occurrence of chaos for system of Fig.1.

3. Chaotic region

In this section the chaotic region in parameter plane for several transfer function will be studied.

(a) $G(s) = 1/(s^3 + a_1 s^2 + a_2 s + a_3)$ (20)

Since $\omega_p = \sqrt{a_2}, I_0 = a_3 - a_1 a_2, g_0 = a_3$, then Eq. (19) becomes

$$\tfrac{a_1 a_2}{2} + a_3 \le k \le 14 a_1 a_2 + a_3. \tag{21}$$

(b) $G(s) = (b_0 s + b_1)/(s^3 + a_1 s^2 + a_2 s + a_3)$ (22)

$$\omega_p = \sqrt{(b_1 a_2 - b_0 a_3)/(b_1 - a_1 b_0)}$$

$$I_0 = (a_3 - a_1 a_2)/(b_1 - a_1 b_0)$$

$$g_0 = a_3 / b_1$$

Then,

$$\tfrac{1}{2} \cdot \tfrac{a_1}{b_1} \tfrac{a_2 b_1 - a_3 b_0}{b_1 - a_1 b_0} + \tfrac{a_3}{b_0} \le k \le 14 \tfrac{a_1}{b_1} \cdot \tfrac{a_2 b_1 - a_3 b_0}{b_1 - a_1 b_0} + \tfrac{a_3}{b_1}. \tag{23}$$

(c) $G(s) = 1/(s^4 + a_1 s^3 + a_2 s^2 + a_3 s + a_4)$ (24)

$$\omega_p = \sqrt{c/a}, \quad I_0 = \tfrac{a_1}{b_1} \cdot \tfrac{a_1(a_3 - a_1 a_2) - a_1^2 a_3}{a_1^2}, \quad g_0 = a_4$$

Then,

$$\tfrac{1}{2} \cdot \tfrac{a_1}{a_1^2}(a_1 a_2 - a_3) + a_4 \le k \le 14 \cdot \tfrac{a_1}{a_1^2}(a_1 a_2 - a_3) + a_4 \tag{25}$$

The parameter regions for the occurrence of chaos for the above transfer functions and examples of chaotic trajectory are shown in Fg. 2.(a) ~ (c). In the shaded region, chaos may occur. In the upper (lower) part of the shaded region, system may converge (diverge).

We can say that the condition given by Eq. (19) is necessary condition and chaos does not always occur even if the parameter values satisfy these conditions.

4. Conclusions

In this paper, a simple method to analyze the occurrence conditions of chaos in a nonlinear control system was investigated. The parameter conditions for several transfer functions and the simulation results were shown.

The method proposed here is simple and applicable. However, since the describing function method is used, the accuracy of the approximation may be problem, if the system has no low pass filter characteristics.

Acknowledgments

The author thanks Ms. M. Fukuda for her helpful suggestions. He also thanks Mr. F. Tan for his assistance of computer simulation.

References

Gelb, A. et al [1968] *Multi-Input Describing Functions and Nonlinear System Design*, (McGrawHill) pp.41-124

Khbnik, A. L et al [1993] "On periodic orbits and homoclinic bifurcations in Chua's circuit with a smooth nonlinearity", *Chua's Circuit*, (World Scientific) pp.145-178

Kuramitsu, M. [1994] "A classification of the 3rd order oscillators with respect to chaos", *Proc. NOLTA 95*, 5E-3, 599-602

Fukuda, M. & Hirai, K. [1995] "Transfer function approach for the analysis of generating mechanism of chaos", *Proc. NOLTA 95*, 5F-1, 603-606

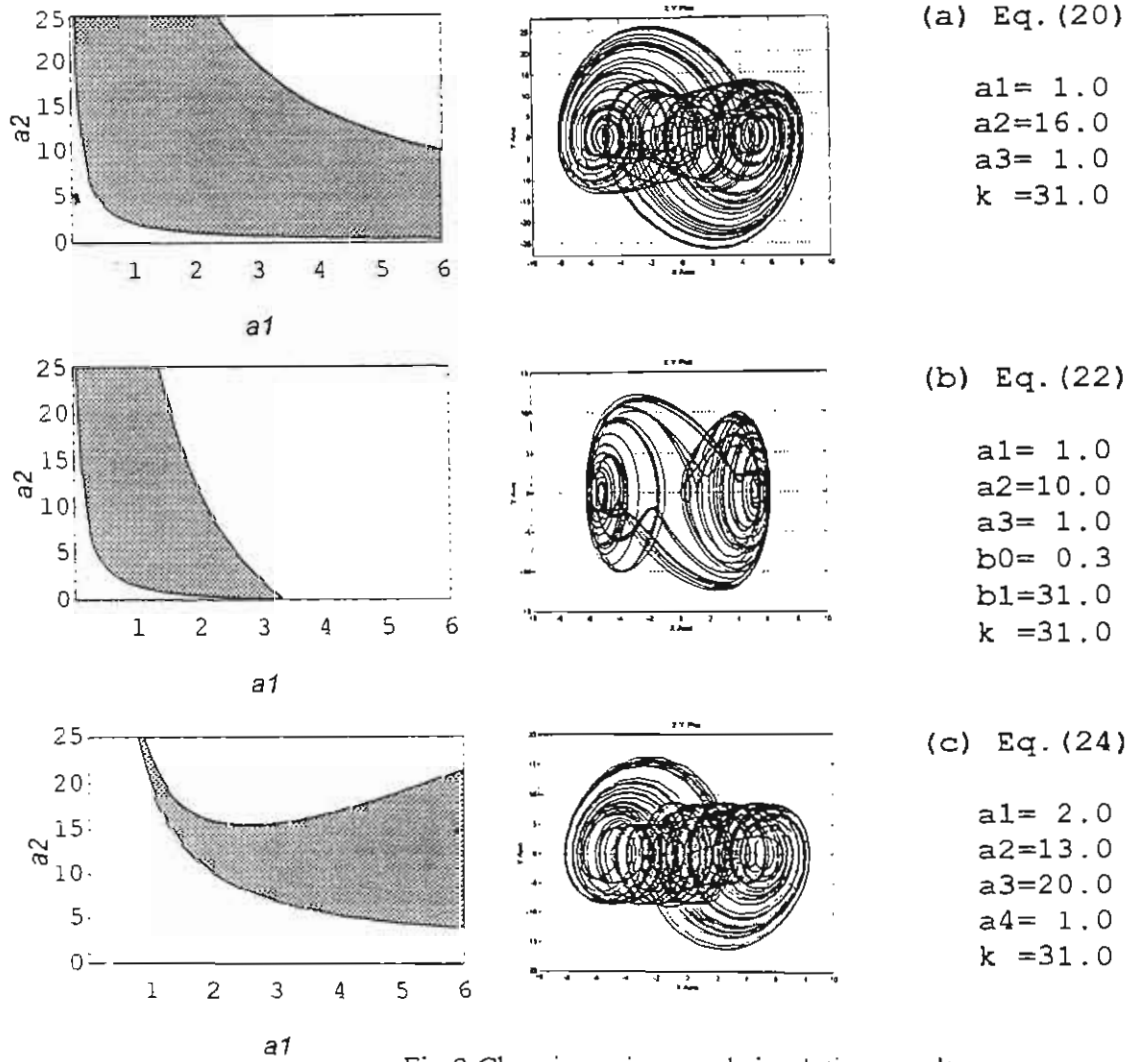

Fig.2 Chaotic regions and simulation results

USING THE CHAOTIC SIGNAL FOR WHITE GAUSSIAN NOISE MODELLING

M. Jessa
Institute of Electronics and Telecommunication, Poznań University of Technology,
ul. Piotrowo 3A, 60-965 Poznań, Poland

Abstract: In this paper a method for generating chaotic signal for white Gaussian noise modelling is considered. It is shown that topological conjunctions between dynamical systems can be used for chaotic signal generation with Gaussian distribution. This signal may be used for white Gaussian noise modelling, e.g. in telecommunication experiments.

1. Introduction

The Gaussian (also called normal) distribution is of the greatest importance in different fields of science. Naturally occurring experiments are often characterised by random variable with Gaussian distribution. A further importance is that the probability distribution of the sum of K statistically independent processes with the same probability density function approaches normalised Gaussian distribution (with zero mean value m_y and standard deviation σ_y equal to unity) in the limit as K approaches infinity (central limit theorem). The values of normally distributed noise-like signal are usually calculated from this theorem. The sequence $\{y_i\}$, where

$$y_i = \frac{(x_1 + x_2 + \ldots + x_K) - \frac{K}{2}}{\sqrt{\frac{K}{12}}} \qquad i = 1, 2, 3, \ldots \tag{1}$$

$x_1, x_2, \ldots, x_K$ - values of uniformly distributed random variable X, has a normalised Gaussian distribution N(0,1) for K approaching infinity. In practice, we assume K=12 [Bratley *at al.* 1991, Knuth , 1981]. The Gaussian distribution $N(m_y, \sigma_y)$ with arbitrary values of mean value m_y and standard deviation σ_y can be generated for random variable $Z=\sigma_y \cdot Y+m_y$.

In this paper we discuss the possibility of generation chaotic signal which properties are close properties of the white Gaussian noise. We use topological conjunctions between chaotic

systems for direct generation of noise-like signal $\{y_n\}$ with Gaussian distribution. We investigate the basic properties of generated chaotic signal which are important for telecommunication applications (the set of properties in commonly depends upon the application). The main are: the accordance of signal distribution with theoretical one, the uniformity of the power spectral density function (the Fourier transform of the autocorrelation function) and values of the cross-correlation function obtained for sequences starting from very close initial points.

2. The Normally Distributed Chaotic Signal

The equation which describes dynamical system with an arbitrary probability density function can be drawn from expression which relates probability density functions of dynamical systems which are topologically conjugate [Jessa & Davies, 1994, Kilias *et al.*, 1994, 1995]. This is relatively simple when one of these systems is ergodic and generates uniformly distributed numbers in the unit interval <0,1) [Jessa & Davies, 1994, Kilias *et al.*, 1994, 1995]. If we assume that some dynamical system $f(X,\mu)$ with probabilistic measure μ is described by tent map with Liapunov exponent equal log2 we obtain the following equation describing dynamical ergodic system $g(Y,\mu)$ with one-sided Gaussian probability distribution function, topologically conjugate to system $f(X,\mu)$

$$y_{n+1} = \frac{1}{k}\ln\left(\frac{3e^{ky_n}-1}{3-e^{ky_n}}\right) \quad for \quad y_n \in \left[0; \sqrt{\frac{\pi}{8}} * \ln 3\right)$$

$$y_{n+1} = \frac{1}{k}\ln\left(\frac{e^{ky_n}+5}{e^{ky_n}-3}\right) \quad for \quad y_n \in \left[\sqrt{\frac{\pi}{8}} * \ln 3; +\infty\right), \qquad k = \sqrt{\frac{8}{\pi}} \qquad (2)$$

The choice of the tent map from the family of piece-wise linear maps results in the conclusions of paper presented by M. Jessa and A.C.Davies [1994]. One of them states that tent maps and sawtoooth maps are related by simple formula. The second is that the maximal cycle length of chaotic numbers generated for tent maps is double greater the maximal cycle length of chaotic numbers obtained for sawtooth maps and for the same precision of calculations.

In Fig. 1 we see the histogram of signal $\{y_n\}$. The histogram was obtained numerically from equation (2) for 10^6 samples. The accordance of signal distribution with theoretical one was verified in chi-square test. The result is the statement: 'There is no reason (with 0.99 probability) to reject the hypothesis that the generated sequence has the Gaussian distribution'.

The uniformity of the power spectral density was checked for map

$$q(y)=g^{\alpha}(y) \qquad \alpha=1,2,... \qquad (3)$$

where g^{α} denotes the functional composition of g α times. The smallest value of the standard deviation of the power spectral density function is equal to 2.5% of the average value. The

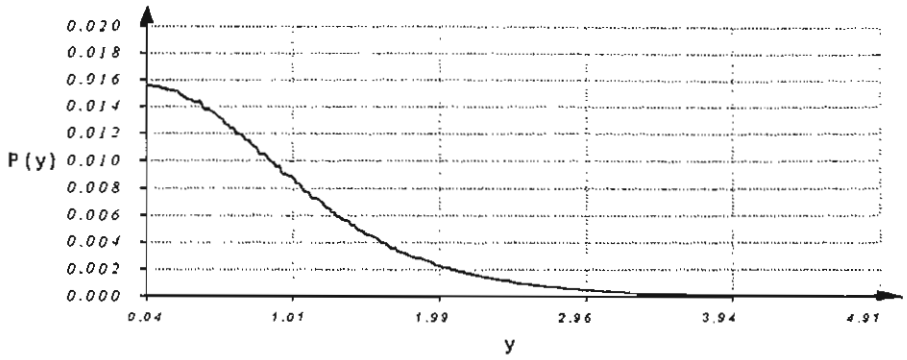

Fig. 1. Histogram of the one-sided Gaussian distribution.

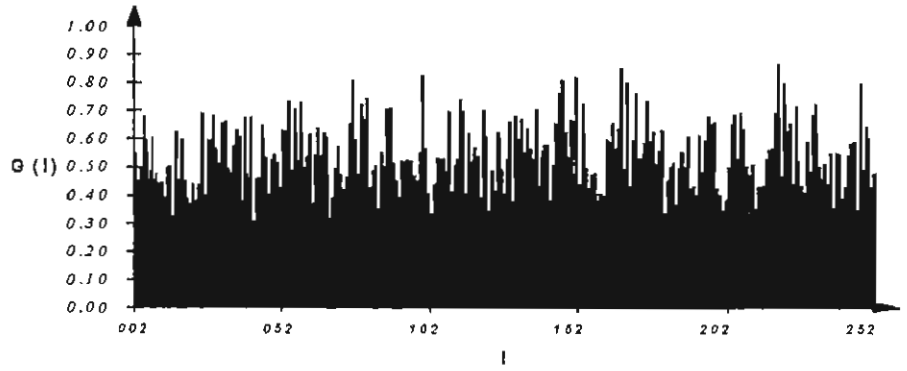

Fig. 2. The power spectral density of sequence $\{y_n\}$ obtained for α=7 and 5000 of trajectory points generated from (2), the average value is equal to 0.538 and standard deviation is equal to 0.0135.

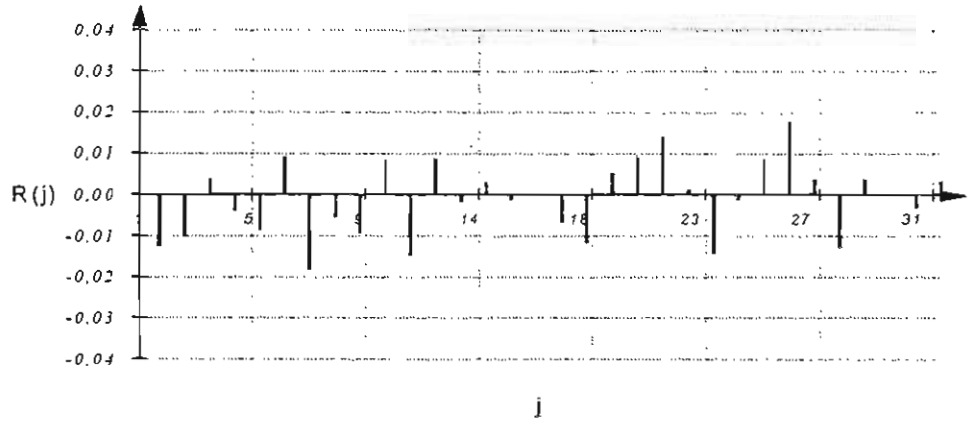

Fig. 3. The cross-correlation function between trajectories started from y_o and y_o+0.0001 obtained from equation (2); 5000 samples, α=7.

largest value is equal to 4.5 % of the average value. This result was obtained for α=7, i.e. for sequence composed of each seventh sample obtained from equation (2). The values of cross-correlation function R(j) between close trajectories (Fig.3) are at least 34 times smaller than the greatest value of the autocorrelation function.

3. Conclusions

In this paper a method for generating chaotic signal for white Gaussian noise modelling for simulation experiments has been considered. We have shown that the topological conjunction method can be used for chaotic normally distributed signal generation. It seems this signal may be used for white noise modelling, e.g. in telecommunication experiments. The calculation of successive samples of normally distributed noise-like signal based on topological conjunctions between dynamical systems is a general method. The complexity of calculations in this method is always less than the complexity of calculations of successive samples in the another general method - the inverse method [Bratley *at al.* 1991, Knuth , 1981]. The latter method requires first a generation of uniformly distributed numbers, while the former leads directly to the generation of samples with desired distribution. The application of central limit theorem requires at least 12 random numbers to produce a single sample of the Gaussian signal. Moreover, this number increases rapidly when large values of noise signal has to taken into account in simulation experiment.

4. References

Bratley P, Fox B.L, Schrage L.E [1991] *A Guide to Simulation* (Springer-Verlag).

Jessa M, Davies A.C [1994] "Generating Pseudochaotic Number Sequences", *Proceedings of the Workshop "Nonlinear Dynamics of Electronic Circuits, Krakow, Poland,* 197-202.

Kilias T,Schwarz W, Davies A.C [1994] " Noise Generators with Adjustable Spectra Based on Discrete-Time Maps", *Proceedings of the Workshop Nonlinear Dynamics of Electronic Circuits, Krakow, Poland,* 85-90.

Kilias T, Kutzer K, Schwarz W [1995] "Discrete-Time Chaos Generators", *ISCAS'95, 'Technology for Multimedia' Seattle, USA,* **Chapter 5.2**, 301-317.

Knuth D.A [1981] *The Art of Computer Programming* (Addison-Wesley), vol.2.

Bifurcation and Chaos Phenomena of Interspike Intervals in Nervous System

Xu Jianxue* , Gong Yunfan* , Ren Wei** , Hu Sanjue** and Wang Fuzhou**

*Department of Engineering Mechanics , Xi'an Jiaotong University , Xi'an , 710049 , P.R.China

**Department of Physiology , Fourth Military Medical University , Xi'an, 710032, P.R.China

Abstract

In this paper , based on the analyses of the β-cell model and the experimental findings , we report the bifurcation and chaos phenomena of the interspike intervals (ISI) in the nervous system . After that , nonlinear forecasting as well as the surrogate data method is applied to analyze the chaotic ISI time series both from the model and the experiment .

Key words : bifurcation , chaos , neural electrophysiological activities , β-cell model , chaotic time series analysis , the surrogate data , nonlinear forecasting method

It is of great interest how the information is coded in the nervous system . Lots of experiments and theoretical investigations have been aimed at this problem . One experimental method widely used is to study the interspike intervals (ISI) of the nervous action potential trains propagated along single nerve fiber . Now , whether the time series of ISI have chaotic structure or are intrinsic noise is still in violent dispute . Some people have the point that they are absolutely noise without deterministic structure [1] , while others are for the point that there is deterministic chaos in the signals [2] . Although different methods have been utilized to analyze the data , actually , the mechanism underlying them is still unknown . There is one fundamental question need to answer , that is , what can be reflected of the original complex nervous system by the ISI data ?

In this paper , we focus our attentions on the model of β-cell proposed by Rinzel et al. [3] . Using the method of the Poincare section which seems to be one of the most powerful tools to study the complicated system , the period doubling to chaos as well as the period adding bifurcation diagram of the ISI with the alteration of the parameter $\bar{g}_{K\text{-}Ca}$ was obtained and

shown in Fig.1 (a) (b) separately . Therefore , if the original nervous system is considered as a continuous dynamical system , the ISI data corresponds to the reduced discrete one . For the purpose of comparison with the experimental case , Figure 1 (c) exhibits the enlargement of the period doubling bifurcation which was contaminated by the Gaussian white noise of the mean value 100 and the variance 50 . The chaotic ISI time series were demonstrated in Fig.1 (d) of which the sum of the ISI number was plotted in sequence on the abscissa .

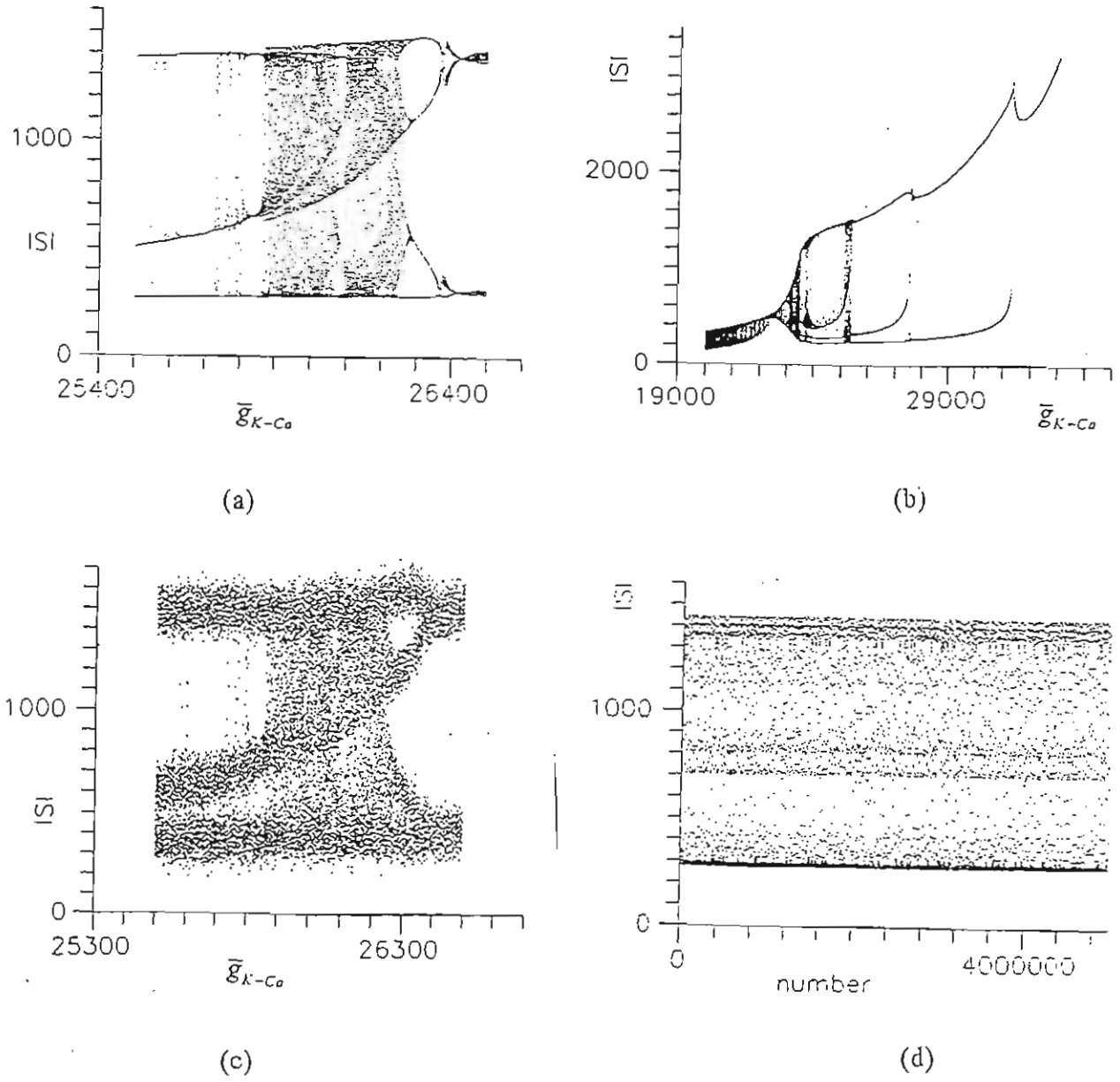

Fig. 1. Bifurcation and chaos of the ISI time series in the β-cell model , with the Poincare section V+35=0 . (a) The period doubling bifurcation to chaos (without noise) . (b) The period adding bifurcation diagram of the ISI time series . (c) Enlargement of the period

doubling procedure (contaminated by the Gaussian white noise) . (d) The chaotic ISI time series (without noise) .

Second , the bifurcation phenomenon of ISI has been found in our experiments too . The surgical operations were carried out using the procedure described by Bennett and Xie [4] . Adult male SD rats were used in the experiments , the discharges along single nerve fiber were input to an A/D converter and the ISI data were recorded by the computer , the activities of the nervous system were monitored on a memory oscilloscope screen (vc-11 system) during the whole experiment . When analyzing the ISI data , attentions were paid to the dynamical change of the data with time rather than the static value . As a result , the bifurcation procedure was found and recorded . Figure 2 (a) exhibits the bifurcation diagram of the ISI data CA381W4 from the experiment . Figure 2 (b) gives another period adding bifurcation of the ISI data EG3803 . It can be seen clearly from both these figures that although the ISI data were corrupted by the measurement noise , they still can reflect the dynamical change from the periodic motion to chaos of the nervous system .

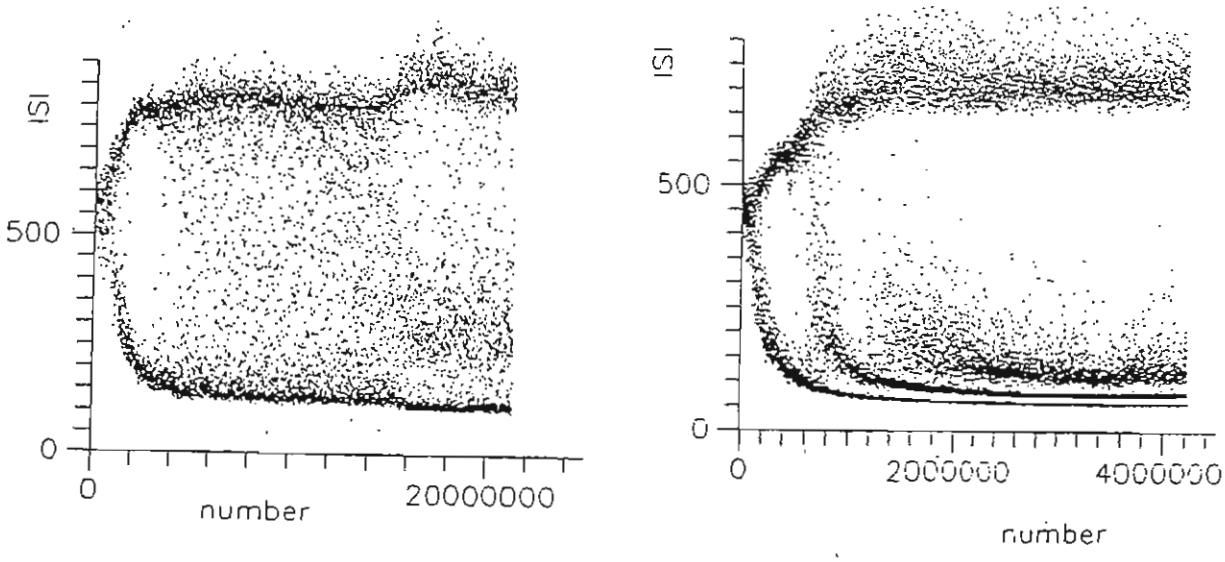

Fig. 2. Bifurcation and chaos of the ISI time series from the experiment . (a) The bifurcation diagram of the ISI data CA381W4 . (b) The period adding bifurcation of the ISI time series EG3803 .

Third , nonlinear forecasting and the surrogate data methods have been combined together to analyze the ISI data both from the experiment and the model [5][6] . Although the data are contaminated by the noise from experimental measurement , correlation coefficient curve has distinct difference from that of their surrogate data . This means that the nervous system was in the state of chaos at that time . The results from the experiment are also consistent with what have been obtained from the model while contaminated by the Guassian white noise . As another important evident to support our finding of chaos , the plot of ISI (n+1) vs. ISI (n) which can reflect the characteristic structure of chaos is reconstructed . It is exciting that there is a good resemblance of the structure between the plot from the model and that obtained from the experiment .

Acknowledgment

This work was supported by National Science Foundation No. 19372044 of P.R.China .

References

[1] J.M.Gilchrist , M.Perrone and J.Ross , " Dynamical analysis of neuromuscular transmission jitter ." , Muscle-Nerve 18 , pp.685 , (1995) .

[2] R.E.Hoffman , W.X.Shi and B.S.Bunney , " Nonlinear sequence-dependent structure of nigral dopamine neuron interspike interval firing patterns ." , J. Biophys. 69 , pp.128 , (1995) .

[3] J.Rinzel , A.Sherman and C.L.Stokes , " Channels , coupling , and synchronized rhythmic bursting activity ." , Analysis and Modeling of Neural Systems , F.H.Eeckman , eds. , pp.29 , Kluner Academic Publishers , (1989) .

[4] G.J.Bennett and Y-K.Xie , " A peripheral mononeuropathy in rat that produces disorders of pain sensation like those seen in man ." Pain 33 , pp.87 , (1988) .

[5] G.Sugihara and R.M.May , " Nonlinear forecasting as a way of distinguishing chaos from measurement error in time series ." , Nature 344 , pp.734 , (1990) .

[6] J.Theiler , S.Eubank , A.Longtin , B.Galdrikian and J.D.Farmer , " Testing for nonlinearity in time series : the method of surrogate data ." , PhysicaD 58 , pp.77 , (1992) .

SYNCHRONIZATION IN THE IDENTICALLY DRIVEN SYSTEMS

B. Kaulakys[1], F. Ivanauskas[2] and T. Meškauskas[2]

[1]Institute of Theoretical Physics and Astronomy, A. Goštauto 12, 2600 Vilnius, Lithuania
[2]Department of Mathematics, Vilnius University, Naugarduko 24, 2006 Vilnius, Lithuania

Abstract: We investigate a transition from chaotic to nonchaotic behavior and synchronization in an ensemble of systems driven by identical random forces. We analyze the synchronization phenomenon in the ensemble of particles moving with friction in the time-dependent potential and driven by the identical noise. We define the threshold values of the parameters for transition from chaotic to nonchaotic behavior and investigate dependencies of the Lyapunov exponents and power spectral density on the nonlinearity of the systems and character of the driven force.

1. Introduction

Trajectories of the nonlinear dynamical systems are very sensitive to initial conditions and unpredictable. The systems exhibit an apparent random behavior. It might be expected that turning on an additional random forces make their behavior even "more random". However, as it was shown by Fahy & Hamann [1992] and Kaulakys & Vektaris [1995a,b] when an ensemble of bounded in a fixed external potential particles with different initial conditions are driven by an identical sequence of random forces, the ensemble of trajectories may become identical at long times. The system becomes not chaotic: the trajectories are independent on the initial conditions. Here we analyze the similar phenomenon in the ensemble of particles moving with friction in the time-dependent potential and driven by the identical noise. We define the threshold values of the parameters for transition from chaotic to nonchaotic behavior and investigate dependencies of the Lyapunov exponents and power spectral density on the nonlinearity of the systems and character of the driven force.

2. Models and Results

Consider a system of particles of mass $m = 1$ moving according to Newton's equations in the time dependent potential $V(\mathbf{r}, t)$, e.g. in the potential $V(x, t) = x^4 - x^2 - ax \sin \omega t$, and with the friction coefficient γ. At time intervals τ the particles are partially stopped and their velocities are reset to the mixture of some part α of the old velocities with

random velocity $\mathbf{v}_i^{ran}$: $\mathbf{v}^{new} = \alpha \mathbf{v}^{old} + \mathbf{v}_i^{ran}$, where i is the stop number. Note that $\mathbf{v}_i^{ran}$ depends on the stop number i but not on the particle. The simplest and most natural way is to choose the random values of velocity $\mathbf{v}_i^{ran}$ from a Maxwell distribution with $k_B T = m = 1$.

A transition from chaotic to nonchaotic behavior in such a system may be detected from analysis of the neighboring trajectories of two particles initially at points $\mathbf{r}_0$ and $\mathbf{r}_0'$ with starting velocities $\mathbf{v}_0$ and $\mathbf{v}_0'$. The convergence of the two trajectories to the single final trajectory depends on the evolution with a time of the small variances $\Delta \mathbf{r}_i = \mathbf{r}_i' - \mathbf{r}_i$ and $\Delta \mathbf{v}_i = \mathbf{v}_i' - \mathbf{v}_i$. From formal solutions $\mathbf{r} = \mathbf{r}(\mathbf{r}_i, \mathbf{v}_i, t)$ and $\mathbf{v} = \mathbf{v}(\mathbf{r}_i, \mathbf{v}_i, t)$ of the Newton's equations with initial conditions $\mathbf{r} = \mathbf{r}_i$ and $\mathbf{v} = \mathbf{v}_i$ at $t = 0$ it follows the mapping form of the equations of motion for $\Delta \mathbf{r}$ and $\Delta \mathbf{v}$. The analysis of dynamics based on these equations has been investigated by Kaulakys & Vektaris [1995a,b].

Here we calculate the Lyapunov exponents directly from the equations of motion and linearized equation for the variances and extend the investigation for the systems with friction in the regular external field and perturbed by the identical for all particles random force. In Fig. 1 we show the dependence on τ of the Lyapunov exponents for the motion in the nonautonomous Duffing potential with friction described by the equations

$$\dot{v} = 2x - 4x^3 - \gamma v + a \sin \omega t, \qquad \dot{x} = v. \tag{1}$$

For the values of parameters corresponding to the positive Lyapunov exponents, i.e. without the random perturbation ($\tau \to \infty$) the system is chaotic. The negative Lyapunov exponents for small τ indicate to the nonchaotic Brownian-type motion.

As it was already been observed in [Kaulakys & Vektaris, 1995b] such systems exhibit the intermittency route to chaos which provides sufficiently universal mechanism for $1/f$-type noise in the nonlinear systems. Here we analyze numerically the power spectral density of the current of the ensemble of particles moving in the closed contour and perturbed by the common for all particles noise. The simplest equations of motion for such model are of the form

$$\dot{v} = F - \gamma v, \qquad \dot{x} = v. \tag{2}$$

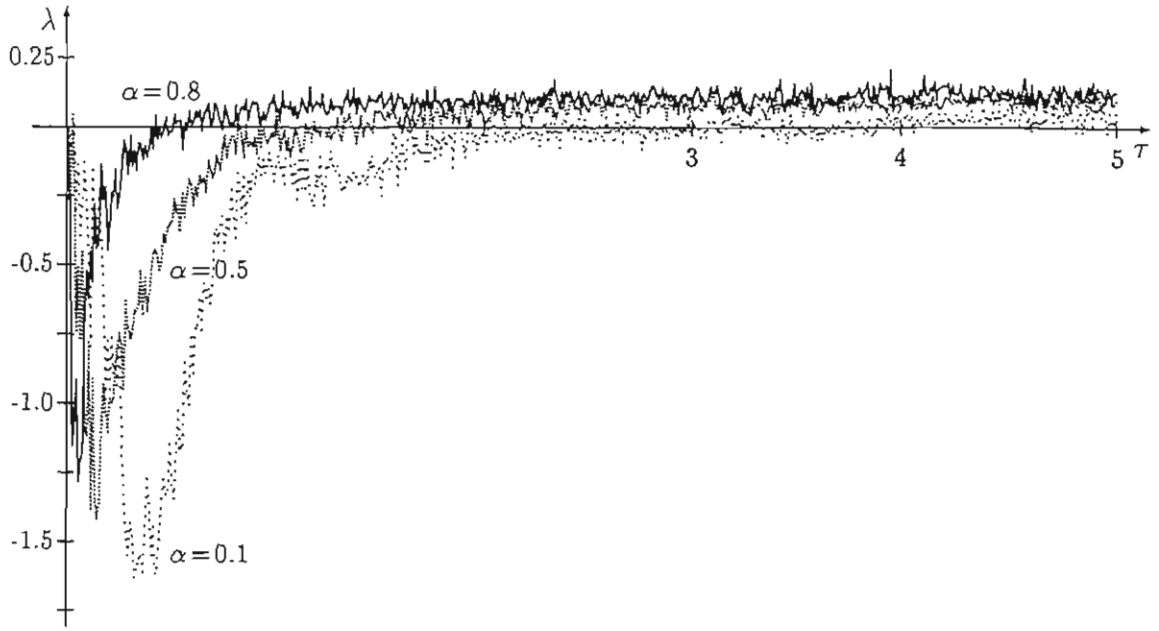

Figure 1: Lyapunov exponents vs the time τ between resets of the velocity for motion in the Duffing potential according to Eq. (1) with $a = 5$, $\omega = 1$, $\gamma = 0.07$ and different α.

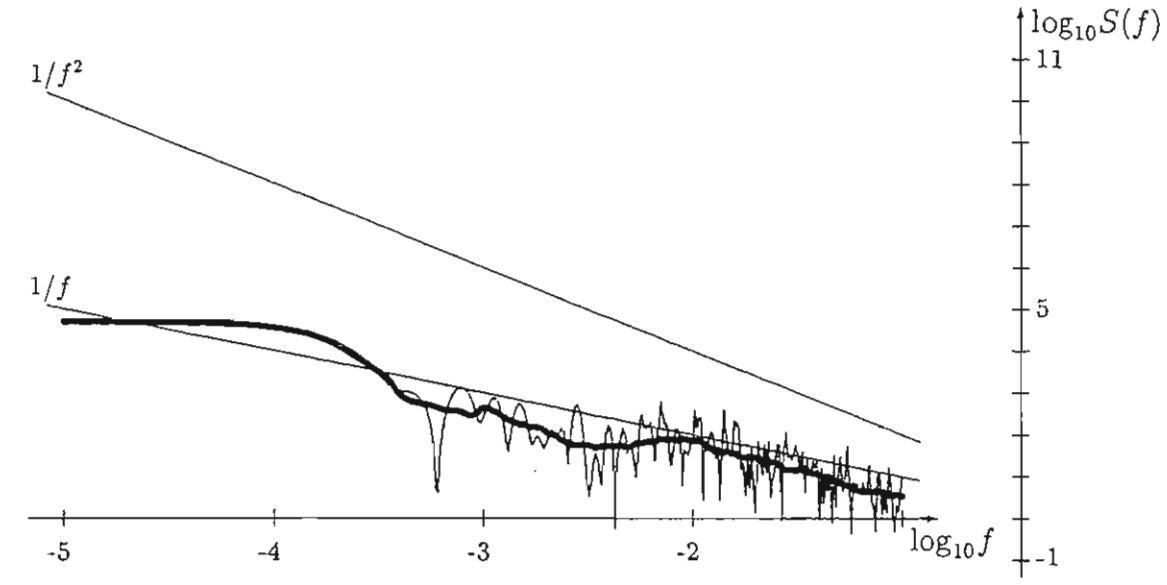

Figure 2: The power spectral density of the current of the ensemble of particles moving according to Eq. (2) with $F = 1$, $\gamma = 0.1$ and perturbed by the common for all particles noise $\mathrm{v}^{new} = \alpha \mathrm{v}^{old} + \mathrm{v}_i^{ran}$ with $\alpha = 1$ and $\tau = 0.1$. The dense line represents the averaged spectrum.

with the perturbation given by the resets of velocity of all particles after every time interval τ according to the identical for all particles replacement $\mathrm{v}^{new} = \alpha \mathrm{v}^{old} + \mathrm{v}_i^{ran}$. We observe the current power spectral density $S(f)$ dependence on the frequency f close to the $1/f$–dependence (see Fig. 2).

Our model may be generalized for systems driven by any random forces or fluctuations. On the other hand, the phenomenon when an ensemble of systems is linked with a common external noise or fluctuating external fields is quite usual. Thus, an ensemble of systems in the external random field may provide a sufficiently universal mechanism of $1/f$–noise.

3. Conclusions

From the fulfilled analysis we may conclude that, first, synchronization and transition from chaotic to nonchaotic behavior in ensembles of the identically perturbed by the random force nonlinear systems may be analyzed as from the mapping form of equations of motion for the distance between the particles and the difference of the velocity as well as from the direct calculations of the Lyapunov exponents and, second, an ensemble of systems linked with a common external noise may exhibit the $1/f$–type fluctuations.

Acknowledgment

The research described in this publication was made possible in part by Grant from the Lithuanian State Science and Studies Foundation.

References

Fahy, S. & Hamann, D. R. [1992] "Transition from chaotic to nonchaotic behavior in randomly driven systems", *Phys. Rev. Lett.* **69(5)**, 761-764.

Kaulakys, B. & Vektaris, G. [1995a] "Transition to nonchaotic behavior in a Brownian-type motion, *Phys. Rev. E* **52(2)**, 2091-2094.

Kaulakys, B. & Vektaris, G. [1995b] "Transition to nonchaotic behavior in randomly driven systems: intermittency and 1/f-noise", *Proc. 13th Int. Conf. Noise in Phys. Syst. and 1/f Fluctuations* (World Scientific, Singapore), pp. 677-680.

ROUTE TO CHAOS, CRISIS AND OSCILLATORY MODE TRANSITION IN A MODEL NEURON

Komendantov A.O.#* and Kononenko N.I.*
Glushkov Institute of Cybernetics, Kiev, Ukraine;
* Laboratory of Neurobiology, Bogomoletz Institute of Physiology
Bogomoletz str., 4, 252601 GSP, Kiev-24, Ukraine

Abstract: The mathematical model of electrical activity of bursting neuron demonstrates period-doubling chaos and crisis as the chemosensitive conductance is increased. This conductance in intact nerve cell depends on neuropeptide released by interneuron. The transition from resting state to bursting activity evoked by short-lasting stimulation is observed in our model. These studies reveal a putative role of nonlinear properties of cellular membrane in information processing at the level of a single neuron.

1. Introduction

In recent years, neurobiological studies gave undoubted evidences of complexity of electrical processes in single nerve cells. Intact nerve cells and their models can demonstrate beating, bursting or chaotic activity [Canavier *et al.*, 1993; Chay *et al.*, 1995; Hayashi & Ishizuka, 1992]. The model presented reproduces behavior of *Helix* identified bursting neuron although the results of our studies have a relevance for more clear understanding of functions of other nerve cells and neuronal assemblies.

2. Model of Electrical Activity of Bursting Neuron

The model is based on experimental data and includes following components: slow-wave generating mechanism (I_K, I_{Na}, $I_{Na(t)}$, I_B); Hodgkin-Huxley spike generating mechanism (I_{NaHH}, I_{KHH}) and fast potassium current (I_{KF}); calcium and calcium-sensitive system (I_{Ca}, $I_{Ca\text{-}Ca}$, I_{CAN}, uptake of $[Ca^{2+}]_{in}$ by intracellular depots). The equations and corresponding parameters are presented in **Appendices.**

3. Bifurcations, Chaos and Crisis in the Model Neuron

The bifurcation diagram in Fig.1 is obtained by numerically integrating the model equations. It shows the interspike interval (ISI) changes with increasing of g_B (hyperpolarization-activated conductance responsible for termination of spike burst) from 0.380 to 0.455 μS. This conductance in intact snail neuron was established to be modulated by neuropeptide released by corresponding interneuron. The model pacemaker neuron changes its monomodal beating activity to chaotic one with increasing of g_B and the diagram demonstrates route to chaos through cascades of period doubling. The dominant Lyapunov exponent to the attractor in the region of chaotic beating activity for time series contained 2600 ISIs was estimated as 0.438 bits/iteration.

The model demonstrates also the features of crisis [Grebogi *et al.*, 1983] which was observed in other models of excitable cells [Chay *et al.*, 1995]. When g_B>0.420 μS the size of attractor changes suddenly. The periods of quiescence are appeared in high firing rates and maximum of ISI value is increased to 10.5 s (It is not shown in diagram).

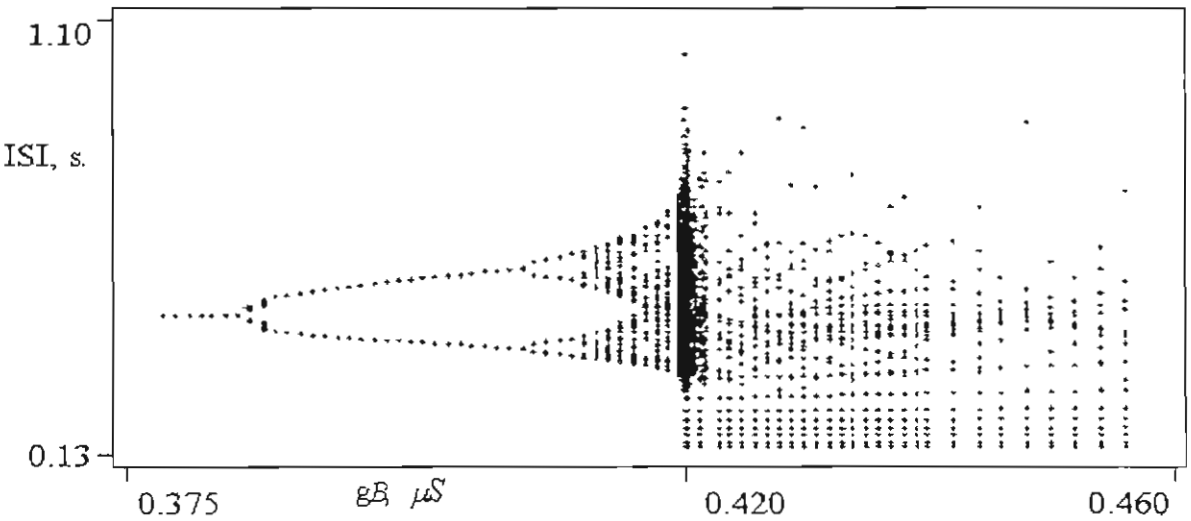

Figure 1. Bifurcation diagram for ISI as a function of g_B.

4. Mode Transition in the Model Neuron

In the previous model [Komendantov & Kononenko, 1995] without I_{KF} and I_{CAN} ($[Ca^{2+}]_{in}$-activated non-specific cation current) we observed stable parameter-independent

mode transitions from periodicity to aperiodicity and vice versa which have been induced by short-lasting membrane polarization. These events simulate activation of synaptic inputs of neuron. The extension of the mathematical model presented in this paper allows us to simulate new interesting features of neuronal behavior. Short lasting depolarizing current can perturb quiescent neuron into persistent bursting activity (Fig.2). Such phenomena take place in some electrophysiological experiments.

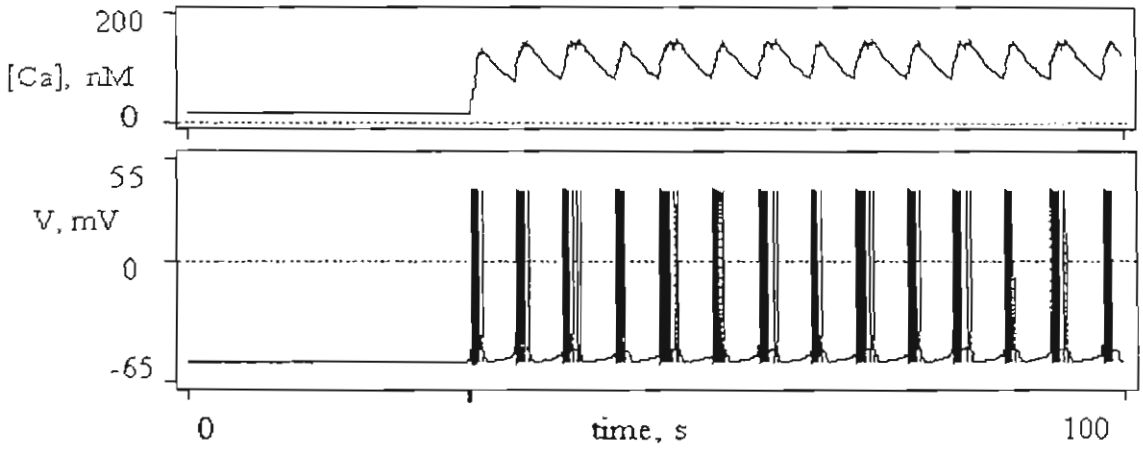

Figure 2.Time course of membrane potential (bottom) and corresponding $[Ca^{2-}]_{in}$ (top). The bar at the bottom graph indicates the spell of current pulse application (-0.5 nA, 1s).

5.Conclusions

Period doubling, crisis and parameter-independent mode transitions were observed also in some other models of excitable cells [Canavier *et al*, 1993; Chay *et al*, 1995; Hayashi & Ishizuka, 1992]. Such phenomena have a biological relevance and nonlinear properties of our model neuron may be considered as putative neuronal mechanism of associative learning, fixed acts, memory, recall.

6. References

Canavier, C.C., Baxter, D.A., Clark, J.W. & Byrne, J.H.. [1993] "Nonlinear dynamics in a model neuron provide a novel mechanism for transient synaptic inputs to produce long term alterations of postsynaptic activity" *J. Neurophysiol.* **69**, 2252-2257.

Chay, T.R., Fan, Y. & Lee, Y.S. [1995] "Bursting, spiking, chaos, fractals, and universality in biological rhythms" *Int. J. Bifurcation and Chaos* **5(3)**, 595-635.

Hayashi, H. & Ishizuka, S. [1992] "Chaotic nature of bursting discharge in the *Onchidium* pacemaker neuron", *J.Theor.Biol.* **156**, 269-291.

Grebogi, G., Ott, E. & Yorke, J.A. [1983] "Crises, Sudden Changes in Chaotic Attractors and Chaotic Transients", *Physica* **D 7**, 181-200.

Komendantov, A.O. & Kononenko, N.I. [1995] "Chaos in mathematical model of pacemaker activity in bursting snail neuron", *Systems Analysis Modelling Simulation* **18-19**, 725-728.

7. Appendices

A.1. The model equations:

$$-C_m\,dV/dt = I_{NaHH}+I_{KHH}+I_{KF}+I_K+I_{Na}+I_{Na(t)}+I_B+I_{Ca}+I_{Ca\text{-}Ca}+I_{CAN};$$

$$I_{NaHH}=g_{NaHH}m^3h(V-V_{Na});\ I_{KHH}=g_{KHH}n^4(V-V_K);\quad I_{KF}=g_{KF}fq(V-V_K);$$

$$dm/dt = (1/(1+\exp(-0.4(V+31)))-m)/0.0005;$$

$$dh/dt = (1/(1+\exp(0.25(V+45)))-h)/0.01;$$

$$dn/dt = (1/(1+\exp(-0.18(V+25)))-n)/0.015;$$

$$df/dt = (1/(1+\exp(-0.2(V-20)))-f)/0.01;$$

$$dq/dt = (1/(1+\exp(0.3(V+80)))-q)/0.1;$$

$$I_{Na(t)} = g_{Na(t)}(1/(1+\exp(-0.4(V+45))))(V-V_{Na});$$

$$I_K = g_K(V-V_K);\ I_{Na} = g_{Na}(V-V_{Na});\ I_B = g_B\,m_B\,h_B(V-V_B);$$

$$dm_B/dt = (1/(1+\exp(0.4(V+38)))-m_B)/0.08;$$

$$dh_B/dt = (1/(1+\exp(-1(V+43)))-h_B)/1.5;$$

$$I_{Ca}=g_{Ca}\,m_{Ca}^2(V-V_{Ca});\quad dm_{Ca}/dt = (1/(1+\exp(-0.2V))-m_{Ca})/0.01;$$

$$d[Ca]/dt = \rho\,(-(I_{Ca}+I_{Ca\text{-}Ca})/2F\upsilon - k_S[Ca]);\qquad \upsilon = 4\pi R^3/3;$$

$$I_{Ca\text{-}Ca}=g_{Ca\text{-}Ca}\,\frac{1}{1+\exp(-0.12(V+45))}\,((Kd_{Ca\text{-}Ca}+[Ca])/Kd_{Ca\text{-}Ca})(V-V_{Ca});$$

$$I_{CAN}=g_{CAN}\,([Ca]^p/(Kd_{CAN}^p+[Ca]^p))\,(V-V_{CAN}).$$

[Ca] is $[Ca^{2+}]_{in}$, F is Faraday number, k_S - rate constant of intracellular Ca-uptake by intracellular stores, ρ - endogenous Ca buffer capacity.

A.2. General parameters for the model equations:

g_{KF}= 100 μS; g_{NaHH}=400 μS; V_{Na}=40 mV; V_K=-70 mV; V_B=-58 mV; V_{Ca}=150 mV; V_{CAN}=10 mV; R=100 μm; ρ = 0.002; k_S=100 1/s; $Kd_{Ca\text{-}Ca}$=1.6 10^{-4} mM.

A.3. Parameters and initial conditions for part 3 (bifurcation diagram):

C_m=0.04 μF; g_K=0.25 μS; g_{Na}=0.02 μS; $g_{Na(t)}$= 0.15 μS; g_{KHH}=150 μS; g_{Ca}= 8 μS; $g_{Ca\text{-}Ca}$=0.04 μS; g_{CAN}=0.005 μS; Kd_{CAN}=2$10^{-5}$ mM; p=1; V=-55 mV; $[Ca]$= 0 mM.

A.4. Parameters and initial conditions for part 4 (quiescent state):

C_m=0.02μF; g_K=0.3 μS; g_{Na}=0.034 μS; $g_{Na(t)}$= 0.1 μS; g_B=0.3 μS; g_{KHH}=250 μS; g_{Ca}= 10 μS; $g_{Ca\text{-}Ca}$=0.03 μS; g_{CAN}=0.017 μS; Kd_{CAN}= 4 10^{-5}mM; p=4; V=-53.5 mV; $[Ca]$= 1.8 10^{-5} mM

SMALL HYSTERESIS PERTURBATIONS IN BIFURCATION PROBLEMS

M.A.Krasnosel'skii, V.S.Kozyakin, N.A.Kuznetsov, D.I.Rachinskii, M.G.Yumagulov

Institute for Information Transmission Problems

Russian Academy of Science

19 Bol'shoy Karetny st., GSP-4, Moscow, 101447, Russia

Abstract: The effects of the Hopf bifurcation type are studied for autonomous systems depending on parameters. An operator approach based on the method of parameter fuctinalization is introduced to analyze the existence of periodic solutions in the neighbourhood of the system equilibrium. The approach is applicable to the study of systems with autonomous hysteresis nonlinearities.

1. Let us begin with a simple example. Consider the system

$$\frac{dz}{dt} = A(\lambda)z + \varphi(z;\lambda), \qquad \lambda \in R,\ z \in R^N. \tag{1}$$

Here $A(\lambda)$ is a real matrix with continuous in λ elements; the vector function $\varphi(z,\lambda)$ is continuous in z,λ and $\varphi(z;\lambda) = O(|z|^2)$, $z \to 0$. Hence, $z = 0$ is an equilibrium of the system (1) for any $\lambda \in R$.

We say that λ_0 is a bifurcation point (in problem of the Hopf bifurcation at zero equilibrium), if for any $\varepsilon > 0$ there exist a number λ_ε and a nontrivial $T(\lambda_\varepsilon)$-periodic solution $z(t;\lambda_\varepsilon)$ of the system (1) for $\lambda = \lambda_\varepsilon$ such that

$$|\lambda_\varepsilon - \lambda_0| < \varepsilon, \qquad |z(t;\lambda_\varepsilon)| < \varepsilon,\ t \in R. \tag{2}$$

Obviously, a necessary condition for λ_0 to be a bifurcation point is that the linear system $z' = A(\lambda_0)z$ have nontrivial periodic solutions.

Suppose that this condition is satisfied and, in addition, the matrix $A(\lambda_0)$ is nonsingular. Then, the matrix $A(\lambda_0)$ has a pair of the pure imaginary eigenvalues $\pm i\beta_0$, where $\beta_0 > 0$. Let the following assumptions hold:

(i) *The eigenvalues* $\pm i\beta_0$ *of the matrix* $A(\lambda_0)$ *are simple;*

(ii) *The numbers* $i\beta_0 k$, *where* $k = 0, \pm 2, \pm 3, \ldots$, *do not belong to the spectrum of* $A(\lambda_0)$.

Note that the spectrum of $A(\lambda_0)$ may include some pure imaginary points $\mu \neq \pm i\beta_0$ (excepting the ones mentioned in (ii)) as well as any point $\mu = \xi + i\eta$, where $\xi \neq 0$ regardless of the sign of ξ.

It follows from (i) that the matrix $A(\lambda)$ has a unique eigenvalue $\alpha(\lambda) + i\beta(\lambda)$ close to $i\beta_0$ for $|\lambda - \lambda_0| \ll 1$. In this notation, $\alpha(\lambda_0) = 0$, $\beta(\lambda_0) = \beta_0$.

Theorem. *Let assumptions* (i)-(ii) *hold. Let for any* $\delta > 0$ *there exist* $\lambda', \lambda'' \in (\lambda_0 - \delta, \lambda_0 + \delta)$ *such that*

$$\alpha(\lambda')\alpha(\lambda'') < 0. \tag{3}$$

Then, λ_0 *is a bifurcation point for the system (1) in problem of the Hopf bifurcation at zero equilibrium. Moreover, the periods* $T(\lambda_\varepsilon)$ *of the cycles* $z(t; \lambda_\varepsilon)$ *satisfy*

$$T(\lambda_\varepsilon) \to 2\pi/\beta_0 \quad \text{as} \quad \varepsilon \to 0. \tag{4}$$

The general approach used to prove this theorem makes it possible to find asymptotic formulas for the cycles $z(t; \lambda_\varepsilon)$ and their periods $T(\lambda_\varepsilon)$, to analyze stability of the cycles etc. The approach can also be applied to analyze problems of nonlinear resonance (bifurcation at infinity).

The idea of the proof is as follows. First, by time rescaling we replace the problem of periodic solutions of unknown period T for the system (1) by the boundary value problem on the segment $[0, 1]$:

$$\frac{dz}{d\tau} = TA(\lambda)z + T\varphi(z; \lambda), \tag{5}$$

$$z(0) = z(1). \tag{6}$$

Here T becomes an additional prameter. Then, we get over to some equivalent to the problem (5)-(6) integral equation. Let us write it in the operator form

$$z(\tau) = B[z(\tau); \lambda, T]. \tag{7}$$

Eq.(7) can be analyzed in various functional spaces, e.g. in the space C of continuous on $[0, 1]$ vector functions $z = z(\tau)$. Operator $B : C \times R \times R \to C$ is completely continuous.

An intrinsic peculearity of Eq.(7) is that the set $Z(\lambda, T)$ of its nonzero solutions $\overline{z}$ does not contain isolated points. Furthermore, if $Z(\lambda, T) \neq \emptyset$, then any connected component of $Z(\lambda, T)$ is a continuum of zero topological index. This complicates the study of Eq.(7).

To overcome the difficulty we introduce the pair of the scalar valued functionals $f_1(\overline{z}; q)$, $f_2(\overline{z}; q)$, where $q > 0$ is an auxiliary parameter. Substituting f_1, f_2 for λ, T in (7), we obtain

$$\overline{z} = B[\overline{z}; f_1(\overline{z}; q), f_2(\overline{z}; q)]. \tag{8}$$

The functionals f_1, f_2 are constructed so that nonzero solutions of Eq.(8) are isolated. It is important that f_1, f_2 are given by simple formulas.

The argument based on standard topological methods of functional analysis shows that Eq.(8) has a nonzero solution $\overline{z}_q$ for any sufficiently small $q > 0$. The function $\overline{z}_q = z_q(\tau)$ determines the nonzero $T(q)$-periodic solution $z(t; \lambda(q))$ of the system (1) for $\lambda = \lambda(q)$, where $\lambda(q) = f_1(\overline{z}_q; q), T(q) = f_2(\overline{z}_q; q)$. Formulas (2),(4) follow from

$$\max_t |z(t; \lambda(q))| \to 0, \quad \lambda(q) \to \lambda_0, \quad T(q) \to 2\pi/\beta_0 \quad \text{as} \quad q \to 0. \tag{9}$$

2. The approach outlined above is applicable to the study of bifurcation in autonomous systems with hysteresis.

Let W be an autonomous hysteresis nonlinearity with inputs $u(t)$ and outputs $x(t)$, their values being elements of R^l and R^m respectively. In particular, W may denote some scalar or multidimensional hysteron, e.g. a play or a stop. It may be as well a complex hysteresis nonlinearity like the models occuring in plasticity and magnetism, e.g. the ones due to A.Yu.Ishlinskii, G.J.Friedman, I.D.Mayergoyz, Z.Mroz, V.V.Novozhilov, F.Preisach etc.

Consider the system with the hysteresis nonlinearity W of the form

$$\frac{dz}{dt} = A(\lambda)z + \psi(z, x; \lambda), \quad z \in R^N, \tag{10}$$

$$\omega(t) = W[t_0, \omega(t_0)]u(t), \quad t \geq t_0, \tag{11}$$

$$u(t) = Pz(t), \quad x = \Phi(\omega). \tag{12}$$

Here ω is a state of the hysteresis nonlinearity W; it is an element of a convex compact subset Ω of some Hilbert space H. Operator (11) determines how the state ω is changed

in time from its initial value $\omega(t_0)$ under the influence of the input $u(t)$. Operators $P : R^N \to R^l$ and $\Phi : \Omega \to R^m$ determine the input and the output of the nonlinearity W.

Initial conditions for the system (10)-(12) consist of two equalities $z(t_0) = z_0$, $\omega(t_0) = \omega_0$. Periodic solutions of the system are the pairs $\{z(t), \omega(t)\}$ of T-periodic functions; their values shape cycles in the system phase space $R^N \times \Omega$.

For the sake of simplicity we restrict our consideration to the case when Eq.(10) has the form

$$\frac{dz}{dt} = A(\lambda)z + \varphi(z;\lambda) + \varepsilon g(z, x;\lambda), \tag{13}$$

where $\varepsilon > 0$ is a small parameter. The system (11)-(13) is considered as a perturbed system (1) with the perturbation term depending on the hysteresis nonlinearity output.

Classical approaches to the Hopf bifurcation problem fail when applied to the study of systems with hysteresis. The reason is that hysteresis nonlinearities are not differentiable. To analyze the problem of small periodic solutions for the system (11)-(13) we use the approach presented in Sec.1. First, the problem is reduced to the analysis of the system

$$\bar{z} = B_1[\bar{z}, \omega; \lambda, T], \quad \omega = B_2[\bar{z}, \omega; \lambda, T]. \tag{14}$$

The structure of its set of solutions is similar to that of Eq.(7). As above, by substituting the functionals f_1, f_2 for λ, T, we get over to the system with isolated solutions. The latter is analyzed by means of standard topological tools, which leads to the result analogous to the Theorem of Sec.1.

DYNAMIC AND STATIC STABILITY OF MULTILAYER CONTACTING SHELLS

V.A. Krysko
Professor, Doctor of Technical Sciences, Honourd Man of Science an Engineering of Russia. The Head of the Hignerst Mathematics chais, addres: B. Sadovaja str., 96a,Slat 77, Saratov, 410054, Russia. E-mail kvm@sstu.saratov.su (88452)255558

There are few works, devoted to dynamic of non-soldered multilayer shells. In given work we aspired to fill this blank.

In given article the dynamic stability of multilayer geometrically nonlinear rectangular in plane shells is discussed. For the first time local and general loss of stability of shells is studied. Offered approach allows to consider both static and dynamic problems.

Let's consider multilayer rectangular in plan cylindrical shell assembled from any number of n +1 layers. Let h is the distance between layers Si and Si+1. Let's designate through S the middle surface of i-th layer (i=0, n). We'll take 0-th middle surface as a coordinate surface z=0. We'll take main curvature lines as curvilinear axes. External normal is directed to center of curvature of the given coordinate surface.

We'll consider each layer Si as an independent thin shell described by the equations of Kirchhoff-Love model:

$$\begin{aligned} &\nabla_{\lambda}^{4} F^{i} + \frac{1}{2} L\left(W^{i}, W^{i}\right) + \nabla_{k}^{2} W^{i} = 0, \\ &\frac{\partial^{2} W^{i}}{\partial t^{2}} + \frac{1}{\chi}\left\{\frac{1}{12\left(1-\nu^{2}\right)} \nabla_{\lambda}^{4} W^{i} - \nabla_{k}^{2} F^{i} - L\left(W^{i}, F^{i}\right) - Q^{i}\right\} = 0. \end{aligned} \tag{1}$$

To integrate the equations of system (1) it is necessary to attach the appropriate initial conditions:

$$W^{i}\Big|_{t=0} = W_{0}^{i}(x,y); \left.\frac{\partial W^{i}}{\partial t}\right|_{t=0} = V_{0}^{i}(x,y). \tag{2}$$

Moreover, it is necessary to satisfy with four boundary conditions in each point of contour $\dot{r}$:

$$\left.\frac{\partial^k W_0^i}{\partial \bar{n}^k}\right|_\Gamma = \Omega_k^i(x,y,t); \left.\frac{\partial^l F^i}{\partial \bar{n}^l}\right|_\Gamma = \Theta_l^i(x,y,t); \qquad (3)$$

where n is normal to border ŕ; k, l, change from 0 up to 3.

Let a normal load Q (x, y, t) is applied to layer Si. Under its influence points of the layer get displacements Wi and can enter into contact interaction with neighboring layers. Let's assume that contact pressure (i.e. tension normal to surface) is much more smaller than normal pressure in sections of shells and shells free slip in zones of contact.

Let's consider balance of an element of shell Si in view of contact interaction with layers S^{i-1} and S^{i+1}:

$$\frac{\partial^2 W^i}{\partial t^2} + \frac{1}{\chi}\left\{\frac{1}{12\left(1-\nu^2\right)}\nabla_\lambda^4 W^i - \nabla_k^2 F^i - L\left(W^i, F^i\right)\right.$$
$$\left. -\underline{Q}^i - \varphi^i R^{i-1} + \varphi^{i+1} R^{i+1}\right\} = 0. \qquad (4)$$

where R^i is contact interaction between layers S^i and S^{i-1}, and

$$\varphi^i = \begin{cases} 1, \text{in case of contact;} \\ 0, \text{contact not present.} \end{cases}$$

Excepting contact pressure R^i from equations (4), we'll get an equation of motion of shells taking into account contact interaction between layers:

$$\nabla_\lambda^4 F^i + \frac{1}{2} L\left(W^i, W^i\right) + \nabla_k^2 W^i = 0,$$
$$\chi\left(\frac{\partial^2 W^i}{\partial t^2} + \varphi^{i+1}\left[\frac{\partial^2 W^{i+1}}{\partial t^2} + \varphi^{i+1}[\ldots]\ldots\right] + \varphi^i\left[\frac{\partial^2 W^{i-1}}{\partial t^2} + \varphi^{i-1}[\ldots]\ldots\right]\right) = \qquad (5)$$
$$\varphi^i + \varphi^{i+1}\left[\varphi^{i+1} + \varphi^{i+1}[\ldots]\ldots\right] + \varphi^i\left[\varphi^{i-1} + \varphi^{i-1}[\ldots]\ldots\right],$$

where $\phi^i = \left\{\frac{1}{12\left(1-\nu^2\right)}\nabla_\lambda^4 W^i + \nabla_k^2 F^i + L\left(W^i, F^i\right) + \underline{Q}^i\right\}, i = \overline{0,n}.$

If an initial arrangement of shells and load are those, that shells are not contacting during movement , j=0 and (5) splits into n independent systems. Otherwise the equations of system (5) are connected.

For example, let's consider a system consisting of two layers. Let a uniformly distributed load Q is applied to layer S. Then equations (5) will take the form:

$$\nabla_{\lambda}^{4} F^{1} + \frac{1}{2} L\left(W^{1}, W^{1}\right) + \nabla_{k}^{2} W^{1} = 0,$$

$$\nabla_{\lambda}^{4} F^{2} + \frac{1}{2} L\left(W^{2}, W^{2}\right) + \nabla_{k}^{2} W^{2} = 0, \qquad (6)$$

$$\frac{\partial^{2} W^{1}}{\partial t^{2}} + \varepsilon \frac{\partial W^{1}}{\partial t} + \varphi\left(\frac{\partial^{2} W^{2}}{\partial t^{2}} + \varepsilon \frac{\partial W^{2}}{\partial t}\right) = \frac{1}{\chi}\left(\left\{\frac{1}{12\left(1-\nu^{2}\right)} \nabla_{\lambda}^{4} W^{1} + \nabla_{k}^{2} F^{1}\right.\right.$$

$$\left.\left.+ L\left(W^{1}, F^{1}\right) - Q\right\} + \left\{\frac{1}{12\left(1-\nu^{2}\right)} \nabla_{\lambda}^{4} W^{2} + \nabla_{k}^{2} F^{2} + L\left(W^{2}, F^{2}\right)\right\}\right),$$

where ε - is the decay factor of medium.
The initial and boundary conditions are :

$$W\big|_{t=0} = \left.\frac{\partial W}{\partial t}\right|_{t=0} = 0;$$

$$W\big|_{x=0,a} = W\big|_{x=0,b} = \left.\frac{\partial^{2} W}{\partial x^{2}}\right|_{x=0,a} = \left.\frac{\partial^{2} W}{\partial y^{2}}\right|_{x=0,b} = 0;$$

$$F\big|_{x=0,a} = F\big|_{x=0,b} = \left.\frac{\partial F}{\partial x}\right|_{x=0,a} = \left.\frac{\partial F}{\partial y}\right|_{x=0,b} = 0;$$

We'll decide system (6) using a finite differences method of O(h2) order. Together with initial and boundary conditions, received equations represent complete system of ordinary differential equations of the second order on time. This system can be integrated as follows:

1. We use Wi, obtained on previous step on time, to form right side of system of algebraic equations for function F.

2. Received F and W are substituted in right side of differential equations, from which using Runge-Kutta's method of fourth order we etermine W for following step. Zones of contact (the functions j) are determined from reasons of mutual non-penetration of shells.

Further the process repeats .

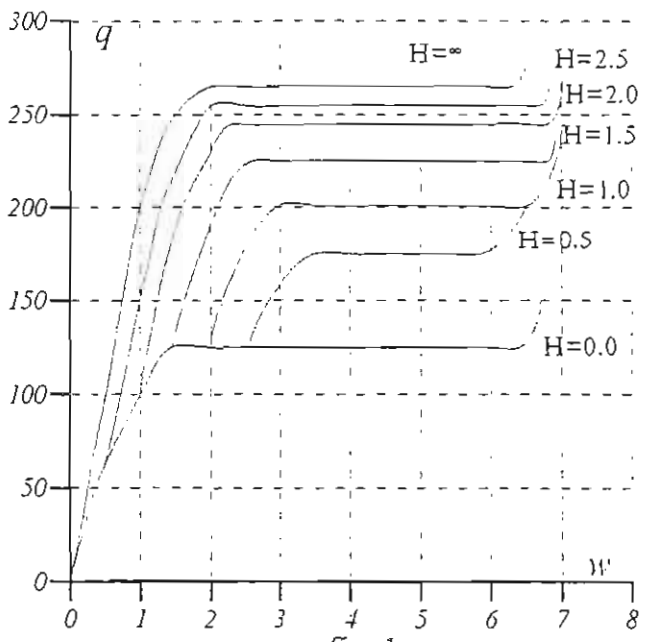

fig.1.

Fig. 1 demonstrates the dependence of a deflection from load for various H (curves 1-7 correspond H=0; 0.5; 1; 1.5; 2; 2.5; x respectively). For K =K = 2a H < 1.5 system losses stability when second shell losses them.

When h increases, process of loss of stability splits on two parts. Shell S losses stability when the shell S still stable (local stability loss of system).

Load to be increased, loss of stability of shell S occurs (general stability loss).

Critical loads were determined according to [1].

The contact pressure has character of concentrated in center load. If load increases, a zone of contact increases too, and maximum of contact pressure moves to the border of a contact zone. It's explained by the fact that in using model the squeeze on thickness of shells in zone of contact is not taking into account.

For H>1.5 contact pressure completely concentrates on the border of a contact zone (in central part the contact pressure is equal to zero). Thus contact of shells breaks in center and contact zone gets a form of ring.

Journal reference:

Крысько В.А.[1979] "Динамическая потеря устойчивости оболочек прямоугольных в плане при конечных прогибах", *Int. J. Прикладная механика 15(11), 58-62.*

Дедюкин И.Ю., Крысько В.А.[1994]"О критерия динамической потери устойчивости оболочек", *Int. J International applied Mechanics 10(30),56-60.*

NONLINEAR VIBRATIONS AND CHAOS IN ELASTIC-PLASTIC STRUCTURES

Ü. Lepik

Institute of Applied Mathematics, Tartu University,

Vanemuise str. 46, EE2400 Tartu, Estonia.

Abstract: Nonlinear vibrations of elastic-plastic beams, flat arches and cylindrical shells are considered. The end sections of the structure are pinned so that membrane forces appear. The equations of motion are integrated by the Galerkin method. Possibility of chaotic behavior of structures is discussed; for this purpose displacement-time histories, phase portraits and power spectrum diagrams are put together.

1. Introduction

Symonds and Yu [1985] considered the following problem: a fixed-ended beam is subjected to a short intensive pulse of transverse loading that produces plastic deformations. Solving the equations of motion they found that permanent deflection may be in the direction opposite to that of load. Such a phenomenon they called "counter-intuitive behavior" of the beam. They also showed that this effect takes place only in a narrow region of beam and load parameters. In the following papers Symonds and his coworkers investigated chaotic character of the vibrations, for this purpose they used Poincaré diagrams and Lyapunov exponents. Symonds and Lee [1993] calculated also the fractal dimensions for this problem. They found for the similarity dimension the value 0.78 and for the correlation fractal dimension ~ 1.44. In most of these papers Symonds and his coworkers for simplicity sake used models which consist of rigid beams connected by small elastic-plastic shells (Shanley-type models). The case of a continuous sandwich-type beam was discussed by Symonds and Yin Qian [1995]. In this paper equations of motion were integrated by the Galerkin method (for two degrees of freedom).

Elastic vibrations of compressed beams under lateral excitation were discussed by

Abhyankar et al [1993]. They considered a beam which is compressed by an axial load greater than the Euler buckling load and then is fixed in its compressed position. After that a transverse load $p = p(x,t)$ will be applied, besides a base excitation $w_B(t)$ may act (Fig. 1). Chaotic behavior of the solutions follows from phase portraits and period doubling bifurcations.

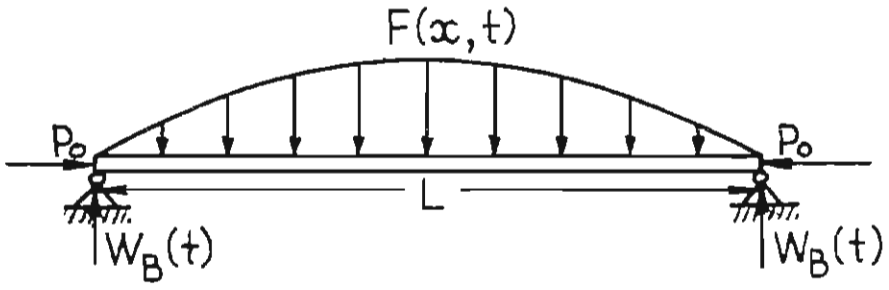

Fig. 1

The author of the present paper has tried to get solutions for continuous beams (i.e. without making use of Shanley-type or analogical models). For this purpose the Galerkin procedure for an arbitrary number of degrees of freedom has been used. The results which are published by Lepik [1993a, 1993b, 1993e, 1995, 1996] refer to beams, swallow arches and cylindrical shells. Here in after a short review about the method of solution and achieved results is presented.

2. Method of solution

To be brief we shall consider only beams with a rectangular cross-section, B, h and L are the width, thickness and length of the beam, respectively. The equations of motion are

$$\Phi_1 \equiv \frac{\partial T}{\partial x} - \rho B h \frac{\partial^2 u}{\partial t^2} = 0$$

$$\Phi_2 \equiv \frac{\partial^2 M}{\partial x^2} + \frac{\partial}{\partial x}\left(T\frac{\partial w}{\partial x}\right) - p(x,t) - \rho B h\left(\frac{\partial^2 w}{\partial t^2} - \frac{\partial^2 w_B}{\partial t^2}\right) \tag{1}$$

where ρ- is density, u- axial displacement, w- deflection. Axial force T and bending moment M we shall calculate from the formulae

$$T = \int_{-h/2}^{+h/2} \sigma(x,z)\, dz, \quad M = \int_{-h/2}^{+h/2} \sigma(x,z) z\, dz \tag{2}$$

We shall assume that the beam material has linear strain-hardening and the stress-strain diagram has the form as shown in Fig. 2. Elastic unloading (line CD) and secondary

plastic loading (line DB) are also taken into account.

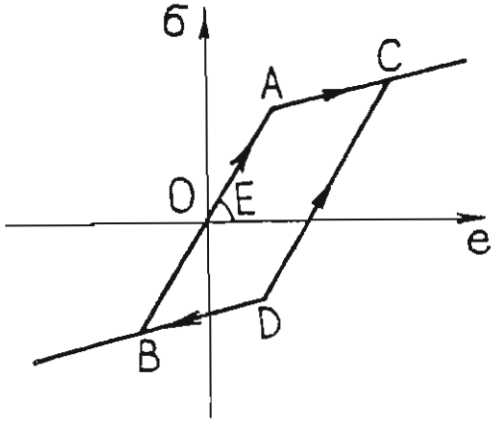

Fig. 2

To the equations (1) we shall apply the Galerkin's procedure

$$\int_0^L \Phi_1 \delta u \, dx = 0, \quad \int_0^L \Phi_2 \delta w \, dx = 0 \tag{3}$$

Here we shall confine us only to the beam with simply supported ends and seek the displacements u and w in the form

$$u = \sum_{i=1}^{n} b_i \sin 2i\pi \frac{x}{L}, \quad w = \sum_{i=1}^{m} f_i \cos(2i+1)\pi \frac{x}{L} \tag{4}$$

The integrals (2)-(3) we shall calculate numerically; by doing this we find the second derivatives $\ddot{b}_i$ and $\ddot{f}_i$. For evaluating the quantities $b_i, \dot{b}_i, f_i, \dot{f}_i$ we shall use the scheme of central finite differences (for getting a stable solution the time increment Δt must be sufficiently small).

3. Discussion

Calculations have been carried out for four problems: (1) beam under short pulse loading, (2) prestressed beam, (3) flat arch under short pulse loading, (4) prestressed cylindrical shell. These calculations showed that the necessary exactness is achieved if we shall take from both of the series (4) only 2-3 terms. The results obtained by our method are quite close to the solution obtained by Abacus technic. Most existing solutions go out from the assumption that the axial force T is constant along the beam. Our computations show that this assertation does not hold in the real case.

For analyzing chaotic behavior of the vibrations deflection history, phase portraits and power spectrum diagrams are put together. It follows from these diagrams that weak chaotic effects in the response of the structure may exist, especially in the initial phase; as to the long-term motion then it transitates to periodic vibrations of smaller amplitude. Most distinguished are these effects in the case of prestressed beams. In the case of flat arches and cylindrical shells the vibrations are considerably more regular as for beams.

References

Abhyankar, N. S. & Hall, E. K. & Hanagud, S. V. [1993] "Chaotic vibrations of beams: numerical solution of partial differential equations",*ASME J. Appl. Mech.* 60, 167-174.

Lee, J. Y. & Symonds, P. S. & Borino, G. [1992] "Chaotic response of a two-degree of freedom elastic-plastic beam model to short pulse loading", *ASME J. Appl. Mech.* **59**, 711–721.

Lepik, Ü. [1993a] "Dynamic response of elastic-plastic beams with axial constraints", *Int. J. Impact. Engng* **15**, 3-16.

Lepik, Ü. [1993b] "Impulsively loaded fully fixed-ended elastic-plastic beams by Galerkin's method", *Int. J. Impact. Engng* **15**, 17-23.

Lepik, Ü. [1993c] "Vibrations of elastic-plastic fully clamped beams and flat arches under impulsive loading", *Int. J. Non-Linear Mech.* **29**, 613-623.

Lepik, Ü. [1995] "Elastic-plastic vibrations of a buckled beam", *Int. J. Non-Linear Mech.* **30**, 129-139.

Lepik, Ü. [1996] "Axisymmetric vibrations of elastic-plastic cylindrical shells by Galerkin's method", *Int. J. Impact. Engng* **18**, 489-504.

Symonds, P. S. & Lee, J. Y. [1993] "Fractal dimensions in elastic-plastic beam dynamics", *Proc. of the 14th Biennal ASME Conference on Vibrations and Noise, Albuquerque, New Mexico.*

Symonds, P. S. & Yu, T. X. [1985] "Counterintuitive behavior in a problem of elastic-plastic beam dynamics", *ASME J. Appl. Mech.* **52**, 517-522.

Symonds, P. S. & Yin, Qian. [1995] "Aspects of chaotic response of an elastic-plastic beam to impulsive loading" *Proc. IUTAM and ISIMM Symp. on Aniosotropy, Inhomogeneity and Nonlinearity in Solid Mech., Univ. of Nothingham (1994), Kluwer.*

REGULAR AND CHAOTIC MOTION OF FROUDE PENDULUM

Grzegorz Litak, Grzegorz Spuz-Szpos, Kazimierz Szabelski, Jerzy Warmiński
Department of Mechanics, Technical University of Lublin,
Nadbystrzycka 36, Lublin 20–618, Poland

(Fax: + 48 81 550808, E-mail: glitak@archimedes.pol.lublin.pl)

Abstract: Vibrations of self–excited Froude pendulum under external excitation with non–linear stiffness. were analyzed. Differential equation of motion includes nonlinear damping term of Rayleigh's type. Vibrations synchronization and chaos were examined in the system.

1. Introduction

Froude pendulum is well known example of self–excited system [Minorski 1962, Moon 1987, Litak *et al.* 1994, Litak *et al.* 1996]. Vibrations of pendulum subjected to external excitation are described by the following differential equation:

$$\ddot{\varphi} - (\tilde{\alpha} - \tilde{\beta}\dot{\varphi}^2)\dot{\varphi} + \sin\varphi = \tilde{B}\cos\omega t \quad , \tag{1}$$

where $\tilde{\alpha}$, $\tilde{\beta}$ denotes non–linear damping coefficients of Rayleigh's type, $\tilde{B}$ excitation amplitude, ω excitation frequency.

The system is described by two characteristic frequencies: the frequency of self–excited vibration p and the external excitation frequency ω. For exiting force amplitude $\tilde{B}$ equal to zero vibration with the same frequency as self–excited appears. For $\tilde{B} > 0$ according to the parameters of the system, it is likely to occur two cases of regular solutions: mono-frequency solution or quasi–periodic solution with modulated amplitude. Besides regular solutions, also chaotic solutions may appear [Litak *et al.* 1994, Litak *et al.* 1996].

2. Vibration in the Vicinity of Fundamental External Resonance

Let us examine small vibrations around $\varphi = 0$. Expanding in Tailor's series up to the third order terms $\sin(\varphi) \approx \varphi - \tilde{\gamma}\varphi^3$, where $\tilde{\gamma} = 1/6$ we get following equation

$$\ddot{\varphi} - (\alpha - \tilde{\beta}\dot{\varphi}^2)\dot{\varphi} + (1 - \tilde{\gamma}\varphi^2)\varphi = \tilde{B}\cos\omega t \quad . \tag{2}$$

For fundamental external resonance $\Omega \approx 1$ we can write:

$$\Omega^2 = 1 + \epsilon\sigma \quad . \tag{3}$$

Introducing the small parameter $\epsilon \ll 1$ into Eq. 2 we get:

$$\ddot{\varphi} + \Omega^2\varphi = \epsilon\left[\sigma\varphi + (\alpha - \beta\dot{\varphi}^2)\dot{\varphi} - (1 - \gamma\varphi^2)\varphi + B\cos\Omega t\right] \quad , \tag{4}$$

where $\tilde{\beta} = \epsilon\beta$, $\tilde{B} = \epsilon B$, $\tilde{\alpha} = \epsilon\alpha$, $\tilde{\gamma} = \epsilon\gamma$.

Proceeding standard multiple-time-scale calculations [Nayfeh 1989] we look for the first order approximation of type:

$$x(t) \approx a\cos\left(\frac{1}{2}\Omega t + \psi\right) \quad , \tag{5}$$

where a and ψ satisfy the following equations:

$$\dot{a} = \epsilon\left(\frac{\alpha}{2} - \frac{3}{8}\beta a^3 - \frac{B}{2\Omega}\sin\psi\right) \tag{6}$$

$$a\dot{\psi} = \epsilon\left(-\frac{\sigma_1}{2\Omega}a - \frac{3\gamma}{8\Omega}a^3 - \frac{B}{2\Omega}a^3\cos\psi\right) \quad . \tag{7}$$

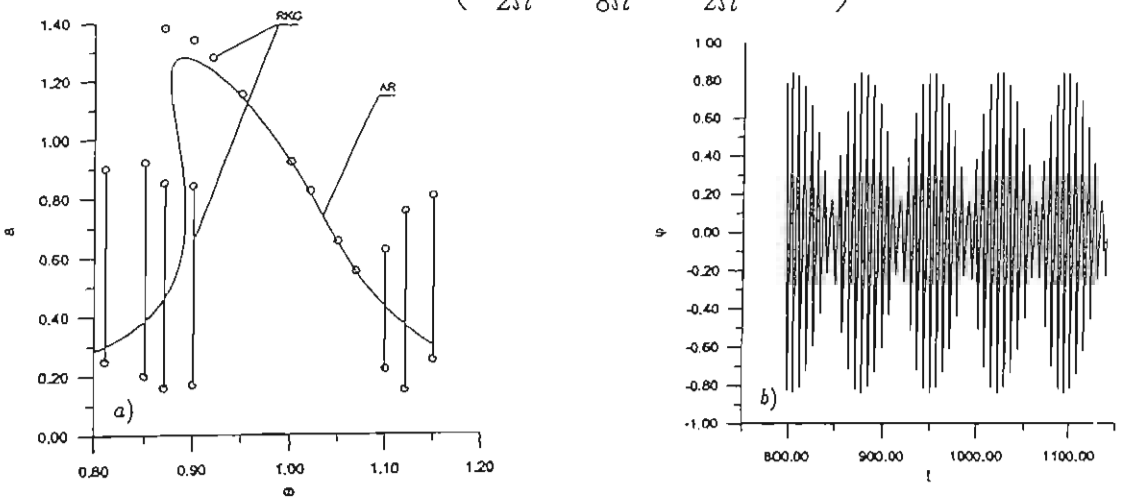

Figure 1. Vibration amplitudes (1a), time history for $\omega = 0.87$ (1b).

Figure 1a shows vibration amplitude a plots versus frequency of parametric excitation ω. They were obtained as result of analytical (AR) investigations in first order approximation (Eqs. 4,5).

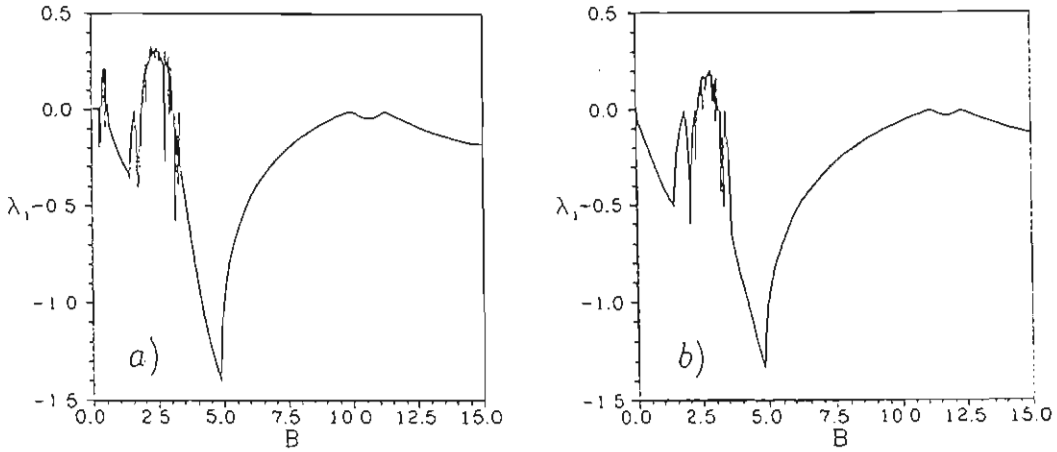

Figure 2. Lapunov exponents: $\tilde{\alpha} = 0.35$ (Fig 2a), $\tilde{\alpha} = 0.035$ (Fig. 2b).

Comparative points obtained during numerical simulation (Eq. 1) were also marked (RKG). Parameters used in investigations were following: $\tilde{\alpha} = 0.035$, $\beta = 0.1$, $\tilde{B} = 0.1$, $\tilde{\gamma} = 1/6$, $\epsilon = 0.1$. Outside the synchronization area beats, i.e. almost periodic vibrations occur. The typical time history in this region is presented in Fig. 1*b*, where ω was chosen to be equal to 0.87.

3. Chaotic Motion of Froude Pendulum.

The most reliable criterion for chaotic motion is positive value of maximal (but nonzero) Lyapunov exponent. Figure 2 presents results values of Lyapunov exponents λ_1 versus excitation amplitude $\tilde{B}$ calculated by Wolf *et al*'s algorithm [1988]. For calculations the following parameters: $\omega = 1$, $\tilde{\beta} = 0.1$, $\tilde{\alpha} = 0.35$ (Fig. 2*a*) and $\tilde{\alpha} = 0.035$ (Fig. 2*b*) the initial conditions: $\varphi_0 = 0$, $\dot{\varphi}_0 = 0.5$ were used.

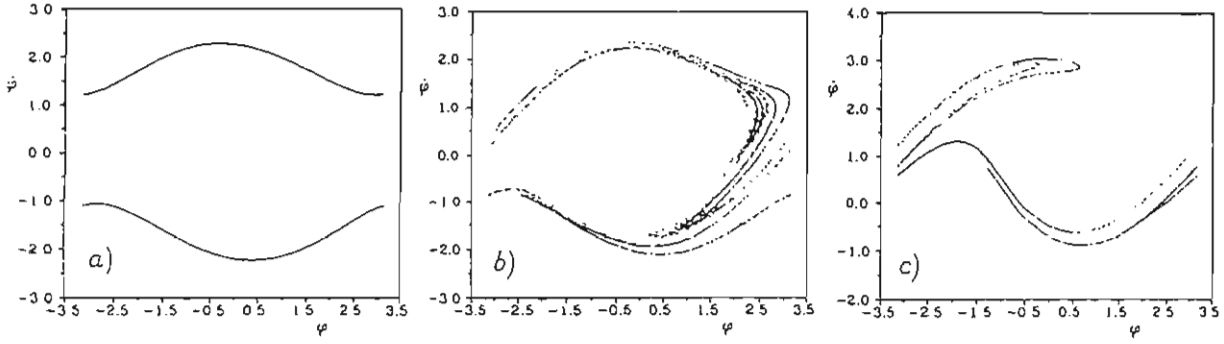

Figure 3. Poincaré maps, Figs.3a, b, c for values of parameter $\tilde{B} = 0.1, 0.42, 2.5$ respectively.

For intervals around $\tilde{B} \approx 2.5$ chaotic motions of pendulum were found in both cases ($\tilde{\alpha} = 0.35$, $\tilde{\alpha} = 0.035$). Additional interval around $\tilde{B} \approx 0.45$ for $\tilde{\alpha} = 0.35$ shows chaotic behavior which is absent in case of smaller $\tilde{\alpha}$.

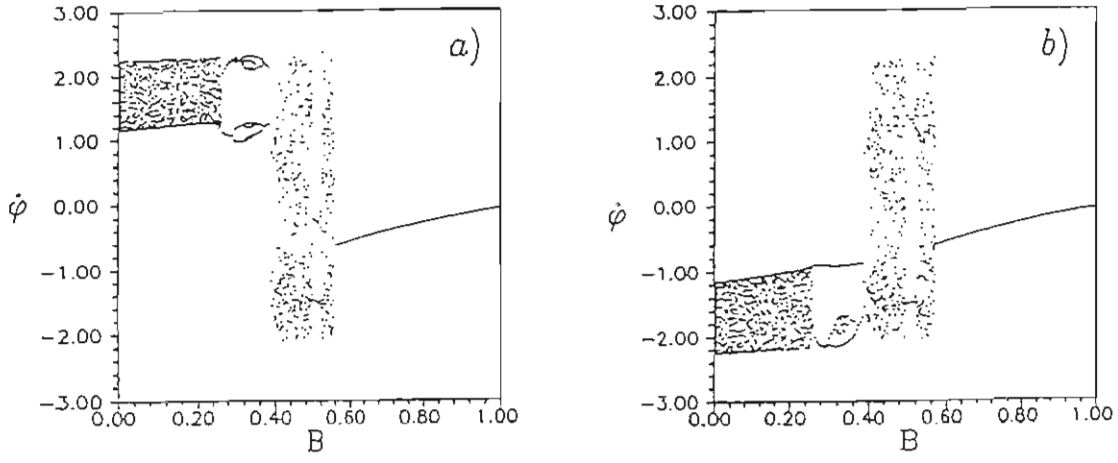

Figure 4. Bifurcation diagrams: for $(x_0, v_0) = (0, 1)$ (Fig. 4*a*), for $(x_0, v_0) = (0, 0.5)$. (Fig. 4*b*)

For three values of the parameter $\tilde{B} = 0.1, 0.42, 2.5$ (other parameter values as in Fig. 2*a*) Poincaré sections are presented (Figs. 3*a*, *b*, *c*) Figure 3*a* shows regular quasi-periodic

motion while Figs. $3b, c$ illustrate the strange attractors of pendulum chaotic motion.

Two different Bifurcation diagrams (all parameters values as in Fig. $2a$) according to different initial conditions (corresponding to upper and lower branches of Poincaré Maps in Fig. $3a$) are connected with rotational motions of pendulum in different directions.

Thus the regular motion of Froude pendulum could be synchronized with external forcing or quasi periodic. We found that quasi periodic vibrations appear outside synchronization region for small $\tilde{alpha}$ (Fig $1b$) while quasi periodic rotations appear for large enough α ($\tilde{\alpha} = 0.35$ ~ Fig. $2a$). We see in Fig. $1a$ for relatively small external excitation $\tilde{B}$, where the quasi periodic rotation appears Lapunov exponent λ_1 has nodal value.

4. Summary

Analytic and numerical investigation was carried on for Froude pendulum. Synchronization region was obtained under certain simplified assumptions and their verification was obtained applying numerical simulation. Chaotic vibrations and quasi-periodic rotation of pendulum was investigated by means of Lyapunov exponent, Poincaré maps and bifurcation diagrams for particular parameters of the system.

5. Acknowledgments

Authors KS, GL, JW, were partially supported by State Committee for Scientific Research (KBN) Grant.

6. References

Litak G., Przystupa W. and Szabelski K., Warmiński J. [1994] "Chaotic Motion of Froude Pendulum" *I.F. UMCS REPORT.*

Litak G., Warmiński J., Spuz-Szpos G. [1996] "Chaos Analysis of the Self-Excited System with External Forcing" *Proceedings of VIBRATIONS IN PHYSICAL SYSTEMS, XVII SYMPOSIUM*, Poznań-Błażejewko, May 22-25 1996, 188-189

Minorsky N. [1962] *Nonlinear Oscillations*, Van Nostrand, Princeton, NJ.

Moon F. C. [1987] *Chaotic vibrations*, John Wiley and Sons, New York.

Nayfeh A.H., Sanchez N.E. [1989] "Bifurcations in a Forced Softening Duffing Oscillator" *Int. J. Non-Linear Mechanics* 24, 483-497.

Wolf A., Swift J.B. Swinney H.L. and Vasano J.A. [1988] "Determining Lyapunov Exponents from a Time Series." *Physica* D16, 285-317.

VIBRATION SYNCHRONIZATION AND CHAOS IN SELF- EXCITED SYSTEM WITH PARAMETRIC FORCING AND NONLINEAR STIFFNESS

Kazimierz Szabelski, Grzegorz Litak, Grzegorz Spuz-Szpos, Jerzy Warmiński
Department of Mechanics, Technical University of Lublin,
Nadbystrzycka 36, Lublin 20-618, Poland

(Fax: + 48 81 550808, E-mail: glitak@archimedes.pol.lublin.pl)

Abstract: Vibrations of self-excited oscillator under parametric excitation with non-linear stiffness were investigated in this paper. Differential equation of motion includes Van der Pol, Mathieu and Duffing terms. Vibrations synchronization and chaos were examined in the system. In the resonance area, self-excited vibrations are dawn by parametric excitation. Outside the synchronization area, almost periodic vibrations appear. According to the parameters, in the system may doubling of the period and transition to the chaos appear. Chaotic solutions were found by means of Lyapunov exponent.

1. Introduction

Let us examine vibrations of parametrically self-excited systems described by differential equation [Szabelski 1984, Huseyin and Rui 1992, Rui and Huseyin 1992]:

$$\ddot{x} - (\alpha_1 - \beta_1 x^2)\dot{x} + (\delta - \mu_1 \cos\Omega t)x + \gamma_1 x^3 = 0 \quad . \tag{1}$$

As far as chaos investigations in this class of system are concerned chaos was discovered for vibrations model with Van der Pol terms, non-linearity of Duffing-type and external excitation in the form [Ueda and Aamatsu 1981, Steeb and Kunick 1987, Kapitaniak and Steeb 1990]:

$$\ddot{x} - (\alpha - \beta\dot{x}^2)\dot{x} + (\delta + \gamma x^2)x = B\cos(\omega t + \phi_0) \quad . \tag{2}$$

For that equation scope of parameters, leading to chaos solutions, was determined. In [Ueda and Akamatsu 1981, Steeb and Kunick 1987] case $\delta = 0$ was examined, and in $\delta \neq 0$ case. In [Kapitaniak and Steeb 1990] case $\delta \neq 0$ and $\gamma \neq 0$, where $\gamma \ll \delta$, was investigated. In [Szabelski *et al.* 1996] system (Eq. 2) of soft type of nonlineatity ($\gamma_1 < 0$) was considered. In this paper we provide the analogous analysis of stiff case ($\gamma_1 > 0$).

2. Vibrations in Case of the Main Resonance

Introducing a small parameter $\epsilon \ll 1$ into Eq. 1 and putting $\delta = 1$, we obtain:

$$\ddot{x} + x = \epsilon \left[(\alpha - \beta x^2)\dot{x} + \mu x \cos\Omega t - \gamma x^3 \right] \quad . \tag{3}$$

In case of the main parametric resonance ($\Omega \approx 2$), we can write:

$$\frac{1}{4}\Omega^2 = 1 + \epsilon\sigma_1 \quad . \tag{4}$$

Introducing this formula into (2), we obtain:

$$\ddot{x} + \frac{1}{4}\Omega^2 x = \epsilon \left[(\alpha - \beta x^2)\dot{x} + \sigma_1 x + \mu x \cos\Omega t - \gamma x^3 \right] \quad . \tag{5}$$

After some algebra [Szabelski *et al.*, 1996] solutions of the equation in the first and second order of perturbation may be presented in the following forms:
(solution in the first order approximation)

$$x(t) \approx a\cos\left(\frac{1}{2}\Omega t + \psi\right) \quad , \tag{6}$$

where a and ψ satisfy the set of equations:

$$\dot{a} = \epsilon\left(\frac{\alpha}{2}a - \frac{\beta}{8}a^3 - \frac{\mu}{2\Omega}a\sin(2\psi)\right) \tag{7}$$

$$a\dot{\psi} = \epsilon\left(-\frac{\sigma_1}{\Omega}a + \frac{3\gamma}{4\Omega}a^3 - \frac{\mu}{2\Omega}a\cos(2\psi)\right) \tag{8}$$

(solution in the second order approximation)

$$x(t) \approx a\cos\left(\frac{1}{2}\Omega t + \psi\right) + \epsilon\left[-\frac{\mu a}{4\Omega^2}\cos\left(\frac{3}{2}\Omega t + \psi\right) + a^3\left(\frac{\gamma}{8\Omega^2} + \frac{i\beta}{4\Omega}\right)\cos\left(\frac{3}{2}\Omega t + 3\psi\right)\right], \tag{9}$$

where a and ψ satisfy the set of equations:

$$\dot{a} = \epsilon\left(\frac{\alpha}{2}a - \frac{1}{8}\beta a^3 - \frac{\mu}{2\Omega}a\sin(2\psi)\right) + \epsilon^2\left(-\frac{3\alpha\gamma}{4\Omega^2}a^3 + \frac{11\beta\gamma}{64\Omega^2}a^5 + \frac{\beta\mu}{16\Omega^2}a^3\cos(2\psi)\right) \tag{10}$$

$$\begin{aligned} a\dot{\psi} &= \epsilon\left(-\frac{\sigma_1}{\Omega}a + \frac{3\gamma}{4\Omega}a^3 - \frac{\mu}{2\Omega}a\cos(2\psi)\right) + \epsilon^2\left[\left(-\frac{\sigma_1^2}{\Omega^3} - \frac{\alpha^2}{4\Omega} + \frac{3\mu^2}{8\Omega^3}\right)a\right. \\ &+ \left.\left(\frac{3\gamma\sigma_1}{2\Omega^3} + \frac{\alpha\beta}{4\Omega} - \frac{\gamma\mu}{4\Omega}\cos(2\psi) - \frac{\beta\mu}{8\Omega^2}\sin(2\psi)\right)a^3 + \left(-\frac{15\gamma^2}{32\Omega^3} - \frac{7\beta^2}{128\Omega}\right)a^5\right] \quad . \end{aligned} \tag{11}$$

Figure 1*a* shows vibration amplitude plots versus frequency of parametric excitation. They were obtained as result of analytical (AR) investigations in first order approximation (Eq. 6). Comparative points obtained during numerical simulation (Eq. 3) were also marked (RKG). Outside the synchronization area beats, i.e. almost periodic vibrations occur. Parameters used in investigations were following: $\alpha = 0.1$, $\beta = 0.5$, $\gamma = 0.5$, $\mu = 1.0$, $\epsilon = 0.1$.

3. Chaotic Vibration of System

Applying Wolf algorithm [Wolf *et al.* 1988], maximal (nonzero) Lyapunov exponent (Eq. 1) $\alpha_1 = 0.2$, $\beta_1 = 0.2$, $\mu_1 = -17$, $\Omega = 4$, $\gamma_1 = 1$ and $\delta = [0, 20]$) was found (Fig. 1*a*).

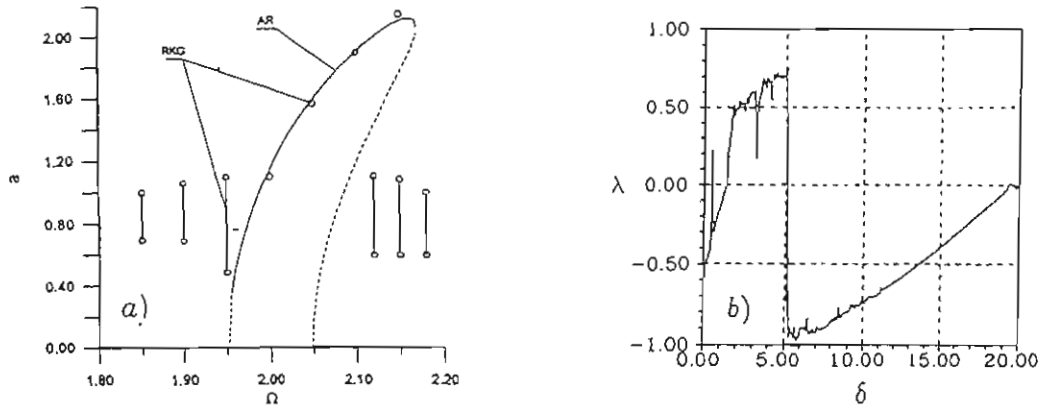

Figure 1. Vibration amplitudes (1*a*), Lyapunov exponent (1*b*).

The following initial conditions were assumed $x_0 = 0.5$ and $\dot{x}_0 = 0.5$. Figure 1*b* shows interval of parameter values ($\delta \approx ([1.5, 5.1]$) for which exponent λ is positive.

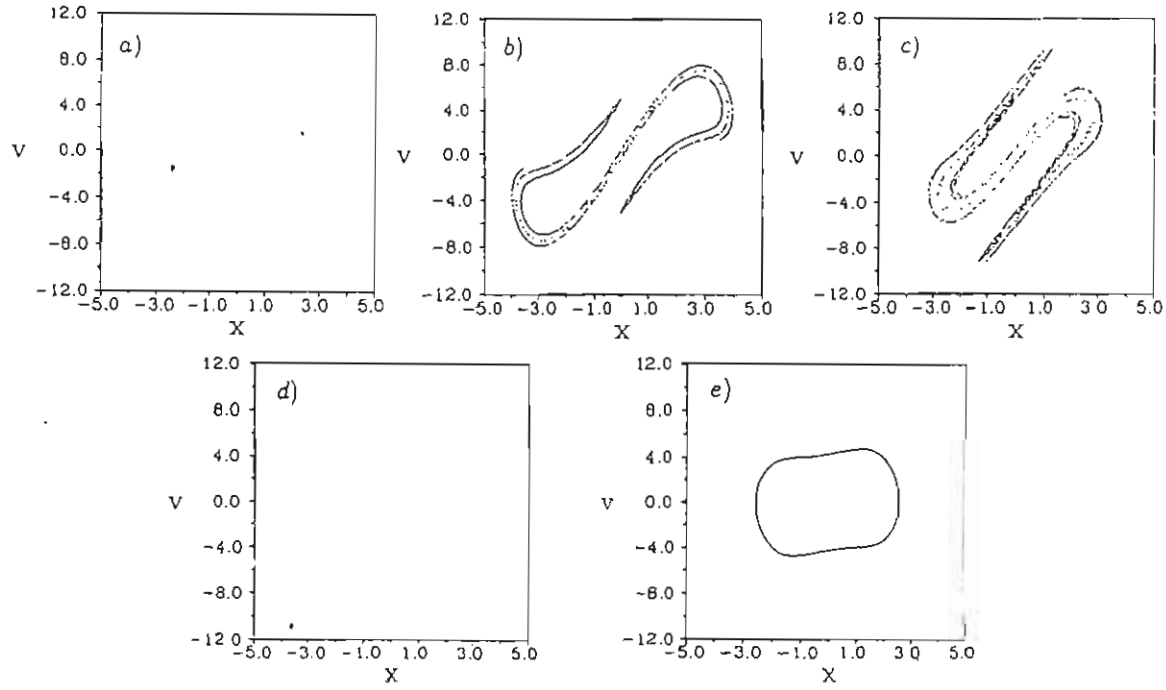

Figure 2. Poincare Maps

For δ values belonging to that interval, the system behaves in chaotic way. Figures 2*a*–*e* shows Poincare maps for chosen values of δ (other parameters are as in Fig. 1*b*). In Figs. 2*a* ($\delta = 1.3$) and 2*d* ($\delta = 1.7$) system vibrations is synchronized. Figures 2*b* and 2*c* show strange attractors of chaotic motion. At last Fig. 2*e* for larger value of δ ($\delta = 20$) presents limit cycle attractor of quasi periodic motion characteristic for self-exited systems.

4. Summary

Considering existing and stability of differential equation solutions, the interaction effects of self-excited and parametric vibrations were determined. It was found that vibrations synchronization in particular frequency interval of parametric excitation took place. Analytic investigation was carried out under certain simplified assumptions and their verification was obtained applying numerical simulation. Applying Lyapunov exponents method, chaotic vibrations were discovered for particular parameters of the system.

5. Acknowledgments

Authors KS, GL, JW were partially supported by KBN Grant.

6. References

Huseyin K. and Rui L. [1992] "A perturbation method for the analysis of vibrations and bifurcations associated with non-autonomous systems -I. Non resonance case." *Int. J. Non-Linear Mechanics* **27**, 203–217.

Kapitaniak T. and Steeb W.-H. [1990] "Transition to chaos in a generalized van der Pol's eguation." *J. Sound and Vibration* **143**, 167–170.

Parlitz U. and Lauterborn W. [1987] "Period-doubling cascades and devil's staircase of the driven van der Pol oscillator." *Phys. Rev.* **A36**, 1428–1434.

Rui L and Huseyin K. [1992] "A perturbation method for the analysis of vibrations and bifurcations associated with non-autonomous systems -II. Resonance case." *Int. J. Non-Linear Mechanics* **27**, 219–232.

Szabelski K. [1984] "Drgania układu samowzbudnego z wymuszeniem parametrycznym i nieliniową sprężystością." *Mechanika Teoretyczna i Stosowana*, **22**, 171–183.

Szabelski K., Litak G., Warmiński J. and Spuz–Szpos G. [1996] "Vibration Synchronization and Chaos in the Parametrically Self–Excited System with Non–Linear Elasticity" in *Proceedings of EUROMECH – 2nd European Nonlinear Oscillation Conference* Prague, September 9–13, 1996.

Steeb W.-H. and Kunick A. [1987] "Chaos in system with limit cycle" *Int. J. Non-Linear Mechanics* **22**, 349–361.

Ueda Y. and Akamatsu N. [1981] "Chaotically Transitional Phenomena in the Forced Negative–Resistance Oscillator." *IEEE Transactions on Circuits and Systems*, CAS-28 217–224.

Wolf A., Swift J.B. Swinney H.L. and Vasano J.A. [1988] "Determining Lyapunov Exponents from a Time Series." *Physica* D16, 285-317.

TRANSITION FROM UNIMODAL TO BIMODAL MAP IN ONE-DIMENSIONAL PIECEWISE LINEAR MODELS

Yu. L. Maistrenko, V. L. Maistrenko and S. I. Vikul
Institute of Mathematics, National Academy of Sciences of Ukraine,
3 Tereshchenkivska st. Kiev, Ukraine, 252601

Abstract: We study transition from unimodal to bimodal maps in a three-segment piecewise linear one-dimensional family. It is shown, that such type bifurcation gives rise to the appearance of the period adding cascades of attracting cycles which assumed a description with use of symbolic dynamics. We obtain exact formulas for the existence regions of these attracting cycles and explain the mechanisms of their destructions.

1. Introduction

We continue the study of attracting cycles as well as cycles of chaotic intervals of bimodal piecewise linear maps of line itself begun in Maistrenko *et al.* [1995a]. Consider the map in the form:

$$f = f_{l,p,b}(x) = \begin{cases} lx - lb - l/p + 1, & x \le b + 1/p, \\ px - pb, & b + 1/p < x < b - 1/p, \\ lx - lb + l/p - 1, & x \ge b - 1/p \end{cases} \tag{1}$$

where parameters l and p are slopes, b is a shift of a graph of $y = f(x)$ with respect to origin. Parameter region to be considered is chosen as:

$$\Pi = \{(l, p, b) : 0 < l < 1, \quad -\infty < p < -1, \quad |b| < 1 + 1/p\}. \tag{2}$$

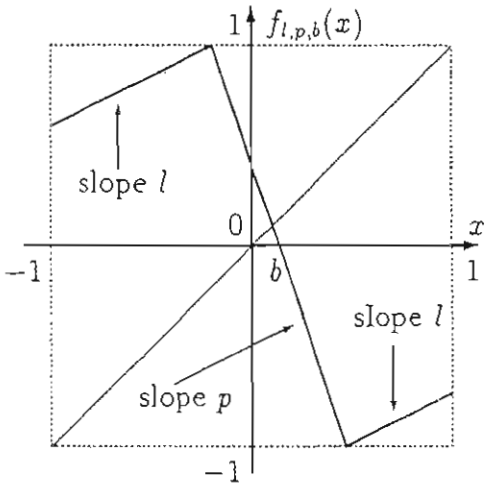

Fig. 1(a)

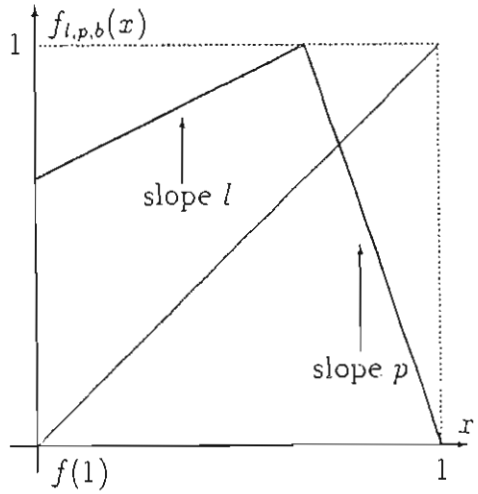

Fig.1(b)

It is simply to check that for all $(l, p, b) \in \Pi$ $f_{l,p,b}$ has unique finite invariant interval [-1,1] (i.e. $f([-1,1]) = [-1,1]$) where f is piecewise linear three-segment (Fig.1(a)). This interval $[-1,1]$ attracts all trajectories of f; more exactly, any trajectory gets into $[-1,1]$ for a finite number of iteration and never leave after. An invariant set possessing this property is called by absorbing area [Gumowski & Mira, 1980]. Thus, for all $(l, p, b) \in \Pi$ $f_{l,p,b}$ has absorbing interval $[-1,1]$ where it is three-segment. If the inequality $|b| < 1+1/p$ is false $f_{l,p,b}$ has not invariant intervals in which it is three-segment.

Nevertheless, if

$$1 + 1/p < |b| < 1 - 1/p,$$

absorbing invariant interval still exists, being equal [f(1), 1] (for $b > 0$) or [-1, f(-1)] (for $b < 0$). In this invariant interval, the map considered is two-segment called a skew tent map (Fig.1(b)). Regular and chaotic attractors of skew tent map, forming period adding cascade were described in Maistrenko *et al.* [1992] and Maistrenko *et al.* [1993]

At last, if

$$|b| > 1 - 1/p,$$

our map does not have any finite nontrivial invariant intervals, and the unique its attractor is an attractive fixed point x^* equals $\frac{lb+l/p-1}{l-1}$ (for $b > 0$) or $\frac{lb-l/p+1}{l-1}$ (for $b < 0$).

When parameter b crosses the surfaces $|b| = 1 - 1/p$ ($|b|$ is decreasing) so-called "border-collision" bifurcation takes place [Nusse & Yorke, 1995]. It consists in passing by the attractive fixed point x^* through the extremum (turning) point which is a border of two intervals at every of which the map is linear. Result of this bifurcation is a birth of absorbing invariant interval, where f is a skew tent map. Just after the bifurcation moment, this appeared interval is infinitesimal, then its size increases linearly with b.

Let's continue decreasing the modulus of the parameter b. When its value passes through the point $1 + 1/p$, (l, p, b)- parameter point enters the region Π - so-called "unimodal-bimodal" bifurcation takes place consisting in the following: in the invariant interval, the map $f_{l,p,b}$ turns to change its form from two-segment to three-segment.

The purpose of this paper is to show that this bifurcation gives rise to the appearance of the attracting cycles of different periods and configurations, to obtain exact formulas for the regions of existence of these cycles and to study the mechanisms of their destructions inside Π.

In Maistrenko *et al.* [1995a], the map $f_{l,p,b}$ was considered under the conditions that the parameter point (l, p, b) enter the region Π through the surface $p = -\infty$, where the

map can be represented as a discontinuous circle map in the form:

$$x \mapsto lx + a \pmod 1 \tag{3}$$

and $a = 1 - l(b+1)/2$. If, additionally, $l = 1$ this map turns to a shift map with a rotation number $\rho = (1-b)/2$ being a rational or irrational depending on b be rational or irrational. In the first (rational) case all trajectories are periodic with the rotation number $\rho \stackrel{def}{=} r/q$; in the second (irrational) case all they are quasiperiodic.

At $l < 1$ (still $p = -\infty$) the regions of synchronization $\Pi_{r/q}$ arise (so-called Arnold's tongues) being regions in the parameter plane (l, b) in which attracting cycle $\gamma_{r/q}$ with rotation number r/q exists for any r and q relatively prime. In contract to the case $l = 1$, this cycle $\gamma_{r/q}$ is global attractor: all other trajectories of $f_{l,-\infty,b}$ are attracted by it.

Let, by this time $p > -\infty$. Consider the map $f_{l,p,b}$ at $(l, p, b) \in \Pi$. This map has unique fixed point $x^* = \frac{pb}{p-1}$, which is repelling. For each period-q cycle

$$\gamma = \{f^n(x_0)\}_{n=0}^{n=q-1}$$

(q be period) of the map $f_{l,p,b}$ we introduce the following proper fraction

$$\rho = \frac{\#\{i = \overline{1,q} : f^i(x) \in (x^*, 1]\}}{q}, \tag{4}$$

which will be called **generalized rotation number** or, simply, **rotation number** of the cycle γ. Numerator of the fraction indicates how many points of γ belong to the interval $(x^*, 1]$. Geometrically, it is a number of inverses of corresponding periodic trajectory for a period. Denominator q equals to the period of trajectory. Note, that this fraction r/q may be reducible.

At $p = -\infty$ this generalized rotation number turns to usual rotation number of circle map [Melo & Strien, 1993] when rotation number of any trajectory is the same for any trajectory. For $f_{l,p,b}$ at $p > -\infty$ it is not the case: different trajectories may have different rotation numbers.

Suppose that γ is a cycle with rotation number $\rho = r/q$, where fraction r/q, generally, may be reducible. Cycle, possessing this property, will be denoted by $\gamma_{r/q}$. Moreover, (l, p, b)-parameter region where $\gamma_{r/q}$ exists and is attracting will be denoted by $\Pi(\gamma_{r/q})$ or, simply, $\Pi_{r/q}$.

2. Regions of Synchronization after Bifurcation "Circle Map - Three-Segment Map"

As it was shown in Maistrenko *et al.* [1995a], bifurcation "via $p = -\infty$" in the family $f_{l,p,b}$ of the form Eq.(1) gives rise to the appearance of the regions of synchronization (Arnold's tongues) $\Pi_{r/q}$. Every this regions $\Pi_{r/q}$ is characterized by the existence of the only one attracting cycle $\gamma_{r/q}$ (r/q is cycle rotation number) which is a continuation of the corresponding attracting cycle incoming from the case $p = -\infty$. Cycle $\gamma_{r/q}$ is characterized as follows: it has r points belonging to the right segment $[b - 1/p, 1]$ and, respectively, $q - r$ - to the left one $[-1, b + 1/p]$ (for a definiteness, we assume $b > 0$).

Analogously to the case $p = -\infty$, these regions $\Pi_{r/q}$ can be ordered in accordance with the levels of complexity [Leonov, 1959; Mira, 1987]. First complexity level consists of the regions $\Pi_{1/q}$ (for $b > 0$) and $\Pi_{(q-1)/q}$ (for $b < 0$) $q = 2, 3, ...$ Between any two such regions of first level, there are two converging sequences of second complexity regions: $\Pi_{n/(nq+1)}$ and $\Pi_{n/n(q+1)-1}$ (for $b > 0$) and $\Pi_{n(q-1)+1/(nq+1)}$ and $\Pi_{(nq-1)/n(q+1)-1}$ (for $b < 0$). And so on.

Recurrent formulas has been obtained for the regions of any level of complexity. Note, that the boundaries of any region $\Pi_{r/q}$ are derived with use of the following criterion: one of the cycle $\gamma_{r/q}$ points passes through the extremum point of f giving rise to a border collision bifurcation.

Regions of the next $(k + 1)$th level of complexity are obtained by the action of some operator of similarity defined on the regions of previous kth level. At this formulas for the boundaries of first level complexity regions can be easily derived directly. For example, for $\Pi_{1/q}$ ($b > 0$) they are:

$$b_{1/q}^{(-)} = \frac{1 - 2l^{q-1} + l^q}{1 - l^q} p' + \frac{1 - 2l^{q-2} + 2l^{q-1} - l^q}{1 - l^q};$$

$$b_{1/q}^{(+)} = -\frac{1 - 2l + l^q}{1 - l^q} p' - \frac{1 - 2l^{q-1} + l^q}{1 - l^q},$$

where $p' \stackrel{def}{=} -1/p$. See, also, Veitch & Glendinning [1990] and Veitch [1992] where formulas for regions $\Pi_{r/q}$ are derived directly (without use of the notion complexity level).

In Maistrenko *et al.* [1995a], also, general bifurcation picture for the destruction of any region $\Pi_{r/q}$ is presented. Depending on parameters, this destruction, being a result of border collision bifurcation, can give rise to attracting point cycle $\gamma_{mr/mq}$, as well as to attracting cycle of chaotic intervals $\Gamma_{mr/mq}$, with a general rotation number mr/mq (see Def.(5)), where m can be any positive integer.

3. Regions of Synchronization as a Result of Bifurcation "From Unimodal to Bimodal Map"

The bifurcation consists in the transition from skew tent map $f_{l,p}$ to bimodal (three-segment) map $f_{l,p,b}$. In parameter space (l,p,b) it occurs at $|b| = 1 + 1/p$.

We find that, typically, this type bifurcation results in period adding sequences of attracting point cycles $\gamma_{a_{11}+a_{12}k/a_{21}+a_{22}k}$, $k = 0, 1, ...$, where a_{ij}, $i,j = 1,2$ are some integer numbers which characterize each sequence. All attracting cycles arising due to this bifurcation have the only one point belonging to the third segment $[b - 1/p, 1]$ $(b > 0)$ or to the first segment $[-1, b + 1/p]$ $(b < 0)$.

With use of computer simulation, two these sequences $\gamma_{2+2k_1/5+4k_1}$ and $\gamma_{1+2k_2/3+4k_2}$, $k_1, k_2 = 0, 1, ...$, can be easily seen between tongues $\Pi_{1/2}$ and $\Pi_{1/3}$. For both sequences, an accumulating point (at the bifurcation curve $b = 1 - 1/p$) is the same, and can be found from the condition of gomoclinic bifurcation of the cycle $\gamma_{1/2}$ of skew tent map $f_{l,p}$.

Below, these facts are formulated as a statement.

Let $f_{l,p,b}$, $(l,p,b) \in \Pi$ be a map in the form Eq.(1). For any its trajectory $\eta = \{f^i(x)\}_{i=0}^{i=\infty}$, the following symbolic sequence

$$\xi_0 \xi_1 ... \xi_n ...$$

of five symbols L, M, R, C_1, C_2 can be constructed by the rule:

$$\xi_i = \begin{cases} L, & if \quad f^i(x) \in [-1, b + 1/p), \\ M, & if \quad f^i(x) \in (b + 1/p, b - 1/p), \\ R, & if \quad f^i(x) \in (b - 1/p, 1], \\ C_1, & if \quad f^i(x) = b + 1/p, \\ C_2, & if \quad f^i(x) = b - 1/p, \end{cases} \tag{5}$$

$i = 0, 1, ...$

Statement. *When the parameter point (l,p,b) enters the region Π through the surface $b = 1 + 1/p$, between the regions $\Pi_{1/2}$ and $\Pi_{1/3}$, two sequences of attracting cycles $\gamma_{\rho_{k_1}}$ and $\gamma_{\rho_{k_1}}$ appear with the following generalized rotation numbers and symbolic sequences:*

$$\rho_{k_1} = \frac{2 + 2k_1}{5 + 4k_1}, \qquad (LM)^{2k_1} LM^2 LR..., \quad k_1 = 0, 1, ...$$

$$\rho_{k_2} = \frac{1 + 2k_2}{3 + 4k_2}, \qquad (LM)^{2k_2} MLR.... \quad k_2 = 0, 1, ...$$

Moreover:

i) numbers of attracting cycles γ_{k_1} and γ_{k_2} are finite at any fixed $l \in (0,1)$, nevertheless these numbers tends to infinity with l tends to 0;

ii) regions of the existence and attraction $\Pi_{\rho_{k_1}}$ and $\Pi_{\rho_{k_2}}$ of these cycles $\gamma_{l\rho_{k_1}}$ and $\gamma_{l\rho_{k_2}}$ are bounded by the following curves:

for $\Pi_{\rho_{k_1}}$: $\quad p = -l^{\frac{2k_1+3}{2k_1+2}}$,

$$b_1^{(-)} = \frac{(l^{2k_1+3}p^{2k_1+2}-1)(1-l^2p^2)+(1-l/p)[(lp)^{2k_1}(1+lp^2(1-l))(1-l^2p^2)+(1+lp)(1-(lp)^{2k_1})]}{l[(lp)^{2k_1}(1+p(1+p)+lp^2(1+l))(1-l^2p^2)+(1+p)(1+lp)(1-(lp)^{2k_1})]},$$

$$b_1^{(+)} = \frac{(1-l^{2k_1+3}p^{2k_1+2})(1-l^2p^2)+(1-l/p)[(l^{2k_1+1}p^{2k_1}(1+lp^2)-1)(1-l^2p^2)+l(1+lp)(1-(lp)^{2k_1})]}{l[l^{2k_1+1}p^{2k_1}(1+p(1+p)+lp^2+1)(1-l^2p^2)+l(1+p)(1+lp)(1-(lp)^{2k_1})]}$$

for $\Pi_{\rho_{k_2}}$: $\quad p = -l^{\frac{2k_2+2}{2k_2+1}}$

$$b_2^{(-)} = \frac{(1-l^{2k_2+2}p^{2k_2+1})(1-l^2p^2)+(1-l/p)[((lp)^{2k_2+1}-1)(1-l^2p^2)+l(1+lp)(1-(lp)^{2k_2})]}{l[(1+l^{2k_2}p^{2k_2+1}(1+l))(1-l^2p^2)+l(1+p)(1+lp)(1-(lp)^{2k_2})]},$$

$$b_2^{(+)} = \frac{(l^{2k_2+2}p^{2k_2+1}-1)(1-l^2p^2)+(1-l/p)[l^{2k_2}p^{2k_2+1}(1-l)(1-l^2p^2)+(1+lp)(1-(lp)^{2k_2})]}{l^{2k_2}p^{2k_2+1}(1+l(1+l))(1-l^2p^2)+l(1+p)(1+lp)(1-(lp)^{2k_2})];$$

iii) when parameter point (l,p,b) leaves region Π_{ρ_1} crossing curve $b_1^{(+)}$ or $b_1^{(-)}$, border-collision bifurcation takes place; it results in a cycle of $5+4k_1$ invariant intervals at every of which the map f^{5+4k_1} is skew tent map with the slopes of linear branches equal to $l^{2k_1+3}p^{2k_1+2}$ and $l^{2k_1+2}p^{2k_1+3}$;

iv) when parameter point (l,p,b) leaves region Π_{ρ_2} crossing curve $b_2^{(+)}$ or $b_2^{(-)}$, an inverse saddle-node bifurcation takes place; it results in appearance everywhere dense in [-1,1] trajectories of $f_{l,p,b}$; moreover, every two neighbor regions $\Pi_{\frac{1+2k_2}{3+4k_2}}$ and $\Pi_{\frac{1+2(k_2+1)}{3+4(k_2+1)}}$ are mutually intersecting (multistability phenomenon takes place).

As further, computer simulation shows there are much more such type period adding sequences in the gap between tongues $\Pi_{1/3}$ and $\Pi_{1/4}$, for all of them $a_{12}=3$ and $a_{22}=6$. And so on, it seems to be true, that number of such sequences between $\Pi_{1/q}$ and $\Pi_{1/q+1}$ tends to infinite when $q \to \infty$ (see also Maistrenko *et al.* [1993b]).

References

Gumowski, I. & Mira, C. [1980] *Dynamique Chaotique* (Toulouse. Cepadues Editions).

Leonov, N.N. [1959] "Map on the line on to itself," *Radiophysics*, 2(6), 942-956 (Russian).

Maistrenko, V.L., Maistrenko, Yu.L. & Sushko, I.M. [1992] "Attractors of piecewise linear maps of straight line and plane," *Preprint* #92.33 Inst. Math. Ukr. Acad. Sci. (Russian) p. 55.

Maistrenko, Yu.L., Maistrenko, V.L. & Chua, L.O. [1993] "Cycles of chaotic intervals in a time-delayed Chua's circuits," *Int. J. Bifurcation and Chaos* 3(6), 1557-1572.

Maistrenko, Yu.L., Maistrenko, V.L., Vikul, S.I. & Chua, L.O. [1995a] "Bifurcation of attracting cycles from time-delayed Chua's circuit", *Int.J.Bifurcation and Chaos* 5(3), 653-671.

Maistrenko, Yu.L., Maistrenko & V.L., Vikul, S.I. [1995b] "Bifurcation of attracting cycles of piecewise linear interval maps", *Proc. NDCCS'95* (to appear).

Marcuard, J.C. & Visinescu, E. [1992] "Monotonicity properties of some skew tent maps", *Probabilities et Statistiques*28(1), 1-29.

Melo, W. de & Strien S. van *One-Dimensional Dynamics* (Springer-Verlag, Berlin Heidelberg New York) Chap.2, pp.14-80.

Mira, C. [1987] *Chaotic dynamics* (World Sci., Singapour).

Nusse, H.E. & Yorke J.A. [1995] "Border-collision bifurcations for piecewise smooth one-dimensional maps", *Int.J.Bifurcation and Chaos* 5(1), 189-207.

Veitch, D & Glendinning, P.[1990] "Explicit renormalisation in piecewise linear bimodal maps", *Physica D* 44, 149-167.

Veitch, D. [1992] "Windows of Stability in Control Chaos", *IEEE Transactions on circuits and systems - I:Fundamental theory and application* 39(10), 808-819.

Image Processing using Applied Bifurcation Theory and Knot Theory

X.Marsault*, E.Salmon**, CH.Lamarque**

(*) Ecole d'Architecture de Lyon, laboratoire Aria, 3 rue Maurice Audin, BP 170, F69512 Vaulx en velin Cedex France

(**) ENTPE / DGCB / LGM / CNRS 1652, 1 rue Maurice Audin, BP 170, F69512 Vaulx en velin Cedex France

1. Introduction

Here, we intend to use tools of the bifurcation theory in order to build either new edge detectors, or new methods of segmentation for noisy and textured images. We describe the method associated with a potential (a "catastroph") ; for this general case, we introduce a m-ary encoding, transition steps on local grids, entropies and energies. We show results for examples and give building braids associated with every pixel of an image. We use knot theory to build a kind of topological filter.

2. Description of the method

2.1. Heuristic

Every "catastroph" or "singularity" [1], [2], [3], [4], is associated to a potential $V(X,\Lambda)$ where $X=(x_1,...,x_n)$ denotes the vector of the variables, and $\Lambda=(a_1,...,a_c)$ the vector of the parameters. The main idea is to use approximation of the discrete starting image, build with a given geometrical pattern (a catastroph). The approximation depends on the step h of the local grid which is choosen. So the pattern can change with the deformations of the grid governed by the step(s) : indeed, there exist somme critical steps which define the bifurcations, and determinate the geometrical change. The number of critical values is related to the set of bifurcation of $grad_X V(X,\Lambda)=0$.

2.2. Method for the general case

2.2.1. Calculation of the codimension coefficients

We generally call "image" the values of a map from a sample of $\Re^n$ into a finite subset of $\Re$ (if n is equal to 2, we find again an usual "image" as values on a grid). Let us consider on the space $\Re^n \times \Re^c$ a catastroph whose potential is $V(x_1,...,x_n)$ and the codimension parameters $(a_1,...,a_c)$. The catastroph surface is defined by : $\forall i \in [1,n] \quad \frac{\partial V}{\partial x_i}=0$. In the space $\Re^n$, a discrete local grid G is introduced related to a reference point $(x_1,...,x_n)$; then the n derivative $\frac{\partial V}{\partial x_i}$ are adjusted in the best way in the sense of local mean squares on the grid of steps $(h_1,...,h_n)$: $\underset{(a_1...a_c)}{Min} \sum_{1\le i\le n}\left(\frac{\partial V}{\partial x_i}(\{x_i,h_i\},a_1,..a_c)-I(\{x_i,h_i\})\right)^2$, and the corresponding parameters $(\bar{a}_1,...,\bar{a}_c)$ are computed by solving a linear system.

2.2.2. Definition of a m-ary encoding

For every pixel and its local associated grid, we computed the "least squares" parameters $(\bar{a}_1,...,\bar{a}_c)$. Then, we solve a system of equations. We obtain a definite number m of real solutions. So we are able to split up the space $\Re^n$ that we analyse into m areas.

2.2.3. Computation of images with transition steps

In the previous splitting, the obtained image depends on the steps h of the given grid of $\Re^n$ and its orientation. So,let us fix this orientation, we are able to compute for every pixel some steps $h^*_{i,k}$ corresponding to the transition between any number k and k+1 (k < m) of solutions. So, every transition k->k+1 could provide one or several images of $h_{i,k}$. This number of co-images can be very large ; then clever choices are to be made.

2.2.4. Image of quadratic norm

Fitting the best way the n derivatives on the local grid produces a « quadratic error» that we intend to show. Parameters of this image called « norm » are n, h and the direction d. Global images (Fig 9) obtained with summing on d are relatively invariant with h. However it is possible to find at which h, the norm is minimum (Fig 11).

2.2.5. Computation of the best fitting catastroph

As in 2.2.4, it is finaly possible to compute the same results, but taking into account which catastroph (among the ombilics, or the cuspoids, or both) leads to the minimum norm. Then, we compute (Fig 7, 8) splitted images (3 gray levels for ombilics, and 4 for cuspoids). Experiments show that norms obtained with cuspoids are almost always inferior to those with ombilics ; then a 7-levels-splitting is impossible to obtain in this way.

3. Analysis with the cusp-catastroph

3.1. Introduction

The cusp-catastroph is defined by a universal unfloding of x^4, the catastrophic surface beeing : $S = \{(x,p,q) / x^3 + px + q = 0\}$, and the potential from which it derives : $V(x,p,q) = x^4/4 + px^2/2 + qx$.

3.2. Calculation of the splitting parameters

We define a n-points local grid by choosing a direction (vector v) of the image (plan) which define the variable x of the given potential V. We choose a step h related to x, and a neighbourhood of n pixels (n generally odd). The pixels are sample according to the grid. For each pixel, except those belonging to the boudary of the image, we compute the couple $(\bar{p},\bar{q})$ so that $\sum_{i=1}^{n}(u_i - \frac{\partial V}{\partial x}(x_i))^2$ is minimized, with $(\frac{\partial V}{\partial x} = x^3 + px + q)$. Then, the equation $x^3 + \bar{p}x + \bar{q} = 0$ is solved, that leads to one, two or three real solutions. So, we are able to split the image into three parts. When n=3, *the parameter* $\bar{q}$ *is equal to the mean of level of the pixels on the neighbourhood, and that* $\bar{p}$ *is related to a h-normalized gradient :* $\bar{p}(h) = \frac{u_3 - u_1}{2h} - h^2$ et $\bar{q}(h) = \frac{u_1 + u_2 + u_3}{3}$.

3.3. Variation of h and edge appearance

If the step h of the grid (the same step h is retained for every grid around every pixel) is varied, and if we use the encoding 1, 2 or 3 (the number of solutions of the cubic equation), we can present the edges that appear : see on Fig 2. The results give information about edges in agreement with the expressions of $\bar{p}(h)$ and $\bar{q}(h)$.

3.4. Computation of the co-image or « dual » image

The number of solutions of $x^3 + \bar{p}x + \bar{q} = 0$ depends on the step h. For large values of h (h > 3), 3 solutions are generally obtained. For small values of h (h < 0.01 for example), only one solution is often carried up. So we look for a critical step h* (for every pixel) corresponding to the transition 1 solution -> 3 solutions (namely 2 solutions). At the end of the computation, we are able to build the "co-image" of the gray-levels of the h*.

For each point, the computation of h* is cheap enough using a numerical dichotomic method for example. But an analytical calculation is possible here : using Cardan-formula, for a three-point grid, somme algebra leads to :

$$h^* = \sqrt{\sqrt[3]{\frac{\delta}{2} - \frac{3}{2}\hat{u}^{2/3}\left(\sqrt[3]{\frac{\delta}{2} - \sqrt{\frac{\delta^2}{4} - \hat{u}^2}} - \sqrt[3]{\frac{\delta}{2} + \sqrt{\frac{\delta^2}{4} - \hat{u}^2}}\right)}} \quad (8)$$

where $\delta = u_3 - u_1$ et $\hat{u} = 1/3.(u_1 + u_2 + u_3)$. We keep only the real positive solution in agreement with this expression. The cusp-method leads to an orientated and selective edge detector. We apply the method to the "girl" image. A result is presented in Fig 3.

3.5. Application to a global edge detection

First, we sum the « co-images » related to each direction (defined by an angle θ), and we use a weight coefficient a_θ. This process provides a mean « co-images » according to : $I_h = \sum_\theta a_\theta . I_{h,\theta}$. Another « co-

images » is interesting : for any given direction, h could be varied (between h_{min}=0.0001 and h_{max}=5.0) in order to compute : $M = \sum_{h=h_{min}}^{h=h_{max}} h.I_h$. We provide an example of image M for the « girl » in Fig 4.

Fig 1 : the « girl » image

Fig 2 : number of cusp solutions for h=1.0 and h=1.4

Fig 3 : dual image in NE direction

Fig 4 : global image M for 3x3

Fig 5 : dual ombilic entropy (h=1.0)

Fig 6 : cusp energy for 3x3, h=0.5

Fig 7 : best cuspoid for 7x7, h=1.0

Fig 8 : best ombilic for 5x5, h=1.0

3.6. Definition of energies and entropies

The "best" local deformation of the grid versus a given catastroph, associated with a "strain" (the image) remembers one of the variationnal principals in the field of mecanics of the continuous media, and of the energy of deformation. Using this analogy, we define for any image I (similar to a strain) and its dual image or « norm » image I* (similar to "local deplacements") one global energy $E = I \otimes I^* = \sum_{P \subset \Re^n} I(x_1,...,x_n).I^*(x_1,...,x_n)$, and two global entropies $E_1(I,I^*) = \sum_{P \subset \Re^n} \log(I(x_1,...,x_n)).I^*(x_1,...,x_n)$, $E_2(I^*,I) = \sum_{P \subset \Re^n} \log(I^*(x_1,...,x_n)).I(x_1,...,x_n)$. Locally, around any pixel, we can also define an energy and two entropies. Fig 5, 6 show images obtained from the "girl" in this way, that seem to put high contrast boundaries into light. It is possible to use these images to

search for local minima or maxima, draw local maps of high or low energy or entropies, or build special splittings.

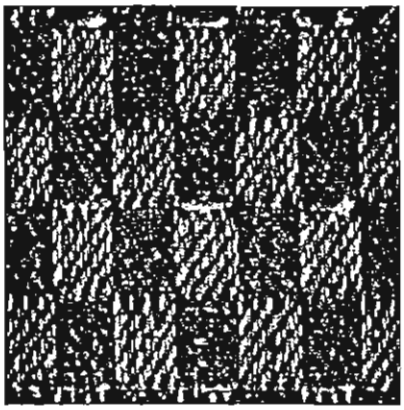

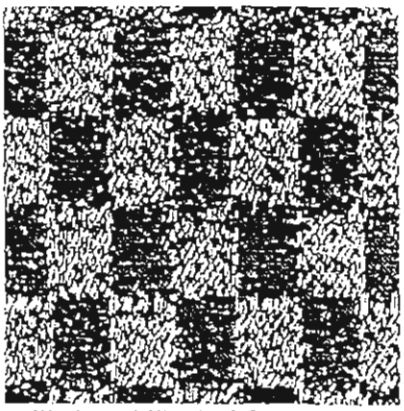

Fig 9 : elliptic ombilic norm at h=1.0 Fig 10 : segmentation of texture by elliptic ombilic (h=0.9)

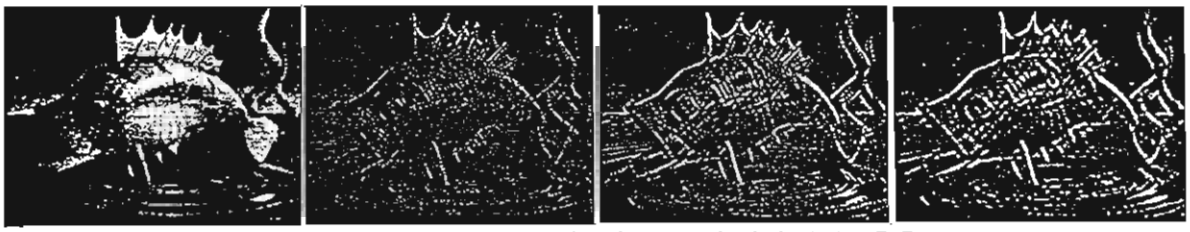

Fig 11 : « fish » images of h where the ombilic norm is minimum, for 3x3, 5x5 et 7x7

4. Braids and knots polynomial filters

A new family of filters for image processing has been developped according to the following procedure : for every pixel of an image, a braid is built using local approximations and arbitrary crossing of strands. Then braids are classified by computing their Jones Polynomial, that are arbitrarily numbered. This procedure leads to image-processing operators which can be useful for edge detection, thresolding, but are sensitive to noise [5].

5. Conclusion

In this paper, we dealt with image processing using "catastroph theory" and braids. We've described the method for general singularities ("catastrophs"). We gave results by using the first "interesting" catastroph (cusp). It seems, which is very interesting in image analysis, that with dual cusp images it is possible to take no account of local contrast : low boundaries appear as bright as reinforced ones, because the technique used leads to calculus of local optimum slopes. With other catastroph, like the elliptic ombilic, we are able to define more complex types of transition, resulting from the multi-dimensional nature of the catastroph ; and we operate new segmentations. Fig 10 show how elliptic ombilic (with $h_x = h_y = 0.9$ in this case) can be used to separate orientation of patterns. Braids and knots polynomial filters lead to noisy results.

Bibliography

[1] V.I. Arnold, *Catastroph Theory*, Springer, 82p, 1984.

[2] V.I. Arnold, Goussein-Zadé, A.Varchenko
Singularités des applications différentiables, Editions de Moscou, Moscou, 1986.

[3] D.P.L. Castrigiano, S.A.Hayes, *Catastrophe Theory*, Addison Wesley, 1993.

[4] R.Thom, *Stabilité structurelle et morphogenèse*, Benjamin Reading, 1972.

[5] E.Salmon, *Application de la théorie des noeuds à l'analyse d'images*, Mémoire de Diplôme d'Etudes Approfondies, Spécialité Image, université de Saint-Etienne, 1995.

A Numerical Illustration of the Quasiperiodic Route to Chaos in a Model for Fluid-Structure Interaction

J.P. Meijaard,

Laboratory for Engineering Mechanics, Delft University of Technology,
Mekelweg 2, NL-2628 CD Delft, The Netherlands.

Abstract: Bifurcations of quasiperiodic solutions of a string excited by flow-induced forces and possible transitions to chaotic motion are studied numerically by calculating Liapunov exponents. It is found that quasiperiodic motion with three independent frequencies may exist. Multiple attractors can exist simultaneously.

1. Introduction

Several transition routes from regular motion to chaotic motion in dynamical systems are known, of which the most important ones are the route via an infinite sequence of period-doubling bifurcations, the intermittency route, and the quasiperiodic route. In low-dimensional mechanical dynamical systems, the usual route is via period doublings, whereas the route via successive Hopf bifurcations and quasiperiodic motion seems to be more relevant to fluid mechanics.

The quasiperiodic route for the transition from laminar to turbulent flow was first proposed by Landau [1944]. He imagined that an infinite sequence of Hopf bifurcations results in the development from stationary motion, via periodic motion and quasiperiodic motion with an increasing number of independent frequencies, to turbulence. This mechanism was replaced by the Ruelle-Takens-Newhouse theory [Ruelle & Takens 1971] [Newhouse *et al.* 1978], which shows that one can obtain, by a small perturbation, so-called strange attractors in the neighbourhood of quasiperiodic motion with three or more independent frequencies, so these quasiperiodic motions are not generic. However, quasiperiodic motions with three or more independent frequencies have sometimes been measured in experiments, which means that these motions may occur for a set of parameter values with positive measure. Indeed, near a bifurcation of a two-dimensional invariant torus, a stable three-dimensional torus may exist if some Diophantine conditions are met, similar to the conditions in the KAM-theory for Hamiltonian systems [Chenciner & Iooss 1979] [Sell 1979]. The quasiperiodic route can now be described as follows. As some parameter is increased, a stationary solution loses its stability in an ordinary Hopf bifurcation, after which a stable periodic solution originates. The periodic solution becomes unstable at a Neimark-Hopf bifurcation, after which an attracting invariant two-dimensional torus originates, on which periodic or quasiperiodic motion is observed. The torus experiences a bifurcation, after which we have periodic, quasiperiodic and chaotic motion mixed in an intricate way.

As no physical model whatsoever was given in the original paper by Ruelle and Takens, and the quasiperiodic route is rarely observed in low-dimensional models, this paper proposes a system of two coupled partial differential equations with one space dimension, which may be regarded as a model for a string that is excited by a transverse fluid flow. Its behaviour has a rich structure, which may serve as an illustration for several bifurcations and routes to chaos. A preliminary analysis of this system by numerical means is given.

2. System Description

The proposed system models a string with a circular cross-section in the flow of a liquid in a direction perpendicular to the string, where the string can make lateral oscillations perpendicular to the flow. The forces induced by the flow are taken into account by means of a wake oscillator model, inspired by the ones proposed by Hartlen and Currie [1970] and others. The model consists of the one-dimensional wave equation coupled to a distributed Rayleigh oscillator with some additional damping and stiffness terms. The scaled equations are

$$\begin{gathered} \ddot{u} - u'' + c_1\dot{u} - c_2\dot{u}'' - \varepsilon(\dot{u} - \dot{v}) + (\dot{u} - \dot{v})^3 + k_1(u - v) - k_2(u'' - v'') = 0, \\ m\ddot{v} - c_4\dot{v}'' + \varepsilon(\dot{u} - \dot{v}) - (\dot{u} - \dot{v})^3 - k_1(u - v) + k_2(u'' - v'') = 0, \\ 0 \le x \le 1, \quad u(0) = u(1) = v(0) = v(1) = 0. \end{gathered} \tag{1}$$

Here, u and v are the lateral displacements of the string and the wake oscillator, dots and primes denote derivatives with respect to the time t and the spatial dimension x, m is the relative mass per unit of length of the wake oscillator, and c_1, c_2, c_4, k_1, and k_2 are positive damping and coupling stiffness coefficients. The parameter ε measures the excitation, which is considered as variable in this model and may be related to the Reynolds number. Some of the terms are only introduced to make the system well-behaved in the high-frequency range, especially the terms involving c_2, c_4 and k_2, and hence small values for these coefficients will be taken. As we are mainly interested in an illustration of phenomena which are typical for a large class of systems, the precise form of the equations is not so important and one may substitute equations which describe a given system more accurately. In calculations, we shall take as values for the parameters, $c_1 = 0.1$, $c_2 = 0.001$, $k_1 = 2.0$, $k_2 = 0.01$, $m = 0.5$, $c_4 = 0.001$, while ε is variable.

3. Analysis

The equations have a left-right symmetry ($x \mapsto (1 - x)$) and an up-down symmetry ($(u, v) \mapsto (-u, -v)$), and there is always the trivial solution $u \equiv 0, v \equiv 0$.

The stability of the trivial solution is investigated by analysing the linearized equations. These linearized equations allow a separation of variables for their solution. The eigenfunctions of the linearized equations, which are sine functions, are used to make a

spectral expansion of the equations. If n pairs of eigenfunctions are kept, the expressions $u = \sum_{i=1}^{n} u_i(t)\sin(i\pi x)$, $v = \sum_{i=1}^{n} v_i(t)\sin(i\pi x)$ are substituted in the equations, and only the contributions of the non-linear terms in the kept eigenfunctions are retained, the discretized equations become

$$\begin{aligned} \ddot{u}_i + (c_1 + i^2\pi^2 c_2 - \varepsilon)\dot{u}_i + \varepsilon\dot{v}_i + (i^2\pi^2 + k_1 + i^2\pi^2 k_2)u_i - (k_1 + i^2\pi^2 k_2)v_i + N_i = 0, \\ m\ddot{v}_i + \varepsilon\dot{u}_i + (i^2\pi^2 c_4 - \varepsilon)\dot{v}_i - (k_1 + i^2\pi^2 k_2)u_i + (k_1 + i^2\pi^2 k_2)v_i - N_i = 0, \end{aligned} \tag{2}$$

where $1 \leq i \leq n$ and N_i represent the contributions of the non-linear term $(\dot{u} - \dot{v})^3$. The linearized equations are obtained by dropping the N_i. In the sequel, we shall take $n = 6$, yielding a system of 24 first-order differential equations.

For each value of i, the two critical values for the parameter can be found, at which Hopf bifurcations occur. These critical values are given in Table 1. The first Hopf bifurcation for $i = 1$ is supercritical, because the non-linear terms are dissipative.

Table 1: Hopf bifurcation values

i	ε_{Hi1}	ε_{Hi2}
1	0.02790 09477 76516	0.05132 23077 46019
2	0.04571 87409 71100	0.11018 50251 51927
3	0.09532 40022 55210	0.16627 18591 71225
4	0.16563 68027 77111	0.23598 32781 69455
5	0.25621 26156 23986	0.32294 92813 04069
6	0.36697 43200 24512	0.42818 24440 12335

One could expect that, due to the many Hopf bifurcations of the trivial solutions, the periodic solution arising from the first Hopf bifurcation would become unstable very soon for increasing values of the parameter ε. However, this is not the case; the periodic solution remains stable for a considerable range of parameter values, and other, initially unstable, periodic solutions may become stable. From an approximate analysis by the harmonic balance, this will become clear. If there is a dominant eigenfunction i, we have approximately for the amplitude a of $u_i - v_i$, $a^2 = 4(\varepsilon - \varepsilon_{Hi1})/3$. This gives an extra positive damping to the other modes of about $3a^2/2 = 2(\varepsilon - \varepsilon_{Hi1})$, so the eigenfunction j is stable when $(\varepsilon - \varepsilon_{Hj1}) < 2(\varepsilon - \varepsilon_{Hi1})$, which condition is always fulfilled if $j > i$. The periodic solution can only become unstable when the shape departs from being nearly sinusoidal if ε reaches a value of the order of one. The picture that there are a number of non-linear oscillators with weak coupling is not valid for this system.

For an approximation with $n = 6$, a Neimark-Hopf bifurcation occurs at the parameter value $\varepsilon = 0.58963\,97506$, after which an invariant two-dimensional torus originates with predominantly quasiperiodic behaviour with two independent frequencies. The behaviour of this torus for increasing values of the parameter is monitored by calculating the Liapunov exponents, for which the algorithm given by Benettin *et al.* [1980] is used. It appears that some characteristic exponents come in pairs, similar to complex conjugate

characteristic multipliers for periodic solutions. The invariant torus becomes unstable at $\varepsilon = 0.60156$, after which we have a quasiperiodic motion with three independent frequencies, that is, there is an invariant three-dimensional torus. As in experimental studies, it is often difficult to distinguish between periodic motion with a long period, quasiperiodic motion and chaotic motion. We assume that a Liapunov exponent is zero if it approaches zero in a more or less linear way if the time interval of simulation is increased. If we increase ε further, the motion returns to quasiperiodic with two independent frequencies at about $\varepsilon = 0.635$. Finally, the motion jumps to a periodic left-right antimetric solution at $\varepsilon = 0.670$, due to a kind of fold of the two-dimensional torus.

4. Conclusions

We have observed the development of quasiperiodic solutions in a discretization by spectral expansion of a continuous model system. The trivial solution may undergo an unlimited number of Hopf bifurcations, resulting in many coexisting attractors. There is a strong coupling between modes. It appeared that quasiperiodic motions on a three-dimensional torus are possible. It remains unclear whether there are interspersed regions of chaotic motions, but these chaotic regions must be very small. The attractors may suddenly disappear by a collision with another periodic or quasiperiodic attractor.

As the approximation with $n = 6$ is still crude, one can question if there is a close connection between the discretized and the full system. For a further analysis, more powerful techniques than simple simulation are needed, such as the direct computation of invariant tori and more ingenious ways of calculating Liapunov exponents.

References

Benettin, G., Galgani, L., Giorgilli, A. & Strelcyn, J.-M. [1980] "Lyapunov characteristic exponents for smooth dynamical systems and for Hamiltonian systems: a method for computing all of them." *Meccanica* **15**, 9–30.

Chenciner, A. & Iooss, G. [1979] "Bifurcations de tores invariants," *Archive for Rational Mechanics and Analysis* 69, 109–198.

Hartlen, R.T. & Currie, I.G. [1970] "Lift-oscillator model of vortex-induced vibration," *Proceedings of the ASCE. Journal of the Engineering Mechanics Division* **96**, 577–591.

Landau, L.D. [1944] "On the problem of turbulence," *Comptes Rendus de l'Académie des Sciences URSS* **44**, 311.

Newhouse, S., Ruelle, D. & Takens, F. [1978] "Occurrence of strange axiom A attractors near quasi periodic flows on T^m, $m \geq 3$." *Communications in Mathematical Physics* 64, 35–40.

Ruelle, D. & Takens, F. [1971] "On the nature of turbulence," *Communications in Mathematical Physics* 20, 167–192, 23, 343–344.

Sell, G.R. [1979] "Bifurcation of higher dimensional tori." *Archive for Rational Mechanics and Analysis* 69, 199–230.

MATCHING OF LOCAL EXPANSION AND A CONSTRUCTION OF HOMOCLINIC TRAJECTORIES

Yu.V.Mikhlin
Kharkov Polytechnic University, Kharkov 310002 Ukraine

Abstract: A similar approach is proposed here for the construction of the homoclinic trajectories. Quasi-Pade'approximants,potentiality and convergence conditions are utilized in the problem.

1. Introduction

The homoclinic and heteroclinic orbits of nonlinear dynamical systems with spaces of dimensions equal two or three are analytically approximated by constructing quasi-Pade' approximants (QPA) containing exponential polynomials and periodical functions. Potentiality and convergence conditions are performed to eliminate initial amplitude values.

2. Convergence Condition

Assume that there are local expansions obtained at small and large values of a parameter σ (for example,the parameter is an amplitude value of the periodic solution) [Mikhlin,1995]:

$$p_i^{(1)}=\sum_{j=0}^{\infty}\alpha_j^{(i)}\sigma^j, \qquad p_i^{(2)}=\sum_{j=0}^{\infty}\beta_j^{(i)}\sigma^{-j}. \tag{1}$$

Consider fractional rational diagonal two-points Pade' approximants (PA) [Baker & Graves-Morris,1981]:

$$p_s^{(i)}=\frac{\sum_{j=0}^{s}a_j^{(i)}\sigma^j}{\sum_{j=0}^{s}b_j^{(i)}\sigma^j}=\frac{\sum_{j=0}^{s}a_j^{(i)}\sigma^{j-s}}{\sum_{j=0}^{s}b_j^{(i)}\sigma^{j-s}} \quad (s=1,2,3,\ldots;i=2,3,\ldots n) \tag{2}$$

Compare the expressions (2) with expansions (1).By preserving only the terms with an order of $\sigma^r(-s\le r\le s)$, n-1 systems of

2(s+1) linear algebraic eqs. will be obtained for determination of $a_j^{(i)}$, $b_j^{(i)}$. Since the determinants of these systems $\Delta^{(i)}$ are generally not equal to zero, the systems have a single exact trivial solution. Select a PA corresponding to the preserved terms in (1) having nonzero coefficients $a_j^{(i)}, b_j^{(i)}$. It can also be assumed that $b^{(i)} = 1$. Now the systems of algebraic eqs. become overdetermined. All unknown coefficients are determined from (2s+1) eqs. while the "error" of this approximate solution can be obtained by substitution of all coefficients in the remaining eq. Obviously, the "error" is determined by the value of $\Delta_s^{(i)}$ since at $\Delta_s^{(i)} = 0$ nonzero solutions and consequently exact PA will be obtained. Hence the following is a necessary condition for convergence of the PA (2), at $s \to \infty$, to fractional rational functions $P_\infty^{(i)}$ [2]:

$$\lim_{s\to\infty} \Delta_s^{(i)} = 0 \quad (i = 2,3,\ldots,n) \qquad (3)$$

It is possible to generalize the condition (3) to quasi-Pade' approximants (QPA).

3. Potentiality Condition

A finite-dimensional system on the closed homoclinic or heteroclinic trajectories behaves like a conservative one having a single degree of freedom: $\ddot{x} + \Pi(x) = 0$. Denoting a line integral along a closed contour by $\oint$, one write a potentiality condition for a system of a general form, $\ddot{x} + f(x) = 0$:

$$\oint f(x)\, dx = 0, \quad \text{or} \quad \oint f(x)\, \dot{x}\, dt = 0 \qquad (4)$$

4. Standing Waves Equation

The equation considered here is obtained in a problem of the analysis axisymmetric, spatially localized standing waves with periodic time dependence (breathers) [Emaci et al., 1996]:

$$y''(x) + (1/x)\, y'(x) - y(x) + y^3(x) = 0, \qquad (5)$$
$$y'(0) = 0; \quad \lim_{x\to\infty} y(x) = 0$$

Since the sought solutions are expected to be analytic functions, they can be expressed in Taylor series about x=0:

$$y(x) = A + A_2x^2 + A_4x^4 + A_6x^6 + \ldots, \qquad (6)$$

where $A_2 = (1/4)\,A\,(1-A^2)$; $A_4 = (1/64)\,A\,(1-A^2)\,(1-3A^2)$; $A_6 = (1/2304)\,A\,(1-A^2)\,(1-3A^2)$, ...

On utilize the potentiality condition (4). Substituting the expansion (6) to (4) and integrating, we construct then the diagonal PA corresponding to the obtained expansion:

$$P^{(4)} = \frac{\alpha_2x^2 + \alpha_4x^4}{1 + \beta_2x^2 + \beta_4x^4},$$

where its coefficients are computed in terms of A. The condition (4) must be realized for x being changeable from zero to infinity. Substituting the limits of integration and taking into account other terms of equation ($y \to 0$ if $x \to \infty$ and $y \to A$ if $x \to 0$), on obtain an algebraic eq. for computing a value of A. The value $A \approx \pm 2.23$ is given by not difficult calculation. The initial value corresponding to the decaying solution was numerically estimated as $A^{num} \approx \pm 2.206$ [Emaci et al., 1996].

The sought solution can be expressed as following local expansion about $x \to \infty$:

$$y = e^{-x}\,x^{-(1/2)}(B + B_1x^{-1} + B_2x^{-2} + \ldots) + e^{-3x}x^{-(3/2)}(C_0 + C_1x^{-1} + \ldots) + O(e^{-3x}), \qquad (7)$$

where B is an arbitrary constant; $B_1 = -(1/8)\,B$, $B_2 = (9/128)\,B$, $C_0 = (1/8)\,B^3$, $C_1 = -(0/64)\,B^3$ etc. The simplest QPA which is described the closed homoclinic trajectories, has the form:

$$P = e^{-z^2}\frac{\alpha_1z^{-1}\; z^{-3}(\alpha_3 + e^{-z^2}\gamma_0)}{1 + \beta_2z^{-2} + \beta_3z^{-3} + e^{-z^2}\delta_0}.$$

To compare QPA with local expansions (6),(7) and using the convergence condition (3), we obtain an algebraic eq. for computing value of B.

5. Nonautonomous Duffing Equation

The same method makes possible to construct separatrix of the nonautonomous Duffing eq.:

$$y'' - y + y^3 = f\cos\omega t$$

The solution can be presented for small values of f as local expansions in the vicinity of zero and infinity:

$$y = a_0 + a_2 t^2 + a_4 t^4 + \ldots (t \to 0)$$
$$y = b_0 e^{-t} + b_1 e^{-3t} + c_0 \cos \omega t + \ldots (t \to \infty) \qquad (8)$$

where a_0, b_0 are arbitrary constants.

The first of the expansions is used in the condition (4). Integrating from zero to infinity (with the help of the reorganization to the PA) on obtain a value a_0. Note that we obtain two values a_0 corresponding to two separatrix (separatrix splitting). Both local expansions (8) can be used for constructing analytical components of the separatrix of the form:

$$QPA = \frac{\alpha_0 e^{-t} + \alpha_1 \cos \omega t + \alpha_2 e^{-3t}}{1 + \beta_1 e^{-2t} + \beta_2 e^{-t} \cos 2\omega t} \qquad (9)$$

The corresponding convergence condition permits to calculate value of b_0. Numerical check computations show good agreement.

6.Lorenz Equation

Similar calculations allow to construct closed homoclinic trajectories of the Lorenz system. The orbits exist in space of dimensions equal three. We take into account that the motion arises on the two-dimension espace. Simplified calculations give us a bifurcational value of the parameter ρ near 15 (other parameters are fixed as in the original Lorenz publication). It is well known that the correct value is near 14, but a precision of the calculations may be excited.

7.References

Baker,G.A. & Graves-Morris P. [1981] *Pade' Approximants* (Addison-Wesley, London).

Emaci,E. & Vakakis,A.F. & Andrianov,I.V. & Mikhlin,Yu.V. *J.of Sound and Vibration* (is submitted).

Mikhlin,Yu.V.[1995] Matching of local expansions in the theory of non-linear vibrations. *J.of Sound and Vibration* 182(4), 577-588.

A NON-LINEAR SHALLOW ARCH THEORY FOR LATERALLY RESTRAINED CONCRETE SLABS

Author: Dr. G. Müller
Lecturer, Civil Eng. Dept., Queen's University Belfast
Stranmillis Road, Belfast BT7 1NN, UK

Abstract: The load bearing capacity of laterally restrained concrete slabs is greatly enhanced by the formation of an internal arch. The arch is very shallow, so that non-linear deformation characteristics have to be taken into account. In this paper, a theory for shallow compression-only arches under uniform loading conditions is developed. The previously undefined arch geometry is determined using complementary energy principles. A comparison with linear theory shows that non-linear behavior has to be taken into account for shallow arches of this type.

1. Introduction

In laterally restrained concrete slabs, a shallow compression arch develops when a load is applied. The arching enhances the load bearing capacity of the slab considerably, see e.g. Herzog [1976]. This effect is known as Compressive Membrane Action and shown in Fig. 1. The compression arch is very shallow, so that its load / deflection curve becomes nonlinear.

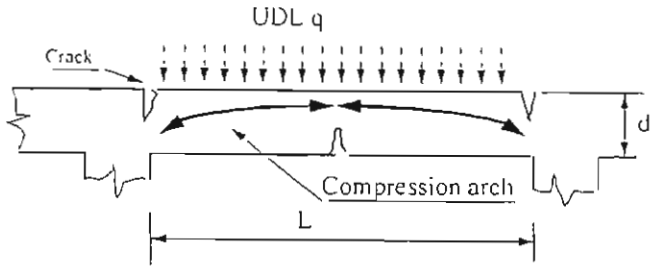

Fig. 1: Concrete beam with compression arch

Classical theory for shallow arches requires bending stiffness for the arch, an assumption which can not be satisfied in concrete since the concrete is assumed to have no tensile resistance. For an arch forming inside a non-tensile resistant material like concrete it will be the compression force that dominates the behavior of the arch. In the following, a theory for a nonlinear compression-only arch will be developed and compared with simple linear theory. The arch will then be used to assess the effect of CMA on the possible loading.

2. Linear analysis

A simple three-hinged arch subjected toa uniformly distributed load (UDL) is shown in Fig. 2. Moments about point a give the thrust N of the arch as $N = qL^2/8h$. The load / deflection curve is linear. For a any given UDL q however the lever arm h is decreased by the deflection, so that the actual load the arch can carry will be less than the assumed load. For very shallow arches where the deflection under working loads can amount to a substantial fraction of the rise, a nonlinear analysis seems necessary.

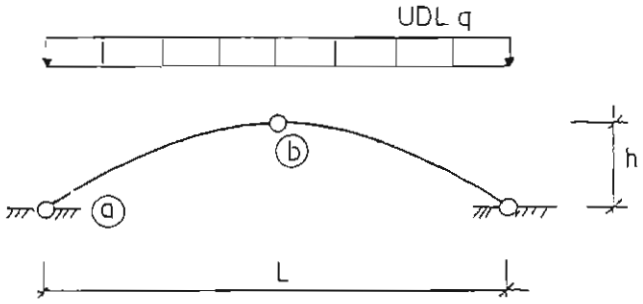

Fig. 2: Three hinged arch

3. Non-linear analysis

For a nonlinear analysis a parabolic arch as shown in Fig. 3 is considered. The parabola is given as y = f(x).

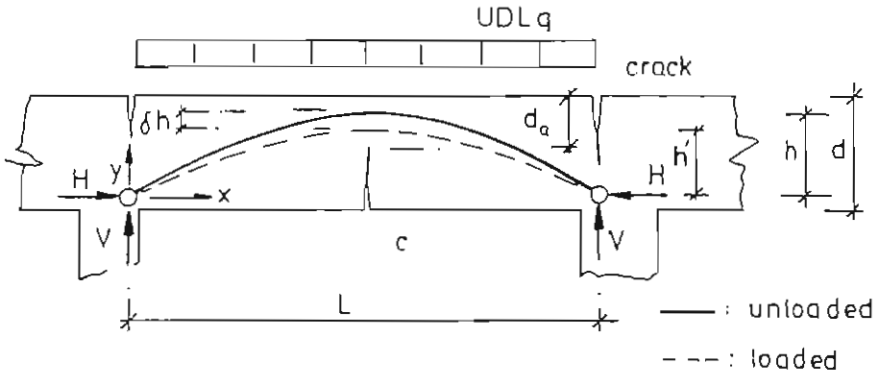

Fig. 3: Compression arch

The loaded deformed shape of the parabola is given as a function of the centre deflection δh with:

$$w_c = (1 - \delta h / h) \text{ and } w(x) = (1 - w_c) \cdot y(x) \tag{1}$$

The normal force N is assumed to be constant throughout the arch. For the analysis of an initially straight membrane, see Kerr et al. (1990), and the strain displacement relation becomes:

$$\varepsilon_{xx}(x) = u'(x) + \frac{1}{2} w'^2(x) \tag{2}$$

However, it must be noted that for the equation the derivative w' is a measure of change of length W' of the deflected curve. In order to use a change of length, the deflected length needs to be subtracted from the original length:

$$W'^2(x) = y'^2(x) - w'^2(x) \tag{3}$$

In order to calculate N for a given deflection w_c equation (2) can be rearranged.

$$u'(x) = \frac{N}{Ed} - \frac{1}{2} W'^2(x) \tag{4}$$

The deflection w_c for each load q is assumed to be a constant. In these derivations, the deformations u(x) are assumed to be very small. Re-arranging and following Marguerre (1938), this leads to a differential equation:

$$\left[Ed \cdot (u' + \frac{1}{2} W'^2) \cdot w' \right]' = -q \tag{5}$$

$$0 \le x \le L$$

$$\left[Ed \cdot (u' + \frac{1}{2} W'^2) \right]' = 0 \tag{6}$$

With the appropriate boundary conditions, and regarding that N can be considered a constant, integration now becomes possible with

$$\int_0^L u'(x)dx = 0 \text{, so that } N = \frac{8}{3} \frac{h^2 Ed}{L^2} \cdot (2 w_c - w_c^2) \tag{7}$$

With this expression for N, the load q for each deflection w_c can be determined easily: Note that for this consideration it is the change of slope of the deflected curve w'' which determines the equilibrium at each individual point.

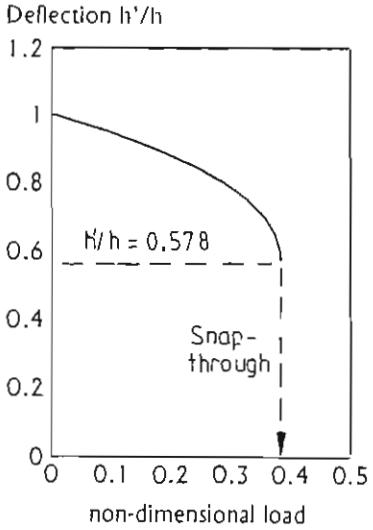

Fig. 4: Load/deflection curve

$$q = -(N \cdot w')' = -N \cdot w''$$
$$= -N \cdot (1 - w_c) \cdot \left(-\frac{8h}{L^2} \right) \tag{8}$$

Combining equations (7) and (8) yields:

$$q = E \cdot d \cdot \frac{64h^3}{L^4} \cdot (1 - w_c) \cdot (2 w_c - w_c^2) \tag{9}$$

Fig. 4 shows the load/deflection curve. It can be seen that for w_c=0.422 snap-through and failure occurs. Elastic buckling can not occur. This seems reasonable as the 'arch' that forms inside a concrete beam is restrained by the surrounding material.

4. Geometry of internal arch

Inside a laterally restrained concrete beam of depth d a variety of trusses can develop, whereby the depth of the arch d_a and the rise h of the arch are related, as $h = d - d_a$. This is illustrated in Fig. 4. The rise h of the internal arch can vary from 0 to d/2. In order to find the most probable rise and area of an arch, the following considerations were made:

(1) The arch is non-linear, so that a complimentary energy approach should be used.
(2) Snap-through failure occurs at w_c = 0.422, so that this point will be used for comparison.
(3) The most probable arch geometry is the one that leads to the maximum energy required to achieve this deflection, as this geometry represents the stiffest arch that can form within the concrete beam. The external energy for a given arch under a UDL

q for a centre deflection of $\delta h = w_c$ is shown in Fig.5. It can be seen that the arch reaches a maximum for $d_a = 0.2d$ and $h = 0.8d$.

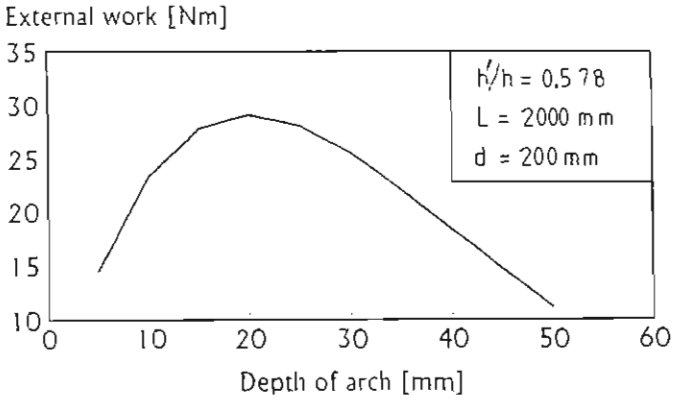

Fig. 5: External work plot for determination of arch geometry

5. Application

A simple compression arch as shown in Fig. 1 in a concrete beam of 100mm thickness and 2m span is considered. Assuming no tensile resistance of the concrete, the thickness of the arch can be estimated as 50mm. Both supports are assumed to be rigid. With equation the maximum load can easily be determined:

$$q_{max} = 30000 \cdot 20 \cdot \frac{64 \cdot 80^3}{3 \cdot 2000^4}(1-.422) \cdot (2 \cdot 0.422 - 0.422^2) = 0.157\, N/mm^2$$

This corresponds to a load of 96 kN/m^2. The in-plane force N can be determined as 1645 kN/m. The resulting concrete stress becomes 82.5 N/mm^2. This is within the range of high strength concrete stresses. In comparison, for the same in-plane force the linear arch would result in a maximum load of 0.273 N/mm^2, ie it would overestimate the ultimate load by 70%.

6. Conclusions

A non-linear shallow arch theory for laterally restrained concrete slabs under uniformly distributed loads was developed. The geometry of the previously undetermined arch was found using a complementary energy approach. A comparison with linear theory showed that linear theory overestimates possible loadings and that, failure can occur through snap-through instability of the arch.

References

Herzog M. [1976] " Die Membranwirkung in Stahlbetonplatten nach Versuchen" (Membrane action in reinforced concrete plates according to tests), *Beton-und Stahlbetonbau*, Vol. 11, pp270-275

Kerr A., Coffin D.W. [1990] "On membrane and plate problems for which the linear theories are not admissible, *Transact. ASME Journal of Applied Mechanics*, Vol. 57, pp 128-133

Marguerre K. [1938] "Über die Behandlung von Stabilitätsproblemen mt Hilfe der energetischen Methode" (on the analysis of stability problems with the aid of energy principles), *Zeitschr. angew. Math. Mech.*, Vol. 18, pp 57-73

Group actions as stroboscopic maps of ordinary differential equations

Andrzej Okniński
Politechnika Świętokrzyska, Physics Division,
Al. 1000-lecia PP 7, 25-314 Kielce, Poland

Abstract

Recently, a method to study noninvertible discrete-time dynamical systems by associating them with group actions was proposed. In the present work possibility of application of this method to systems of ordinary differential equations is studied. Invertible group actions on a group are considered as possible candidates for stroboscopic maps of ordinary differential equations. In this work maps on $SU(2)$ group are studied. It is shown that after proper choice of the initial conditions the map describes within arbitrary accuracy a flow on a sphere generating a stroboscopic map of Landau-Lifshitz type equation.

1 Introduction

Let us consider a dynamical system given by a set of ordinary differential equations (ODE)

$$\dot{\boldsymbol{x}} = f[\boldsymbol{x}(t), t] \tag{1}$$

where $\boldsymbol{x} = [x_1, x_2, \ldots, x_n]$, $f = [f_1, f_2, \ldots, f_n]$ and dot indicates differentiation with respect to time.
Let $\boldsymbol{x}(t)$ be a solution to Eq.(1). Then the map

$$S : x(t) \longmapsto \boldsymbol{x}(t+T) \tag{2}$$

is a stroboscopic map of strobe time T.

Stroboscopic maps are standard tools to solve differential equations. The archetype of numerical methods based on this concept is the Euler method. Let us consider for simplicity the system (1) for $n = 1$

$$\frac{dx}{dt} = f[x(t), t], \quad x(t_0) = x_0 \tag{3}$$

Let us consider time instants $t_0, t_1 = t_0 + T, t_2 = T_1 + T, \ldots$ and introduce shorthand notation $x_0 = x(t_0), x_1 = x(t_1), x_2 = x(t_2), \ldots$. In the Euler method the derivative is approximated by a finite difference

$$\frac{dx}{dt}(t_k) = \lim_{T \to 0} \frac{x(t_k + T) - x(t_k)}{T} \cong \frac{x(t_k + T) - x(t_k)}{T} \tag{4}$$

and hence the original ODE, Eq.(3), is substituted by a stroboscopic map (a difference equation)

$$x_{k+1} = x_k + T f(x_k, t_k) \tag{5}$$

2 Group dynamical systems

Let us consider a dynamical system defined by the following iterative scheme

$$G_{N+1} = \varphi(G_N, \ldots) \tag{6}$$

where $G_N \in \mathcal{G}$, $\mathcal{G}$ being a Lie group. Let $\mathcal{G}$ be a simple Lie group and $\boldsymbol{g}$ its Lie algebra. G_N's can be parameterized in exponential form

$$G_N = exp\left(\sum_{k=1}^{n} I^k c_N^k\right) \tag{7}$$

where real parameters $c_N^1, \ldots, c_N^n$ are local coordinates in $\boldsymbol{g}$ [Barut, 1977].

Let us consider Eqs. (6), (7). Substituting Eq. (7) into Eq. (6) we get a discrete-time dynamical system in parameter space [Okniński, 1992]

$$c_{N+1}^j = F^j(c_N^1, \ldots c_N^n), \quad j = 1, \ldots, n \tag{8}$$

where F^j's are continuous functions [Pontryagin, 1966].

3 Dynamics on the sphere

Let us consider invertible discrete-time dynamical system for $\mathcal{G} = SU(2)$

$$R_{N+1} = Q_1 R_N Q_2 R_{N-1} Q_2^{-1} R_N^{-1} Q_1^{-1} \tag{9}$$

i.e. $\varphi = Q_1 R_N Q_2 R_{N-1} Q_2^{-1} R_N^{-1} Q_1^{-1}$ in Eq.(6).
Let ω_N, $q_{1,2}$ be unit vectors and $R_N, Q_{1,2}$ are defined as

$$R_N = exp(i\frac{\chi_N}{2}\ \sigma \cdot \omega_N) \tag{10}$$

$$Q_{1,2} = exp(i\frac{\alpha_{1,2}}{2}\ \sigma \cdot q_{1,2}) \tag{11}$$

where $i^2 = -1$, and $\sigma = [\sigma^1, \sigma^2, \sigma^3]$ is the pseudo vector with the Pauli matrices as components [Okniński , 1994]. Then Eq.(9) induces dynamics of vectors ω_N on unit sphere.

We shall consider Eq.(9) in the case $Q_1 = Q_2 = Q$, $Q \neq 1$

$$R_{N+1} = Q R_N Q R_{N-1} Q^{-1} R_N^{-1} Q^{-1} \tag{12}$$

where $Q = exp(i\frac{\alpha}{2}\ \sigma \cdot q)$.

We note that Eq.(12) can be reduced to two simpler equations

$$\begin{array}{rcl} S_{N+1} & = & Q S_N Q_{N-1} \\ R_{N+1} & = & S_N R_{N-1} S_N^{-1} \end{array} \tag{13}$$

$S_N \equiv Q R_N Q R_{N-1}$ and can be parameterized as $S_N = exp(i\frac{\beta}{2}\ \sigma \cdot s_N)$.

4 Differential equation

Let us consider Eq.(13). It can be written in equivalent form

$$\begin{array}{rcl} S_{N+1} S_N^{-1} & = & Q S_N Q_{-1} S_N^{-1} \\ R_{N+1} R_{N-1}^{-1} & = & S_N R_{N-1} S_N^{-1} R_{N-1}^{-1} \end{array} \tag{14}$$

Let $\beta = \chi_0, \alpha = \mu\chi_0$. We assume that $\mid \chi_0 \mid \ll 1$, $\mu = O(1)$.

In what follows we shall use two operator identities

$$\begin{array}{l} e^{i\epsilon X} e^{-i\epsilon Y} = 1 + i\epsilon(X - Y) + O(\epsilon^2) \\ e^{i\epsilon X} e^{i\epsilon Y} e^{-i\epsilon X} e^{-i\epsilon Y} = 1 + \epsilon^2 [X, Y] + O(\epsilon^3) \end{array} \tag{15}$$

where $[X,Y] \equiv XY - YX$. Applying identities (15) to Eq.(14) we get

$$\begin{array}{rcl} \frac{s_{N+1}-s_N}{\chi_0} & = & \mu\, s_N \times q \\ \frac{\omega_{N+1}-\omega_{N-1}}{\chi_0} & = & \omega_{N-1} \times s_N \end{array} \tag{16}$$

For $\chi_0 \to 0$ the following set of ODEs is obtained

$$\begin{array}{rcl} \dot{s} & = & 2\mu\, s \times q \\ \dot{\omega} & = & \omega \times s \end{array} \tag{17}$$

which is analogous to the Landau-Lifshitz equation [Landau & Lifshitz, 1935; Brown, 1963]

$$\dot{M} = M \times H_{eff} \tag{18}$$

describing evolution of magnetization vector M in effective magnetic field H_{eff}. Equations (17), (18) become equivalent for $M = \omega, \quad H_{eff} = s$. It follows from the first of Eqs.(17) that the effective magnetic field rotates with angular velocity 2μ.

Finally, let us note that Eq.(12) (or equivalent Eq.(14)) approximates Eq.(17) within the Euler method, c.f. Eq.(4).

References

[1] Barut, A.O. & Rączka, R. [1977] *Theory of Group Representations and Applications* (PWN - Polish Scientific Publishers, Warszawa).

[2] Brown Jr., W.F. [1963] *Micromagnetics* (John Wiley and Sons, New York-London).

[3] Landau, L. & Lifshitz, E. [1935] *Phys. Z. Sowietjunion* **8**, 153.

[4] Okniński, A. [1992] "Groups and dynamical systems. Discrete-time dynamics on the E(2) group", *Physica* **D55**, 358-367.

[5] Okniński, A. [1994] "Three dimensional rotations and discrete-time dynamical systems: discrete symmetries in chaos-order transitions", *Int. J. Bifurcation and Chaos* **4**, 209-218.

[6] Pontryagin, L.S. *Topological groups* (Gordon and Breach, New York).

CHAOS INDUCED BY THERMAL MODULATION OF A FLUID MIXTURE IN A POROUS MEDIUM

M.N. OUARZAZI(*), J.-M. MALASOMA(**), C.-H. LAMARQUE(**)

(*) Laboratoire de Mécanique de Lille - U.R.A. 1441- CNRS

Bd Langevin - F 59 655 Villeneuve d'Ascq - FRANCE

(**) Département Génie Civil Bâtiment / LGM - U.R.A. 1652 - CNRS

1 Rue Audin - F 69 518 Vaulx-en-Velin Cédex - FRANCE

Abstract:

The results of the study of the global behaviour of the convective flow of a binary mixture in a porous medium are presented. Bifurcation diagram, fixed points, periodic, chaotic solutions, stable and unstable manifolds, and basins of attraction have been calculted.Different behaviours (chaos, undecidable, ...) have been found.

1 Introduction

The problem considered here deals with the convective flow of a binary mixture in a porous medium. Two parameters determine mainly the convective flow: the filtration Rayleigh number Ra and the separation ratio Ψ which determines whether gradients in the concentration help or hinder the convection. The system may develop two types of instabilities. The instabilities are oscillatory or stationary and their threshold curve in the (Ra, Ψ) plane intersect at a polycritical point which caracterizes a bifurcation of codimension 2 (C.T.). The aim of this study is to describe the influence of a small sinusoidal time variation of the thermal boundary conditions. In a previous work [1] concerning the linear stability analysis, it is shown that for low frequencies and in the vicinity of C.T. point, the motion appears as the solution of a Mathieu equation. It is well known that its stability diagram contains so-called Arnold tongues, where the motion is mode locked. The study of this phenomenon must take into account the nonlinear effects. For this purpose, according to some hypothesis ,the problem maybe reduced to a second order normal form équation:

$$\frac{d^2W}{dt^2} = \mu_1 W + f_1 W^3 + (\mu_2 - f_2 W^2)\epsilon\frac{dW}{dt} + \epsilon f_3 W\cos(\omega t) + h.o.t. \qquad (1)$$

where $\mu_1 = \mu_2 = 0$ corresponds to the C.T. point. f_1, f_2, f_3 are constants and ϵ is related to the low-frequency modulation $\overline{\omega} = \epsilon\omega$ with $\omega = O(1)$. "h.o.t." stays for "higher order terms". For $\epsilon = 0$ the ordinary differential equation (1) is one-degree-of-freedom Hamiltonian system. It possesses heteroclinic and periodic solutions. When $\epsilon \neq 0$ integrability is generically lost. Therefore, we show that the system may exhibit a chaotical regime of Smale horseshoe type. We estimate, by means of Melnikov theory, the threshold of the onset of the chaotic regime as well as the curve at which saddle-node bifurcation occurs: $\epsilon f_3 \geq 0.32$.

We propose a global numerical study of equation (1). We show numerically that the behaviour of the fixed points strongly depends on the parameter ϵf_3 and that chaos may occur. Phase space plots, Lyapunov exponents, stable and unstable manifolds, periodic solutions quasi-periodic solutions, attractors and basins of attraction have been computed in order to provide the global behaviour of the nonlinear oscillator. The following values of the parameters are used here after: $\mu_1 = 1; \mu_2\epsilon = 0.1; f_1 = 1; f_2\epsilon = 1.; \omega = 2$. The parameter ϵf_3 is the free parameter.

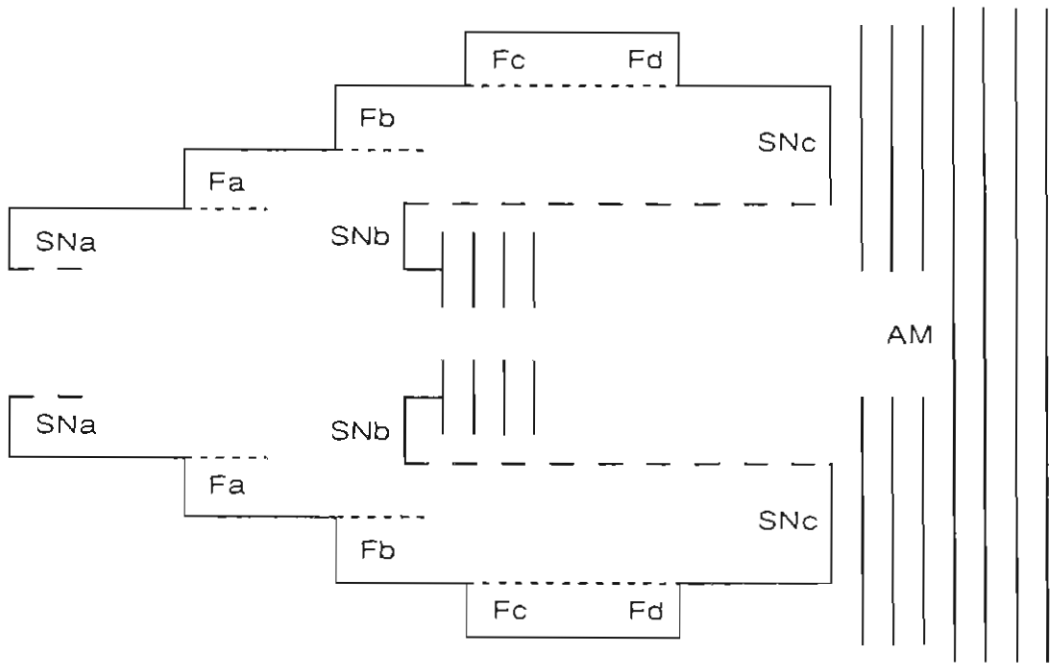

Figure 1: Symbolic bifurcation diagram in the range $0.3 - 0.35$

2 Bifurcation diagram

Extensive numerical simulations have revealed that this system exhibits a complex dynamics with a rich structure of coexisting attractors. For example, the symbolic diagram in figure 1 gives a quick overview of the dynamical behaviour of the system for the previous parameter values when the amplitude of the parametric excitation is varied in the range $0.30 - 0.35$. The solide lines denote stable periodic solutions, while dashed lines denote unstable periodic solutions of flip or saddle types. In the diagram, bifurcations are symbolised by vertical lines, denoted by SN for saddle-node bifurcation and by F for flip bifurcation. Many vertical paralell lines denote a chaotic attractor.

At $SNa = 0.307$ two stable period-7 solutions are created together with two regular saddles of same period. These solutions are symetric by pair with respect to the origin of the phase space. The two stable ones undergoe two successive flip bifurcations in $Fa = 0.326$ and $Fb = 0.343$ and then two stable period-28 coexist. At $SNb = 0.3455$ two new stable period-28 solutions are created wich undergoe complete cascades of period doublings giving rise to two chaotic attractors symetric with respect of the origin. At last two other flip at $Fc = 0.3464$ and at $Fd = 0.3469$ give two period-56 solutions and the system return to two period-28 stable solutions. Theses solutions are destroyed in a final saddle-node bifurcation at $SNc = 0.346934$ and two chaotic attractors are created in type I intermittency. When the amplitude is increased further the two chaotic attractors merge in a symetric one.

3 Undecidable behaviour - Stable and unstable manifolds of a fixed saddle point via Lattés method

When ϵf_3 increases a saddle fixed point occurs the location of which is obviously depending on ϵf_3: it is possible to use the Lattés method [3] in order to compute the stable and the unstable manifolds of this fixed point. According to the value of ϵf_3 a new chaotic attractor may appear if stable and unstable manifold of the fixed point are intersected curves. In figure 3 a) to 3 d), stable and unstable manifolds are shown for $\epsilon f_3 = 0.32; 3a)$, $\epsilon f_3 = 0.37; 3b)$, $\epsilon f_3 = 0.39; 3c)$, $\epsilon f_3 = 0.41; 3d)$. In figure 3 a) there is no

intersection between stable and unstable manifold. The fixed point is not responsible for chaos. In figure 3 b) and 3 c), one can see that intersection is about to occur. In figure 3 d), intersection occurs: "full chaos" is not observed but a complex boundary occurs given by the stable manifold of the saddle point. This implies a second undecidability. Collision between the attractor and this stable manifold is observed for $0.39 < \epsilon f_3 < 0.41$ providing a crisis. The greatest Lyapounov exponent associated with trajectory issued from point $(0.95, 0.)$ has been computed. Its value is 0.06 for $\epsilon f_3 = 0.39$ and Lyapunov dimension 1.51.

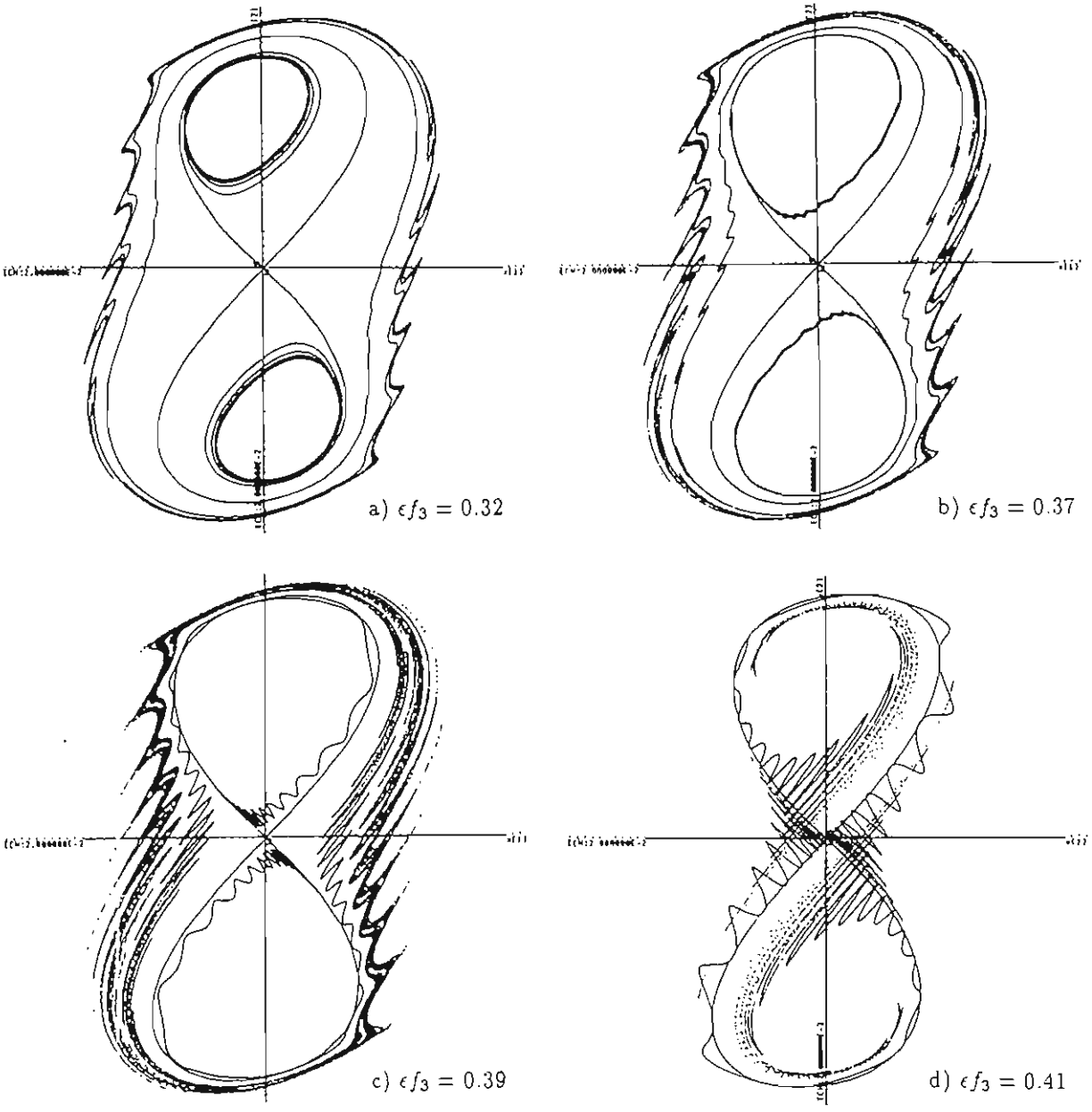

Figure 3. Stable and unstable manifolds. Horizontally: W, vertically $\frac{dW}{dt}$. W and $\frac{dW}{dt}$ both in the range $[-1.; 1.]$. a) $\epsilon f_3 = 0.32$ b) $\epsilon f_3 = 0.37$ c) $\epsilon f_3 = 0.39$ d) $\epsilon f_3 = 0.41$

4 Basins of attraction

Basins of attraction of the different attractors have been computed in the $(W, \frac{dW}{dt})$ plane. The pictures provided correspond to the square $[-1,1] \times [-1,1]$ of initial conditions. Figure 4 a) corresponds to $\epsilon f_3 = 0.39$ and Figure 4 b) corresponds to $\epsilon f_3 = 0.41$. In figure 4 a), the Poincaré section of the chaotic attractor is presented inside its basin. In figure 4 b), there is no more chaotic attractor.

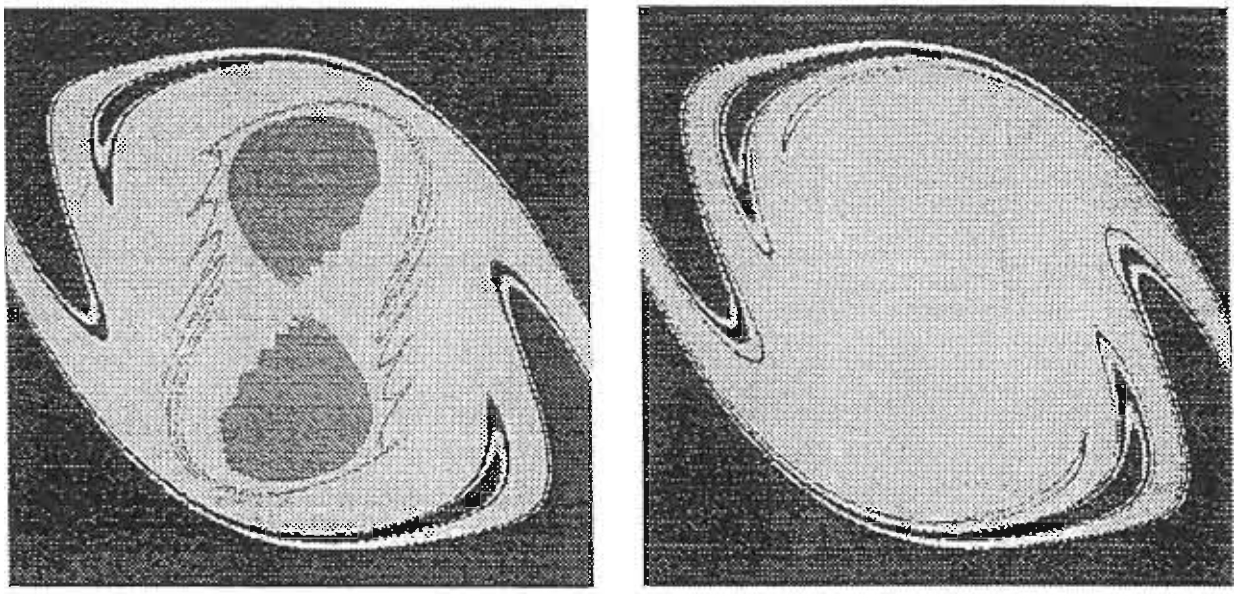

a) $\epsilon f_3 = 0.39$ b) $\epsilon f_3 = 0.41$

Figure 4. Basins of attraction a) $\epsilon f_3 = 0.39$ b) $\epsilon f_3 = 0.41$

5 Conclusion

A global analysis of the behaviour of a one degree of freedom system has been briefly presented. Chaotic behaviour has been numerically depicted. Numerical values of the different parameters may possess physical meaning.

References

[1] M.N.N OUARZAZI, P. BOIS, Linear convection of a fluid mixture in a porous medium with time-dependant temperature gradient, Eur. J. Mech., B/Fluids, 13, n° 3, 275-298, 1994.

[2] V.K. MELNIKOV, On the stability of the Center for time periodic perturbation. Transaction of the Moscow Math. Soc. 12 (1), 1-57,1963

[3] R.L. CLERC, C. HARTMANN, Méthodes constructives pour l'étude des bifurcations de quelques systèmes dynamiques, 289-327, Numéro spécial 1984, Journal de mécanique théorique et appliquée.

Synchronization of Chaotic Systems

U. Parlitz and *L.Kocarev
Drittes Physikalisches Institut, Universität Göttingen,
Bürgerstraße 42-44, D-37073 Göttingen, Federal Republic of Germany
*Department of Electrical Engineering,
Ss. Cyril and Methodius University, Skopje, PO Box 574, Republic of Macedonia

Abstract

The synchronization of chaotic dynamical systems based on active-passive decomposition and sporadic coupling is discussed and illustrated using two unidirectionally coupled arrays of Chua oscillators. Furthermore, we give a brief review of possible applications and generalizations of chaos synchronization including parameter identification, generalized synchronization and phase synchronization.

1. Introduction

Synchronization of periodic signals is a well-known phenomenon in physics, engineering and many other scientific disciplines. However, even chaotic systems may be linked in a way such that their chaotic oscillations are synchronized. In particular, the case of one-directional coupling has been investigated intensely during the last years [Fujisaka & Yamada, 1983; Afraimovich *et al.*, 1986; Pecora & Carroll, 1990; Kocarev & Parlitz, 1995] because of its potential application in communication systems (see, for example, [Parlitz *et al.*, 1996a] and references cited therein). In this article we briefly discuss further applications and generalizations, in particular the synchronization of spatially extended arrays of coupled oscillators.

2. Active-Passive Decomposition

The basic idea of the following synchronization method consists in a decomposition of a given (chaotic) system into an active and a passive part, where different copies of the passive part synchronize when driven by the same active component. Consider an arbitrary N-dimensional (chaotic) dynamical system

$$\dot{\mathbf{z}} = \mathbf{F}(\mathbf{z}). \tag{1}$$

The goal is to rewrite this autonomous system as a non-autonomous system that possesses certain synchronization properties. Formally, we may write

$$\dot{\mathbf{x}} = \mathbf{f}(\mathbf{x}, \mathbf{s}), \tag{2}$$

where $\mathbf{x}$ is the new state vector corresponding to $\mathbf{z}$ and $\mathbf{s}$ is some vector valued function of time given by $\mathbf{s} = \mathbf{h}(\mathbf{x})$ or $\dot{\mathbf{s}} = \mathbf{h}(\mathbf{x}, \mathbf{s})$. The pair of functions $\mathbf{f}$ and $\mathbf{h}$ constitutes a decomposition of the original vector field $\mathbf{F}$. The crucial point of this decomposition is that for suitable choices of the function $\mathbf{h}$ any system

$$\dot{\mathbf{y}} = \mathbf{f}(\mathbf{y}, \mathbf{s}) \tag{3}$$

that is given by the *same* nonautonomous vector field $\mathbf{f}$, the *same* driving s, but *different* variables $\mathbf{y}$, synchronizes with the original system (2), i.e., $\|\mathbf{x} - \mathbf{y}\| \to 0$ for $t \to \infty$. More precisely, synchronization occurs if the driven dynamical system is asymptotically

stable which can be proved via a stability analysis of the linearized system, by means of a (global) Lyapunov function, or numerically using the fact that synchronization occurs if all conditional Lyapunov exponents of the nonautonomous system (2) are negative [Pecora & Carroll, 1990]. In this case, system (2) is a passive system and we call the decomposition an *active-passive decomposition (APD)* of the original dynamical system [Halle *et al.*, 1993; Wu & Chua, 1993; Kocarev & Parlitz, 1995; Parlitz *et al.*, 1996a].

What makes this method for constructing synchronized systems interesting for applications is the fact that in many cases the function $s(t)$ can be rather general. In particular, it may depend not only on the state $\mathbf{x}$ but also on some information signal $i(t)$, i.e., $s = h(\mathbf{x}, i)$. In the case of synchronization ($\mathbf{y} \to \mathbf{x}$), this information i can be recovered from $s = h(\mathbf{x}, i) = h(\mathbf{y}, i)$ if this equation is uniquely solvable for i. This communication method can also be implemented using hyperchaotic dynamics [Kocarev & Parlitz, 1995; Parlitz *et al.*, 1996a].

3. Sporadic Coupling

To achieve synchronization of two *continuous* systems it is *not* necessary to couple them *continuously*. Even if the coupling is switched on at *discrete* times $t_n = nT$ only, synchronization may occur if the coupling and the time interval T are suitably chosen [Amritkar & Gupte, 1993; Stojanovski *et al.*, 1996]. In particular, this kind of *sporadic coupling* leads also to a correct interpolation of the continuous time evolution during the intervals *between* the coupling times t_n. In those cases where the coupling signal or variable is chosen such that the corresponding *continuous* coupling would lead to synchronization in the sense of Pecora and Carroll [1990] it was shown by Stojanovski *et al.* [1996] that a threshold value T_h exists with synchronization for all $T < T_h$.

4. Synchronizing Arrays

We shall now consider one-dimensional arrays of diffusively coupled Chua oscillators (4) with periodic boundary conditions. The equations for the array are given by:

$$\begin{aligned}
\frac{dV_{C1}^i}{dt} &= G(V_{C2}^i - V_{C1}^i) - g(V_{C1}^i) + G_c(V_{C1}^{i-1} - 2V_{C1}^i + V_{C1}^{i+1}) \\
\frac{dV_{C2}^i}{dt} &= G(V_{C1}^i - V_{C2}^i) + I_L^i \\
\frac{dI_L^i}{dt} &= -V_{C2}^i - R_0 I_L^i
\end{aligned} \tag{4}$$

where the index i denotes the i-th oscillator in the array. The coupling conductance G_c is given by $G_c = 1/R_c$ with $R_c = 100\text{k}\Omega$ and the other parameters equal $m_0 = -0.405\text{mS}$, $m_1 = -0.756\text{mS}$, $G = 1/R$ with $R = 1740\Omega$, $B_p = 1.08\text{V}$, $L = 18\text{mH}$, $R_0 = 20\Omega$, $C_1 = 10\text{nF}$, and $C_2 = 100\text{nF}$. A copy of this array may be synchronized by applying the sporadic coupling described in the previous section sequentially to the individual elements of both arrays. One can, for example, start with the first oscillator of the response array and set the value of its V_{C2}-variable at time t_n to the corresponding value $V_{C2}(t_n)$ of the first oscillator of the drive array. Then, at time $t_{n+1} = t_n + T$ the second elements of both arrays are sporadically coupled and so on. Finally, when the last two oscillators have been coupled we start with the first pair again. The results of a numerical simulation based on this coupling scheme with $T = 0.001$ is shown in Fig. 1 for an array consisting of 100 oscillators. Figure 1a gives the spatio-temporal evolution of

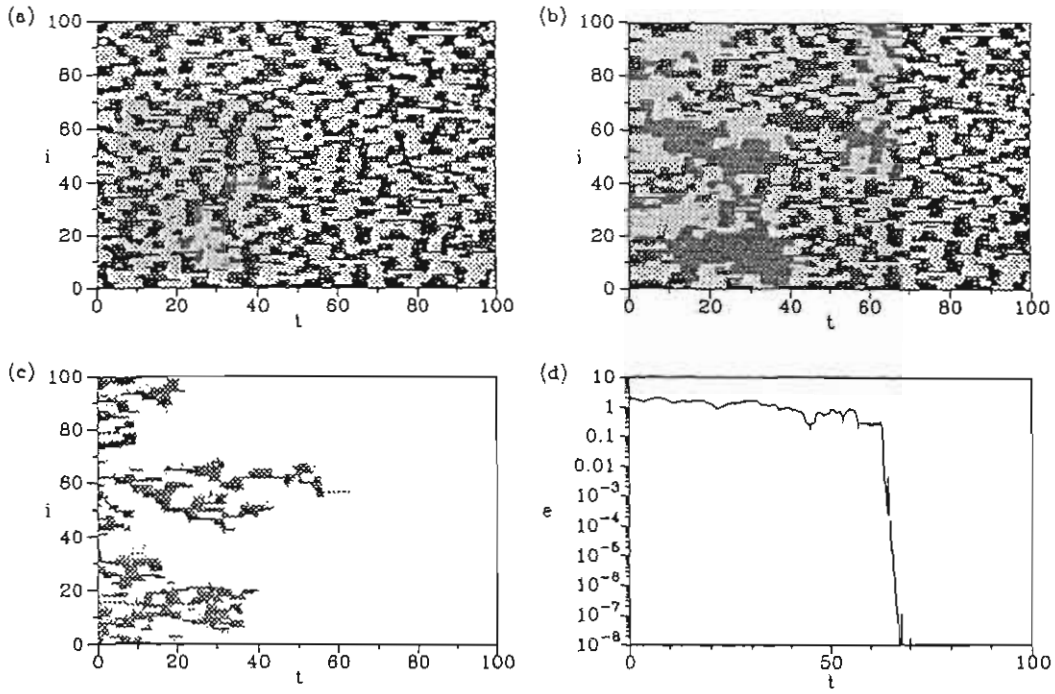

Figure 1: Spatiotemporal evolution of coupled Chua oscillators (4).

the drive array in terms of gray-coded values of $V_{C2}(t)$ vs. time t and oscillator position i. Figure 1b shows the corresponding diagram for the response system. As can be seen both arrays are synchronized for $t > 65$ and generate the same spatio-temporal pattern. To visualize the synchronization transient the magnitude of the difference is plotted in Fig. 1c vs. time t and position i, where dark regions denote large differences. Figure 1d gives the spatially averaged synchronization error e as a function of time. As soon as the last "synchronization defect" died out (compare Fig. 1c) the error drops down to the resolution of the numerical simulation. The dynamics of the drive array is hyperchaotic with a Lyapunov dimension of $D_L > 200$ and thus provides a rather complex encoding when used in a communication system.

5. Parameter Identification

A potential application of synchronization consists in parameter estimations from time series. Assume that a (chaotic) experimental time series has been measured and the structure but not the parameter values of a model describing the underlying process are known. The goal is to find these unknown parameters and perhaps also the time evolution of the variables that have not been measured. This problem can be tackled using synchronization. The basic strategy consists in finding the right parameter values by minimizing the synchronization error of a numerical model driven by the given data. More details about the algorithm and experimental results may be found in Parlitz *et al.* [1996b]. In those cases where a continuous coupling between the experiment a computer model is possible, similar methods may be applied [Parlitz, 1996; Parlitz & Kocarev, 1996].

6. Phase Synchronization

The synchronization of two systems in the sense that both state vectors converge to the same value is not the only possibility. If, for example, a well defined phase variable

can be identified in both systems, the phenomenon of *phase synchronization* may occur [Rosenblum *et al.*, 1996; Parlitz *et al.*, 1996c]. In this case the difference between both phases is bounded and the average values of the resulting angular rotation frequencies are equal after some synchronization transient, while the corresponding amplitudes of both systems remain uncorrelated. This phenomenon may be used in technical or experimental applications where a coherent superposition of several output channels is desired.

7. Generalized Synchronization

Another concept of synchronization is the notion of *generalized synchronization* where the existence of a functional relationship between the states of the coupled systems is required (in the limit $t \to \infty$) [Afraimovich *et al.*, 1986; Rulkov *et al.*, 1995; Kocarev & Parlitz, 1996]. This type of synchronization occurs for uni-directionally coupled systems when the driven system is asymptotically stable [Kocarev & Parlitz, 1996] and is therefore very robust with respect to parameter mismatch.

This work was supported by the German-Macedonian project No. 6.J1A.6.A.

References

Afraimovich, V.S., Verichev, N.N. & Rabinovich, M.I. [1986] "Stochastic synchronization of oscillations in dissipative systems," *Radiophys. Quantum Electron.*, 29, 795-803.

Amritkar, R.E. & Gupte, N. [1993] "Synchronization of chaotic orbits: The effect of a finite time step," *Phys. Rev. E*, 47(6) 3889-3895.

Fujisaka, H. & Yamada, T. [1983] "Stability theory of synchronized motion in coupled-oscillator systems," *Prog. Theor. Phys.*, 69, 32-46.

Halle, K.S., Wu, C.W. Itoh, M. & Chua, L.O. [1993] "Spread spectrum communication through modulation of chaos," *Int. J. Bifurcation and Chaos*, 3, 469-477.

Kocarev, L., & Parlitz, U. [1995] "General approach for chaotic synchronization with applications to communcation," *Phys. Rev. Lett.*, 74, 5028-5031.

Kocarev, L. & Parlitz, U. [1996] "Generalized synchronization, predictability and equivalence of unidirectionally coupled dynamical systems," *Phys. Rev. Lett.*, 76(11), 1816-1819.

Parlitz, U., Kocarev, L., Stojanovski, T. & Preckel, H. [1996a] "Encoding messages using chaotic synchronization," *Phys. Rev. E*, 53, 4351-4361.

Parlitz, U. & Kocarev, L. [1996] "Multichannel communication using auto-synchronization," *Int. J. Bifurcation and Chaos*, 6(3), 581-588.

Parlitz, U., Junge, L., & Kocarev, L. [1996b] "Synchronization based parameter estimation from time series," submitted for publication.

Parlitz, U. [1996] "Estimating model parameters from time series by auto-synchronization," *Phys. Rev. Lett.*, 76, 1232-1235.

Parlitz, U., Junge, L., Lauterborn, W. & Kocarev, L. [1996c] "Experimental observation of phase synchronization," to appear in: *Phys. Rev. E.*

Pecora, L.M., & Carroll, T.L. [1990] "Synchronization in chaotic systems," *Phys. Rev. Lett.*, 64, 821-824.

Rosenblum, M.G., Pikovsky, A. & Kurths, J. [1996] "Phase synchronization of chaotic oscillators," *Phys. Rev. Lett.* 76, 1804-1807.

Rulkov, N.F., Sushchik, K.M., Tsimring, L.S., & Abarbanel, H.D.I. [1995] "Generalized synchronization of chaos in directionally coupled chaotic systems," *Phys. Rev. E*, 51, 980-994.

Stojanovski, T., Kocarev, L. & Parlitz, U. [1996] *Driving and Synchronising by Chaotic Impulses*, to appear in: Phys. Rev. E.

Wu, C.W. & Chua, L.O. [1993] "A simple way to synchronize chaotic systems with applications to secure communication systems," *Int. J. of Bifurcation and Chaos*, 3, 1619-1627.

Theory of resonant transmission. Wave propagation in a medium of coupled harmonic oscillators

V.I. Petrosyan, Yu.V. Gulyaev, V.A. Krysko ,
E.A. Zhitenyova, V.A. Yelkin, N.I. Sinitsin, D.V. Krysko
Professor, Doctor of Technical Sciences,
Honoural Man of Science and Engineering of Russia,
The Head of the Highest Mqathematics chais
B. Sadovay str., 96a, flat 77, Saratov, 410054 Russia

A "paradoxical" phenomenom of resonant transmission of water media, involving biological objects, has been revealed for electro magnetic radiation (EMR) with an extremely high frequency (EHF of 30...300 GHz in the millimeter-wavelength band, 10...1 mm) and is described in RE, 1995, V. 40, No 1, p. 127.

To understand and model the mechanism of EHF-wave propagation in water media and that of active interaction between these waves and biological objects we consider the molecular structure of identical coupled oscillators (librators). The system of these oscillators may be treated as that of one-dimensional chains extended in the direction of wave propagation. According to the theory of oscillation in the field of an electromagnetic wave that propagates in these chain we have.

$$E(l,t) = E_0 \exp(i\omega t - i\chi l) , \tag{1}$$

The oscillators undergo the action of periodic force

$$f(l,t) = f_0 \exp(i\omega t - i\chi l) = f_0 \exp(i\omega t - i\chi n\alpha), \tag{2}$$

where ω and χ are the frequency and the wave number, respectively; $f_0 = qE_0 / m$ is the amplitude of external force (per unit mass); E_0 is the amplitude of electric field strength; q and m are the oscillator's charge and mass; t is the time; $l = na$ is the depth of penetration into the medium; α is the intermolecular spacing; and n is the number of oscillator in the chain. The oscillators are shifted as forced by their neighbours

$$f = (k / m)\Delta\varphi_n , \tag{3}$$

where k and φ_n are the elasticity constant for interconnection between the oscillators and the oscillator's shift; and

$$\Delta\varphi_n = \varphi_{n+1} - \varphi_n - (\varphi_n - \varphi_{n-1}) = \varphi_{n+1} + \varphi_{n-1} - 2\varphi_n$$

defines the resulting shift of the oscillator with respect to its nearest neighbours. The differential equation with no attenuation has the form

$$\ddot{\varphi}_n(l,t) + \omega_0^2 \varphi_n(l,t) = (k/m)\Delta\varphi_n(l,t), \tag{4}$$

where $\omega_o = (k_0/m)^{1/2}$ and k_0 are the resonant frequency of an autonomaus oscillator and its elasticity counstant.Its solution is as follows

$$\varphi_n(l,t) = \varphi_0 \exp(i\omega t - i\chi n\alpha), \tag{5}$$

where φ_o is the shift amplitude for the oscillator. Substituting (5) into (4) yields the following dispertion equation

$$\omega^2 = \omega_0^2 + 4(k/m)\sin(2\chi\alpha/2), \tag{6}$$

As seen, χ is real for the frequency band $\omega_0 < \omega < \omega^*$ and imaginary for $\omega < \omega_0$ and $\omega > \omega^*$. Here

$$\omega^* = \omega_0 + (4k/m)^{1/2} \tag{7}$$

and $\omega^* \cong \omega_0$ with weak interation.

By this is meant that the EMR amplitude in the resonant band $[\omega_0, \omega^*]$ is maintained and the wave propagates freely in the medium [see (5)]. Outside this band the amplitude decreases exponentially and the wave attenuates at the surface

$$\varphi(l) = \varphi_0 \exp(-\chi l) = \varphi_0 \exp(-2\pi l/\lambda), \tag{8}$$

where $\lambda = 2\pi c_0/\sqrt{\mu\varepsilon}\,\omega$ is the wavelength of the wave in the medium; μ and ε are the permeability and the permittivity of the medium; and c_o is the EMR propagation velocity in vacuum.

The aforesaid can give an insight into the mechanism of EMR penetration through the medium and into the existence of physical resonant frequencies of interation between the EHF radio waves and the biobjects.

Linear oscillation regime with attenuration (anharmonism)

In real media the forced oscillation of interacting oscillators proceed with a certain attenuation and for small amplitudes they are described with the following linear differential equation

$$\ddot{\varphi}(t) + 2\gamma_0\dot{\varphi}(t) + \omega_0^2\varphi(t) = f_0 \exp(i\omega t), \tag{9}$$

where $2\gamma_o$ is the coefficient of linear dissipative loss per unit mass (viscosity, molecular friction). Its solution are the functions

$$\varphi(t) = \varphi_0\left[1 - \exp(-\gamma_0 t)\right]\exp\left[i(\omega t - \theta)\right] \tag{10}$$

and

$$\varphi(t) = \varphi_0 \exp(-\gamma_0 t) \exp\left[i(\omega t - \theta)\right] , \tag{11}$$

where $\theta = arctg\left[2\gamma_0 \omega / \left(\omega_0^2 - \omega^2\right)\right]$ is the phase difference between the external force and the oscillator's shift. There functions were obtained for boundary conditions $t = (0,\infty)$: $\varphi(t) = (0,\varphi_0)$ $\varphi(t) = (\varphi_0,0)$ which corresponds to the EMR source on- and off-switching.

From the stationary solution [see (10)]

$$\varphi(t) = \varphi_0 \exp(i\omega t) . \tag{12}$$

By its substitution into (9) we find the oscillation intensity for the oscillators with the frequency detuning $(\omega - \omega_0 \neq 0)$ and in the resonance with the natural frequencies of the autonomous oscillator $(\omega - \omega_0 = 0)$:

$$\varphi_0^2 = f_0^2 / \left[\left(\omega_0^2 - \omega^2\right)^2 + \left(2\omega\gamma_0\right)^2\right] , \tag{13}$$

$$\varphi_0^2 \cong f_0^2 / 4\omega_0^2\left[\left(\omega_0 - \omega\right)^2 + \gamma_0^2\right] \text{ for } \omega \cong \omega_0 , \tag{13'}$$

$$\varphi_\infty^2 = f_0^2 / (2\omega_0\gamma_0)^2 , \quad \varphi_{0r}^2 = f_0^2 / \left[(2\omega_0\gamma_0)^2 - \left(2\gamma_0^2\right)^2\right] , \tag{14),(15}$$

$$\omega_r = \left(\omega_0^2 - 2\gamma_0^2\right)^{1/2} , \quad \omega_r \cong \omega_0 \text{ for } \gamma_0 << \omega_0 , \tag{16),(16'}$$

$$\gamma_0 = \left|\omega_0 - \omega_{1/2}\right| , \quad Q = \omega_0 / 2\gamma_0 , \tag{17),(17'}$$

where ω_r is the resonant frequency of the oscillator with losses (obtained from the extremum condition $d\left(\varphi_0^2\right)/d\omega = 0$), φ_0, φ_∞, φ_{0r} are the oscillation amplitudes of frequencies $\omega, \omega_0, \omega_r$; $\omega_{1/2}$ is the frequency at the level $\varphi_0^2 / 2$, Q is the Q-factor. The intersity of resonant oscillations of the oscillators is thus seen to substantially exceed that of incident waves.

Nonlinear oscillation regime with attenuation

As the intensity of forced oscillation of the oscillators is raised at resonant frequencies, the energy dissipation also increases and transmission decreases.

It follows from the noustationary solution of (10) that, starting with the point of the EMR source on-switching at the resonant frequency $\omega = \omega_r$, the oscillation amplitude is greater with time according to the exponential law

$$\varphi_0(t) = \varphi_\infty\left[1 - \exp(-\gamma t)\right] , \tag{19}$$

Due to this fact, the oscillators pass to the nonlinear oscillation regime as their oscillation amplitudes approach the maximum values. Nonlinearity is induced by nonlinear loss in this case which are related to a stronger intermolecular interaction as the magnitude of the

oscillationamplitude approaches the intermolecular spacing. This dependence must be quadratic due to its being even

$$\gamma = \gamma_0\left[1 + \alpha\left(\varphi_0/\alpha\right)^2\right], \tag{20}$$

where γ and α are the shift and the amplitude of nonlinear dissipative loss and proportionallity factor. The substitution of (20) into (9) yields the nonlinear Van der Pole equation with the difference that the quadratic term is not a variable, but the parameter:

$$\ddot{\tilde{\varphi}}(t) + 2\gamma_0\left[1 + \alpha\left(\tilde{\varphi}_0/\alpha\right)^2\right]\dot{\tilde{\varphi}}(t) + \omega_0^2\,\tilde{\varphi}(t) = f_0\exp(i\omega t), \tag{21}$$

where $\tilde{\varphi}(t), \tilde{\varphi}_0$ are the shift and the amplitude of nonlinear oscillation.

This representation gives a possibility to exploit the results of linear solutions(13) - (16) with substituting γ_0 by (20):

$$\tilde{\varphi}_0^2 = f^2 / \left\{\left(\omega_0^2 - \omega^2\right)^2 + \left[2\omega\gamma_0\left(1 + \alpha\,\tilde{\varphi}_0^2/\alpha^2\right)\right]^2\right\}, \tag{22}$$

$$\tilde{\varphi}_\infty^2 = f_0^2 / \left[2\omega_0\gamma_0\left(1 + \alpha\,\varphi_\infty^2/\alpha^2\right)\right]^2, \tag{23}$$

$$\varphi_{0r}^2 = f_0^2 / \left\{2\omega_0\gamma_0\left[1 + \alpha\left(\varphi_0/\alpha\right)^2\right]\right\}^2 - \left\{2\gamma_0^2\left[1 + \alpha\left(\varphi_0/\alpha\right)^2\right]^2\right\}^2, \tag{24}$$

$$\tilde{\omega}_r^2 = \omega_0^2 - 2\gamma_0^2\left(1 + \alpha\,\tilde{\varphi}_\infty^2/\alpha^2\right),\ \gamma^2 = \omega_0\left(\omega_0 - \tilde{\omega}_r\right) \text{ as } \tilde{\omega}_r \equiv \omega_0. \tag{25}$$

where $\tilde{\omega}_r$ is the resonant frequency of the nonlinear attenuation oscillator. Since the resonant frequency of the oscillator is lowered with the oscillation amplitude increase (see (24)), $\omega_0 \Rightarrow \tilde{\omega}_r$, the system leaves the resonance and the transmission of energy from the external source becomes weaker or ceases depending on the EMR intensity. As a result the resonance curve is shifted

$$\varphi_\infty(\omega_r, \omega_0) \Rightarrow \tilde{\varphi}_\infty(\tilde{\omega}_r, \omega_0) \tag{26}$$

and the oscillation intensity of the oscillators and thus energy dissipation ,falls exponeutially in accord to (11);

$$\varphi_0(t) = \left[\varphi_{0r}(\omega_r, \omega_0) - \varphi_{0r}(\tilde{\omega}_r, \omega_0)\right]\exp(-\gamma t) + \tilde{\varphi}_{0r}(\tilde{\omega}_r, \omega_0) \tag{27}$$

where the functions $\varphi_{0r}(\omega_0, \omega_0), \tilde{\varphi}_{0r}(\omega_r - \omega_0)$ are defined by (15) and (24) and the difference between them reflects the amplitude decrease. Within a pause in absorbing the EMR energy the system of the oscillators returns to its initial resonant state, $\tilde{\omega}_r \Rightarrow \omega_0$, and the cycle is automatically repeated. Self-o scillations of the medium transmission were observed for the EMR. With futher EMR power increasig its penetration into the medium becomes stochastic. This is the mechanism of resonant interaction between the EMR and molecular media.

FORCED CHAOTIC AND IRREGULAR OSCILLATIONS – COMPARISON OF FIRST APPROXIMATION AND NUMERICAL SIMULATION

L. Půst

Institute of Thermomechanics, Academy of Sciences, Dolejškova 5, CZ–182 00 Prague 8, Czech Republic

Abstract: The behaviour of the two DOF non-linear mechanical system excited by the harmonic force is studied by the first approximation (averaging and asymptotic) method and by the numerical simulation.
The response curves, instability domains, motion versus time dependencies and phase plane portraits are ascertained. By means of the first approximation solution we receive three instability domains, connected with bifurcation, where jumps occur, or in which the beats and chaotic motions emerge.
The numerical simulation confirmed these properties, but showed that there exist several bifurcation and new instability domains, in which the response on the harmonic excitation is chaotic. These oscillations depend on the history, i.e. on the way and speed of the frequency change with which the system has got into the current state. The responses at increasing or decreasing frequencies differ, the hysteresis loops exist.

1. Introduction

Mechanical systems with the nonlinear springs show a variety of complicated responses on the deterministic harmonic forces. The important typical properties of the responses on the nonlinear systems are the existence of the instabilities and bifurcations connected with the occurence of jumps, beats, irregular quasiperiodic motions and chaotic oscillations. Some of these properties can be explained by the application of the first approximation methods as are equivalent linearization, averaging method, Poincaré method of small parameter etc. But the detailed study of these irregular phenomena can be realised only by the more exact simulation method, i.e. by the numerical solution of the differential Eqs. of motion.

The main attention is given in this contribution to the behaviour of two degrees of freedom (2DOF) nonlinear system containing the stiffening spring with the cubic characteristic and to the comparison of the results gained by the aproximate and exact solutions.

2. Studied system

Mechanical system with 2DOF is excited by the harmonic force, acting on the lower mass m_1 (Fig.1). The nonlinear spring connects masses m_1 and m_2. For simplicity we assume that the system is damped only by linear viscous damping. The differential equations of motion are

$$\begin{aligned} m_1\ddot{x}_1 + b_1\dot{x}_1 + k_1x_1 - f_2(x_2) - b_2\dot{x}_2 &= F_0\cos\omega t \\ m_2(\ddot{x}_1 + \ddot{x}_2) + f_2(x_2) + b_2\dot{x}_2 &= 0 \end{aligned} \qquad (1)$$

where x_2 is the relative displacement between masses m_1 and m_2. The nonlinear function let us suppose in cubic form $f_2(x_2) = k_2x_2 + k_3x_2^3$ $(k_2, k_3 > 0)$. After some transformation and introducing the dimensionless parameters and variables

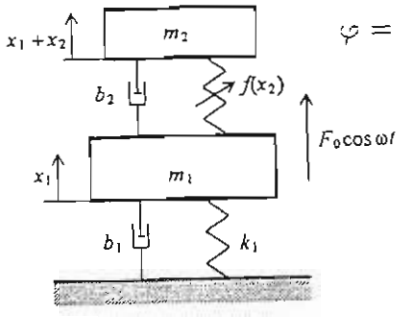

Fig. 1

$$\varphi = \omega t, \quad \eta = \omega\sqrt{m_1/k_1}, \quad \mu = m_2/m_1$$

$$y_j = k_1x_j/F_0, \quad B_j = b_j/\sqrt{k_1m_1}, \qquad j = 1,2 \tag{2}$$

$$f(y_2) = \kappa y_2 + \kappa_3 {y_2}^3, \quad \kappa = k_2/k_1, \quad \kappa_3 = k_3{F_0}^2/{k_1}^3$$

we get

$$\begin{aligned} \eta^2 y_1'' + \eta B_1 y_1' + y_1 - \kappa y_2 - \kappa_3 {y_2}^3 - \eta B_2 y_2' &= \cos\varphi \\ \mu\eta^2(y_1'' + y_2'') + \kappa y_2 + \kappa_3 {y_2}^3 + \eta B_2 y_2' &= 0. \end{aligned} \tag{3}$$

3. Method of solution in first approximation

At the study of the forced oscillation, we shall concerned on the first approximation and therefore we use the averaging method combined with the equivalent linearization method.

These methods are based on the application of the transformation of variables y_j to slowly varying variables C_j, S_j

$$y_j = C_j\cos\omega t + S_j\sin\omega t \qquad j = 1,2 \tag{4}$$

Introducing the auxiliary conditions

$$C_j'\cos\omega t + S_j'\sin\omega t = 0 \tag{5}$$

we receive (after short calculation) four ordinary differential eqs. of the first order. These eqs. exactly describe the behaviour of the system from Fig. 1 and are fully identical with eqs. (1). As their analytical solution is not possible, there it is advantageous to split the right hand sides into the parts containing only members independent explicitly on the time t and the parts periodic in ωt. In the first approximation we can neglect the periodic members and receive the eqs. of motion in the averaged form:

$$\begin{aligned} C_1' &= \tfrac{1}{2\eta^2}\{-\eta B_1C_1 + (1-\eta^2)S_1 + \eta B_2C_2 - \kappa_e(a_2)S_2\} \\ S_1' &= \tfrac{1}{2\eta^2}\{\eta^2 - 1)C_1 - \eta B_1S_1 + \kappa_e(a_2)C_2 + \eta B_2S_2 + 1\} \\ C_2' &= \tfrac{1}{2\eta^2}\{\eta B_1C_1 - S_1 - (1+1/\mu)\eta B_2C_2 + ((1+1/\mu)\kappa_e(a_2) - \eta^2)S_2\} \\ S_2' &= \tfrac{1}{2\eta^2}\{C_1 + \eta B_1S_1 - ((1+1/\mu)\kappa_e(a_2) - \eta^2)C_2 - (1+1/\mu)\eta B_2S_2 - 1\} \end{aligned} \tag{6}$$

where the equivalent linear stiffness $\kappa_e(a_2)$ was introduced instead of the nonlinear function $f(y_2)$ according to the relation

$$f(y_2) \doteq \kappa_e(a_2)y_2 = (\kappa + \frac{3}{4}\kappa_3{a_2}^2)y_2 \tag{7}$$

The amplitude a_2 of the relative motion y_2 is given by

$$a_2 = \sqrt{{C_2}^2 + {S_2}^2}. \tag{7a}$$

Response curves of stationary forced oscillation with the period $T = \frac{2\pi}{\omega}$ can be ascertained from the algebraic eqs., received by setting $C_1' = S_1' = C_2' = S_2' = 0$ into the eqs. (6):

The coefficients in these eqs. depend only on two variables a_2 and ω. This property enables easy construction of response curves a_2, η and a_1, η. The examples of response curves are given in Fig. 2.

The stationary states of the periodic forced vibration are not stabil in all points of the response curves. The study of stability is based on the perturbation theory. To the equilibrium state at the fixed frequency η and constant values C_1, S_1, C_2, S_2 fulfilling the equations of response curves, we add the small perturbations c_1, s_1, c_2, s_2 and receive the perturbed motions:

$$C_j^* = C_j + c_j, \qquad S_j^* = S_j + s_j \qquad j = 1,2 \tag{8}$$

After substituting (8) into eqs. (6), developing in the powers of small quantities $c_1, \ldots, s_2$ and neglecting the powers higher than one we receive the linear differential eqs. in c_1, s_1, c_2, s_2.

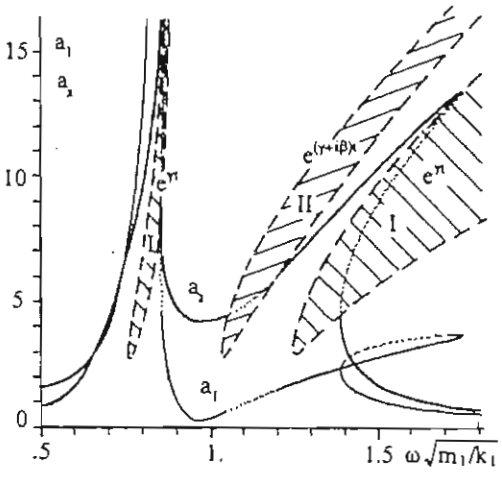

Fig. 2

From the coefficients of these equations of perturbation we can construct the characteristic eq. The stability of the periodic motion is determined according to the real parts of the roots of the characteristic equation written in the form

$$\lambda^4 + A_3\lambda^3 + A_2\lambda^2 + A_1\lambda + A_0 = 0. \tag{9}$$

For the asymptotic stability we use the Routh-Hurwitz criteria. It can be proved that all coefficients A_0, A_1, A_2, A_3 depend only on two variables a_2 and η. Therefore also the roots λ of the characteristic equation depend on these variables and it is possible to draw the instability regions in the coordinates a_2, η in which also the response curve is drawn.

In our case the most important are the instability regions with the boundaries given by the equations

$$A_0 = 0 \qquad \text{(region I)} \tag{10}$$

$$A_1A_2A_3 - A_1^2 - A_3^2A_0 = 0 \qquad \text{(region II)} \tag{11}$$

As an example of the response curves and instability regions are in the Fig. 2 the results of calculation for the 2DOF system with the parameters

$$\kappa_e(a_2) = 0.2 + 0.003a_2^2, \quad \mu = 0.25, \quad B_1 = 0.02, \quad B_2 = 0.01$$

The parts of the response curve a_2, η going through the regions of instability I or II are unstable (see dashed line). Unstable parts of response curve a_1, η have the boundaries at the same η as the curve a_2, η.

The regions I ascertain the same types of unstable motions as in the nonlinear system with 1DOF. There are exponential increase of perturbations given by the law $e^{\alpha t}$, typical for the beginning of the jumps to the other stable periodic states. The more interesting is the region II, where no jump can occur, as there exists only one periodic but unstable solution. Therefore the motion must pass into another, nonperiodic motion. There are complex roots $\lambda = \gamma \pm i\beta$ with the positive real part $\gamma > 0$ and the motion has the form of exponentially increasing beats with the period $2\pi/\beta$.

Let us show the motion in this region of instability. The course of the components of amplitudes C_1, C_2, S_1, S_2 after small perturbation from the stationary state is in Fig. 3 for $\varphi = 0 \div 200$. The motion begins with the exponential increase of beats of amplitudes. At certain distance from the stationary state the beats change over into the irregular-quasichaotic motion. This phenomena is demonstrated also in the phase diagram C_1, S_1 and C_2, S_2 for the same time interval $\varphi = \omega t = 0 \div 200$ in Fig. 4.

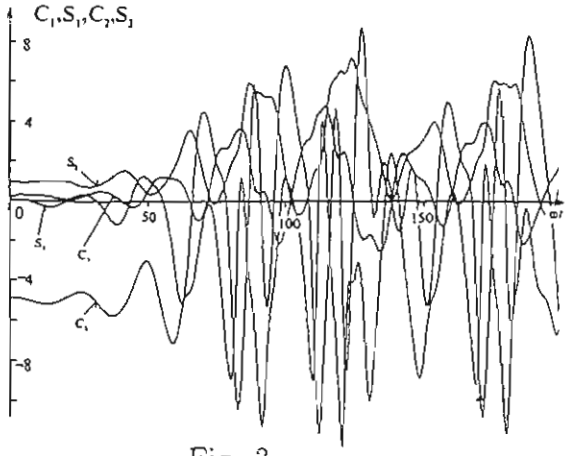

Fig. 3

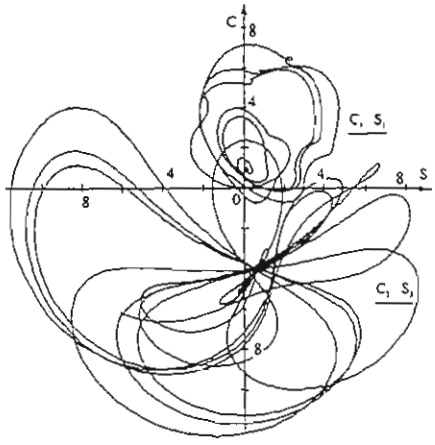

Fig. 4

The response curves out of the instability regions are smooth without any bifurcation and any change of character of motion.

4. Numerical simulation

The method of first approximation based on the equivalent linearization takes into account only first harmonic component with the frequency ω. However the higher components, which always exist in nonlinear systems, can significantly change not only the form of oscillation but also the course of response curves (given by the maxima of displacement) and their stability.

For the more exact study of this behaviour it is very convenient to use the numerical simulation i.e. the direct solution of differential equations (1).The programme package. prepared by F.Peterka [1] for the 1DOF system with impacts, was extended for 2DOF nonlinear systems.

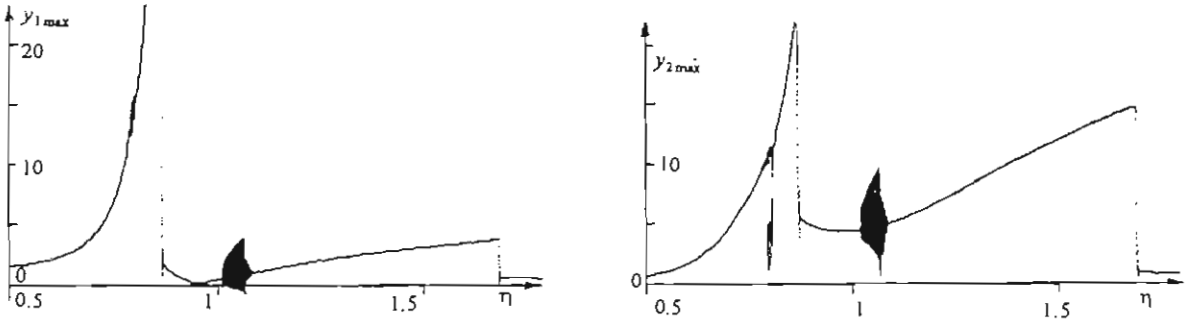

Fig. 5

The behaviour of the system in the second resonance, where the node lies in the nonlinear spring between the masses m_1 and m_2 is very similar to the behaviour of 1DOF system. The properties of the system in the zone near antiresonance i.e. in the instability region II are described in [Půst, 1995] and [Půst & Szöllös, 1996].

In this contribution we shall pay attention to the first resonance peak. The response

curves were gained by the very slow change of frequency approx. 10% in 1000 periods so that the response curves can be supposed to be stationary. The used software package [1] indicates the maxima of chosen coordinate during the motion and plots them into the diagram in dependence on the frequency. Such response curves are in Fig. 5. Besides of two jumps (at $\eta = 0.88$ and 1.70) and one chaotic beats region ($\eta = 1.02 - 1.09$), which were ascertained also by the approximate solution, the irregular motion occurs at $\eta = 0.8$. The isolated branch of response curves means, that there is strong influence of higher harmonics resulting in the occurrence of new maximum in the time history of motion. The influence of the control of frequency variation from $\eta = 0.79$ to 0.87 up and down is shown in Fig. 6 and 7 ($\kappa_5 = 0.0003, B_1 = 0.01, B_2 = 0.05$).

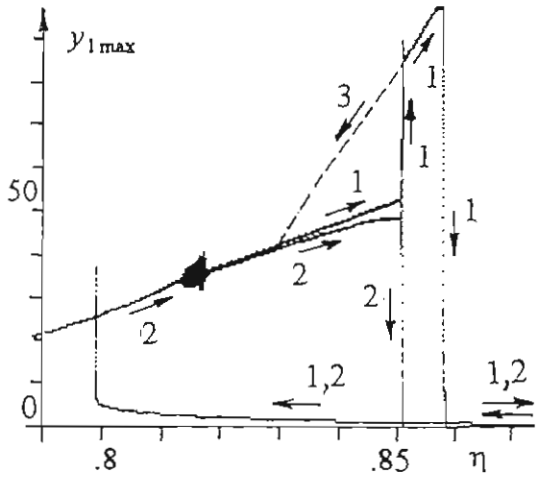

Fig. 6

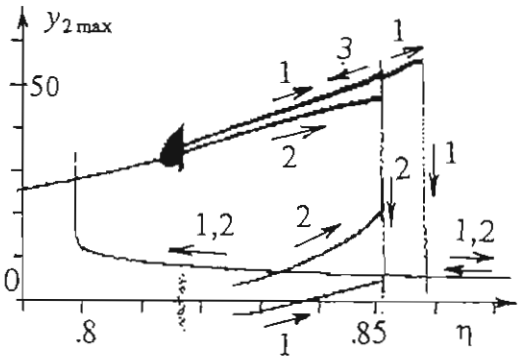

Fig. 7

The region of beat-chaotic motion is in all repeated cycles the same, but the peak itself has different forms according to the speed of frequency change and to the other random influences. The first cycle (1) was done at very low increase of frequency. The jump to higher displacement occurs at $\eta = 0.852$. After reaching the peak maximum ($y_{1max} = 98.$) the amplitudes jump down at $\eta = 0.858$. The vibrations at descending frequency follow the lower branch. Repeating this cycle at 10 times higher increase of frequency, the curves (2) differ from (1). Above the region of chaotic beats the curves bifurcate and the oscillations ($\eta = 0.825 - 0.852$) follow lower branch in y_{1max}, η diagram. In y_{2max}, η there are again two branches. The jump to postresonance solution occurs now at $\eta = 0.852$.

The third cycle (3) consists of the way identical with cycle 1 up near to the peak and then the frequency was running down, as can be seen in Fig. 6. In diagram y_{2max}, η, the response curve was nearly identical with the case (1). (Fig. 7).

The time variation of the displacement $y_1(t)$ and $y_2(t)$ together with the velocity variation is demonstrated in the phase planes in Fig. 8, at $\eta = 0.815$. The motion was recorded in the time interval of 10 periods. From the longer time record it was seen that, the motion can be interpreted as transient chaotic process between two forms of oscillations, seen in next fig. After increasing the exciting frequency to $\eta = 0.83$ this chaotic motions pass over into two separate periodic trajectories shown in Fig. 9a, 9b. These portraits correspond to the upper branches 1 and 2 in Fig. 6 and 7. The portrait of vibration in the branch 3 is seen in Fig. 10. The oscillations $y_1(t)$ are very harmonic,

the nonlinearity manifests itself in the motion $y_2(t)$.

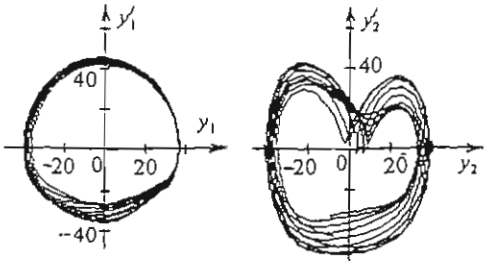

Fig. 8

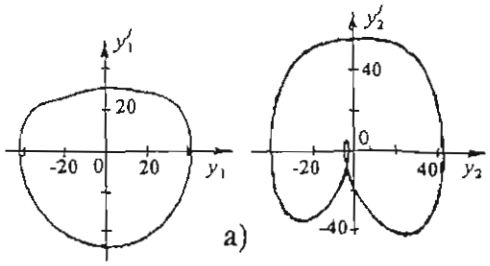

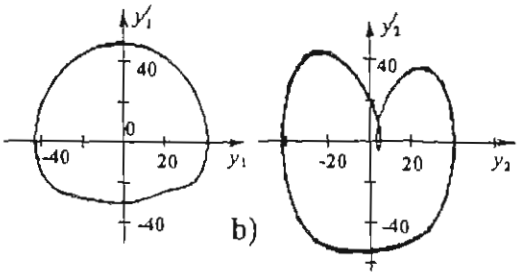

Fig. 9

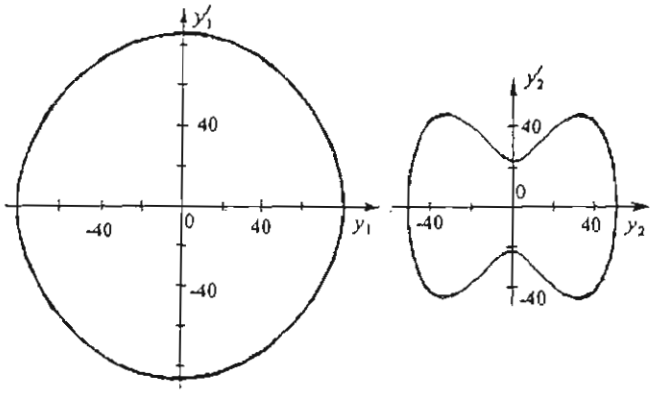

Fig. 10

5. Conclusion

The study of the forced vibrations of the nonlinear two-degrees-of-freedom system showed that:

- the response curves obtained by the approximate and simulation methods are qualitative the same,
- the main regions of instability I (jumps) and II (beats) were ascertained by both methods and have the similar properties. From the quantitative point of view there are self-evidently important differences,
- the new region of chaotic beats, bifurcations and new jump phenomena were found out near the first resonance peak.

Ackonwledgement. This research was supported by Grant Agency of Czech Republic (No.101/94/0126).

6. References

Peterka, F. & Formánek, P. [1994] "Simulation of motion with strong nonlinearities", *Proc. CISS, ETH Zürich*, 137–141.

Půst, L. [1995] "Stability and transient phenomena in the nonlinear systems", *Proc. 9th World Congress on TMM, Milano*,1489–1493.

Půst, L. & Szöllös, O. [1996] "Forced irregular oscillations of the two degrees of freedom nonlinear system" *2nd ENOC, Prague*, 367–370.

Thompson, J.M.T. & Stewart, H.B. [1986] *Nonlinear Dynamics and Chaos* (John Wiley & Sons, New York).

LIE–TROTTER FORMULA AND POISSON DYNAMICS

M.Puta

Seminarul de Geometrie–Topologie, University of Timişoara,
1900 Timişoara, Romania

Abstract. We construct via the Lie–Trotter formula some explicit Poisson integrators for the Maxwell–Bloch equations from laser–matter dynamics, the Euler equations of the free rigid body and the equations of the rigid body with a spinning rotor.

1. Introduction

Let $(R^n, \{\cdot,\cdot\}, H)$ be a Hamilton–Poisson mechanical system. Its dynamics is described by the following system of differential equations:

$$\dot{x}_i = \{x_i, H\} = X_H(x_i), \quad i = 1, 2, \ldots, n.$$

Of course, one of the most interesting problems is to try to construct for this system an explicit numerical integrator such that to preserve as much as possible from its Poisson geometry. Such integrators have been constructed via the Lie–Trotter formula by [Wisdom & Holman, 1991] for the n–planet solar system, by [McLachlan, 1995] for the 2–dimensional Euler equations of an incompressible fluid and by [Hüper et al., 1995] for the Toda lattice.

The goal of our paper is to complete the above list with the cases of Maxwell–Bloch equations, the free rigid body and the rigid body with a spinning rotor.

2. Lie–Trotter Formula and Poisson Geometry

The Lie–Trotter formula, see [Trotter, 1959], applies when one can write the Hamiltonian H as

$$H = H_1 + H_2$$

in such a way that $exp(tX_{H_1})$ and $exp(tX_{H_2})$ can both be explicitly computed. Then the Lie–Trotter formula is given by:

$$\Phi_t : x \in R^n \longmapsto \Phi_t(x) = exp(tX_{H_2})exp(tX_{H_1})x = exp(tX_H)x + O(t^2). \qquad (1)$$

Now we have:

THEOREM 2.1. The Lie–Trotter formula (1) satisfies the following properties:
(i) It preserves the Poisson structure of the phase space $(R^n, \{\cdot,\cdot\})$.
(ii) It preserves the symplectic leaves of the Poisson configuration.

It is clear that the formula (1) is only first order. The order can be increased to m, by composing many such stages, namely:

$$exp(b_m t X_{H_2}) exp(a_m t X_{H_1}) \dots exp(b_1 t X_{H_2}) exp(a_1 t X_{H_1}),$$

with coefficients chosen in such a way, that the above composition approximates $exp(t X_H)$ with error $O(t^{m+1})$.

3. Applications

EXAMPLE 3.1. The Maxwell-Bloch equations from laser–matter dynamics can be written in the following form:

$$\dot{x}_1 = x_2; \quad \dot{x}_2 = x_1 x_3; \quad \dot{x}_3 = -x_1 x_2. \tag{2}$$

They can be realized as a Hamilton–Poisson mechanical system with the phase space R^3, the Poisson bracket given by the matrix

$$\Pi_{MB} = \begin{bmatrix} 0 & -x_3 & x_2 \\ x_3 & 0 & 0 \\ -x_2 & 0 & 0 \end{bmatrix}$$

and the Hamiltonian H given by

$$H = \frac{1}{2} x_1^2 + x_3.$$

The symplectic leaves of our Poisson manifold (R^3, Π_{MB}) are the pairs $(\mathcal{O}_k, \omega_k)$, where

$$\mathcal{O}_k = \{(x_1, x_2, x_3) \in R^3 \mid x_2^2 + x_3^2 = k^2\}$$

and

$$\omega_k = \frac{1}{k}(x_3 dx_1 \wedge dx_2 - x_2 dx_1 \wedge dx_3).$$

The Lie–Trotter formula (1) gives rise to an explicit Poisson integrator for the Eq. (2), namely:

$$\begin{cases} x_1^{k+1} = x_1^k + x_2^k \\ x_2^{k+1} = x_2^k \cos x_1(0) t + x_3^k \sin x_1(0) t \\ x_3^{k+1} = -x_2^k \sin x_1(0) t + x_3^k \cos x_1(0) t \end{cases} \tag{3}$$

Moreover, its restriction to each coadjoint orbit $(\mathcal{O}_k, \omega_k)$ gives rise to an explicit symplectic integrator.

EXAMPLE 3.2. The Euler's equations of the free rigid body can be written in the following form:

$$\dot{x}_1 = a_1 x_2 x_3; \quad \dot{x}_2 = a_2 x_1 x_3; \quad \dot{x}_3 = a_3 x_1 x_2 \tag{4}$$

They can be realized as a Hamilton–Poisson mechanical system with the phase space R^3, the Poisson structure given by the matrix

$$\Pi_{RB} = \begin{bmatrix} 0 & -x_3 & x_2 \\ x_3 & 0 & -x_1 \\ -x_2 & x_1 & 0 \end{bmatrix}$$

and the Hamiltonian H given by

$$H = \frac{1}{2}\left[\frac{x_1^2}{I_1} + \frac{x_2^2}{I_2} + \frac{x_3^2}{I_3}\right].$$

The symplectic leaves of our Poisson manifold (R^3, Π_{RB}) are the pairs $(\mathcal{O}'_k, \omega'_k)$, where

$$\mathcal{O}'_k = \{(x_1, x_2, x_3) \in R^3 \,|\, x_1^2 + x_2^2 + x_3^2 = k^2\},$$

and

$$\omega'_k = \frac{1}{k}(x_2 dx_1 \wedge dx_3 - x_3 dx_1 \wedge dx_2 - x_1 dx_2 \wedge dx_3).$$

The Lie–Trotter formula (1) gives rise to an explicit Poisson integrator for the Eq. (4), namely:

$$[x_1^{k+1}, x_2^{k+1}, x_3^{k+1}] = ABC[x_1^k, x_2^k, x_3^k]^t. \tag{5}$$

where A, B, C are respectively the flows of the Hamiltonian vector fields $X_{x_1^2/2I_1}$, $X_{x_2^2/2I_2}$, $X_{x_3^2/2I_3}$. Moreover, its restriction to the coadjoint orbits $(\mathcal{O}'_k, \omega'_k)$ gives rise to an explicit symplectic integrator.

Let us finish with the observation that similar results also hold for the rigid body dynamics with a spinning rotor.

Acknowledgements. I want to express here all my thanks to Professors J. Marsden and T.Ratiu for some stimulating discussions on this topic.

References

Hüper, K., Paul, S. & Pauli, R. [1995] "Isospectral matrix flow and Lie–Poisson integrators", Systems and networks: mathematical theory and applications vol. 2 - invited and contributed papers, eds. Helmke, U., Mennicken, R. & Sauer, J. (Mathematical Research vol. 79, Akademie Verlag), 239–245.

McLachlan, R.I. [1993] "Explicit Lie-Poisson integration and Euler equations", *Phys. Rev. Lett.* **71**, 3043–3046.

Trotter, H.F. [1959] "On the product of semigroups of operators", *Proc. Amer. Math. Soc.* **10**, 545–551.

Wisdom, J. & Holman, M. [1991] "Symplectic maps for the N–body problem", *Astron. J.* **102**, 1528–1538.

ATTRACTOR-BASIN SUDDEN BIFURCATION MECHANISMS IN NONLINEAR STRUCTURAL DYNAMICS

G. Rega[†] and A. Salvatori[‡]
[†] Dipartimento di Ingegneria Strutturale e Geotecnica
Università di Roma "La Sapienza", via A. Gramsci 53, 00195 Roma, Italy
[‡] Dipartimento di Ingegneria delle Strutture, delle Acque e del Terreno
Università di L'Aquila, Monteluco di Roio, 67040 L'Aquila, Italy

Abstract: The nonlinear oscillations of an elastic suspended cable are analyzed through different geometrical and computational tools. In particular, cell mapping, chaotic saddle analysis and invariant manifolds evolution allow to deeply investigate bifurcations, crises and chaotic phenomena for a sdof model representing the in-plane motion of the cable. A complete computational and geometrical study is performed both in the $\frac{1}{2}$ and $\frac{1}{3}$ subharmonic resonance ranges, highlighting the main rôle played by direct and inverse saddles in the continuing evolution of the attractors and of their basins of attraction.

1. Introduction

Nonlinear modelling in the dynamics of structural systems is strictly related to the availability of techniques suitable to furnish understanding of the relevant complicated behaviour. Though some mdof models have recently been developed to describe various response aspects, the numerical and geometrical analysis of simple sdof models still allows to gain deep insight into some main bifurcational and chaotic phenomena of the system, not yet completely understood. Here the attention is focused on the understanding of sudden change mechanisms [Park *et al.*, 1992], which furnishes detailed information about the global dynamics of the nonlinear system. The approach followed consists in a combined bifurcational analysis of the attractor-basin-manifold-phase-portrait structure, and of the whole chaotic saddle [Lai *et al.*, 1992]. Reference is made to the sdof nonlinear equation:

$$\ddot{q} + \mu\dot{q} + q + c_2 q^2 + c_3 q^3 = P\cos(\Omega t) \qquad (1)$$

which describes the finite dynamics of an elastic suspended cable vibrating under harmonic forcing with its first in-plane symmetric mode [Rega *et al.*, 1995], and which exhibits several nonlinear dynamic phenomena: primary, subharmonic and superharmonic resonances, due to quadratic and cubic terms, various local and global bifurcations, multiple coexisting regular and strange attractors, crises entailing sudden evolutions of chaotic attractors, fractal basin boundaries involving the chaotic saddle, which also determines the topology and evolution of chaotic attractors in state space [Rega & Salvatori, 1996].

2. Attractor-Basin-Manifold-Phase-Portrait for Characterization of Global Dynamics.

Analysis of bifurcation and chaotic dynamics of Eq. (1) has been made in the neighbourhood of the $\frac{1}{2}$ and $\frac{1}{3}$ subharmonic resonances [Rega *et al.*, 1995], [Rega & Salvatori, 1996]. Here some further interesting results are reported. Together with path following curves, cell mapping and bifurcation diagrams give an overall picture of global

attractor-basin structure, and a pictorial introduction to the crises phenomena. Moreover, the superimposition of basins of attraction and manifolds of saddle points gives the construction of attractor-basin-manifold phase portraits (ABMPP) allowing a complete topological interpretation of crisis phenomena in terms of intersection of stable and unstable manifolds of direct or inverse saddles, which involves homoclinic and heteroclinic tangencies.

When varying a control parameter, attention is focused on the merging and switching crises (interior crises of the first and second kind), occurrying in the ABMPP. These crises deeply involve a local/global evolution of chaotic attractors with meaningful rôle played by various geometrical entities: the direct (inverse) saddles of some periodic solution, their relevant stable (unstable) manifolds $W_j^{s(u)}(D_i^k)$, $W_j^{s(u)}(I_i^k)$, the chaotic saddle and the chaotic attractors. All these geometric entities are obviously correlated to the basins of attraction of the actual solution of the nonlinear system (1). Interior crises play a relevant rôle in the evolution in shape and size of chaotic attractors, in conjunction with topology of chaotic saddle, which also determines the evolution of the complete ABMPP [Park *et al.*, 1992]. That's why main attention will be focused on some mechanisms which determine the interior crises 1 and 2 in Eq. (1).

3. Merging Crisis: Multi-Band Chaotic Attractors, Invariant Manifolds and Chaotic Saddle.

Interior crises 1 involve the sudden enlargement in size of the $n-$band chaotic attractor together with its band-halving. In Eq. (1) behaviour of this kind can been easily seen both in $\frac{1}{2}$ and in $\frac{1}{3}$ subharmonic ranges, (for example, at the values $P = 0.04$, $\Omega = 1.817$, and $P = 0.40$, $\Omega = 4.03$ respectively). In Fig. 1 ($\frac{1}{2}$-subharmonic range) mergings of the 4 bands of the C^4 chaotic attractor to form a 2-bands C^2 chaotic attractor, which definitely merge into a broad chaotic attractor C, are shown together with the relevant inverse saddle (I^4,I^2,I^1) stable and unstable manifolds responsible for the heteroclinic tangles, and with the chaotic saddles. It's worth noticing that this crisis, which is local to the basin of the chaotic attractor, is caused by *heteroclinic tangle* $W_j^s(I_i^{n/2}) \cap W_k^u(I_h^n)$, (where n is the number of band of C^n). The chaotic attractor which enlarges itself by this tangle, really touches an infinite number of times the stable manifold $W_j^s(I_i^{n/2})$, in this manner tresspassing the inaccessibility topological boundary represented by this manifold in its own domain of attraction; this implies that, in this case of interior crisis 1, $\overline{W_k^u(I_h^n)} \supset C_p^n$. It can be properly conjectured that these manifolds belong, all together, to the chaotic saddle, which is formed by the union of the infinitely existing unstable periodic orbits due to classical evolution of secondary attractors (i.e., generation by saddle-node bifurcation, period doubling to chaos, boundary crisis due to its own direct saddle generated by the same SN, and collection of all direct and inverse saddles, to form the chaotic saddle).

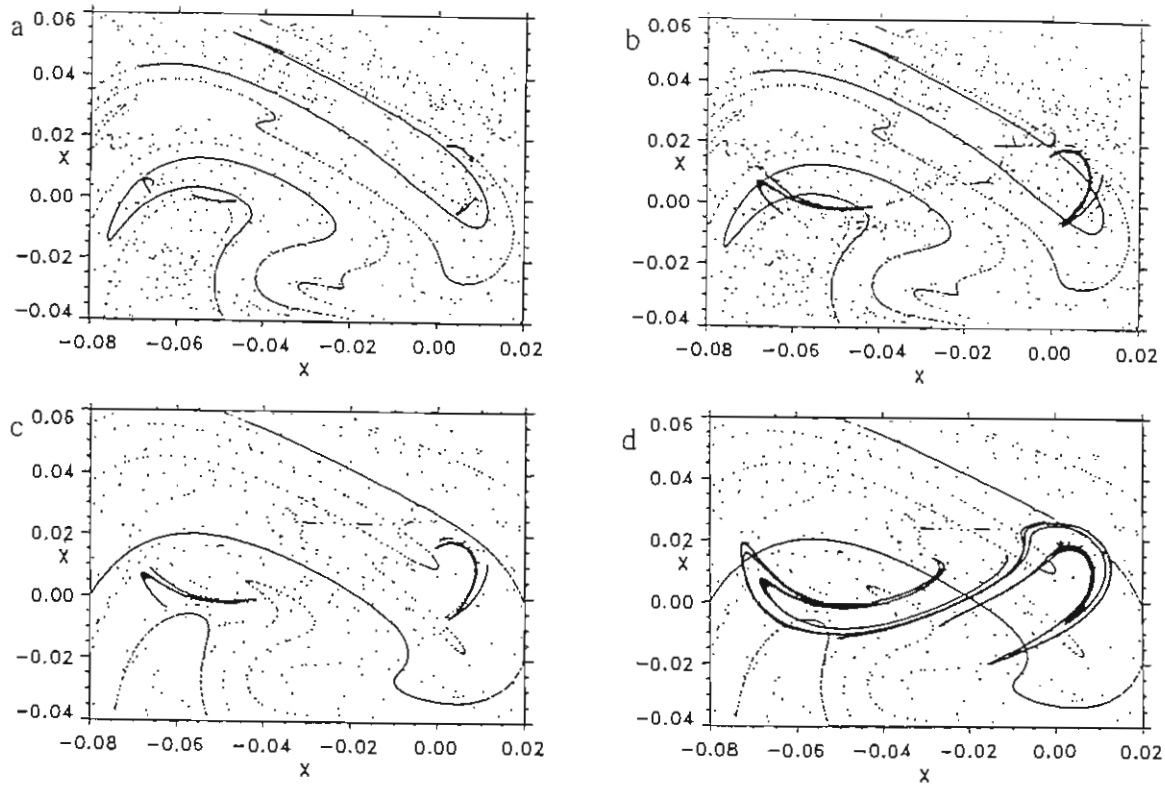

Figure 1: Interior crisis 1, $P = 0.04$, $\Omega = 1.827$ (a-b), $\Omega = 1.8267$ (c-d)

Several chaotic saddles were calculated with PIM-triple procedure [Lai et al., 1992] for Eq. (1), always showing the mechanism of englobing of chaotic saddle trajectories into the band-halving chaotic attractor, when crisis occurs.

4. Switching Crisis: Narrow-to-Large Chaotic Attractor, Invariant Manifolds and Chaotic Saddle.

Differently from previous mechanism, the interior crisis 2 depends on only one saddle. This crisis involves the chaotic attractor and the direct saddle of a secondary p-periodic solution in the control parameter space; before the crisis, its relevant stable manifolds, say $W_j^s(D_i^p)$, form a boundary which delimitates an inaccessible region inside the same domain of attraction. At the crisis a *homoclinic tangle* between stable and unstable manifolds $(W_j^s(D_i^p) \cap W_j^u(D_i^p))$ occurs, and, because of $\overline{W_k^u(D_i^p)}$ contains the narrow chaotic attractor, the latter touches an infinite number of times $W_j^s(D_i^p)$, and then tresspass the inaccessible boundary formed by it, notably enlarging itself until a new topological boundary has been reached. The chaotic attractor englobes portion of the chaotic saddle in its enlarging, after the infinite numher of tangencies with the chaotic saddle itself deriving from the homoclinic tangle mechanism evidenced before. Actually, it is also possible to identify specific saddles responsible for the enlargement. As an example, in Fig. 2 a switching crisis is shown at $P = 0.04$, $\Omega = 1.749$, where the enlargement is seen to be connected with the tangency with the D_i^5 direct saddle and its relevant stable manifold $W_j^s(D_i^5)$,

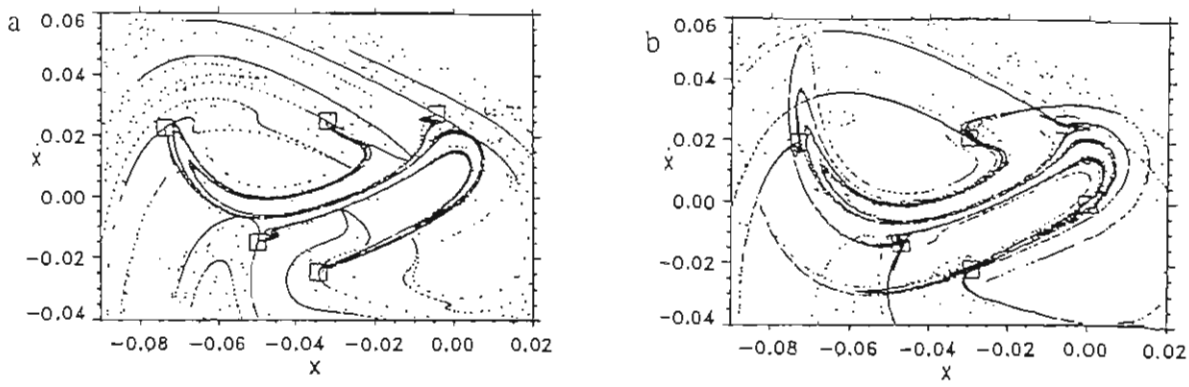

Figure 2: Interior crisis 2, $P = 0.04$, $\Omega = 1.749$ (a), $\Omega = 1.75$ (b)

(Fig. 2a); in Fig. 2 also the chaotic saddle is shown, evidencing the above mentioned englobing phenomenon, when passing through the crisis. In the $\frac{1}{3}$-subharmonic range [Rega & Salvatori, 1996] it has even been possible to identify two different enlargements associated with two very high-periodic unstable orbits belonging to the chaotic saddle, which occur in a extremely narrow range of the control parameter values.

5. Concluding Remarks.

The rôle played by the sub-domains of attraction and by their boundaries and the topology of some global bifurcation mechanisms has been highlighted. Complex and time consuming computations, concerned both with the ABMPP structure, and with the chaotic saddle, were needed to understand the complete bifurcational picture of the system. Passing to more reliable mdof models of the considered mechanical system, a question arises whether it's still possible to obtain such a deep description of the system topological and bifurcational behaviour with reasonably affordable calculations. A positive answer likely relies in using the powerfulness of parallel computing, which permits to obtain complex mdof entities at lower effort.

6. References.

Lai, Y.C., Grebogi, C. & Yorke, J.A. [1992] "Sudden Change in the Size of Chaotic Attractors: How Does it Occur?", in J.H.Kim and J.Stringer Eds., *Applied Chaos*, 441-455.

Park, B.S., Grebogi C., Lai Y.C., [1992] "Abrupt Dimension Changes at Basin Boundary Metamorphoses", *International Journal of Bifurcation and Chaos*, 2(2), 533-541.

Rega, G., Salvatori, A. & Benedettini, F. [1995] "Numerical and Geometrical Analysis of Bifurcation and Chaos for an Asymmetric Elastic Nonlinear Oscillator", *Nonlinear Dynamics*, 7, 249-272.

Rega, G. & Salvatori, A. [1996] "Bifurcation Structure at $\frac{1}{3}$ Subharmonic Resonance in an Asymmetric Nonlinear Elastic Oscillator.", *International Journal of Bifurcation and Chaos*, 6(8).

SELF-ORGANIZATION AND CHAOS IN ATMOSPHERE

Cz. Rymarz
Military University of Technology
01-489 Warsaw S.Kaliski str. 2 POLAND

Abstract. The coexisting phenomena of self-organization and deterministic chaos can form some sequence, which consists of three parts: Birth - Evolution - Death modelling living systems. Such kinds of systems are universal in atmosphere (fronts and cyclones). In this lecture the modern thermodynamics of processes running far from the equilibrium has been used for investigations of atmospheric instabilities of westerly, zonal flow. These are instabilities of the type of self-organization. To investigate these instabilities or unstable processes, the method of Lapunov function has been applied. Following the procedure of non-equilibrium thermodynamics, the necessary conditions for zonal barotropic and baroclinic instabilities of the self-organization type have been formulated. The simple example of the sequence of phenomena from a heat conductivity to deterministic chaos, induced by the gradient of temperture is presented.

1. Introduction

Self-organization and chaos phenomena neighbour each other forming some sequence. They produce an order and disorder. They belong to different philosophical categories. Disorder, according to the general conclusion of classical thermodynamics, is growing permanently (entropy's production), and the useful energy is degradating. As a consequence the Universe should tend to the thermal death.The universal observations contradict this pessimistic philosophy. It is a living matter, which exists due to evolution and to a growing of order or organization. The coexistence of these opposite phenomena creates the following threefold sequence, which can be treated as an essence of the life

$$\textbf{BIRTH} \Rightarrow \textbf{EVOLUTION} \Rightarrow \textbf{DEATH}$$

Such a kind of sequences is very universal in the terrestrial atmosphere. Atmospheric fronts, cyclones (cetnres of low pressure) and other organized strutures appear in some area, pass serie of transformations, which being stable, allow them to survive some period, and after that they desapear. Hence we can say, that the atmosphere is some kind of living structure, and the weather can be predicted for the period of the „life" of atmospheric structure.

The phenomena of self-organization and deterministic chaos have been investigated by D.Benard (self-organization) and E.N. Lorenz separatelly, applying different theoretical approaches. In the first case the theory of non-equilibrium thermodynamics for processes far from equilibrium in variational formulation has been applied. In the second case the procedure of dynamics' analysis of nonlinear system has been used. In both approaches systems of nonlinear PDE or ODE are solved numerically. If the self-organization is investigated, the solutions' of PDE, modeling the dynamic of atmosphere, are used for calculation of excess entropy production. When this production in running process is negative, the self-organizing phenomena in system may take place (necessary condition). For the case of deterministic chaos

the solutions of ODE or trajectories in the phase space are analysed, for finding they singularities and strange atractors. The both mehods are modern, promising and effective, and are able to follow runnig unstable processes, not only the threshold parameters of instsbilities like in the classical approach.

The aims of this lecture is to present the following contributions in compact form:

- thermodynamic global approch to investigation of two kinds of main atmospheric instabilities of a self-organization type,
- linearized method for analysing the sequence, which models the atmospheric „life", it means heat conductivity, convective instability and chaos.

More informations on the first subject can be find in [2],[3].

2. Barotropic and baroclinic instabilities of the type of self-organization.

I. Prigogine and P. Glansdorff formulated the modern thermodynamics of processes running far from an equilibrium [1] . It allows to investigate the phenomena of self-organization , which can occur in such processes. The necessary conditions for the self-organization to appear are:

-nonlinearity in the investigated process ,

- remaining it far from the thermodynamic equilibrium,

-existing of bifurcation points and enough great fluctuations in their vicinity.

Since fluctuations can be great, the linear approximation is invalide and global formulation of the instability criterion should be proposed. The Lapunov function (functional) of the following form is proposed

$$L = \delta^2(Z) = \delta^2 \int_V (\rho z) dv = \int_V \delta^2 (\rho z) dv \qquad (1)$$

where $\delta^2(\rho z)$ - second variation of the ρz function, where ρ is mass density, and s entropy

$$z = s - T^{-1} v^2 \qquad (2)$$

It can be proved that the above definition satisfies the requirements for Lapunov function, when the following condition for local thermodynamic equilibrium is true

$$\delta^2(\rho z) < 0 \qquad (3)$$

This condition for the process to be negative definete is satisfied in majority of the real situations The main condition for thermodynamical stability is following:

$$\partial_t(\delta^2 S) > 0 \quad \text{or} \quad \partial_t \int_V \delta^2(\rho z)dv > 0 \tag{4}$$

If this condition is satisfied, the non-equilibrium process is stable, what means that excess entropy or disorder is growing. In the opposite case the production of excess entropy is decreasing in time and the order or organization is growing. It can be interpreted that useful potential or kinetic energies prevail over the dissipations. Hence to recognize that, the organization is growing, one need to check as the relations (4) is satisfied. It can be done for real data of the actually going process.

The balance of the excess entropy has the following form:

$$\frac{\partial}{\partial t}\left[\delta^2(\rho z)\right] = \sigma\left[\rho z\right] - \Phi_{j,j} \tag{5}$$

were $\sigma(\rho z)$ is the excess entropy production and Φ_j the flux of the entropy. For closed sytem $\Phi_j = 0$ and the condition of stability is equivalent to the sign of integral for σ. The function σ has the following form:

$$\begin{aligned}\sigma(\rho z) = \sum_i \delta X_i \delta J_i - [\delta(\rho e)\delta v_j + \delta \sigma_{ij}\delta v_i + \tfrac{1}{2}(\delta v)^2 \rho v_j]T^{-1}_{,j} - \\ -[\delta T^{-1}\delta\sigma_{ij} - T^{-1}\delta v_i \delta(\rho v_j]v_{i,j} - \\ -[\delta T^{-1}\delta(\rho e)_{,j} - \delta T^{-1}_{,j}\delta(\rho e)]v_j - \\ -F_i\delta\rho\delta v_i + \tfrac{1}{2}T^{-1}(\delta v)^2(\rho V_j)_{,j}\end{aligned} \tag{6}$$

where

$$\sum_i \delta X_i \delta J_i = -\delta(T^{-1}\sigma_{ij})\delta v_{j,i} + \delta T^{-1}_{,j}\delta W_j - \delta T^{-1}\delta(\rho e v_{j,j}) \tag{7}$$

The relation for σ contains 12 or 13 terms, which consist of fluctuations δT, δv_i... and non-perturbated value T, v_i..., which describe the basic state, which stability is investigated We investigate two kinds of stabilities of zonal westerly atmospheric flow:

-barotropic, when the stationary westerly wind changes with the geographic latitude,

-baroclinic, when the stationary westerly wind changes with the altitude and temperature changes with the latitude.

In both cases the conditions for 12 or 13 terms to be negative have been established. Among them only two are always positive. They model the groving of disorder or positive entropys' production. Remaining can be positive or negative. The instability of zonal flows of

of the type of self-organization occurs and is developing, when

$$P(z) = \int_{V} \sigma(\rho z) dv < 0 \qquad (8)$$

The necessary conditions for zonal flows to remain in the unstable state of self-organization are following:

-for barotropic flow

1 for the flow- ,$\delta v > 0$, $\delta w > 0$, $\delta u \delta v > 0$ or $\delta u \delta v < 0$

2- for the deformations of the flow - $\frac{dU}{dy}(\delta u_{,y} + \delta v_{,x}) < 0$

3- for the zonal gradient of the temperature- $\delta T_{,x} > 0$

-for baroclinic flow

1. for the flow - $\delta v > 0$, $\delta w > 0$, $\delta u \delta w > 0$, or $\delta u \delta w < 0$,

2- for the gradient of temperature - $\delta T_{,x} > 0$,

3- for the deformation of the flow- $\frac{dU}{dz}(\delta u_{,z} + \delta w_{,x}) < 0$,

4.- energetic condition - $((\delta \mathbf{v})_{,y}^{2} + \delta \mathbf{v} \cdot \nabla \delta v) < 0$.

Applying this method some preliminary results for the barotropic flow have been obtained. They was performed at assumed atmospheric fields stationary and perturbated being comparable with the stationary ones, since the self-organization phenomena run at the great fluctuations.

3. Example containing self- organization and chaos

It is for the generalized Benard poblem. Applying the known Lorenz approach the problem of the Benard instability is reduced to the set of three nonlinear ODE. Following the known procedure of linearization the eigen values and eigen vectors have been determined. Analyzing the changes of eigen values in function of the gradient of temperature, we observe in layer of the fluid heated from below, the transitions of the states from the thermal conductivity by the convective Benards' stracure to the chaotic instabilities. More informations on this subject will be given at the lecture.

4 References

1. Glansdorff P. & Prigogine I. [1970], Thermodynamic Theory of Structure. Stability an Fluctuations (Wiley-Interscience)
2 Rymarz Cz. [1995], „Barotropic instability of the type of self-organization in westerly zonal flow, *Journ. Tech. Phys.*, **36**, 4, 501-515.
3 Rymarz Cz.. [1996], „Baroclinic instability of the type of self-organization in westerly zonal flow", *Journ.Tech.Phys.*, **37**, 1, 51-65.

3-D CHAOS IN THE THIN ELASTIC ROD

E.L. Starostin

Keldysh Institute of Applied Mathematics, Russian Academy of Sciences,

Miusskaya Sq. 4, 125047 Moscow, Russia

Abstract: Equilibrium shapes of a thin homogeneous elastic rod are considered. It is assumed that the rod is straight and twisted in its relaxed state and it is submitted to external forces at its ends only. The torsional stiffness and two principal bending stiffnesses are assumed to be constant and all different. The initial twisting rate is also taken to be constant along the rod. These assumptions turn out to be sufficient to produce chaotic 3-D shapes of the rod. The phase space of the system under consideration is investigated by reducing it to a mapping of two-dimensional Poincaré sections. The results obtained are illustrated graphically.

1. Introduction

Equilibrium shapes of a thin homogeneous elastic rod obey equations identical to those governing the rotation of a gyrostat spinning about a fixed point in a constant homogeneous gravitational field (the Kirchhoff analogy). The equations are integrable when the rod has a circular cross section and its bending stiffness coefficients are equal. This model has been widely used for investigation of shapes of a DNA molecule, e. g., see [Šelepová & Kypr, 1985]. Equilibrium configurations of the axisymmetric rod closed into a ring were studied in [Starostin, 1996].

On the other hand, the problems of spatial chaos were considered in [Davies & Moon, 1993] for an infinitely long elastic rod for two cases: when one of bending stiffness coefficients or initial curvatures changes periodically along the rod while all other stiffnesses and initial curvatures are constant.

In this paper, the torsional stiffness and two principal bending stiffnesses are assumed to be constant and different. The initial twisting rate is also taken to be constant along the rod. These assumptions turn out to be sufficient to produce chaotic 3-D shapes of the rod. It should be noted that chaos is treated here in the limiting sense [El Naschie & Kapitaniak, 1990].

The phase space of the system under consideration may be investigated by reducing it to a mapping of two-dimensional Poincaré sections. The Poincaré maps were built numerically for various values of parameters of the rod. Different choice of Poincaré sections was tried in order to obtain thorough data on the whole phase space structure. The maximum Lyapunov exponents were computed to identify chaotic trajectories and to characterize the level of chaoticity. The results obtained are illustrated graphically.

2. Equations

We consider an initially curved and/or twisted thin elastic rod which is deformed by the forces and moments at its ends only. Its equilibrium state is described by the following

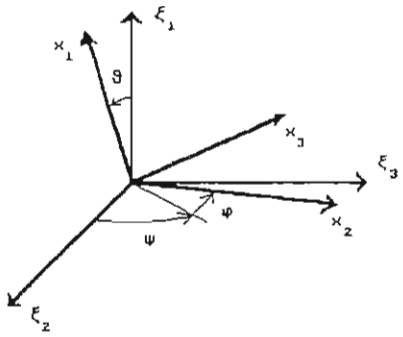

Figure 1: The Euler angles ψ, φ, and ϑ specify the attitude of the principal axes of bending and twisting $x_1x_2x_3$ with respect to the coordinate system $\xi_1\xi_2\xi_3$ fixed in space. The axis x_1 is along the center line of the rod. The direction of the axis ξ_1 is coincident with the direction of the end force.

system of differential equations [Ilyukhin, 1979]:

$$b\frac{d\omega_1}{ds} + c\omega_2(\omega_3 - \omega_3^0) - \omega_3(\omega_2 - \omega_2^0) = 0, \tag{1}$$

$$\frac{d\omega_2}{ds} + b\omega_3(\omega_1 - \omega_1^0) - c\omega_1(\omega_3 - \omega_3^0) - \frac{p}{2}\sin\vartheta\cos\varphi = 0,$$

$$c\frac{d\omega_3}{ds} - b\omega_2(\omega_1 - \omega_1^0) + \frac{p}{2}\sin\vartheta\sin\varphi = 0,$$

where ω_1 is the torsion of the cross section about the tangent to the center line of the rod, ω_2 and ω_3 are projections of the curvature of the center line onto the principal axes of bending, s the arc coordinate along the center line, which extension is neglected, ω_1^0 an initial value of the torsion in the relaxed state, ω_2^0 and ω_3^0 initial values of the curvature projections in the relaxed state, $b = B_{11}/B_{22}, c = B_{33}/B_{22}(B_{22} \neq 0), B_{11}$ the torsional stiffness coefficient, B_{22} and B_{33} the principal bending stiffness coefficients, $p = -2P/B_{22}, P$ the value of the end force.

The attitude of the principal axes of bending and twisting $x_1x_2x_3$ with respect to the fixed coordinate system $\xi_1\xi_2\xi_3$ is given by the three Euler angles ψ, φ, ϑ (Fig. 1). The axis ξ_1 is aligned with the direction of the end force.

The vector $\vec{\omega} = (\omega_1, \omega_2, \omega_3)$ specifies the angular velocity of rotation of the axes $x_1x_2x_3$ with respect to the fixed coordinate system. An analog of the Euler kinematic equations is valid

$$\frac{d\psi}{ds} = \frac{\omega_2\sin\varphi + \omega_3\cos\varphi}{\sin\vartheta}, \tag{2}$$

$$\frac{d\varphi}{ds} = \omega_1 - \cot\vartheta(\omega_2\sin\varphi + \omega_3\cos\varphi),$$

$$\frac{d\vartheta}{ds} = \omega_2\cos\varphi - \omega_3\sin\varphi.$$

The system of Eqs. (1),(2) allows for the invariants

$$b(\omega_1 - \omega_1^0)\cos\vartheta + (\omega_2 - \omega_2^0)\sin\vartheta\sin\varphi + c(\omega_3 - \omega_3^0)\sin\vartheta\cos\varphi = l, \tag{3}$$

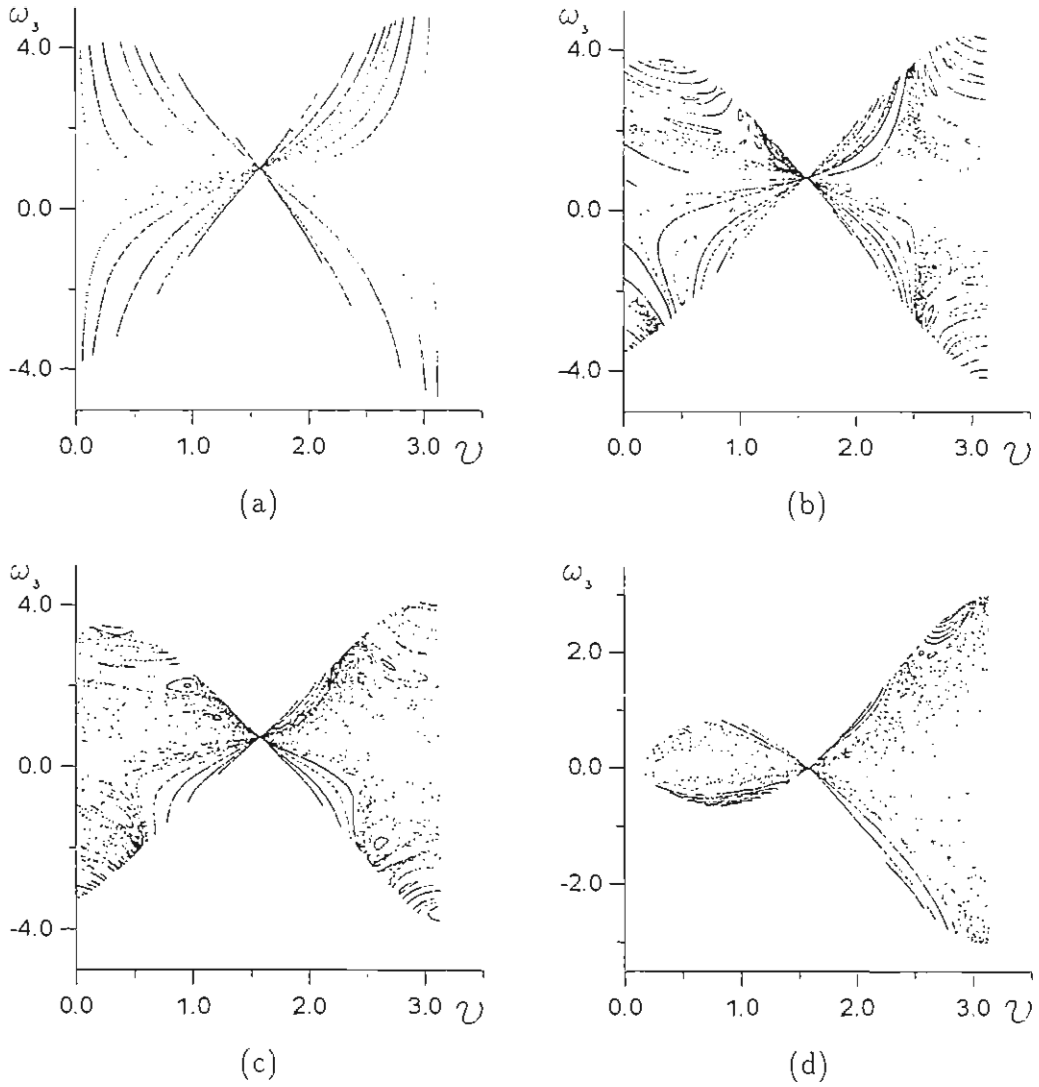

Figure 2: Poincaré maps of (ϑ, ω_3) plane. (a) $B_{11}/B_{22} = 0.8, B_{33}/B_{22} = 1.0, p = 3., l = 1., e = 20., \omega_1^0 = 0.2$. A symmetric rod, an integrable case. (b) $B_{11}/B_{22} = 0.8, B_{33}/B_{22} = 1.2, p = 3., l = 1., e = 20., \omega_1^0 = 0.2$. (c) $B_{11}/B_{22} = 0.8, B_{33}/B_{22} = 1.4, p = 3., l = 1., e = 20., \omega_1^0 = 0.2$. (d) $B_{11}/B_{22} = 0.8, B_{33}/B_{22} = 1.1, p = 5., l = 0., e = 5., \omega_1^0 = 0.2$.

$$b\omega_1^2 + \omega_2^2 + c\omega_3^2 + p\cos\vartheta = e, \tag{4}$$

3. The Poincaré Mapping

In what follows, we assume that the rod is straight in the relaxed state, then $\omega_2^0 = \omega_3^0 = 0$. However, the rod may be twisted (generally, $\omega_1^0 \neq 0$). This case corresponds to the model of DNA [Šelepová & Kypr, 1985], [Starostin, 1996].

The system (1), (2) is not integrable in the general case. Note that the variable ψ does not appear in the right sides of Eqs. (1), (2) and the first Eq. (2) may be solved after the solution of the rest 5 equations. Since the variable φ appears in the right sides as an argument of trigonometric functions, we may study the system's configurations only at the time moments when $\varphi = 2\pi k, k$ integer. The configuration is completely described by the values of $\omega_1, \omega_2, \omega_3$ and ϑ, which satisfy (3) and (4). ω_1 may be eliminated from (3)

and (4) and we obtain one equation that constrains the values of ω_2, ω_3 and ϑ:

$$b\left(\omega_1^0 + \frac{l - c\omega_3 \sin\vartheta}{b\cos\vartheta}\right)^2 + \omega_2^2 + c\omega_3^2 + p\cos\vartheta = e. \tag{5}$$

For a fixed ϑ, Eq. (5) defines a second-order curve on the plane (ω_2, ω_3). It is easy to show that this curve may be only an ellipse (real or imaginary) or a pair of imaginary straight lines having a common real point. The second case always takes place when $\vartheta = \frac{\pi}{2} : \omega_2 = 0, \omega_3 = \frac{l}{c}$.

We will consider such values of parameters when a real ellipse exist at least for some interval(s) of ϑ. Then there is a surface in the space $(\omega_2, \omega_3, \vartheta)$. We choose this surface as a surface of section and we compute the Poincaré maps of it. Numerical integration is applied to obtain the Poincaré maps.

4. Numerical Results

The Poincaré maps are presented as projections on (ϑ, ω_3) plane in Fig. 2. The maps (a)–(c) are computed for the following values of the parameters: $b = B_{11}/B_{22} = 0.8, p = 3., l = 1., e = 20.$, and $\omega_1^0 = 0.2$. The parameter $c = B_{33}/B_{22}$ was taken different: (a) $c = 1.0$, (b) $c = 1.2$, (c) $c = 1.4$. The graph (a) corresponds to the symmetric rod. This case is integrable and one can see no chaotic trajectories on the map. To the contrary, there are chaotic regions on maps (b) and (c). The more the rod differs from symmetric, the more chaotic the map appears. Also, a complex structure of the phase space can be observed in Fig. 2 (b). There exist all kinds of solutions: periodic, quasiperiodic and chaotic.

The map (d) is presented for a lower energy level $e = 5.$ and for different $p = 5.$ and $l = 0$. The rod is close to symmetrical: $c = 1.1$. However, there is a strong chaoticity of the map along with some islands of regular solutions. Further decrease in the energy implies an increase of the chaotic region. There exist such values of the parameters when no regular solutions were found.

5. Concluding Remarks

The results obtained may help in better understanding complexity of spatial configurations formed by long biopolymer molecules: DNAs, RNAs and proteins. In nature and technics, there are also many other long coiled structures which demonstrate similar properties and whose essential features may be approximately described by the same equations.

Acknowledgements

This research is supported by the Russian Foundation of Basic Research Grant No. 95-01-00308 and by INTAS Grant No. 94-0643.

References

Davies, M.A. & Moon, F.C. [1993] "3-D spatial chaos in the elastica and the spinning top: Kirchhoff analogy", *Chaos* **3**(1), 93–99.

El Naschie, M.S. & Kapitaniak, T. [1990] "Soliton chaos models for mechanical and biological elastic chains", *Physics Letters A* **147**(5, 6) 275–281.

Ilyukhin, A.A. [1979] *Spatial Problems of the Nonlinear Theory of Elastic Rods* (Naukova Dumka, Kiev) Chap. 1, pp. 7–34 [in Russian].

Šelepová, P. & Kypr, J. [1985] "Computer simulation of DNA supercoiling in a simple elastomechanical approximation", *Biopolymers* **24**, 867–882.

Starostin, E.L. [1996] "Three-dimensional conformations of looped DNA", *Meccanica* [in press].

THE ANALYSIS OF CHAOTIC BEHAVIOUR USING FRACTAL AND WAVELET THEORY

W.J. Staszewski and K. Worden
Department of Mechanical and Process Engineering
University of Sheffield
Mappin Street, Sheffield S1 3JD, UK

Abstract: The continuous and orthogonal wavelet transform is used to analyse chaotic behaviour. The analysis involves signal decomposition into the scale components. Statistical measures of similarity are applied to study chaotic vibration. The Ueda oscillator is used as an example.

1. Introduction

Methods of diagnosing chaos can be divided in two major groups: non-parametric techniques (power spectra, Lyapunov exponents, correlation dimensions, Poincare sections, etc.) and prediction-based techniques (based on prediction errors). Variance and correlation analysis only provide statistical information about the system. This can be dynamically inappropriate and further analysis of nonlinear dynamics is necessary.

Recent years have shown increased interest in wavelet-based fractal analysis [Wornell 1996]. Statistical analysis, when combined with wavelets, can provide useful information about chaos. One of the forms of fractal geometry arises from statistical scaling behaviour of physical systems. This can be studied using the variances and correlations of wavelet coefficients.

2. Wavelet Theory

For the sake of completeness a brief description of the relevant wavelet theory is given. More detailed analysis can be found in [Chui 1992]. Let $L^2(\Re)$ denote the space of measurable square-integrable functions $x(t)$ defined on $= (-\infty; +\infty)$ which represent analog signals with finite energy. The wavelet transform is a linear transformation on this space that decomposes a given function $x(t)$ into a superposition of the elementary functions $g_{a,b}(t)$ derived from an analysing wavelet $g(t)$ by scaling and translation i.e.,

$$g_{a,b}(t) = g^*(\frac{t-b}{a}) \tag{1}$$

where $*$ denotes complex conjugation, b is a translation parameter indicating the locality and a is a dilation or scale parameter. The continuous Grossman-Morlet wavelet transform is defined as,

$$W_g^x(a,b) = \frac{1}{\sqrt{a}} \int_{-\infty}^{+\infty} x(t)\, g^* \left(\frac{t-b}{a} \right) dt \tag{2}$$

For the function $g(t)$ to qualify as an analysing wavelet, it must satisfy appropriate admissibility conditions [Chui 1992]. In this paper, the Morlet wavelet function is used, defined by,

$$g(t) = e^{2\pi i f_0 |t|} e^{-\frac{|t|^2}{2}} \tag{3}$$

Using a binary dilation and a dyadic translation, the orthogonal wavelet transform can be defined. A function $g(t)$ is called an orthogonal wavelet if the family $g_{m,k}(t) = 2^{m/2} g(2^m t - k)$ forms an orthonormal basis of $L^2(\Re)$, that is $< g_{m,k}, g_{n,l} >= \delta_{m,n} \cdot \delta_{k,l}$, for all integer m, n, k, l, where $<\ ,\ >$ is the usual inner product and $\delta_{m,n}$ is the Kronecker symbol.

In the following, the wavelets of Daubechies [Chui 1992] are used in the orthogonal wavelet decomposition,

$$x(t) = \sum_{m,k} x_k^m g_{m,k}(t) \tag{4}$$

where the x_k^m are the coefficients. The orthonormal basis is obtained using Mallat's pyramid algorithm [Meyer 1993].

3. Wavelets and Fractal Dynamics

In order to show the importance of wavelet-based fractal analysis, consider a Gaussian noise process $x(t)$. The log variance of the wavelet coefficients of Gaussian noise is of the order of 2^{-m} times a constant. In fact, [Wornell 1996]

$$var\ x_n^m = \sigma^2 2^{-m} \sum_n g(2^{-m}t - n)^2 \tag{5}$$

where σ is a common standard deviation, that of the noise. Eq. (5) shows that the variances of the wavelet coefficients obey a geometric progression consistent with the structure of statistically self-similar processes. In general,

$$var\ x_n^m = \sigma^2 2^{-(2H+1)m} \tag{6}$$

where H is the self-similarity parameter; $H = -1/2$ for Gaussian noise. It can be shown that there is strong relationship between the self-similarity parameter H and the fractal dimension D of the signal $x(t)$ considered as a curve in $\Re^2$. In fact, if $0 < H < 1$, then $D = 2 - H$ [Wornell, 1996]. It can further be shown that if the noise is a 1/f process, i.e. has a spectrum of the form,

$$S_x(\omega) = \frac{\sigma_x^2}{|\omega|^\gamma} \tag{7}$$

that $\gamma = 2H + 1$.

The normalised wavelet correlation can be defined as [Wornell, 1996],

$$\rho_{n,n-l}^{m,m} = \frac{E\left[x_n^m x_{n-l}^m\right]}{\sqrt{(var\ x_n^m)(var\ x_{n-l}^m)}} \tag{8}$$

and, for a given value of scale m, the normalised wavelet correlation is a function of lag l only. Wavelet coefficients of Gaussian noise are uncorrelated and form an independent family of Gaussian random variables.

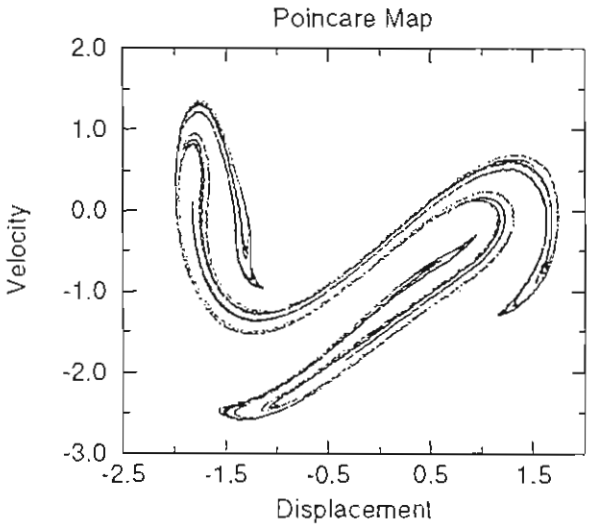

Figure 1. Poincare map for Ueda system.

4. Simulation Results

In order to show the usefulness of the wavelet transform for the study of chaotic behaviour, the Ueda variant of the Duffing oscillator [Ueda 1985],

$$\ddot{y} + 0.1\dot{y} + y^3 = 11.5\sin(t) \tag{9}$$

is analysed using the continuous and orthogonal wavelet transform. Fig. 1 shows the Poincare map of simulated data from the Ueda oscillator; the chaotic nature of the system

can be clearly observed. Fig. 2 gives the phase of the continuous wavelet transform of the data $y(t)$. The random convergence points of the constant phase lines can be observed in the transform from Gaussian white noise (Fig. 2a) The chaotic behaviour of the Ueda oscillator produces a transform with a higher degree of order in the distribution of the convergence points.

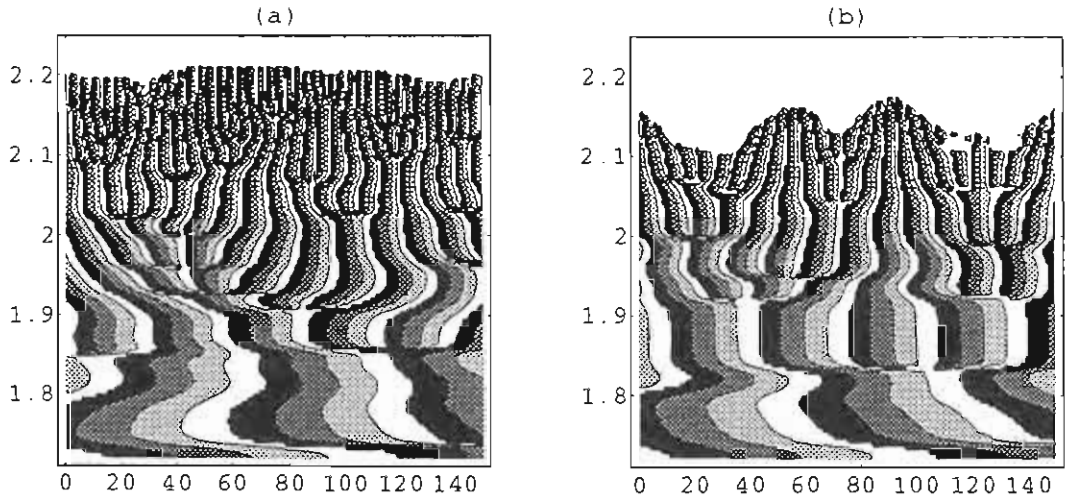

Figure 2. Wavelet phase for (a) Gaussian noise (b) Ueda system. Vertical axis is log scale, horizontal axis is time.

Fig. 3a shows the values of variance of the orthogonal wavelet transform of Gaussian white noise and the Ueda oscillator plotted on a semi-logarithmic scale. The self-similarity parameter $H = -1/2$ for the Gaussian white noise can be obtained from the slope of a straight line fitted to the variances. The Ueda oscillator shows different behaviour; the averaged (over l) values of the the wavelet correlation functions are presented in Fig. b3. It can be seen that the wavelet coefficients are uncorrelated for the small scale parameters in the case of the Gaussian white noise. The correlation among wavelet coefficients in the case of Ueda oscillator is small only for level $m = 7$ which corresponds to the driving frequency.

5. Conclusions

The wavelet transforms, continuous and orthogonal, show promise as a means of estimating the degree of self-similarity in chaotic time-series and thus providing a characterisation The fractal dimension of the graph $x(t)$ will follow directly if $0 < H < 1$.

References

Chui, Ch.K [1992] "*An Introduction to Wavelets.*" (Academic Press, Inc., San Diego).

Meyer, Y. [1993] "*Wavelets. Algorithms & Applications.*" (SIAM, Philadelphia).

Ueda, Y. [1985] " Random phenomena resulting from nonlinearity in the system described by Duffing's equation", *Int. J. Non-Linear Mech* **20**, 481-491.

Wornell, G.W. [1996] "*Signal Processing with Fractals: A Wavelet-Based Approach.*" (Prentice Hall PTR, Upper Saddle River, NJ).

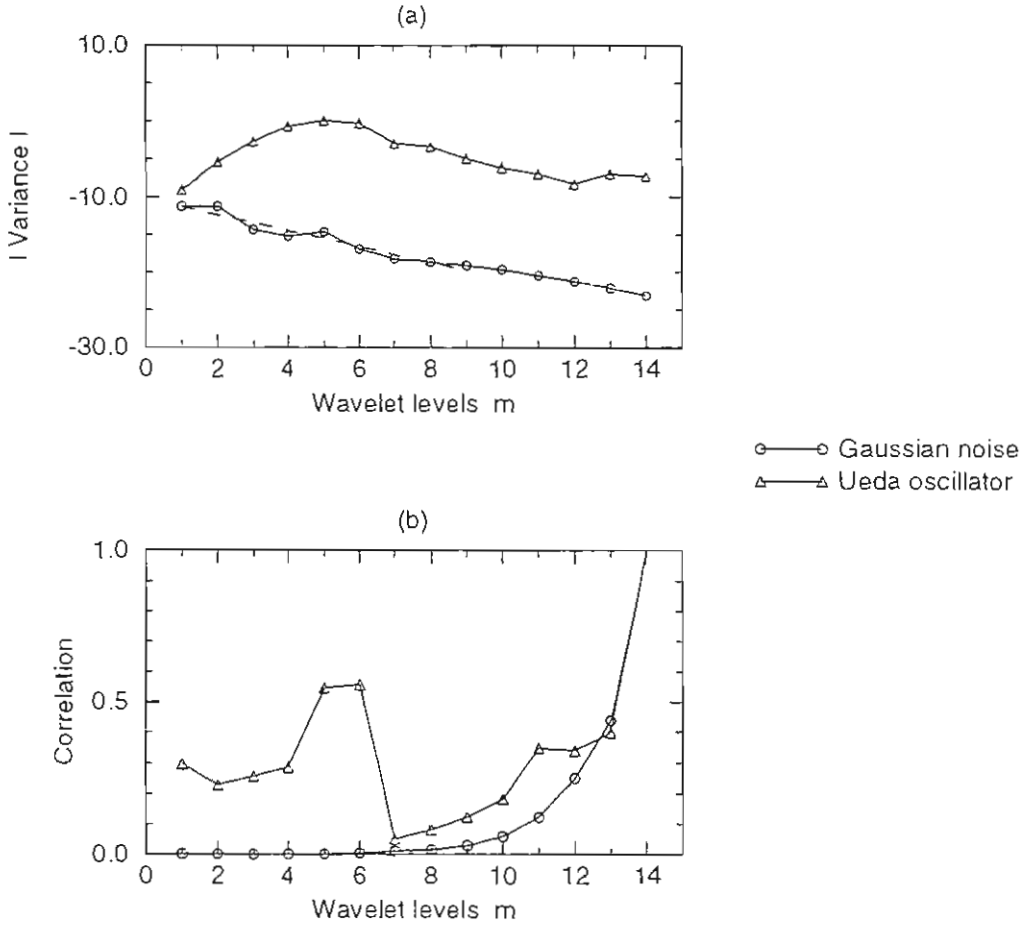

Figure 3. Coefficient variances and wavelet correlations.

Homoclinic Chaos in Bistable Optical Systems

Majid Taki

Laboratoire de Spectroscopie Hertzienne, CNRS URA 249
UFR de Physique, Universite de Lille,
59655 Villeneuve d'Ascq Cedex, France.
e-mail: taki@lsh.univ-lille1.fr

Abstract: It is shown analytically and numerically that a single-mode bistable optical system, under a modulated incident field, may undergo a chaotical behavior of Smale horseshoe type. The threshold for the onset of chaos together with the bifurcating curves for nonlinear resonances are derived semi-analytically, by means of Melnikov method, and numerically checked. We also demonstrate the existence of multistable attractors, namely, two time-periodic states and a strange attractor are shown to coexist for a certain range of parameters.

1 Introduction

The response of nonlinear dynamical systems to the external periodic forcing may exhibit a large variety of complex behavior, including phase-locked phenomena, quasiperiodicity and chaos. One of these problems is that of optical bistability (OB) which has become one of the most active fields in nonlinear optics because of the potential applications of the optical bistable devices. Although, in general, these complexe systems have high dimentional phase space, their chaotic attractors are often low dimentional, and reduced dynamical models, still provide a good theoretical description of experimental observations[1]. In this paper, we show that optical bistable systems may exhibit Smale horseshoes chaos and derive the analytical expressions for the threshold of the onset of chaos, and bifurcating curves for nonlinear resonances, by means of Melnikov method.

2 A Reduced Model System

In order to keep analysis as simple as possible, we consider the good cavity case where the transmitted field is given by[2] :

$$\kappa^{-1}\frac{dF}{dt} = y - F\left[1 + \frac{2C}{1+\Delta^2+|F|^2} + i\left(\theta - \frac{2C\Delta}{1+\Delta^2+|F|^2}\right)\right]. \qquad (1)$$

For the sake of simplicity, let us consider conditions of purely dispersive OB[2] :

$$\Delta^2 \gg 1, \quad \Delta\theta \gg 1 \quad \text{and} \quad \theta \gg \Delta.$$

In that case it is convenient to rescal F, y, and t by setting $\tau = \kappa\theta t$, $X = (\frac{\theta}{2C\Delta})^{\frac{1}{2}}F$, and $Y = (\frac{\theta}{2C\Delta})^{\frac{1}{2}}\frac{y}{\theta}$. Thus, we write Eq.(1) as a first order system :

$$\frac{dx_1}{d\tau} = y_0 + x_2\left(1 - \frac{1}{a+|X|^2}\right) - \varepsilon\left[x_1\left(\delta_1 + \frac{\delta_2}{a+|X|^2}\right) + A\sin\omega\tau\right] \qquad (2)$$

$$\frac{dx_2}{d\tau} = -x_1\left(1 - \frac{1}{a+|X|^2}\right) - \varepsilon x_2\left(\delta_1 + \frac{\delta_2}{a+|X|^2}\right) \qquad (3)$$

where $a = \frac{(1+\Delta^2)\theta}{2C\Delta}$, $\delta_1\varepsilon = \frac{1}{\theta}$, and $\delta_2\varepsilon = \frac{1}{\Delta}$. The amplitude modulation was written in the form $y = y_0 + \varepsilon A\sin\omega\tau$ where ε is a small parameter and the field variable $F = x_1 + ix_2$.

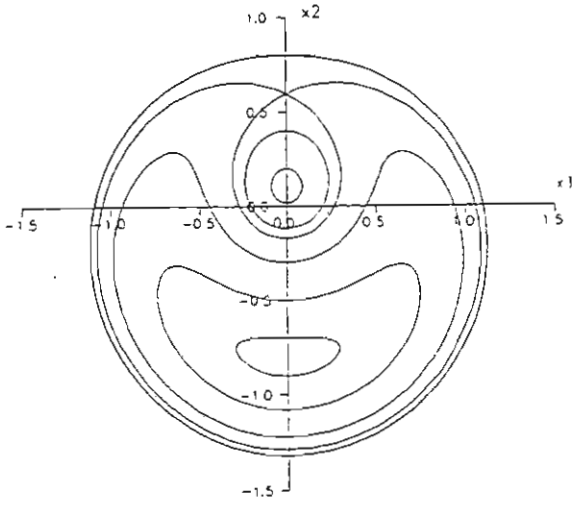

Fig. 1. The phase space of the unperturbed ($\varepsilon = 0$) system(2-3) with $a = 0.5$, and $y_0 = 0.1$. Note the heteroclinic connection

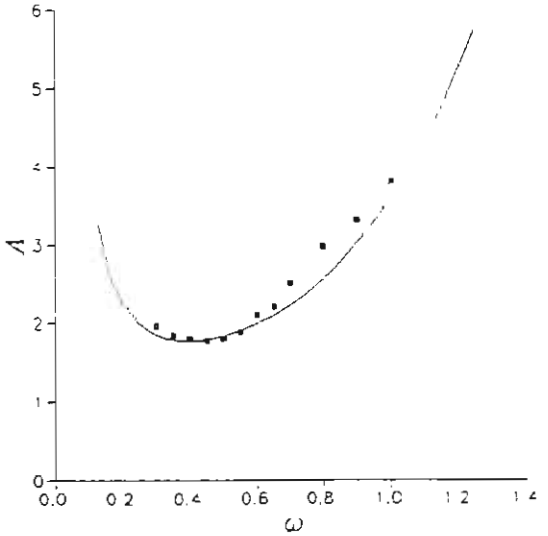

Fig. 2. The critical curve for the onset of chaos. Discrete symbols correspond to numerical thresholds of chaos. For comparison and clarity we have set the other parameters to $a = 0.5$, $\delta_1\varepsilon = \delta_2\varepsilon = 0.05$, $y_0 = 0.1$, for all figures.

3 Temporal Chaos and Nonlinear Resonances

We return now to the system(2-3) and set $\varepsilon = 0$, the unperturbed Hamiltonian reads :

$$H(x_1, x_2) = \frac{1}{2}({x_1}^2 + {x_2}^2) + x_2 y_0 - \frac{1}{2}\ln(a + {x_1}^2 + {x_2}^2) + cste \qquad (4),$$

and it constitutes a one parameter family of level curves in the phase plan (x_1, x_2). Figure(1) displays the phase plan with the heteroclinic connection, via a saddle point, of

the two homoclinic loops. To evaluate the threshold of chaos, we intruduce Melnikov function $M(t_0)$ for the homoclinic loops $X_h = (x_{1,h}, x_{2,h})$ (setting h for both inner and outer loops) :

$$\begin{aligned} M(\tau_0) &= -\int_{-\infty}^{+\infty} \left(\delta_1 + \frac{\delta_2}{a+|X_h|^2}\right)\left[y_0 x_{2,h} + \left(1 - \frac{1}{a+|X_h|^2}\right)|X_h|^2\right] d\tau \\ &+ A\cos\omega\tau_0 \int_{-\infty}^{+\infty} \left(1 - \frac{1}{a+|X_h|^2}\right) x_{1,h}\sin\omega\tau\, d\tau, \end{aligned}$$

where the homoclinic loops have their time dependence determined by Eq.(4). Figure(2) shows the critical curve for the onset of chaos, which separates the parameter plan (A,ω) in two regions. Namely, the upper region where there exist, in the phase space, sets of chaotic orbits of Smale horseshoe type[3]. In the lower region no intersection can occur at all and the whole system is not chaotic. We have not shown the critical curve for the outer homoclinic loop which is similar to that of the inner one translated towards high values of the amplitude field A. Numerical thresholds for different frequencies are also illustrated in the figure, which are in a very goog agreement with the analytical predictions. We have numerically integrated the system(2-3) and the only route to chaos we have observed is the classical periode doubling route as displayed in the figure (3), for a typical value of the external frequency.

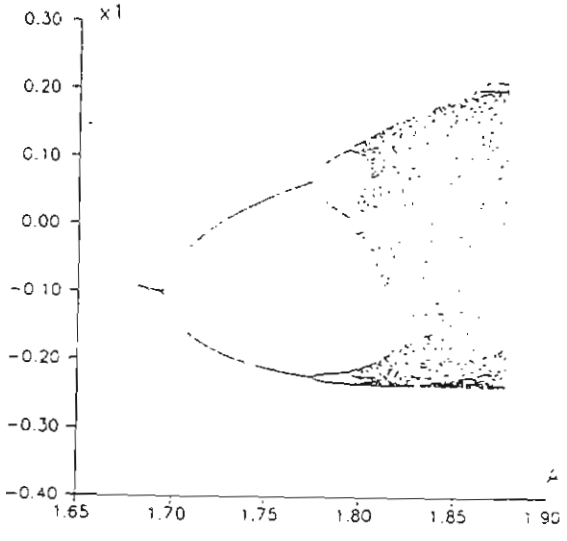

Fig. 3 Bifurcation diagram of the real part x_1 for $\omega = 0.5$

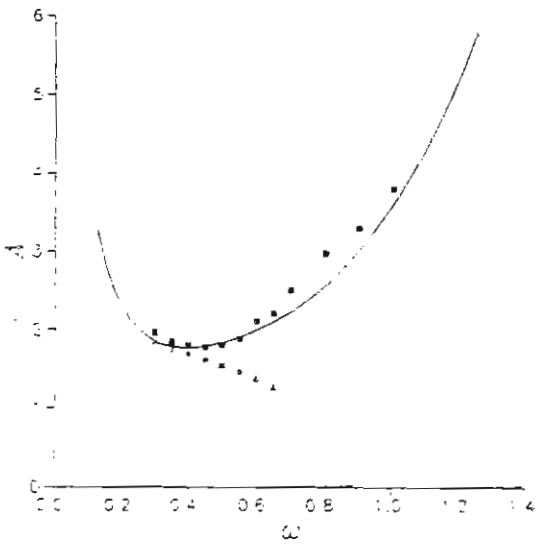

Fig. 4. Comparison between thresholds for chaos and subharmonic orbits to exist respectively. Melnikov prediction of chaos (solid line) corresponding numerical thresholds (squares ■). Melnikov thresholds for subharmonic orbites to exist (crosses ×) and coresponding numerical thresholds (triangles ▲). Note the coexistence of time-periodic states and chaos

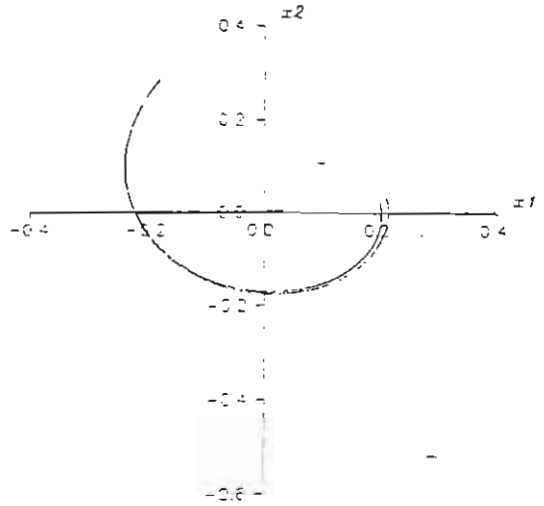

Fig. 5. Coexistence of a strange attractor and two time-periodic states in Poincaré section, where points are marked at phase $\phi = 0$ and $A = 1.577$

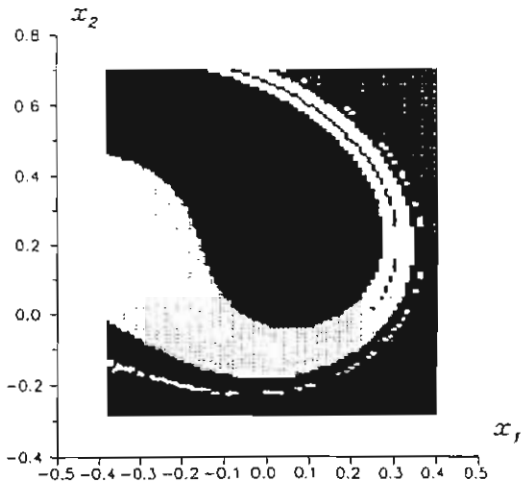

Fig. 6. Basins of coexisting attractors of fig.(5). Here, crosses denote the basin of lower time-periodic state. Black squares denote the basin of the upper one and dots denote the basin of the strange attractor

We have observed that the Smale horseshoe chaos may be related to phase-locked phenomena. Again we have evaluated Melnikov function for these resonant orbits and the agreemant is satisfactory. However, an important feature is the coexistence between the strange attractor and time-periodic states which may also be explained by Melnikov analysis. Indeed, figure(4) shows the critical value of the amplitude modulation necessary for subharmonic orbits to exist virsus frequency. Note that, for low frequencies (left on the figure) the existence of subharmonics coincides with the chaotical region. This is exactely what we have observed. Figure(5) illustrates a typical situation where two different time-periodic states coexist with a strange attractor. To get more insight about the coexistence of these states, we have shown in figure(6) the complexity of the corresponding attracting basins.

References

[1] J. Zemmouri, W. sergent, and B. Ségard, Opt.Commu. 84, 199(1991); B. Ségard and B. Macke, Phys. Rev. Lett. 60, 412 (1988).

[2] L. A. Lugiato,in *Progress in Optics*, ed. by E. Wolf (North-Holland, Amsterdam, 1984), Vol. 21.

[3] M. Taki, J. C. Fernandez, and G. Reinisch, Phys. Rev. A38,3086 (1988).

SELF-ORGANIZATION AND NONLINEAR DYNAMICS OF NUCLEIC ACID-WATER SYSTEM

M. Ye. Tolstorukov and S. V. Gatash

Radiophysics Department, Chair of Molecular and Applied Biophysics,

Kharkov State University, Svobody Sq. 4, 310077 Kharkov, Ukraine

Abstract: We proceed our research on the physical modeling of the conformational transitions in the nucleic acid molecule during the water desorption-resorption cycle. The nucleic acid-water system is considered as an open system and simulated with a trigger model. The analysis of kinetic equations and the analysis based on the nonlinear master equations show the non-trivial bifurcation behavior of the system which leads to the multistability. Besides, autowave processes, such as traveling fronts of a new conformation (trigger waves), oscillations are possible in the corresponding distributed parameter system, if the diffusion of the water molecules is taken into account. The problem of self-organization in the nucleic acid-water system is of great importance for revealing physical mechanisms of the functioning of nucleic acids and for many specific practical fields.

1. Introduction

In macromolecular systems, such as nucleic acids (NA), self-organization and nonlinear dynamic effects draw the attention of both the experimentators and theoresists, (review of Volkov [1992]).

Conformational changes of NA are tightly connected to the rebuilding of its hydration shell [Maleyev *et. al.*, 1993]. Taking into account the hydration shell of the NA and the possibility of the water content changing we are forced to consider the water+NA as an open system. In the present paper a theoretical model taking into account the interdependence of hydration and NA conformation transition processes is offered.

2. The Model

We consider a finite space, which contains the nucleic acid sample and is in contact with a bath of water or water vapor with "concentration" of water molecules equals X_e. A biopolymer molecule is simulated by the sequence of N identical units with n binding sites for water molecules. Every unit can reversibly transit between two conformational states (e.g. A- and B-form). Both the water molecule sorption and the transition of biopolymer

units are assumed to be cooperative processes. The set of the partial differential equations describes the processes of sorption and unit transitions [Tolstorukov *et. al.*]:

$$\begin{aligned} \frac{\partial X}{\partial t} &= k_x^+ X_e \left(1 - \left(1 + \frac{1}{X_e} \exp\left(\Delta F_w - \beta\theta(r) - \gamma X(r)\right)\right) X\right) + D\frac{\partial^2 X}{\partial r^2} \\ \frac{\partial \theta}{\partial t} &= k_\theta^+ \left(1 - \left(1 + \exp\left(\Delta F_p + 2\mu\left(1 - \theta(r-a) - \theta(r+a)\right) - \beta n X(r)\right)\right)\theta(r)\right) \end{aligned} \tag{1}$$

where θ- fraction of units in the B-form, X - occupied binding site fraction. Parameters of the Set (1) depend on the nature of the biopolymer considered.

3.Autowave Processes and Critical Fluctuations in the System

The treatment of the spatially independent model (with $4\mu<4$, $\gamma>4$, $\beta>0$) has been done [Tolstorukov *et. al.*, 1996]. The Set (1) has two steady, in respect to the small fluctuations, (points 1, 3 in Fig. 1) and one unsteady (point 3 in Fig. 1) stationary homogeneous solutions in some interval of the values of X_e. So, there will be the hysteresis of the equilibrium values of θ and X.

The separation of the variables on "fast" (X) and "slow" (θ) can be used to describe the inhomogeneous solutions of the Set (1). The inhomogeneous 0solutions appears to be only in the multistable interval and are described, in the "fast" phase, by the two steady traveling fronts switching the system from one steady branch of N-shaped isocline, Fig. 1, to the other one. The velocity of these waves is determined as eigenvalue of the corresponding boundary problem in the form $V = V(\theta)$ [Tolstorukov *et. al.*].

If equilibrium value of $\theta_{eq1}(\theta_{eq3})$, Fig. 1, is greater (less) than θ_c ($V(\theta_c) = 0$) the edges of the fluctuation, occurred in the initially homogeneous system, move in opposite directions, Fig. 3b, and the system is being switched to the other homogeneous state. If the value of $\theta_{eq1}(\theta_{eq3})$ is less (greater) than θ_c the edges of the fluctuation move one toward another, Fig. 3a, and fluctuation disappears for the finite time. However, very large fluctuations can trigger the system before reaching the value of $\theta_{eq} = \theta_c$. In this case fluctuation initially shrinks and then growing occupies whole volume of the system, Fig. 3a-3c, [Tolstorukov *et. al.*]. The size of these fluctuations can be estimated from following inequality: $L > 6V(\theta_{eq})\tau(X^*, X_3)$ where $\tau(X^*, X_3)$ determines the time of variation of the variable in the "slow" phase along steady branches of N-shaped null-isocline.

The trigger switching occurs only if the size of initial fluctuation is greater than some critical value [Prigogine *et. al.*, 1975]. The behavior of any small element of biopolymer with N units, coupled by diffusion of bound water molecules with other elements of

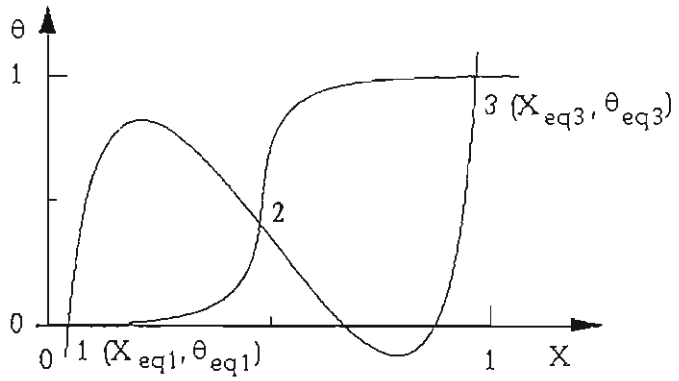

Fig.1 Phase-plane picture of set (1)

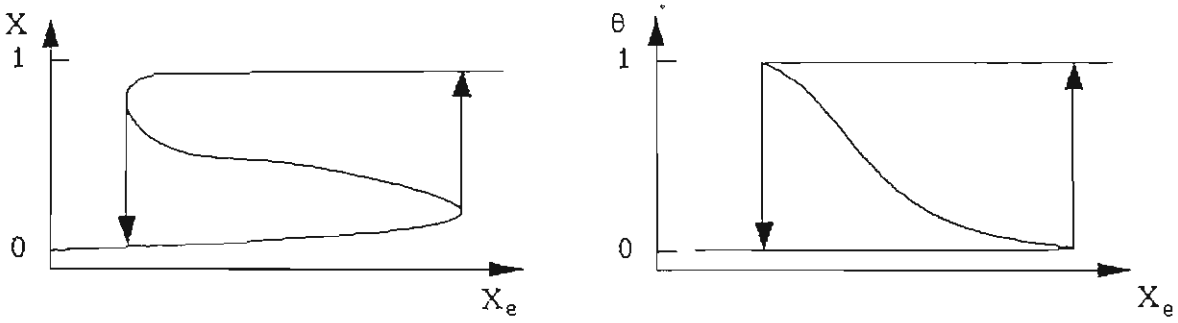

Fig. 2 Stationary homogeneous solutions of set (1)

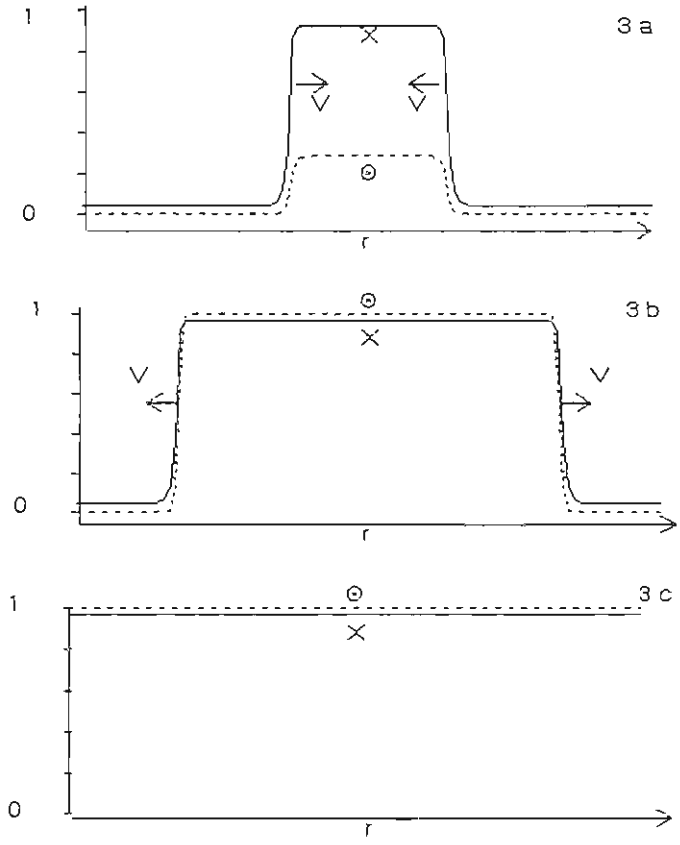

Fig.3 Evolution of the fluctuation in the initially homogeneous system (r- arbitrary units)

biopolymer, is described by a set of non linear master equations with stationary solutions (in the approximation $P(X,t) = P_X(X) \cdot P_\theta(\theta)$) in the form [Tolstorukov *et. al.*, 1996]: $P_X = P_X(X, \langle X \rangle, \langle \theta \rangle, D)$; $P_\theta = P_\theta(\theta, \langle X \rangle, \langle \theta \rangle)$, where D is the function of the fluctuation size in the form $D = f(T) \cdot S/V = F(N)$, here V and S are the volume and the surface square of considered biopolymer element. The distribution $P_\theta(\theta)$ has always a single maximum, while the distribution $P_x(X)$ has two maxima situated near the left and the right branches of N-shaped null-isocline, Fig. 1. The ratio of the maxima heights is in dependence on the value of parameter D and therefore on value of the considered biopolymer element. So, one can estimate the value of critical fluctuation N_c switching the system from one steady state to the other one. It appears that N_c is finite only if:

$$\int_{X_1}^{X_3} \ln \frac{1-x}{\frac{x}{X_e} \exp\left(\Delta F_w - \beta \langle \theta \rangle - \gamma x\right)} dx > 0 \qquad (2)$$

From Eq. (2) $(X_e)_c$ can be determined. Thus, the system has the metastable states, i.e., when the fluctuation is greater than N_c it switches the system from one steady state to the other one.

The model suggested describes the real NA-water system. The trigger systems of type, described in the paper are not studied enough, but they demonstrate complex behavior and could be applied to many practical problems. It is not hard to think very interesting biological applications of hysteresis and trigger waves in the DNA-water system.

4. References

Maleyev, V. Ya., Semenov, M. A., Gasan, A. I., Kashpur, V. A. [1993] "Physical propoties of the DNA-water system ", *Biopysics*, **38**, 789-801.

Prigogine, I., Lefever, R., Turner, J. S., Turner J. W. [1975] "Stochastic theory of metastable states and nucleation, *Physics Letters*, **51A**, 317-319.

Tolstorukov, M. Ye., Gasan, A. I., Gatash, S. V., Maleyev V. Ya. [1996] "Molecular mecanism of the sorption hysteresis in the DNA-water system", *Biophysics*, in press

Tolstorukov, M. Ye., Gatash, S. V., Maleev V. Ya., "The dynamical behavior of the macromolecule + water system", to be submitted to *Physics Letters.*

Volkov, S. N. [1990] "Development of the DNA nonlinear dynamics", *Biopolymers and Cell*, **6**, 21-31, in Russian.

DIFFUSIVE CUT-OFF OF FRACTAL SURFACES IN CHAOTIC MIXING

V. Toussaint and Ph. Carrière
Laboratoire de Mécanique des Fluides et d'Acoustique
ECL, UCB Lyon I, UMR CNRS 5509
36, avenue Guy de Collongue
69131 Ecully Cedex, FRANCE

Abstract: Results concerning the fractal properties of isovalue surfaces of a passive, diffusive scalar field being advected by a three-dimensional, steady flow exhibiting chaotic streamlines are presented. For all Péclet numbers and flow fields studied, the mixing efficiency is shown to be related to the extent of the so-called advective zone for which the capacity D is optimal in the sense of mixing ($D = 3$). For global chaos, the effective mixing time can be related to the diffusive cut-off scale which bounds this zone. For partial chaos, this cut-off corresponds to the size of the regular region which limits asymptotically the mixing.

1 Introduction

In terms of fluid mechanics, chaotic advection which means passive scalar transport by a flow exhibiting chaotic trajectories is found to provide an efficient process of mixing [Aref. 1984, Ottino, 1989].

The aim of this study is to determine some fractal properties of isovalue surfaces of a scalar field being advected by a three-dimensional, steady velocity field consisting of two two-dimensional recirculating flows with perpendicular axes of rotation (Fig. 1), defined by

$$\vec{U} = -U_1 \sin(\pi x)\cos(\pi z)\vec{e}_x - 2\,U_2 \sin(\pi y)\cos(2\pi z)\vec{e}_y$$

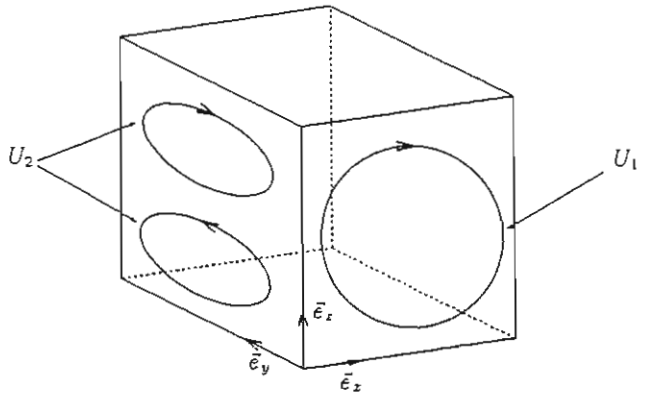

Figure 1: Sketch of the flow field.

$$+ [U_1 \cos(\pi x) \sin(\pi z) + U_2 \cos(\pi y) \sin(2\pi z)] \vec{e}_z, \tag{1}$$

where the amplitudes U_1 and U_2 of each contribution are related by

$$U_1^2 + \frac{25}{4} U_2^2 = 1, \tag{2}$$

in order to perform comparisons for comparable energy costs. The main advantage of this flow is that it allows all possible topologies of the streamlines depending on the parameter U_1. The capacity D of isoscalar surfaces (obtained by numerical simulations of the advection-diffusion equation [Toussaint *et al.*, 1995]), defined by

$$D = \lim_{r \to 0} \frac{\ln(N(r))}{\ln(1/r)}, \tag{3}$$

where $N(r)$ is the number of cubic boxes of size r necessary to cover the surface, is studied by a box-counting method for different amplitudes U_1 of the flow and different Péclet numbers.

2 Results

Figure 2 shows a typical result for the evolution of $\ln(N(r))$ for global chaos: it appears that for large scales (great values of r), $N(r)$ behaves like r^{-3}, which indicates a capacity D equal to 3; the evolution changes progressively so as to behave like r^{-2} for small r, indicating a capacity of 2. Such a behaviour is due to the relative importance of the mechanisms of advection and of diffusion at the considered scale. Thus, for great values

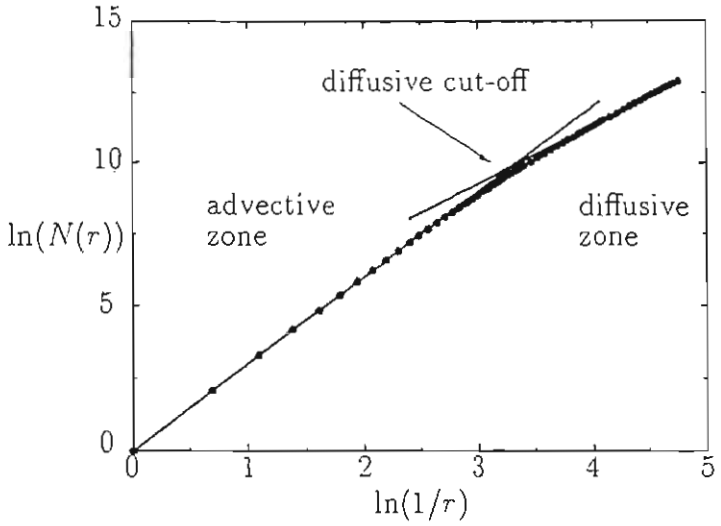

Figure 2: Typical evolution of $\ln(N(r))$ versus $\ln(1/r)$ for global chaos, here for the amplitude $U_1 = 0.25$ of the flow and the Péclet number $Pe = 10^5$.

of r, in the so-called advective zone, the surface is advected along the streamlines, it is highly stretched and folded by chaotic advection and thus has a tendency to fill the entire domain. In contrast, for small values of r, the value of D reflects the fact that the surface has been smoothed by the diffusion. The main feature is that one finds a similar behaviour of $N(r)$ for all the globally chaotic flows and the Péclet numbers considered: the difference between two configurations is due to the *extent of the advective zone* which we characterise by a diffusive cut-off scale r_D defined by the intersection of straight lines of slopes 2 and 3.

For globally chaotic flows, the scale r_D is found to decrease when the Péclet number increases, because of the fact that the mixing occurs at scales which are decreasing when the Péclet number increases. In the same way, the value of r_D decreases when the amplitude U_1 increases, reflecting the fact that the mixing is more efficient for a great amplitude U_1. The value of r_D gives thus quite a satisfactory estimate of the mixing time.

In the case of partial chaos the behaviour of $\ln(N(r))$ varies in time (Fig. 3). For times greater than 120, the cut-off scale r_D is approximately equal to 0.15 and the size of the regular region can be estimated as 0.17: this allows us to conclude again that the mixing is governed asymptotically by a diffusion mechanism at the scale of the regular region [Toussaint *et al.*, 1995]. For times smaller than 100, the cut-off does not make sense since

the asymptotic form of the surface is not attained.

References

[Aref, 1984] Aref, H. [1984] "Stirring by chaotic advection" *J. Fluid Mech.*, 143, 1–21.

[Ottino, 1989] Ottino, J. [1989] *The Kinematics of Mixing: Stirring, Chaos and Transport* Cambridge University Press.

[Toussaint *et al.*, 1995] Toussaint, V., Carrière, P., and Raynal, F. [1995] "A numerical Eulerian approach to mixing by chaotic advection" *Phys. Fluids*, 7(11), 2587–2600.

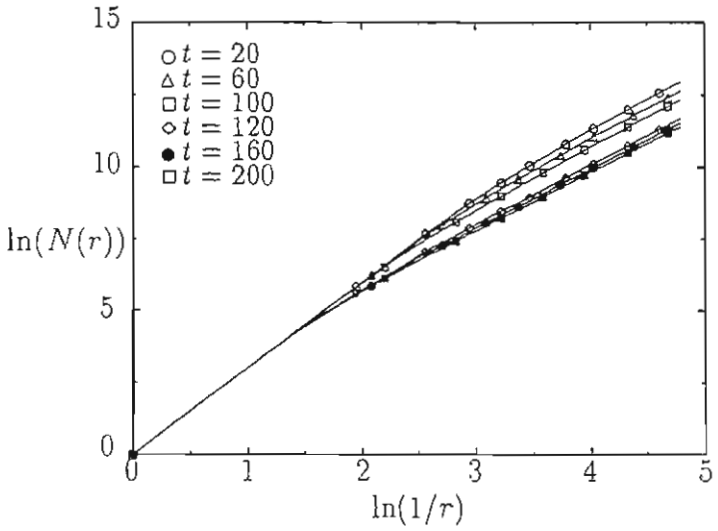

Figure 3: Evolution of $\ln(N(r))$ versus $\ln(1/r)$ for different times, the amplitude $U_1 = 0.35$ of the flow (partial chaos) and the Péclet number $Pe = 10^5$.

SYNTHESIS OF CHAOTICALLY SYNCHRONIZED SYSTEMS BASED ON OBSERVERS

Toshimitsu Ushio
Dept. of Electronic Engineering, Osaka University,
2-1 Yamadaoka, Suita, Osaka 565 Japan
E-mail: *ushio@ele.eng.osaka-u.ac.jp*

Abstract

This paper proposes an observer based approach to synthesis of chaotically synchronized systems. We consider a linear system with nonlinear feedback which exhibits chaos. Using an observer for the linear system, we design chaotically synchronized systems. Moreover, we introduce a new concept of synchronization called (M, c)-synchronization. We also propose a synthesis method for (M, c)-synchronized systems by modifying the observer based method.

1. Introduction

Chaotic synchronization has been observed in various fields. Fujisaka and Yamada[1983] showed criterion of chaotic synchronization using Lyapunov exponents. Since Pecora and Carroll[1990] proposed a synthesis method for chaotically synchronized systems, many methods have been proposed, and its applications in chaos communication are very fascinating studies[Pecora, 1993].

Synchronization systems are classified into mutual synchronization and master-slave synchronization according to coupling configuration. The former is a system with bidirectional coupling, and the latter is that with unidirectional coupling. In the Pecora-Carrol's method, master-slave synchronization is achieved if the conditional Lyapunov exponent is negative. But in general, the exponent can not be obtained in closed form so that careful experiments are required for checking the achievement of synchronization. Wu and Chua[1993] proposed a method for master-slave synchronization. Their method is very simple but the condition that a linear part of a synchronized system is stable is needed. Wu and Chua[1994] extend it by using Lyapunov functions. Moreover, Lai and Grebogi[1993] apply the OGY method to control of chaotic synchronization.

This paper proposes a synthesis method of chaotically synchronized systems applying observers which is commonly used in the control engineering field. We consider a linear system with nonlinear feedback which exhibits chaos. We can construct an observer for the linear system if it is detectable. It is shown that coupled systems with mutual synchronization and master-slave synchronization are synthesized by the observer. So the convergence to synchronized steady states are tuned by selecting an observer gain. Moreover, we introduce a new concept of synchronization called (M, c)-synchronization, and propose a synthesis method of (M, c)-synchronized systems.

This paper deals with discrete-time systems. But the same discussion also holds for continuous-time systems.

2. Nonlinear Feedback Systems and Observers

We consider a linear system S with nonlinear feedback described by

$$\begin{cases} x(k+1) &= Ax(k) + Bu(k) \\ y(k) &= Cx(k) \\ u(k) &= f(x(k)) \end{cases} \tag{1}$$

where $x(k) \in R^n$, $y(k) \in R^\ell$ and $u(k) \in R^m$ are the state, the observed output and the input of the system at time $k \in Z$ respectively, and $f : R^n \to R^m$ is a nonlinear function. We assume that the nonlinear feedback system is chaotic. We apply observer theory[Wonham, 1985] to the linear system S. Then a full-order observer for S is described by

$$z(k+1) = (A + HC)z(k) + Bu(k) - Hy(k) \tag{2}$$

where $z(k)$ is the state of the observer, and H is an $n \times \ell$ matrix such that the absolute values of all eigenvalues of $A+HC$ are less than one. Note that such a matrix H always exists if and only if the pair $(C,\ A)$ is detectable, that is, for any unstable eigenvalue λ of the matrix A,

$$\text{rank} \begin{bmatrix} \lambda I - A \\ C \end{bmatrix} = n \tag{3}$$

Moreover, all eigenvalues of $A + HC$ can be assigned arbitrarily if and only if $(C,\ A)$ is observable, that is, Eq. (3) holds for any eigenvalue λ of A.

If $A + HC$ is stable, the state $z(k)$ becomes an estimated value of the state $x(k)$, that is, for any input $u(k)$

$$\lim_{k \to \infty} \| \ x(k) - z(k) \ \| = 0$$

Thus, the convergence condition is independent of the nonlinear feedback f at all.

3. Chaotic Synchronization

In this section, It is shown that, based on the observer, we can construct various types of chaotically synchronized systems such as master-slave synchronization and mutual synchronization, and we can specify any convergence rate to the synchronized steady state by selection of H if $(C,\ A)$ is observable. If we select H such that all eigenvalues of $A+HC$ are 0, the states $x(k)$ and $z(k)$ become equal in at most n times. Such a observer is called a deadbeat observer.

3.1. Master-slave synchronization

We consider the case that all states are used for coupling. We have $C = I$ and $y(k) = x(k)$. From Eqs. (1) and (2), we can construct the following systems S_1 and S_2 coupled in master-slave configuration.

$$\begin{array}{lll} S_1 & x(k+1) &= Ax(k) + Bf(x(k)) \\ S_2 & z(k+1) &= (A+H)z(k) + Bf(x(k)) - Hx(k) \end{array}$$

where $x(k)$'s and $z(k)$'s are the states of S_1 and S_2, respectively. The system S_1 and S_2 are the master and the slave system respectively, and $x(k)$ is also a coupling signal.

Moreover, in the case that the absolute values of all eigenvalues of A are less than one, we can set $H = 0$ so that the system with $H = 0$ is equivalent to a chaotically

synchronized system obtained by the Wu and Chua's method. So the proposed method is its generalization.

We consider a chaotic output-feedback system described by

$$\boldsymbol{x}(k+1) = A\boldsymbol{x}(k) + Bf(\boldsymbol{y}(k))$$

where $f : R^{\ell} \to R^{m}$. Then, based on the above system, we can construct the following system:

$$\mathcal{S}_3 \quad \begin{cases} \boldsymbol{x}(k+1) &= A\boldsymbol{x}(k) + Bf(\boldsymbol{y}(k)) \\ \boldsymbol{y}(k) &= C\boldsymbol{x}(k) \end{cases}$$

$$\mathcal{S}_4 \quad z(k+1) = (A+HC)z(k) + Bf(\boldsymbol{y}(k)) - H\boldsymbol{y}(k)$$

where $\boldsymbol{y}(k)$ is a coupling signal. Obviously, the systems $\mathcal{S}_3$ and $\mathcal{S}_4$ are synchronized.

3.2. Mutual synchronization

Using $\boldsymbol{u}(k)$ and $\boldsymbol{y}(k)$ as coupling signals, we can construct the following coupled systems $\mathcal{S}_5$ and $\mathcal{S}_6$:

$$\mathcal{S}_5 \quad \begin{cases} \boldsymbol{x}(k+1) &= A\boldsymbol{x}(k) + B\boldsymbol{u}(k) \\ \boldsymbol{y}(k) &= C\boldsymbol{x}(k) \end{cases}$$

$$\mathcal{S}_6 \quad \begin{cases} z(k+1) &= (A+HC)z(k) + B\boldsymbol{u}(k) - HC\boldsymbol{y}(k) \\ \boldsymbol{u}(k) &= f(\boldsymbol{z}(k)) \end{cases}$$

where $\boldsymbol{x}(k)$ and $\boldsymbol{z}(k)$ are the states of $\mathcal{S}_5$ and $\mathcal{S}_6$, and $\boldsymbol{y}(k)$(resp. $\boldsymbol{u}(k)$) is a coupling signal from $\mathcal{S}_5$ to $\mathcal{S}_6$(resp. from $\mathcal{S}_6$ to $\mathcal{S}_5$).

4. A Generalization of Chaotic Synchronization

Synchronization of periodic behaviors with different phases have been reported. In chaotic synchronization, the concept of phase can not be defined because of its aperiodicity. So we propose a new type of synchronization based on linear dependence. We consider two systems whose states are denoted by $v_i(k)(i = 1, 2)$. We say that they are $(M,\ c)$-synchronized if

$$v_1(k) - Mv_2(k) = c \tag{4}$$

where M is a square matrix and c is a constant vector. If $c = 0$, then, we say simply that they are M-synchronized. As a special case, let $M = I$ and $c = 0$, and we have

$$v_1(k) - v_2(k) = 0$$

and this phenomenon is called in-phase synchronization or simply synchronization. When $M = -I$ and c = 0, it is called anti-phase synchronization. So the concept of $(M,\ c)$-synchronization is a generalization of synchronization and applied to chaotic behaviors.

We propose a synthesis method for $(M,\ c)$-synchronized systems by modifying the observer based method. We assume that M is nonsingular, and its inverse matrix M^{-1} exists. We consider the following linear system:

$$w(k+1) = M^{-1}(A+HC)Mw(k) + M^{-1}B(\boldsymbol{u}(k)+d) - M^{-1}H\boldsymbol{y}(k) \tag{5}$$

where $\boldsymbol{d}$ is a constant vector. Then we have

$$\boldsymbol{x}(k+1) - M\boldsymbol{w}(k+1) = (A+HC)(\boldsymbol{x}(k) - M\boldsymbol{w}(k)) - B\boldsymbol{d}$$

By selecting H such that $A+HC$ is stable, we have

$$\lim_{k-\infty} (\boldsymbol{x}(k) - M\boldsymbol{w}(k)) = -(I - A - HC)^{-1}B\boldsymbol{d} \tag{6}$$

Thus, we can construct $(M,\ \boldsymbol{c})$-synchronized systems based on Eq. (1) and (5). For example, we consider the following system S_7.

$$S_7 \quad \begin{cases} \boldsymbol{w}(k+1) &= M^{-1}(A+HC)M\boldsymbol{w}(k) + M^{-1}B(\boldsymbol{u}(k)+\boldsymbol{d}) - M^{-1}H\boldsymbol{y}(k) \\ \boldsymbol{u}(k) &= f(\boldsymbol{w}(k)) \end{cases}$$

Then the mutually coupled systems S_3 and S_7 are $(M,\ \boldsymbol{c})$-synchronized where $\boldsymbol{c} = -(I - A - HC)^{-1}B\boldsymbol{d}$. If A is stable, we can select $H = 0$, and the resulting system becomes an $(M,\ \boldsymbol{c})$-synchronized system in the Wu and Chua's configuration.

As an another example, we consider the following system S_8:

$$S_8 \quad \boldsymbol{w}(k+1) = M^{-1}(A+HC)M\boldsymbol{w}(k) + M^{-1}B(f(\boldsymbol{y}(k)) + \boldsymbol{d}) - M^{-1}H\boldsymbol{y}(k)$$

Then, the systems S_3 and S_8 are coupled in master-slave configuration, and $(M,\ \boldsymbol{c})$-synchronized.

5. Conclusions

This paper proposed an observer based synthesis method for chaotically synchronized systems, and introduced a concept of $(M,\ \boldsymbol{c})$-synchronization. It is noted that the proposed idea is applicable for a class of nonlinear systems for which nonlinear observers exists.

The $(M,\ \boldsymbol{c})$-synchronization can be applied to M-ary chaotic phase shift keying.

References

Fujisaka, H. & Yamada, T.[1983], "Stability theory of synchronized motion in coupled-oscillator systems", *Prog. Theor. Phys.* 69(1), 32–47.

Pecora, L. M. & Carroll, T. L.[1990], "Synchronization in chaotic systems", *Phys. Rev. Lett.* **64**(8), 821–824.

Pecora, L. M. Ed.[1993], Chaos in Communication, *Proc. SPIE* **2038**.

Wu, C. W. & Chua, L. O.[1993], "A simple way to synchronize chaotic systems with applications to secure communication systems", *Int. J. Bifurcation and Chaos* **3**(6), 1619–1627.

Wu, C. W. & Chua, L. O.[1994], "A unified framework for synchronization and control of dynamical systems", *Int. J. Bifurcation and Chaos* 4(4), 979–998.

Lai, Y.-C. & Grebogi, C.[1993], "Synchronization of chaotic trajectories using control", *Phys. Rev. E*, **47**(4), 2357–2360.

Wonham, W. M.[1985] *Linear Multivariable Control*, 3rd Edition(Springer Verlag, New York), Chap. 3.

STUDY OF THE SENSITIVE DEPENDENCE ON INITIAL CONDITIONS OF PERIODIC ORBITS OF THE FORCED PENDULUM USING NONSMOOTH TRANSFORMATIONS

Valery N. Pilipchuk
Department of Applied Mathematics
State Chemical and Technological University
Gagarin Str. 8, Dniepropetrovsk 320005, Ukraine

Alexander F. Vakakis and M.A.F. Azeez
Department of Mechanical and Industrial Engineering
University of Illinois
1206 W. Green Street, Urbana, IL 61801, USA

Abstract: We employ nonsmooth transformations to analytically construct families of strongly nonlinear periodic solutions of the harmonically forced nonlinear pendulum. Each family is parametrized by the period of oscillation, and the solutions are based on piecewise constant generating solutions. By examining the behavior of the constructed solutions for large periods, we find that the periodic orbits develop sensitive dependence on initial conditions.

1. Introduction

We study strongly nonlinear periodic motions of the forced, undamped pendulum:

$$\ddot{x}(t) + \sin x = F\cos\omega t + G\sin\omega t \qquad (1)$$

In [Wiggins, 1989].analytical methodologies for proving the existence of transverse heteroclinic intersections in the weakly forced system (1) are discussed. The existence of arbitrarily large numbers of nonlinear subharmonic orbits in (1) has been analytically proved [Veerman and Holmes, 1985]. We use the method of nonsmooth temporal transformations (NSTTs) [Pilipchuk, 1985; Vakakis et al., 1996], to study the sensitive dependence on initial conditions of strongly nonlinear subharmonic motions of (1). The analysis is carried out in neighborhoods of the heteroclinic orbits of the unforced system for O(1) forcing amplitudes F and G.

2. Analysis

The variable t is replaced by the following two nonsmooth variables (cf. Fig. 1):

$$\tau(t) = (2/\pi)\arcsin[\sin(\pi t/2)]\,,\quad e(t) = \dot{\tau}(t)\,,\quad e^2(t) = 1\,,\quad t \in R \qquad (2)$$

A periodic response x=x(t) of (1) with normalized period T=4 can be expressed as:

$$x(t) = x(\tau,e) = X(\tau) + e\,Y(\tau) \qquad (3)$$

where $X(\tau) = (1/2)[x(\tau)+x(2-\tau)]$, $Y(\tau) = (1/2)[x(\tau)-x(2-\tau)]$, $x(\tau,e) \equiv x(\tau(t),e(t))$. The derivatives $\dot{x}(t)$ and $\ddot{x}(t)$ can be expressed as smooth functions of $X(\tau)$ and $Y(\tau)$,

$$\dot{x}(t) = Y'(\tau) + eX'(\tau), \quad \ddot{x}(t) = X''(\tau) + eY''(\tau) \tag{4}$$

provided that the following smoothness (boundary) conditions are imposed:

$$Y|_{\tau=\pm1} = 0 \quad \text{and} \quad X'|_{\tau=\pm1} = 0 \tag{5}$$

Any function $f(x(t))$ of the periodic function $x(t)$ can be similarly transformed as:

$$f(x) = f(X+eY) = R_f + I_f\, e \tag{6}$$

where $R_f = (1/2)[f(X+Y)+f(X-Y)]$ and $I_f = (1/2)[f(X+Y) - f(X-Y)]$ are termed the R- and I-components of $f(x)$, respectively.

Assuming that $x=x(t)$ is a periodic solution of (1) of period $T=4a$, using (2-6), and setting the R- and I-components of the resulting equation separately equal to zero, we obtain the following two coupled nonlinear boundary value problems (NBVPs) governing $X(\tau)$ and $Y(\tau)$:

$$Y'' + (a^2/2)\,[\sin(X+Y) - \sin(X-Y)] = Fa^2\cos(\Omega_k\tau)\,, \quad Y|_{\tau=\pm1} = 0 \tag{7}$$

$$X'' + (a^2/2)\,[\sin(X+Y) + \sin(X-Y)] = Ga^2\sin(\Omega_k\tau)\,, \quad X'|_{\tau=\pm1} = 0 \tag{8}$$

where $-1 \le \tau \le +1$ (cf. Fig. 1), and the *resonance condition* $\omega a = \Omega_k \equiv (1+2k)(\pi/2)$, $k = 0,1,2,\ldots$, is imposed to indicate an integral relation between the frequency of the excitation and the frequency of the periodic response. Hence, the problem of computing the periodic responses of (1) is converted to the problem of solving the NBVPs (7-8) in the closed interval $-1 \le \tau \le +1$.

Analytic solutions of (7-8) in near-separatrix regimes of (1) are constructed as,

$$Y(\tau) = Y_0(\tau) + Y_1(\tau) + Y_2(\tau) + Y_3(\tau) + \ldots\,, \quad X(\tau) = X_0(\tau) + X_1(\tau) + X_2(\tau) + X_3(\tau) + \ldots \tag{9}$$

and the quarter-period of the motion is expressed as,

$$a^2 = a_0^2\,(1 - z_1 - z_2 - \ldots)^{-1}\,, \; O(z_i) >> O(z_{i+1})\,, \; i = 1,2,\ldots \tag{10}$$

where a_0 is the period of an 'unperturbed' periodic orbit of (1). The O(1) terms in (9) are computed as:

$$Y_0'' = 0 \Rightarrow Y_0(\tau) = +\pi, \quad X_0'' = 0 \Rightarrow X_0(\tau) = 0, \quad -1 \le \tau \le +1 \tag{11}$$

The first order solutions are computed by solving the linear BVPs,

$$Y_1'' - a_0^2\, Y_1 = F\, a_0^2\cos(\Omega_k\tau)\,, \; Y_1|_{\tau=\pm1} = -\pi$$
$$X_1'' - a_0^2\, X_1 = G\, a_0^2\sin(\Omega_k\tau)\,, \; X_1'|_{\tau=\pm1} = 0 \tag{12}$$

with solutions given by:

$$Y_1(\tau) = -\pi\cosh(a_0\tau)/\cosh(a_0) - F\cos(\Omega_k\tau)/(1+m_k^2)\,, \quad X_1(\tau) = -G\sin(\Omega_k\tau)/(1+m_k^2) \tag{13}$$

where $m_k^2 = \Omega_k^2/a_0^2$. Next, we find $Y_2(\tau) = X_2(\tau) = z_1 = 0$, and the third order BVPs:

$$Y_3'' - a_0^2\, Y_3 = z_2\,[a_0^2\, A_1\cosh(a_0\tau) - \Omega_k^2\, B_1\cos(\Omega_k\tau)] -$$
$$(a_0^2/6)\,[A_1\cosh(a_0\tau) + B_1\cos(\Omega_k\tau)]\,[\,3\,C_1^2\sin^2(\Omega_k\tau) + (A_1\cosh(a_0\tau) + B_1\cos(\Omega_k\tau))^2\,] \tag{14}$$

$$X_3'' - a_0^2\, X_3 = -z_2\,\Omega_k^2\, C_1\sin^2(\Omega_k\tau) -$$

$$(a_0^2/6)\, C_1 \sin^2(\Omega_k\tau)\, [\, C_1^2 \sin^2(\Omega_k\tau) + 3\,(A_1 \cosh(a_0\tau) + B_1 \cos(\Omega_k\tau))^2\,] \qquad (15)$$

with $Y_3|_{\tau=\pm1} = 0$ and $X_3'|_{\tau=\pm1} = 0$, and $A_1 = -\pi/\cosh(a_0)$, $B_1 = -F/(1+m_k^2)$, $C_1 = -G/(1+m_k^2)$. The solutions of the BVPs (14-15) were computed in [Pilipchuck and Vakakis, 1996]. The perturbation analysis can be carried out to higher orders of approximation using symbolic algebra.

Summarizing, the periodic motions of the forced pendulum are approximated as follows,

$$x(t) = X(\tau) + e\,Y(\tau) = \left[X_1(\tau) + X_3(\tau) + \ldots\right] + e\left[\pi + Y_1(\tau) + Y_3(\tau) + \ldots\right] \qquad (16)$$

and the quarter-period of the motion by $a^2 = a_0^2[1 - z_2 - \ldots]^{-1}$. The family of periodic solutions (16) is parametrized by the 'unperturbed' period a_0. The convergence properties of the series (16) are discussed in [Pilipchuck et.al., 1996]. At $\tau = \pm1$, the solutions develop a singularity (discontinuity in slope), which, however, is eliminated by adding higher order terms in the series. In Figure 2 we present the periodic with $\omega=1$, $F=1$, $G=10$, $k=5$, $a=17.2788$ and $a_0=7.38909$.

Setting $G=0$, keeping the amplitude and frequency of the forcing function constant, and increasing the period $a = \Omega_k/\omega \equiv (1+2k)\pi/(2\omega)$ by increasing k, the period a_0 also assumes arbitrarily large values. For $a_0 >> 1$, $m_k = \Omega_k/a_0 \rightarrow (\mu-1)^{1/2}$, where $\mu \geq 1$ is the real solution of $(\mu-1)(\mu^2-F^2/4)-\omega^2\mu^2=0$, and,

$$x(t) \sim \left[\, \pi - F\cos[\Omega_k\tau(t/a)] / (1+m_k^2) - \pi \cosh[a_0\tau(t/a)] / \cosh(a_0)\right] e(t/a) \quad \text{as } a_0 \rightarrow \infty \qquad (17)$$

$$a^2 = a_0^2[1 - z_2 - \ldots]^{-1}\ ,\quad z_2 \sim F^2/(4\mu^2) \text{ as } a_0 \rightarrow \infty \qquad (18)$$

The leading approximations dominate over higher-order ones for large periods. For $0 \leq t/a \leq 1$,

$$x(t) \sim \pi - (F/\mu)\cos\omega t - 2\pi e^{-a_0}\cosh(1-z_2)^{1/2}t\ ,\quad 0 \leq t \leq a\ ,\quad \text{as } a, a_0 \rightarrow \infty \qquad (19)$$

and we note that as a, $a_0 \rightarrow \infty$, the response is composed of an oscillatory term (the 'outer solution'), and an exponentially small nonoscillatory one ('inner solution'). Hence, the solutions are composed of localized periodic oscillations close to the unperturbed saddles $(x,\dot{x}) = (\pm\pi,0)$, and of 'jumps' in the time-scale (t/T) in the phase plane between the two neighborhoods of the unperturbed saddles. As $a_0 \rightarrow \infty$ the projections of the periodic orbits in the plane $(x,\dot{x})$ sensitive dependence on initial conditions develops. In Figure 3 periodic orbits with $\omega = 1$, $F = 1$, $G = 0$ are shown. The three orbits possess exponentially close initial conditions but eventually become O(1) apart. The orbits with $k = 4$ and 6 are nearly identical in the projection of the phase space, and the orbit with $k = 5$ nearly coincides with the other two close to $(\pm\pi,0)$ but is distinct in the region of the 'inner' solutions.

3. References

Pilipchuk V.N., 1985. The calculation of strongly nonlinear systems close to vibration-impact systems, PMM, 49 (5), pp. 572-578.

Pilipchuk V.N., Vakakis A.F., and Azeez M.A.F., 1996. Study of a class of subharmonic motions using a non-smooth temporal transformation (NSTT). Physica D (in press).

Pilipchuck V.N., and Vakakis A.F., 1996. Sensitive dependence on initial conditions of strongly nonlinear periodic orbits of the forced pendulum. Journal of Mathematical Problems in Engineering (submitted).

Vakakis A.F., Manevitch L.I., Mikhlin Yu.I., Pilipchuk V.N., and Zevin A.A., 1996. *Normal Modes and Localization in Nonlinear Systems*. Wiley Interscience, New York.

Veerman P., and Holmes P., 1986. Resonance bands in a two-DOF hamiltonian System. Physica 20D, pp. 413-422.

Wiggins S., 1990. *Introduction to Applied Nonlinear Dynamical Systems and Chaos*. Springer Verlag, Berlin and New York.

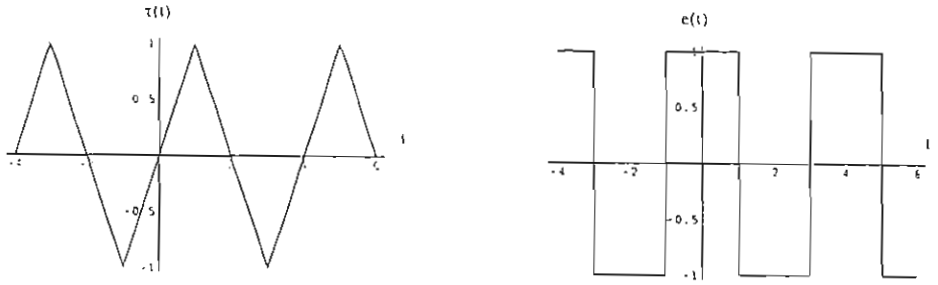

1. The non-smooth variables used in the method of NSTTs.

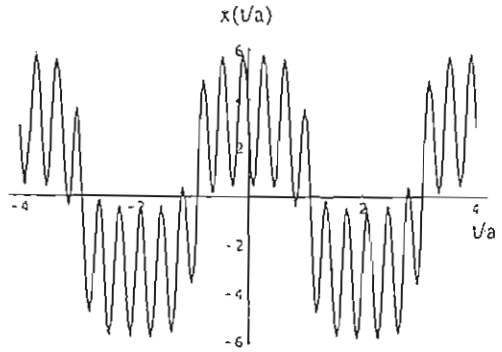

2. Analytical approximation of a strongly nonlinear periodic response of the forced pendulum.

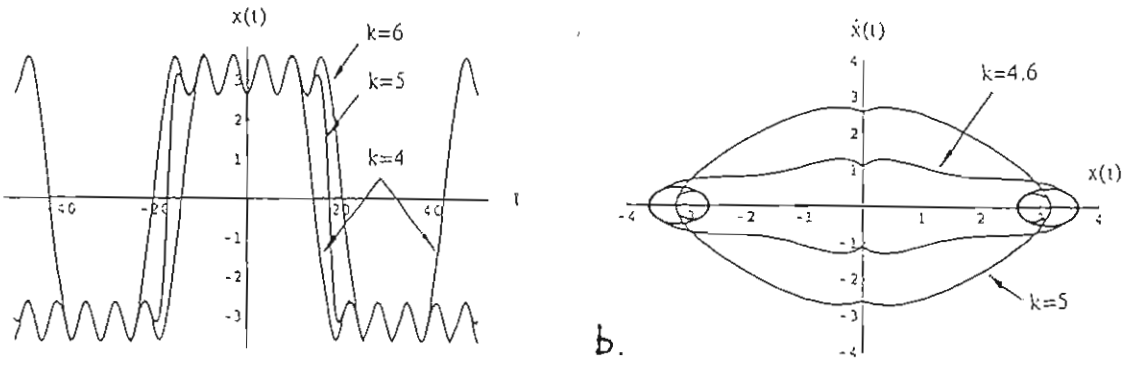

3. Three periodic orbits of the family (16): (a) solutions in time domain, (b) trajectories in the projection of the phase space $(x,\dot{x})$.

DYNAMICS OF MULTIBODY SYSTEMS WITH UNILATERAL CONSTRAINTS

M. Wösle, F. Pfeiffer
Lehrstuhl B für Mechanik, Technische Universität München, 80290 München, GERMANY

Abstract: Mechanical systems containing couplings with dry friction are modelled as multibody systems with unilateral constraints. The description of the system dynamics is structure-varying. In the following, the differential-algebraic equations are transformed into a resolvable mathematical form and we use the homotopy method for the solution of the three-dimensional contact problem.

1. Introduction

Unilateral constraints can have three different states: Separation, sticking and sliding. For a mechanical system with n unilateral constraints, the number of possible combinations of the states of constraints is 3^n. But only one of these combinations is compatible with all kinematic and kinetic conditions of the system.

2. Contact Kinematics

A set of generalized coordinates $q \in \mathbb{R}^f$ is used for the mathematical description of the dynamics of the unconstrained system with f degrees of freedom. In order to take into account additional unilateral constraints, we have to derive some kinematic contact conditions. The possible motion of each body in a multibody system, which is compatible to the kinematic conditions, is restricted by conditions for normal distances $g_N \in \mathbb{R}^{n_N}$, relative velocities $\dot{g}_N \in \mathbb{R}^{n_N}$, $\dot{g}_T \in \mathbb{R}^{2n_T}$ and relative accelerations [Glocker, 1995]

$$\ddot{g}_N = W_N^T \ddot{q} + \overline{w}_N \in \mathbb{R}^{n_N}, \quad \ddot{g}_T = W_T^T \ddot{q} + \overline{w}_T \in \mathbb{R}^{2n_T} \tag{1}$$

in the potential contact points. n_N and n_T are the numbers of the potentially active normal and tangential constraints. $W_N \in \mathbb{R}^{f,n_N}$ and $W_T \in \mathbb{R}^{f,2n_T}$ are the constraint matrices. The vectors $\overline{w}_N$ and $\overline{w}_T$ contain terms of relative kinematics.

3. Dynamics of Rigid Bodies with Superimposed Unilateral Constraints

Describing the motion of a structure-varying system, we start from the differential equations of motion of the unconstrained system [Glocker, 1995]. In a system with additional unilateral constraints, the occurring contact forces $\lambda_N \in \mathbb{R}^{n_N}$ and $\lambda_T \in \mathbb{R}^{2n_T}$ are taken

into account in the equations of motion [Wösle & Pfeiffer, 1996]

$$M\ddot{q} - h - [W_N + H_R]\lambda_N - W_T\lambda_T = 0 \tag{2}$$

as Lagrange multipliers. By the constraint matrices they are expressed in the configuration space. The mass matrix M is symmetric and positive definite. $h \in \mathbb{R}^f$ contains the gyroscopical accelerations together with the sum of all active forces and moments. By means of the matrix $H_R \in \mathbb{R}^{f,n_N}$ of the sliding constraints, the sliding friction forces are taken into account, which obey Coulomb's friction law [Wösle & Pfeiffer, 1996]. In Sec. 4, the system of Eqs. (1) and (2) will be completed by the missing contact laws.

4. Contact Laws

We consider rigid bodies under the assumption of impenetrability ($g_N \geq 0$). The normal contact problem with all closed contacts i ($g_{Ni} = \dot{g}_{Ni} \equiv 0$) is unambiguously determined by the n_N complementary conditions [Glocker, 1995]

$$\ddot{g}_N \geq 0\,, \quad \lambda_N \geq 0\,, \quad \ddot{g}_N^T\lambda_N = 0\,. \tag{3}$$

For the tangential contact problem, we use a representation of Coulomb's friction law on the acceleration level [Wösle & Pfeiffer, 1996]. To get complementary conditions, we introduce the friction saturation $\lambda_{T0i} = \mu_{0i}\lambda_{Ni} - |\lambda_{Ti}|$, as well as the direction angles φ_i and the amounts of the relative accelerations κ_i. Thus the friction forces and relative accelerations can be written in the form

$$\lambda_{Ti} = \begin{pmatrix} \cos\varphi_i \\ \sin\varphi_i \end{pmatrix} |\lambda_{Ti}| = G_{Ti}(\mu_{0i}\lambda_{Ni} - \lambda_{T0i})\,, \quad \ddot{g}_{Ti} = -G_{Ti}\kappa_i \tag{4}$$

with the coefficients of static friction μ_{0i}. By means of the quantities λ_{T0i} and κ_i Coulomb's friction law distinguishes between the both cases for $i = 1, \ldots, n_T$

$$\left.\begin{array}{lll} \text{sticking:} & \lambda_{T0i} > 0 & \Rightarrow \quad \kappa_i = 0 \\ \text{sliding:} & \lambda_{T0i} = 0 & \Rightarrow \quad \kappa_i > 0 \end{array}\right\} \quad \Rightarrow \quad \kappa \geq 0\,, \quad \lambda_{T0} \geq 0\,, \quad \kappa^T\lambda_{T0} = 0 \tag{5}$$

and we obtain the n_T nonlinear complementary conditions for the active tangential constraints.

5. Contact Problem in Mathematical Form

One possibility to solve the contact problem is to transform the complementary conditions into equations. For that purpose, we apply the theorem of Mangasarian to the

contact laws. For the complementary conditions (3) and (5) exist the equivalent equations [Mangasarian, 1976]

$$\begin{aligned} |\lambda_{Ni} - \ddot{g}_{Ni}|^3 - \lambda_{Ni}^3 - \ddot{g}_{Ni}^3 = 0\,, \quad i = 1, \ldots, n_N \\ |\lambda_{T0i} - \kappa_i|^3 - \lambda_{T0i}^3 - \kappa_i^3 = 0\,, \quad i = 1, \ldots, n_T\,. \end{aligned} \tag{6}$$

The Eqs. (1), (2), (4) and (6) form the nonlinear system of equations $F(z) = 0$ with the vector $z^T = [\ddot{g}_N \;\; \lambda_N \;\; \kappa \;\; \varphi \;\; \lambda_{T0} \;\; \lambda_T \;\; \ddot{q}] \in \mathbb{R}^{1,f+2n_N+5n_T}$. This zero-finding problem can be solved by the homotopy method [Watson, 1979] with the choice for the homotopy map

$$\rho(a, \lambda, z) = \lambda F(z) + (1 - \lambda)(z - a) = 0\,. \tag{7}$$

First, we pick a starting point a and get the known solution $z = a$ of $\rho(a, \lambda = 0, z) = z - a$. Then we track the zero curve of ρ with the additional parameter $\lambda \in [0, 1[$. For $\rho(a, \lambda = 1, \bar{z}) = F(\bar{z})$, we get the solution $\bar{z}$ of our zero-finding problem. The numerical integration of the generalized accelerations yields the velocities and coordinates, which are needed to calculate the indicators for state transitions. With them we have the actual state of our mechanical system and so we can determine the new constraint matrices.

6. Application to a Mechanical System

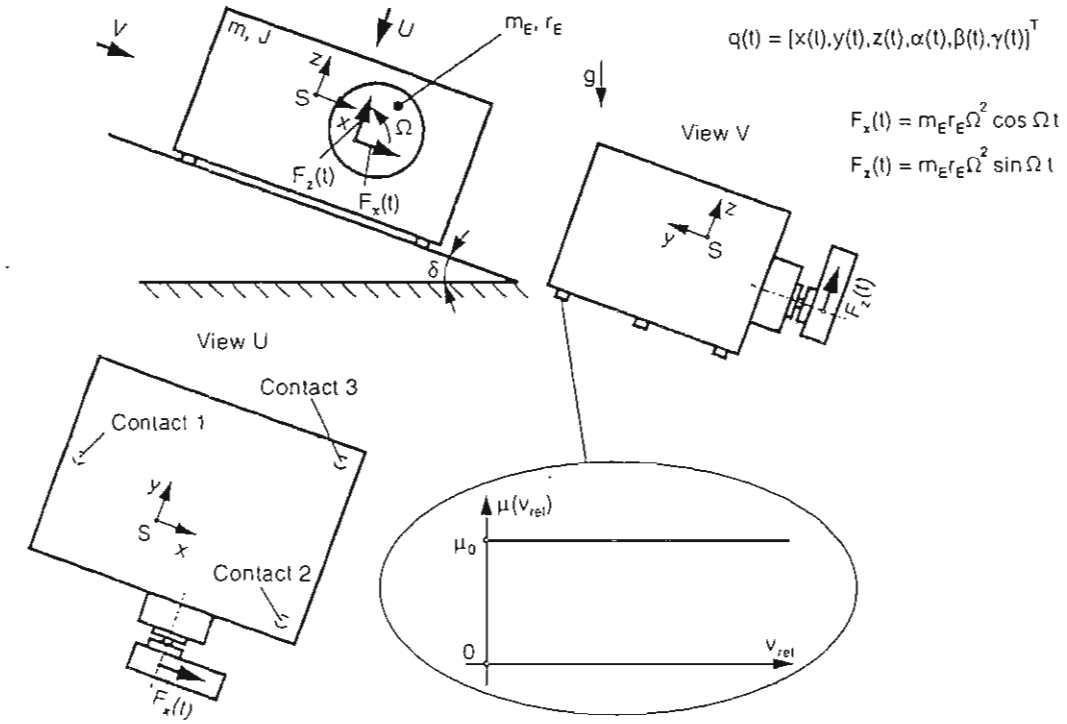

Figure 1: Mechanical Model

The theory is applied to an oscillator on an oblique plane containing one mass and three contact points (Fig. 1). The unconstrained body has six degrees of freedom x, y, z and α.

β, γ. The angles α, β and γ describe the twistings around the three axes. A periodically rotating unbalanced mass excites the rigid body. Because of the selected test conditions no detachment occurs. The diagrams in Fig. 2 show the computed accelerations as a function of their velocities. The unsteady changes in the accelerations are due to stick-slip transitions.

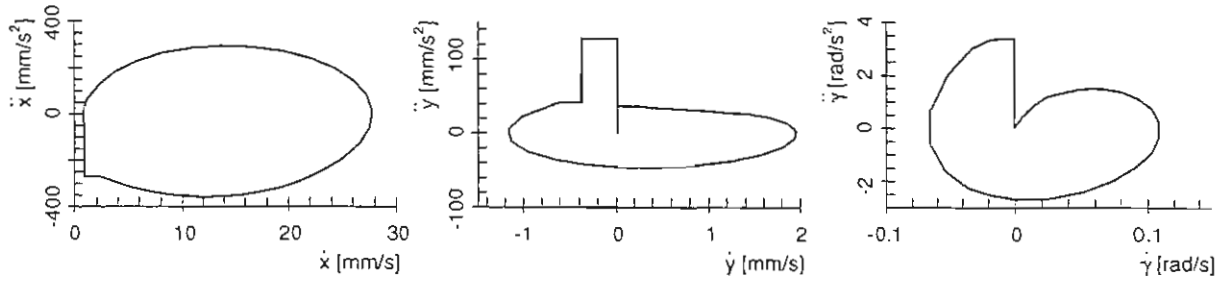

Figure 2: Phase Diagrams

7. Conclusions

Stick-slip phenomena in rigid multibody systems with many frictional contacts imply some fundamental problems. The behaviour of one contact can influence the state of all others. This situation leads to a compatibility problem with respect to constraint dynamics. Only one combination of the states of constraints satisfies all kinematic and kinetic conditions. For three-dimensional problems, the friction direction is unknown in the first moment after the transition from sticking to sliding. This situation leads to nonlinear complementary conditions.

9. References

Glocker, Ch. [1995] *Dynamik von Starrkörpersystemen mit Reibung und Stößen*. VDI-Fortschrittberichte, Reihe 18, Nr. 182, VDI-Verlag, Düsseldorf.

Mangasarian, O. L. [1976] "Equivalence of the complementarity problem to a system of nonlinear equations". *SIAM Journal of Applied Mathematics* 31(1), 89-92.

Watson, L. T. [1979] "Solving the nonlinear complementarity problem by a homotopy method". *SIAM Journal of Control and Optimization* 17(1), 36-46.

Wösle, M. & Pfeiffer, F. [1996] "Dynamics of multibody systems containing dependent unilateral constraints with friction". *Journal of Vibration and Control* 2, 161-192.

HIGHER-ORDER AVERAGING FOR PERIODICALLY FORCED, WEAKLY NONLINEAR SYSTEMS

K. Yagasaki and T. Ichikawa
Department of Mechanical Engineering, Gifu University, Gifu, Gifu 501-11, Japan

Abstract: We perform a higher-order averaging analysis by the Lie transforms for periodically forced, weakly nonlinear systems with the assistance of the computer algebra system, Mathematica. We give an example for a single-degree-of-freedom system to demonstrate our results.

1. Introduction

The averaging method is one of most useful perturbation techniques to study nonlinear systems (e.g, [Sanders and Verhulst, 1985]), and its higher-order approximation results are also available (e.g., [Murdock, 1988]). In particular, the higher-order terms can be computed by the Lie transform algorithm [Nayfeh, 1973], [Chow & Hale, 1982], which is easy to be implemented on computers. Rand & Armbruster [1988] also presented a computer algebra program for higher-order averaging but used a different, primitive algorithm.

In this paper, we perform the higher-order averaging analysis for periodically forced, weakly nonlinear systems. We describe an algorithm for computing the higher-order averaging terms by the Lie transforms, which is implemented on a developed package of the computer algebra system, Mathematica [Wolfram, 1991]. We also give an example for a single-degree-of-freedom system to demonstrate our results.

2. Higher-Order Averaging

Consider systems of the form

$$\dot{x} = \epsilon f(x, \theta, \epsilon), \quad \dot{\theta} = \omega, \quad (x, \theta) \in \mathbb{R}^n \times \mathbb{R}, \quad 0 < \epsilon \ll 1, \tag{1}$$

where $f(x, \theta, \epsilon) \in \mathbb{R}^n$ is analytic and of period 2π in θ. We expand $f(x, \theta, \epsilon)$ in power series of ϵ:

$$f(x, \theta, \epsilon) = \sum_{m=1}^{\infty} \frac{\epsilon^{m-1}}{m!} f_m(x, \theta) \tag{2}$$

Let $w(x, \theta, \epsilon)$ be an analytic function of the form

$$w(x, \theta, \epsilon) = \sum_{m=0}^{\infty} \frac{\epsilon^m}{m!} w_{m+1}(x, \theta). \tag{3}$$

Define a near-identity transformation

$$x = u(y, \theta, \epsilon), \quad y \in \mathbb{R}^n \tag{4}$$

such that $u(y, \theta, \epsilon)$ is a solution of the equation

$$\frac{\partial u}{\partial \epsilon} = w(u, \theta, \epsilon), \quad u(y, \theta, 0) = y. \tag{5}$$

Applying the general theory of the Lie transforms [Nayfeh, 1973], [Chow & Hale, 1982], we see that under the transformation $(x, \theta) = (u(y, \theta, \epsilon), \theta)$, Eq. (1) becomes

$$\dot{y} = \sum_{m=1}^{\infty} \frac{\epsilon^m}{m!} g_m(y, \theta), \quad \dot{\theta} = \omega, \tag{6}$$

where $g_m(y, \theta)$, $m = 1, 2, \ldots$, can be computed by the recursive relations

$$\begin{aligned} f_k^{(0)}(y, \theta) &= f_k(y, \theta), \\ f_k^{(1)}(y, \theta) &= f_{k+1}^{(0)}(y, \theta) + \sum_{j=0}^{k-1} C_j^k L_{j+1} f_{k-j}^{(0)}(y, \theta) - \omega \frac{\partial w_{k+1}}{\partial \theta}(y, \theta), \\ f_k^{(l)}(y, \theta) &= f_{k+1}^{(l-1)}(y, \theta) + \sum_{j=0}^{k} C_j^k L_{j+1} f_{k-j}^{(l-1)}(y, \theta) \quad \text{for} \quad l \geq 2, \end{aligned} \tag{7}$$

and

$$g_m(y, \theta) = f_0^{(m)}(y, \theta) \tag{8}$$

with

$$L_j g(y, \theta) = \mathrm{D}_y g(y, \theta)\, w_j(y, \theta) - \mathrm{D}_y w_j(y, \theta)\, g(y, \theta) \quad \text{and} \quad C_j^k = \frac{k!}{(k-j)!j!}. \tag{9}$$

Let $m \geq 2$ be fixed. Suppose that in the recursive relations (7) we use

$$f_{m-1}^{(1)}(y, \theta) = f_m^{(0)}(y, \theta) + \sum_{j=0}^{m-2} C_j^{m-1} L_{j+1} f_{m-j-1}^{(0)}(y, \theta) \tag{10}$$

instead of the second equation for $k = m - 1$ and denote by $f^{(m)}(y, \theta)$ the final output $f_0^{(m)}(y, \theta)$. Then Eq. (8) becomes

$$g_m(y, \theta) = f^{(m)}(y, \theta) - \omega \frac{\partial w_m}{\partial \theta}(y, \theta). \tag{11}$$

Here $f^{(m)}(y, \theta)$ is independent of $w_m(y, \theta)$. We also set $f^{(1)}(y, \theta) = f_1(y, \theta)$, so that Eq. (11) still holds for $m = 1$.

Define

$$\bar{f}^{(m)}(y) = \frac{1}{2\pi} \int_0^{2\pi} f^{(m)}(y, \theta) \mathrm{d}\theta. \tag{12}$$

Let

$$f^{(m)}(y, \theta) = \bar{f}^{(m)}(y) + \tilde{f}^{(m)}(y, \theta) \tag{13}$$

be split into its mean part $\bar{f}^{(m)}(y)$ and oscillating part $\tilde{f}^{(m)}(y, \theta)$. Choosing $w_m(y, \theta)$ such that

$$\omega \frac{\partial w_m}{\partial \theta}(y, \theta) = \tilde{f}^{(m)}(y, \theta), \tag{14}$$

we obtain

$$g_m(y,\theta) = \bar{f}^{(m)}(y), \tag{15}$$

so that Eq. (6) becomes

$$\dot{y} = \sum_{m=1}^{\infty} \frac{\epsilon^m}{m!} \bar{f}^{(m)}(y), \quad \dot{\theta} = \omega. \tag{16}$$

We refer to Eq. (16) as the m_0-th order averaged system when the summation is truncated at $m = m_0$.

3. Applications to Weakly Nonlinear Systems

We next consider periodically forced, wealy nonlinear n-degree-of-freedom systems

$$\ddot{x} + \omega_i^2 x_i = \epsilon F_i(x, \dot{x}, \omega t, \epsilon), \quad i = 1, \ldots, n, \tag{17}$$

where $x = (x_1, \ldots, x_n)^{\mathrm{T}}$ (T denotes the transpose operation), and $F_i(x, \dot{x}, \theta, \epsilon) \in \mathbb{R}$ is analytic and 2π-periodic in θ. We assume that ultra-subharmonic resonances occur simultaneously such that $\omega_i/\omega \approx l_i/k_i$ with k_i and l_i relatively prime integers for $i = 1, \ldots n$, and set

$$\epsilon^j \Omega_i = \frac{l_i^2\omega^2 - k_i^2\omega_i^2}{k_i}. \tag{18}$$

Then, using the van der Pol transformation

$$\begin{pmatrix} u_i \\ v_i \end{pmatrix} = \begin{pmatrix} \cos\dfrac{l_i}{k_i}\omega t & -\dfrac{k_i}{l_i\omega}\sin\dfrac{l_i}{k_i}\omega t \\ -\sin\dfrac{l_i}{k_i}\omega t & -\dfrac{k_i}{l_i\omega}\cos\dfrac{l_i}{k_i}\omega t \end{pmatrix} \begin{pmatrix} x_i \\ \dot{x}_i \end{pmatrix} \tag{19}$$

in Eq. (17), we obtain

$$\begin{pmatrix} \dot{u}_i \\ \dot{v}_i \end{pmatrix} = -\frac{k_i}{l_i\omega}[\epsilon^m \Omega_i x_i + \epsilon F_i(x, \dot{x}, \omega t, \epsilon)] \begin{pmatrix} \sin\dfrac{l_i}{k_i}\omega t \\ \cos\dfrac{l_i}{k_i}\omega t \end{pmatrix}, \quad i = 1, \ldots, n, \tag{20}$$

where x_i and $\dot{x}_i$ are expressed by u_j and v_j through Eq. (19). Equation (20) can be written as the form (1) and we can apply the averaging method to it.

The developed package of Mathematica contains two programs haverage and Vander-Pol that implement the higher-order averaging procedure for Eq. (1) given in Sec. 2 and the van der Pol transformation from Eq. (17) to Eq. (20).

4. An Example

As an example, we take the nonlinear oscillator with nonsymmetric restoring force,

$$\ddot{x} + \omega_1^2 x = -\epsilon\beta x^2 + \epsilon^2(-\alpha x^3 - \delta\dot{x} + \gamma\cos\omega t), \quad \alpha, \delta, \gamma > 0. \tag{21}$$

We first apply the van der Pol transformation with $k_1 = l_1 = 1$ and $j = 2$:

```
F[1]=e(-beta x[1]^2) +e^2(-delta y[1]-alpha x[1]^3+gamma Cos[phi]);
```

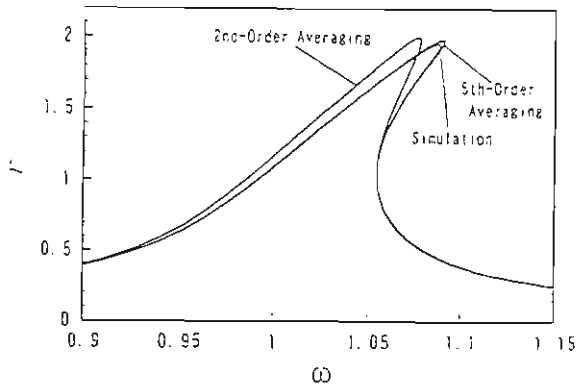

Fig. 1. Resonance curves by second- and fifth-order averaging and direct numerical integrations for Eq. (21) when $\epsilon = 0.2$, $\alpha = 2.5$, $\beta = 1$, $\gamma = 2$, $\delta = 1$ and $\omega_1 = 1$.

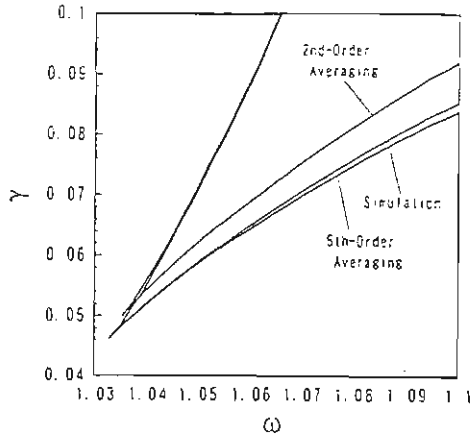

Fig. 2. Bifurcation sets by second- and fifth-order averaging and direct numerical integrations for Eq. (21) when $\epsilon = 0.2$, $\alpha = 2.5$, $\beta = 1$, $\delta = 1$ and $\omega_1 = 1$.

```
g=VanderPol[F,x,y,u,v,psi,omega,e^2 Omega,1,1,1];
```

We carry out averaging up to fifth-order for the resulting equation:

```
Do[f[j]=j!  Coefficient[g,e^j]/psi->theta,j,1,5];
haverage[f,barf,u[1],v[1],theta,omega,2,5];
```

Figures 1 and 2 show comparisons among the second- and fifth-order averaging analyses and direct numerical integrations for resonance curves and bifurcation sets. Here we used the computer software, AUTO [Doedel & Kernévez, 1986], to obtain these results.

References

Chow, S.-N. & Hale, J. K. [1982] *Methods of Bifurcation Theory* (Springer-Verlag, New York).

Doedel, E. & Kernévez, J. [1986] "AUTO: Software for continuation and bifurcation problems in ordinary differential equations," *Appl. Math. Reports*, Caltech.

Murdock, J. [1988] "Qualitative theory of nonlinear resonance by averaging and dynamical systems methods," in *Dynamics Reported*, Vol. 1, eds. Kirchgraber, U. and Walther, H. O. (Wiley, New York).

Nayfeh, A. [1973] *Perturbation Methods* (Wiley, New York).

Rand, R. H. and Armbruster, D. [1987] *Perturbation Methods, Bifurcation Theory and Computer Algebra* (Springer-Verlag, New York).

Sanders, J. A. & Verhulst, F. [1985] *Averaging Methods in Nonlinear Dynamical Systems* (Springer-Verlag, New York).

Wolfram, S. [1991] *Mathematica, A System for Doing Mathematics by Computer*, 2nd ed. (Addison-Wesley, Redwood City).

A METHOD TO CALCULATE HOMOCLINIC POINTS OF A NONINVERTIBLE MAP

T. YOSHINAGA† and H. KAWAKAMI‡

†School of Medical Sciences *and* ‡Faculty of Engineering,
The University of Tokushima, Tokushima, 770 JAPAN
yosinaga@medsci.tokushima-u.ac.jp kawakami@ee.tokushima-u.ac.jp

Abstract

A numerical method is presented for calculating transverse and non-transverse (or tangent) types of homoclinic points of a two-dimensional noninvertible map having an invariant set that reduces to a one-dimensional noninvertible map. To illustrate bifurcation diagrams of homoclinic points and transitions of chaotic states near the bifurcation parameter values, two systems including coupled chaotic maps are studied.

1 Introduction

Recently there are many investigations on coupled discrete maps[1, 2, 3], which are considered as models of coupled oscillators derived from physical systems. Several phenomena observed in coupled chaotic oscillators can be reproduced by a coupling of one-dimensional noninvertible maps. Using a model described by discrete dynamical system, we may clarify mechanisms of generation of chaos, transition or bifurcation of chaos, chaotic synchronization and so on.

The appearance of homoclinic structure in dynamical systems is a global phenomenon and important on the occurrence of chaotic behavior. But it is not possible to obtain homoclinic solutions for a general noninvertible map. On the other hand, there is a method to calculate homoclinic solutions and their bifurcation set for forced differential equations as well as invertible maps[4]. In this paper, we propose a computational method to calculate homoclinic solutions of a noninvertible map for a special case.

We consider a discrete map as a function of a real parameter vector λ, defined by

$$T_\lambda \; : \; R^2 \to R^2 \; ; \; (x, y) \mapsto (x', y') \qquad (1)$$

where the system has an invariant set such that the restriction to the line $px + qy = r$ $(p^2 + q^2 \neq 0)$ reduces to a one-dimensional noninvertible map. We also suppose that Eq. (1) has a saddle type of fixed or periodic point, say D_0, on the line $px + qy = r$, and a homoclinic point Q_0 exists as an intersection of α- and ω-branches (or unstable and stable manifolds, respectively) of the point D_0. Moreover we treat a special case where the ω-branch is restricted to the invariant set $px + qy = r$, so the point Q_0 is located on the line, although the ω-branch itself may be folded. Indeed, this situation is typically observed in, e.g., a coupling of identical chaotic maps as shown in Sec. 3 and this phenomenon is related to a transition of chaos with a symmetric property. From the above assumption, we can obtain the point Q_0 using a similar computational method for invertible maps, because it is not necessary to calculate the ω-branch of the noninvertible map.

2 Method

In this section, we show methods for calculating transverse and non-transverse (or tangent) types of homoclinic solutions. The two situations are sketched in Fig. 1. Note that a periodic point with period k can be studied by replacing T_λ with ${T_\lambda}^k$, k-th iterates of T_λ, in Eq. (1). Therefore in the following we consider only homoclinic point of the fixed point of T_λ. Similar argument can be applied to the periodic point of T_λ.

2.1 Transverse type of homoclinic point

We first consider a method for obtaining a transverse type of homoclinic point Q_0 using a local representation of α-branch. Let the point D_0 be a saddle type of fixed point:

$$T_\lambda(D_0) - D_0 = 0 \qquad (2)$$

We take an ϵ-neighborhood $U(\epsilon, D_0)$ as shown in Fig. 1(a), then there exists a positive integer M

such that

$$T_\lambda^M(Q_{-M}) = Q_0, \quad Q_{-M} \in U(\varepsilon, D_0) \qquad (3)$$

Because Q_0 is on the line $px + qy = r$, the point Q_{-M} satisfies

$$(p \quad q)\, T_\lambda^M(Q_{-M}) - r = 0 \qquad (4)$$

Hence the problem for obtaining the point Q_0 reduces to a problem to find the point Q_{-M} ($\in$ α-branch) that satisfies Eq. (4) and is included in the region $U(\varepsilon, D_0)$.

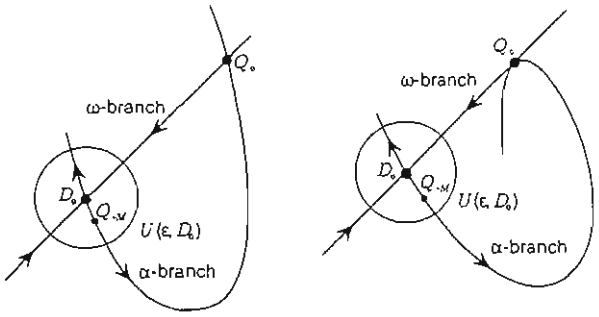

Figure 1: Schematic diagrams for (a) transverse and (b) non-transverse (or tangent) types of homoclinic points.

Now, we use the first order approximation or eigenvector as the local representation of α-branch in the ε-neighborhood. The condition such that the point Q_{-M} is included in the α-branch is written as

$$W_\alpha^*(Q_{-M} - D_0) = 0 \qquad (5)$$

where the row vector W_α^* is

$$W_\alpha^* = (1 \quad 0)(\mu_\alpha I - DT_\lambda), \text{ or}$$
$$(0 \quad 1)(\mu_\alpha I - DT_\lambda) \qquad (6)$$

In the equation, DT_λ indicates the derivative of T_λ with respect to the fixed point D_0, and $|\mu_\alpha| > 1$ denotes the characteristic multiplier.

If the α-branch intersects the ω-branch or the line $px + qy = r$ at the point Q_0, then Eq. (5) is independent of Eq. (4). Therefore we can determine variables $Q_{-M} \in R^2$ for the set of Eqs. (4) and (5), using, e.g., Newton's method.

2.2 Non-transverse or tangent type of homoclinic point

Then we consider a homoclinic point such that the α-branch is tangent to the ω-branch (or the line $px + qy = r$) at the point Q_0. This is a problem for obtaining a bifurcation of homoclinic motion.

The calculation is done by solving homoclinic point and an element of the parameter vector λ, say λ_1, simultaneously, for equations of 2nd order tangent homoclinicity. Figure 1(b) shows a schematic diagram for the situation. Let

$$\phi : R \to R^2 ; s \mapsto \phi(s) \qquad (7)$$

be a representation of the α-branch in $U(\varepsilon, D_0)$, where $\phi(0) = D_0$ and $\phi(s_\alpha) = Q_{-M}$.

We now consider the derivative of ϕ with respect to s, that is,

$$\frac{d\phi}{ds}(s) = W(\phi(s)) \qquad (8)$$

then we have a tangent vector of the α-branch at the point Q_0

$$\left.\frac{d(T_\lambda^M \circ \phi)}{ds}\right|_{s=s_\alpha} = DT_\lambda^M(\phi(s_\alpha))\frac{d\phi}{ds}(s_\alpha)$$
$$= DT_\lambda^M(Q_{-M})W_\alpha \qquad (9)$$

where $W(\phi(s_\alpha)) = W_\alpha$, for simplicity. Hence we have a condition for coincidence of the directions W_α and the line $px + qy = r$:

$$\det\left(DT_\lambda^M(Q_{-M})W_\alpha \vdots \begin{pmatrix} -q \\ p \end{pmatrix}\right) = 0 \qquad (10)$$

where W_α is a vector transposed to W_α^*, that is,

$$W_\alpha^T = W_\alpha^* \begin{pmatrix} 0 & 1 \\ -1 & 0 \end{pmatrix} \qquad (11)$$

where ^{T} indicates the transpose. Hence the problem is reduced to determine variables $(D_0, Q_{-M}, \lambda_1) \in R^5$ for the set of Eqs. (2), (4), (5) and (10).

3 Examples

We illustrate some numerical results of calculating homoclinic bifurcations showing several interesting phenomena related to a transition of chaos. In bifurcation diagram, we use notations: H_l^m for homoclinic tangency, G_l^m for tangent bifurcation, D_l^m for D-type of branching, I_l^m for period-doubling bifurcation and N_l^m for the Neimark-Sacker bifurcation, where m and l respectively denote the order of period and the number to distinguish several same sets of $(\ )^m$, if they exist. If $m = 1$, it will be omitted.

3.1 A coupled system of chaotic neurons

The system of our first example is a coupling of two identical chaotic neurons[3]:

$$T_\lambda \left\{ \begin{pmatrix} x' \\ y' \end{pmatrix} = \begin{pmatrix} 0.8x + a - h(x) + wh(y) \\ 0.8y + a - h(y) + wh(x) \end{pmatrix} \right. \tag{12}$$

where $h(u) = 1/(1+\exp(-u/0.03))$ and $\lambda = (a, w)$. Note that the restriction to $x = y$ reduces to a one-dimensional system.

We obtain parameter sets of local and global bifurcations as shown in Fig. 2. In the region shaded by [ ], there exists a stable fixed point satisfying $x \equiv y$. By passing through the curve I_1 from this region, we have ${}_1I$-type of fixed point which exists in the region [ ]. The point ${}_1I$ has an ω-branch on the line $x = y$, and, if only the saddle exists, the α- and ω-branches intersect each other and form a transverse type of homoclinic structure at every parameter point in the region shown in Fig. 2. The curve H in Fig. 2 denotes the parameter set on which a non-transverse type of homoclinic point of the fixed point ${}_1I$ appears. Phase portraits of attractors and α-branchs of the fixed point observed at the parameter points a–c in Fig. 2(b) are shown in Fig. 3, where the coordinate system is transformed by $u = (x + y)/\sqrt{2}$ and $v = (x - y)/\sqrt{2}$ to see the detail near the line $x = y$ or $v = 0$. In each phase portrait, the α-branch is drawn up to a first transverse with the ω-branch, and another α-branch that is symmetric with respect to the line $v = 0$ is omitted.

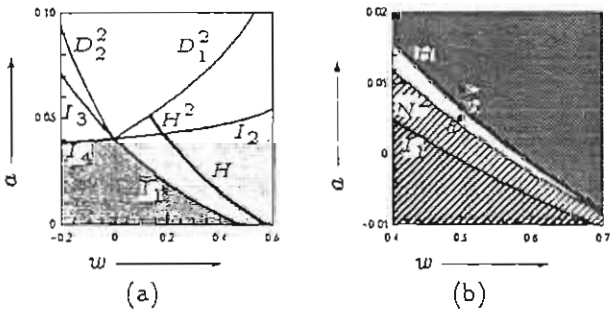

Figure 2: Bifurcation diagrams for Eq. (12). Note that, in the figure (a), several bifurcation curves, e.g., the curve N^2 observed in the figure (b), are omitted for the simplicity.

We have an attractive invariant closed curve of the iterations of Eq. (12) with parameter values indicated by the point a, see Fig. 3(a). This invariant closed curve is generated by the Neimark-Sacker bifurcation, denoted by the curve N^2 in Fig. 2(b), of a stable 2-periodic point with property $T_\lambda(x, y) = (y, x)$, which exists in the region with shading [ ]. By increasing the value of the parameter a for fixed $w = 0.5$, at the point b or on the curve H in Fig. 2(b), we observe a non-transverse type of homoclinic point as shown in Fig. 3(b). The homoclinic point is indicated by the point Q_0 in Fig. 3(c) showing an enlargement of Fig. 3(b). When the homoclinic point becomes to a transverse type, due to more increase of the parameter a, we see that the invariant closed curve changes to a chaotic attractor near the α-branch which forms the transverse homoclinic structure as shown in Fig. 3(d), occurring at the point c in Fig. 2(b). Therefore the curve H shows a bifurcation set for the transition between the invariant closed curve and the chaotic attractor. The parameter region in which the chaotic attractor exists is indicated by the shading [ ] in Fig. 2(b). Note that the attractor shown in Fig. 3(d) is a characteristic chaos observed in the neuron model[3]. It is an advantage of our method to be able to obtain bifurcation parameters at which the chaos generates.

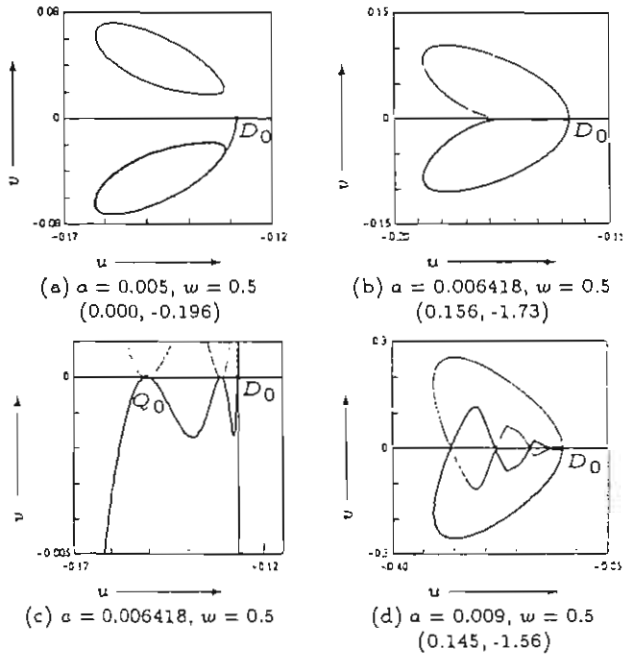

Figure 3: Phase portraits for Eq. (12) in the transformed coordinate system. The point with symbol D_0 and the curve denote the fixed point and its α-branch, respectively. Parameter values are denoted by the points (a) a, (b) b, and (d) c. The figure (c) is for an enlargement of (b). The values of the Lyapunov exponents appear in parentheses.

3.2 A two-dimensional version of Myrberg's map

As the second example, we treat the system taken from Ref. [5]:

$$T_\lambda \left\{ \begin{pmatrix} x' \\ y' \end{pmatrix} = \begin{pmatrix} x^2 - y^2 - \alpha + \varepsilon x \\ 2xy - 2.5\varepsilon y \end{pmatrix} \right. \tag{13}$$

where $\lambda = (\alpha, \varepsilon)$. Note that the restriction to $y = 0$ reduces to the Myrberg map.

Figure 4 is for showing schematic bifurcations of first homoclinic tangencies, denoted by symbols H and H^m, of fixed and m-periodic points, where $m = 2, 4, 8$. The fixed and periodic points are observed on the line $y = 0$ and there is a doubling process of their period-doubling bifurcations indicated by the curves I and I^m, $m = 2, 4, 8$. We see that there exist successive occurrences of the homoclinic bifurcations together with the period-doubling bifurcations. The occurrence of the infinite doubling processes is conjectured. At the points c and d, we have chaotic states restricted to the set $y = 0$. In Fig. 5, phase portraits of attractors with and without homoclinic structures, which can be called as connected ((a) and (c)) and disconnected ((b) and (d)) chaotic attractors, respectively, are shown. Note that, for each figure on the right ((b) and (d)), another attractor that is symmetric with respect to the line $y = 0$ is omitted. The transition between the two types of chaotic attractors occurs on the curves of the first homoclinic tangencies.

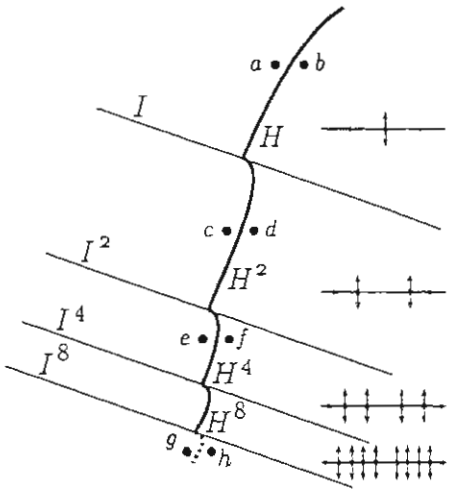

Figure 4: Schematic bifurcation diagram in parameter plane $\lambda = (\varepsilon, \alpha)$ and locations of periodic points on the line $y = 0$ are schematically shown. The periodic points on the line $y = 0$, which exist in regions separated by the period-doubling bifurcations are also illustrated in the diagram.

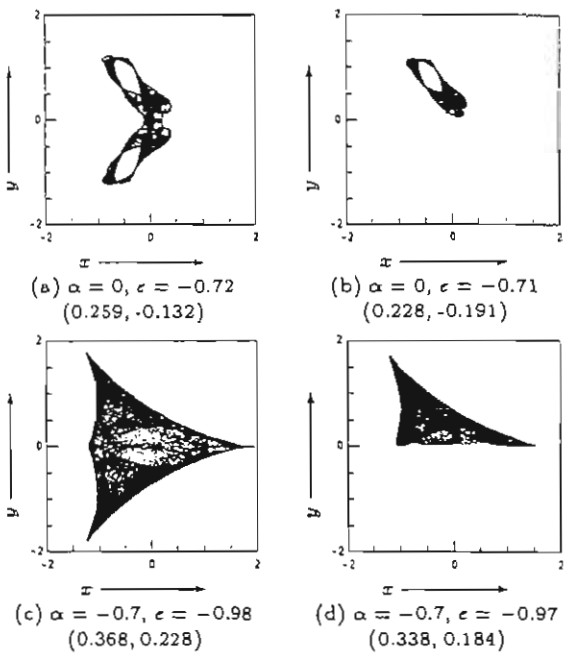

Figure 5: Phase portraits for attractors observed in Eq. (13) with parameter values denoted by the point (a) a, (b) b, (c) g and (d) h in Fig. 4.

4 Conclusion

Using the method for obtaining homoclinic tangencies, the following results were obtained: (1) We obtained bifurcation parameter set that causes the generation of a chaotic attractor, which is a characteristic chaos observed in a coupling of two identical chaotic neurons. (2) A doubling process of homoclinic structures together with period-doubling bifurcations was found in a two-dimensional version of Myrberg's map.

Finally we should note that although we only consider, in this paper, the case where the restriction to ω-branch is the line $px+qy = r$, it is possible to apply to more general case such as $h(x, y) = 0$, where h is a known C^∞ function.

References

[1] Kaneko, K. [1986] *Collapse of Tori and Genesis of Chaos in Dissipative Systems* (World Scientific, Singapore).

[2] Gardini, L., Abraham, R., Record, R. & Fournier, D. [1994] "A double logistic map," *Int. J. Bifurcation and Chaos*, 4 (1), 145–176.

[3] Aihara, K. [1989] "Chaotic neural networks," in *Bifurcation Phenomena in Nonlinear Systems and Theory of Dynamical Systems*, ed. H. Kawakami, 143–161 (World Scientific, Singapore).

[4] Kawakami, H. [1981] C.R. Acad. Sc. Paris, 293, Série I, 401–403.

[5] Mira, C. & Narayaninsamy, T. [1993] "On behaviors of two-dimensional endomorphism: role of critical curves," *Int. J. Bifurcation and Chaos*, 3 (1), 187–194.

Bifurcation and Chaos of Nonlinear Vibration Systems with Parametric Excitation

Chen Yushu

(Department of Mechanics, Tianjin University, Tianjin, China, 300072)

Abstract This paper introduces the local and global bifurcations and chaos of nonlinear vibration systems with parametric excitation obtained by us since 1986.

The vibration equation of such systems is as follows

$$\frac{d^2x}{dt^2} + \delta\left[\frac{dx}{dt} + h\left(x,\frac{dx}{dt},\delta\right)\right] + (1+\mu)x + f\left(x,\frac{dx}{dt},\mu\right) + 2\varepsilon\cos 2t\left[x + g\left(x,\frac{dx}{dt},\mu\varepsilon\right)\right] = 0 \tag{1}$$

here x—vibration displacement, δ—damping coeffecient, ε—amplitude of parametric excitation, μ—tuning parameter, f, g, h—nonlinear functions of $x,\frac{dx}{dt}$, and f and g—even functions of $\frac{dx}{dt}$, h—odd function of $\frac{dx}{dt}$.

In the local bifureation part, defining periodic function spaces, and using subgroup property of (1), and Liapunov–Schmidt reduction, we got the analytical expression of local bifurcation equation and the first order approximate bifurcation equation. Then 6 persistent and 6 nonpersistent (transition) bifurcation diagrams (frequency–response curves) are obtained by using singularity theory. The experimental results at the mechanical model are coincident with above theoretical ones. From here we get vibration utilization theory: vibration damping and vibration utilization in resonant mechanical machines. The second order approximate bifurcation equation is obtained by generalized Green's function.

$$(f^2 + d^2)A^9 + 2(cd + ef)A^7 + (c^2 + e^2 + 2bd - 2\alpha f)A^5 + 2(bc - \alpha e)A^3 + (\alpha^2 + b^2 - g^2)A = A(r(u,\alpha) + \varepsilon_1 + 2\varepsilon_2 u) \tag{2}$$

Defining a modal parameter

$$m = \left|\frac{r_{u\alpha}}{2\sqrt{r_{uu}\,|r_{\alpha\alpha}|}}\right|_{u=0,\alpha=0} \tag{3}$$

We have Moduli Bracelet (see Figure 1), here r is a function of u and system parameters a, b, c, d, e, f, and g. It is main part of second order approximate bifurcation equation and called a germ.

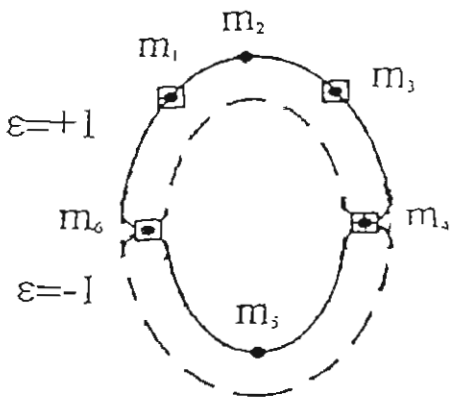

Fig.1 Moduli Bracelet

For non–degenerate cases, that is, system parameters at the interval between modal points, $m \in m_2\ m_3$, $m_3\ m_4$, or $m_4\ m_5$,the first order approximate bifurcation equation can describe the complete dynamical behavior of the original systems. There are 6 persistent bifurcation diagrams [4] . For degenerate cases, that is, at the modal points m_2 , m_5 and part of points m_1 , m_3 ,m_4 ,m_6 may use only the second order approximate bifurcation equation. It is possible for the system to have 14 persistent bifurcation diagrams [5] . For $cd+ef=0$ of m_4 may use the third order approximate bifurcation equation. But for $cd+ef=0$ of m_3 it needs the higher order approximate bifurcation equation than third order. There are more 14 bifurcation diagrams [7] .

The procedure of solving the bifurcation equation is called by the bifurcation theory method in nonlinear vibration. The modern mathematical method introduced by Chen can reveal the bifurcations and rich dynamical behavior of nonlinear vibration systems. The results obtained by modern mathematical method basically interpret the contradictory results obtained by Bogoliubov [2] and Nayfeh [3] . The modern mathematical method carries the nonlinear vibration a new step forward from the classical theory. Especially, from here one can get vibration utilization theory: vibration damping (such as the system parameters in regions ① and (2) of Fig.4 in [4]) and vibration utilization in resonant vibration machines (such as the system parameters in regions ④ and (3) of Fig.4 in [4]). The results of Moduli Bracelet give us part answer about the questions what order approximate solution should be taken for complete revealing the dynamical behaviors of original nonlinear vibration systems. For nondegenerate cases as $m \in \{m_2\ m_3\}$, $m \in \{m_3\ m_4\}$, $m \in \{m_4\ m_5\}$ in Fig.1, one can take the first order approximate bifurcation equation in order to universal unfolding. For degenerate case $cd+ef=0$ of m_4 –the third order approximate bifurcation equation, and $cd+ef=0$ of m_3 –the higher order approximate than third. For other degenerate cases except above two, the second order approximate bifurcation equation is enough.

Chen, Wang and Ye studied the global bifurcation and chaos of a beam under longitudinal excitation [16] . The dynamical model of a beam under the longitudinal excitation has been developed, and the averaging equation by the method of multiple scales is obtained. The theory of normal form and universal unfolding as well as the Melnikov's method are used to determine the parametric domain in which the global bifurcation and chaos can occur. The analytic result indicates that the dynamical response is abundant near degenerate points. In the corrsponding mechanical device the experiment about periodic, quasi–periodic and chaotic motion has been found. Meanwhile, the numerical simulation verifies the results of analysis and experiment by them. The global bifurcations and chaos

are investigated also by Chen etc [18,19] for a van der pol–Duffing–Mathieu system with a single–well potential energy and a three–well potential energy by means of semi–analytical and semi–numerical method. Semi–analytical and semi–numerical means that the autonomous system, called van der Pol–Duffing system, is analytically studied to draw global bifurcation diagrams in parameter space. These diagrams are called basic bifurcation diagrams. Then fixing parameter in every space and taking parametrically excited amplitude as a bifurcation parameter, we can observe how to evolve from a basic bifurcation diagram to chaotic pattern by numerical methods. They observe also nature of basins of attraction noting the appearance of fractal basin boundaries which herald the onset of a loss of structural integrity in order to consider how to control the extent and the rate of the erosion.

This paper is joint with Professor W. F. Langford, Doctors K. J. Zhan, J. Xu, M. Ye, and L. T. Mei, W. Y. Zhang.

Acknowledgement

This research was supported by National Nature Science Foundation of China and National Education Committee of China.

References

1. Krylov, N. & Bogoliubov, N.[1934] Les methodes de la mecanique nonlieaire (Monographie 8, Chaire de la Phys. Math. Acad. Sci. U.K.)
2. Bogoliubov, N. & Mitropolsky, Y. A.[1961] Asyniptotic Methods in the Theory of Nonlinear Oscillations (Gordon and Breach, New York)
3. Nayfeh, A. H. & Mook, D. T.[1979] Nonlinear Oscillations (John Wiley and Sons, New York)
4. Chen, Y. S. & Langford, W. F.[1988] "The subharmonic bifurcation solution of nonlinear Mathieu's equation and Euler dynamically bucking problem", Acta Mechanica Sinica 20(4), 522–532.
5. Chen, Y. S. & Zhan, K. J.[1988] "Some generalization on bifurcation theory of subharmonic resonance in nonlinear Mathieu's equation", Applied Mathematics and Mechanics 11(3), 239–245.
6. Chen, Y. S., Zhan, K. J. & Langford, W. F.[1990] "New results on bifurcation theory of subharmonic resonance in nonlincar system with parametric excitation: Degenerate bifurcation xolution", Journal of Vib. Rngineering 3(2), 38–47.
7. Chen, Y. S. & Mei, L. T.[1990] "Bifurcation solutions of general resonant cases of nonlincar Mathicu equations", Scence in China (Series A) 33(12), 1469–1476.
8. Chen, Y. S. Yie, M., & Zhan, K. J.[1990] "Experiment investigation of 1/2 subharmonic bifurcation solution in Mathieu's equation", Journal of Applied Mechanics 7(4), 11–16.
9. Chen, Y. S. & Xu, J.[1993] "Periodic responses and bifurcations in nonlinear Hill's sys-

tem (Ⅰ)", Jowrnal of Nonlinear Dynamics in Sci. Tech. 1(1), 1–14.
10. Chen, Y. S. & Xu, J.[1994] "Periodic responses and bifurcations in nonlinear Hill's system (Ⅱ)", Jowrnal of Nonlinear Dynamics in Sci. Tech. 1(3), 214–223.
11. Bolotin, V. V.[1964] The Dynanic Stability of Elastic Systems (Holden–Day, San Francisco)
12. Chen, Y. S. & Xu, J.[1993] "Nonlinear dynamical bifurcations of a thin circular plate subjected to the radial disturbing force", Proc. of ICNM Ⅱ, Beijing, 483–486.
13. Chow, S. Y. & Hale, J. K.[1982] Methods of Bifurcation Theory (Springer–Verlag, New York)
14. Golubisky, M. & Schaeffer, D. G.[1985] Singularities and Groups in Bifurcation Theory, Vol.1 (Springer–Verlag, New Tork)
15. Schmidt, G. & Tondl, A.[1986] Non–linear Vibrations (Cambridge University Press)
16. Chen, Y. S., Wand D. S. & Ye M.[1993] "Chaotic motion of beem under longitudinal excitation", Journal of Nonlinear Dynamics in Sci. Tech. 1(2), 124–135.
17. Chen, Y. S. & Xu, J.[1995] "Universal classification of bifurcating solutions to a primary parametric resonance in van der Pol–Duffing–Mathieu's systems", Science in China (Series A) 25(12), 1287–1297.
18. Chen, Y. S. & Xu, J.[1995] " Global bifurcations and chaos in a van der Pol–Duffing–Mathieu system with a single–well potential oscillator", Proc. of the Inter. Conf. on Structural Dynamics, Vibration, Noise and Control, Hong Kong, 511–516.
19. Chen, Y. S. & Xu, J.[1995]" Global bifurcations and chaos in a van der Pol–Duffing–Mathieu system with a single–well potential oscillator", Acta Mechanica Sinica, 11(4), 357–372.

CHAOS AND TRANSFORMATIONS OF STOCHASTIC PROCESSES IN NONLINEAR SYSTEMS WITH INTENSITY DEPENDENT PHASE ROTATIONS

V.V.Zverev,
Physics-Technical Department, Ural State Technical University,
620002 Ekaterinburg, Russia

Abstract: The statistical behavior of mappings with nonlinearities caused by rotations is studied. To describe dynamics under the external noise perturbation we use the Kolmogorov-Chapman equations for the multi-time probability distributions. We obtain the stationary (asymptotic) solutions in the long-time limit as the expansion in a power series with respect to the deviation from the state with complete angle randomization ("phase mixing").

1. Introduction.

In this work we focus on the important class of multidimensional mappings with nonlinearities originated by usual or generalized rotations. Typically a mapping under consideration consist in the successive fulfillment of the transformations stated below: (i) a transformation belonging to the rotation (orthogonal, unitary) group (the angles of rotation are functions of the original vector), (ii) a space contraction associated with dissipation, (iii) a constant shift. A well-known example of the mapping under discussion arise from the analysis of a circuit with nonlinear element and delayed feedback (Ikeda model [Ikeda,1979] of the optical ring cavity, nonlinear electric circuits, etc.). Other mappings belonging to the above-mentioned class often arise from reduction of the differential equations of motion to the difference equations (for example, [Zverev,1993] - for a nuclear magnetization, [Safonov & Zverev,1994] - for parametrically driven spin waves in ferromagnets).

2. A Basic Model: Nonlinear Circuit With Delay.

Here we restrict our consideration to the 2D (complex) model of the circuit with delay proposed by Ikeda [1979]:

$$X(t) = \xi(t) + F(X(t - T_d)) \equiv \xi(t) + 1 + \kappa \exp\left\{ i\lambda |X(t - T_d)|^2 + i\phi_0 \right\}, \qquad (1)$$

where κ is the dissipation parameter ($\kappa<1$), T_d is the delay time, $\xi(t)$ is the noise component of the external signal ($\langle \xi(t) \rangle = 0$). In fact, Eq.(1) is equivalent to the 2D mappings family: $X_N \to X_{N+1}$ for $X_N \equiv X(t_0 + NT_d)$, $0 \le t_0 < T_d$. Using the short notation for the multi-time distribution functions

$$P_N((X_s), \xi) \equiv P(X_0[NT_d + \tau_0], \ldots, X_n[NT_d + \tau_n], \xi[NT_d]), \qquad (2)$$

we may write the corresponding generalized Kolmogorov-Chapman equation as

$$\begin{aligned} P_{N+1}((X_s), \xi_{n+1}) &= \int dY d\xi d\eta P_N((Y_s), \xi_0) \\ &\times \prod_{k=0}^{n} \delta^{(2)}(X_k - \xi_k - \eta_k - F(Y_k))\, p(\eta_k)\, \omega(\xi_{k+1}, \xi_k[\tau_{k+1} - \tau_k]), \end{aligned} \qquad (3)$$

where $dA = dA_0 \ldots dA_n$, $0 = \tau_0 < \ldots < \tau_{n+1} = T_d$ and $\delta^{(2)}$ is 2D delta-function. Above, we assume that the external noise consist of two components: first, Gaussian noise with $\tau_{cor} << T_d$ (the Fourier transformation of its probability distribution function $p(\eta)$ is $\Lambda(U) = \exp\left(-\frac{1}{4} Q |U|^2\right)$), and second, Gaussian or Kubo-Andersen Markowian random process with arbitrary τ_{cor} and the transition densities $\omega(\xi, \eta[\tau])$.

3. Limiting Case of Intense Phase Mixing.

We analyze the stationary solution of equation

$$\Psi_{N+1} = \left(\hat{R} + \varepsilon \delta \hat{R}\right) \Psi_N \xrightarrow{\lambda \to \infty} \hat{R} \Psi_N \quad , \qquad (4)$$

where Ψ_N is the Fourier-image of P_N and ε is a formal "small parameter" (in reality $\varepsilon \delta \hat{R} \sim \lambda^{-1}$ as $\lambda \to \infty$). The zero-order approximate (asymptotic) solution corresponding to the conditions $N, N+1 \to ST$, $\lambda \to \infty$, takes the form

$$\Psi_{ST}^{(0)} = \lim_{N \to \infty} \hat{R}^N \Psi_{INIT} \quad , \quad \Psi_{ST}^{(0)} = \hat{R} \Psi_{ST}^{(0)} \qquad (5)$$

(the problem of convergence of iterative process in (5) was considered in [Zverev & Rubinstein,1991]). Note that

$$\hat{R}^N f\left((U_s),\Omega\right) \xrightarrow{N\to\infty} f\left((0),0\right)\cdot \lim_{N\to\infty}\hat{R}^N 1 \tag{6}$$

and $\Psi_{INIT}\left((0),0\right)$ is the normalization constant. This circumstance reflects the fact of "memory loss" in the system under consideration.

4. Iterative Series Representation of the Exact Solution.

Let us seek the solution of Eq.(4) in the form

$$\Psi_{ST} = \Psi_{ST}^{(0)} + \delta\Psi_{ST} = \sum_{i=0}^{\infty}\varepsilon^i\,\Psi_{ST}^{(i)} \tag{7}$$

Taking into account the normalization condition $\delta\Psi_{ST}\left((0),0\right)=0$ and Eq.(6), one can obtain

$$\Psi_{ST} = \Psi_{ST}^{(0)} + \sum_{i=1}^{\infty}\left[\sum_{k=0}^{\infty}\hat{R}^k\delta\hat{R}\right]^i\Psi_{ST}^{(0)} . \tag{8}$$

The expression (8) may be treated as the "stationary point" of the certain operator:

$$\Psi_{ST} = \hat{A}\Psi_{ST} \quad , \quad \hat{A}\Psi = \Psi_{ST}^{(0)} + \varepsilon\left[\sum_{k=0}^{\infty}\hat{R}^k\right]\delta\hat{R}\Psi \tag{9}$$

Using the norm

$$\|\Psi\| = \sup_{((U_S),\Omega)\in C^{n+2}}\left\{\prod_{k=0}^{n}N(U_k)\left|\Psi\left((U_s),\Omega\right)\right|\right\} \tag{10}$$

with $N(U)=\Lambda^{-1/2}(U)$, we find

$$\left\|\hat{A}\Psi_2 - \hat{A}\Psi_1\right\| \le \alpha\left\|\Psi_2-\Psi_1\right\| , \tag{11}$$

where the estimation for α is given by

$$\alpha = (1-\kappa)^{-1}\left[\left(\frac{4\kappa}{Q\lambda-1}+1\right)^{n+1}-1\right] . \tag{12}$$

Therefore, if $Q\lambda$ is enough large and $\lambda < 1$, existence of Ψ_{ST} follows from the contraction mapping principle.

5. Conclusions and Acknowledgment.

We report the significant result consisting in the rigorous proof of the convergence of asymptotic expansions (8) for the certain models of noise. This expansions can be useful in investigations of the chaotic dynamics with intense mixing. In addition it is shown that noise transformation process in the systems under investigation may be described in terms of two sorts of the fractal domain integrals. The conditions of convergence of this integrals are analyzed in [Zverev,1996].

Work has been partially supported by RF State Committee on High Education (grant 95-0-8.3-14).

6. References.

Ikeda,K.[1979], *Opt.Comm.*,40,68.

Zverev V.V.[1993], *Izv.Vuzov-Prikladnaja Nelinejnaja Dinamika (Applied Nonlinear Dynamics)* **1**,72 (Saratov, in Russian).

Safonov V.L. & Zverev V.V.[1994], *Fizika Tverdogo Tela (Solid State Physics)* **36**, 1939.

Zverev V.V. & Rubinstein B.Ja.[1991], *J.Stat.Phys.*,63,221.

Zverev V.V.[1996], *Teoreticheskaja i Matematicheskaja Fizika (Theoretical and Mathematical Physics)*,(in print).

INDEX